

STU TZIMAN

**NATIONAL ACADEMIES OF SCIENCE AND ENGINEERING  
NATIONAL RESEARCH COUNCIL  
of the  
UNITED STATES OF AMERICA**

**UNITED STATES NATIONAL COMMITTEE  
International Union of Radio Science**



**National Radio Science Meeting  
7-10 January 1992**

Sponsored by USNC/URSI  
in cooperation with  
Institute of Electrical and Electronics Engineers

University of Colorado  
Boulder, Colorado  
U.S.A.

**National Radio Science Meeting  
7-10 January 1992  
Condensed Technical Program**

**Monday, 6 January**

2000-2400  
USNC-URSI Meeting

Broker Inn

**Tuesday 7 January**

0835-1200

A-1 REVIEW OF THERMAL NOISE MEASUREMENTS AT NIST CR2-06  
E-1 SPECTRUM MANAGEMENT IN A CHANGING TELECOMMUNICATIONS ENVIRONMENT CR1-9

0855-1200

G-1 IONOSPHERIC IRREGULARITIES CR0-36  
J-1 INTERPLANETARY AND INTERSTELLAR SCATTERING-I CR2-26

0915-1200

B-1 WAVEGUIDES CR2-28  
C-1 STATISTICAL SIGNAL PROCESSING CR1-46

1335-1700

A-2 NOISE METROLOGY CR2-06  
A-3 NEAR FIELD ANTENNA MEASUREMENTS SESSION CR0-30  
B-2 ANTENNAS CR2-28  
C-2 GEOMAGNETIC INDUCTION EFFECTS CR1-46  
F-1 ATMOSPHERIC PROPAGATION CR1-40  
G-2 IONOSPHERIC MODELING AND PROPAGATION CR0-36  
JE-1 SPECTRUM USEAGE CONSIDERATIONS IN RADIO ASTRONOMY AND REMOTE SENSING CR1-9

1355-1700

H-1 PLASMA WAVES IN THE POLAR MAGNETOSPHERE CR1-42  
J-2 INTERPLANETARY AND INTERSTELLAR SCATTERING-II CR2-26

1700-1800

Commission A Business Meeting CR0-30  
Commission C Business Meeting CR1-46  
Commission F Business Meeting CR1-40

**Wednesday, 8 January**

0815-1200

PLENARY SESSION Duane Physics G0-30

1335-1700

C-3 COMMUNICATION THEORY CR2-06  
G-3 HIGH LATITUDE EFFECTS AND IONOSPHERIC TECHNIQUES CR0-36  
J-3 POINTING AND METROLOGY OF RADIO TELESCOPES CR2-26

1335-1520

B-3 ROUGH SURFACES AND EXOTIC MEDIA CR2-28

United States National Committee  
INTERNATIONAL UNION OF RADIO SCIENCE  
PROGRAM AND ABSTRACTS

National Radio Science Meeting  
7-10 January 1992

Sponsored by USNC/URSI in cooperation  
with IEEE groups and societies:

Antennas and Propagation  
Circuits and Systems  
Communications  
Electromagnetic Compatibility  
Geoscience Electronics  
Information Theory  
Instrumentation and Measurement  
Microwave Theory and Techniques  
Nuclear and Plasma Sciences  
Quantum Electronics and Applications

NOTE:

Programs and Abstracts of the USNC/URSI Meetings are available from:

USNC/URSI  
National Academy of Sciences  
2101 Constitution Avenue, N.W.  
Washington, DC 20418

at \$5 for 1983-1992 meetings.

The full papers are not published in any collected format; requests for them should be addressed to the authors who may have them published on their own initiative. Please note that these meetings are national. They are not organized by the International Union, nor are the programs available from the International Secretariat.

MEMBERSHIP

United States National Committee  
INTERNATIONAL UNION OF RADIO SCIENCE

Chairman: Chalmers M. Butler\*  
Vice Chairman: David C. Chang\*  
Secretary: Charles M. Rush\*  
Immediate Past Chairman: Sidney A. Bowhill\*

Members Representing Societies, Groups, and Institutes:

American Geophysical Union Dr. George W. Reid  
American Astronomical Society Dr. William J. Welch  
IEEE Antennas & Propagation Society Dr. W. Ross Stone  
IEEE Microwave Theory and Techniques Society Dr. A. A. Oliner  
American Meteorological Society Dr. Richard Hahlgren

Members-at-Large: Dr. Susan Avery  
Dr. Lewis Duncan  
Dr. Robert Mattauch\*\*  
Dr. R. M. Price  
Dr. David J. Thompson  
Dr. Donald Wilton\*\*

Liaison Representatives from Government Agencies:

National Telecommunications & Information Administration Dr. Hans Liebe  
National Science Foundation Dr. Julie Lutz  
Federal Communications Commission Mr. William A. Daniel  
Department of Defense Mr. William J. Cook  
Department of the Army Mr. Earl J. Holliman  
Department of the Air Force Dr. Allan C. Schell

Chairmen of the USNC/URSI

Commissions:

Commission A Dr. Motohisa Kanda  
Commission B Dr. Ralph E. Kleinman  
Commission C Dr. Raymond Pickholtz  
Commission D Dr. James W. Mink  
Commission E Dr. Emil F. Soderberg  
Commission F Dr. Juergen H. Richter  
Commission G Dr. Haim Soicher  
Commission H Dr. William Taylor  
Commission J Dr. James M. Moran  
Commission K Dr. James C. Lin

\* Member of USNC/URSI Executive Committee

\*\* Pending approval

Chairmen and Vice Chairmen of  
Commissions of URSI resident  
in the United States:

Vice Chairman, Commission C	Dr. A. D. Wyner
Vice Chairman, Commission D	Dr. T. Itoh
Vice Chairman, Commission F	Prof. R. K. Moore
Chairman, Commission H	Dr. R. F. Benson

Foreign Secretary of the U.S. National Academy of Sciences	Dr. James B. Wyngaarden
---	-------------------------

Chairman, National Research Council, Commission on Physical Sciences, Mathematics, and Resources	Dr. Norman Hackerman
---	----------------------

Chairman, National Research Council, Board on Physics and Astronomy	Frank Drake
---	-------------

Honorary Members	Dr. Harold H. Beverage Dr. Ernst Weber
------------------	---

NRC Staff Director	Dr. Donald C. Shapero
--------------------	-----------------------

NRC Program Officer	Dr. Robert L. Riemer
---------------------	----------------------

NRC Administrative Associate	Ms. Susan M. Wyatt
------------------------------	--------------------

DESCRIPTION OF THE  
INTERNATIONAL UNION OF RADIO SCIENCE

The International Union of Radio Science is one of 18 world scientific unions organized under the International Council of Scientific Unions (ICSU). It is commonly designated as URSI (from its French name, Union Radio Scientifique Internationale). Its aims are (1) to promote the scientific study of radio communications, (2) to aid and organize radio research requiring cooperation on an international scale and to encourage the discussion and publication of the results, (3) to facilitate agreement upon common methods of measurement and the standardization of measuring instruments, and (4) to stimulate and to coordinate studies of the scientific aspects of telecommunications using electromagnetic waves, guided and unguided. The International Union itself is an organizational framework to aid in promoting these objectives. The actual technical work is largely done by the National Committee in the various countries.

The officers of the International Union are:

President:	E. V. Jull (Canada)
Past President:	Dr. A. L. Cullen (U.K.)
Vice Presidents:	Prof. J. Bach Anderson (Denmark) Dr. P. Bauer (France) R. L. Dowden (N.Z) Prof T. O'Koshi (Japan)
Secretary-General	J. Van Bladel (Belgium)
Honorary Presidents:	G. Beynon (U.K.) W. Dieminger (West Germany) W. Christiansen (Australia) W. Gordon (U.S.A.) F. L. H. M. Stumpers (Netherlands)

The Secretary-General's office and the headquarters of the organization are located at Avenue Albert Lancaster, 32, B-1180 Brussels, Belgium. The Union is supported by contributions (dues) from 38 member countries. Additional funds for symposia and other scientific activities of the Union are provided by ICSU from contributions received for this purpose from UNESCO.

The International Union, as of the XXth General Assembly held in Washington, DC in August 1981, has nine bodies called Commissions for centralizing studies in the principal technical fields.

Every three years the International Union holds a meeting called the General Assembly. The next is the XXIVth, to be held in 1993. The Secretariat prepares and distributes the Proceedings of the General Assemblies. The International Union arranges international symposia on specific subjects pertaining to the work of one or several Commissions and also cooperates with other Unions in international symposia on subjects of joint interest.

Radio is unique among the fields of scientific work in having a specific adaptability to large-scale international research programs, since many of the phenomena that must be studied are worldwide in extent and yet are in a measure subject to control by experimenters. Exploration of space and the extension of scientific observations to the space environment are dependent on radio for their research. One branch, radio astronomy, involves cosmic phenomena. URSI thus has a distinct field of usefulness in furnishing a meeting ground for the numerous workers in the manifold aspects of radio research; its meetings and committee activities furnish valuable means of promoting research through exchange of ideas.

Steering Committee:

S. W. Maley, Chairman (303) 492-7004  
D. C. Chang  
D. S. Cook  
P. L. Jensen

Technical Program Committee:

C. M. Rush, Chairman	J. Richter
M. Kanda	E. Soderberg
R. Kleinman	H. Soicher
S. W. Maley	W. Taylor
J. Mink	D. J. Thompson
J. Moran	E. Westwater
R. Pickholtz	

*Tuesday Morning, 7 January, 0855-1200*

Session A-1 0835-Tues. CR2-06

REVIEW OF THERMAL NOISE MEASUREMENTS AT NIST

Chairman: David F. Wait, National Institute of Standards and Technology,  
Boulder, CO 80303

A1-1 INTRODUCTION TO THERMAL NOISE

0840

Sunchana Perera

Electromagnetic Fields Division

National Institute of Standards and Technology

Boulder, CO 80303

Fundamental concepts are reviewed: a blackbody radiator, Planck's law, Rayleigh-Jean's law, spectral power density, Nyquist equation, noise bandwidth, unavailability of thermal noise. An introduction to the theory of random processes is given: ergodicity, amplitude distribution, effects of linear filtering. The concept of correlation is discussed; powers of uncorrelated signals add linearly.

A1-2  
0920

## FUNDAMENTALS OF NOISE MEASUREMENTS

Sunchana Perera

Electromagnetic Fields Division

National Institute of Standards and Technology

Boulder, CO 80303

A distinction between the available and delivered powers is reviewed. The output power of noise passing through a 'passive' two-port is calculated; the available power ratio  $\alpha$ , and the efficiency  $\eta$ , are '*in situ*' quantities and characterize two-port lossiness. The concepts of the available power gain, also an '*in situ*' quantity, and the effective input noise temperature for *active* linear two-ports, are introduced. The repercussions for the noise figure measurements are briefly discussed.

Fundamental principles of noise measuring systems are outlined. An overview of noise standards and radiometers is given. Good design practices in noise metrology are discussed.

A1-3  
1000

COMPARING NOISE SOURCES WITH DIFFERENT CONNECTORS  
W.C. Daywitt  
National Institute of Standards and Technology (NIST)  
Electronic and Electrical Engineering Laboratory  
Electromagnetic Fields Division  
Boulder, CO 80303

Having a separate noise standard for each type of connector would be ideal since the calibration of a DUT (a noise source with an unknown noise temperature) with a particular connector type would then be simpler and more accurate. Unfortunately, building a noise standard for each type of connector is prohibitively expensive and time consuming. Consequently, comparing two noise sources with different connectors must be done through an adapter attached to one of the sources that produces two sources with like connectors.

Alternatively, the adapter can be attached to one port of a switch on the front end of the comparison radiometer, the other input port of the switch having the same type of connector as the other noise source. An absolute adapter efficiency measurement must be performed on the configuration in the first paragraph in order to determine the DUT noise temperature. However, only a relative measurement need be performed for the switch/adapter configuration in the present paragraph.

An ANA measurement of these two adapter configurations will be reviewed and measurement errors assigned.

A1-4  
1040

THE MEASUREMENT OF AMPLIFIER NOISE

D.F.Wait

National Institute of Standards and Technology (NIST)  
Electronic and Electrical Engineering Laboratory  
Electromagnetic Fields Division  
Boulder, CO 80303

The recent emergence of low noise, broad band microwave systems have increased the demand for accurate amplifier noise measurements. In response, NIST is currently developing a measurement service. This presentation will discuss current progress. I begin with the basic definition of noise figure, show that a complete description of amplifier noise at a single frequency requires a four parameter characterization, indicate the motivation and selection of a particular four parameter set, and discuss measurement approach. The paper concludes with comments on current measurement results and error estimates.

A1-5  
1120

THERMAL NOISE MEASUREMENT SERVICES AT NIST  
J.W. Allen  
National Institute of Standards and Technology (NIST)  
Boulder, CO 80303

In the past few years, the National Institute of Standards and Technology (NIST) has significantly expanded the thermal noise calibration services. Presently, we have services for all frequencies between 1 GHz and 12.2 GHz for most of the popular waveguide and coaxial connector types. For selected frequencies and connector types we have services between 0.030 GHz and 95 GHz.

NIST is currently has programs to provide complete coverage between 0.010 GHz and 95 GHz, to reduce the cost of noise calibration services, and to improve the accuracy of existing services. New to NIST are programs to develop amplifier noise calibration services. It is our goal to provide amplifier noise services for all frequency and connector types covered for thermal noise measurements, and to extend the services to MMIC amplifiers.

Chairman: P.L.E. Uslenghi, Dept. of Electrical Engineering and Computer Science, Univ. of Illinois at Chicago, Chicago, IL 60680

B1-1  
0920

## CHARACTERIZING THE RADIATION SPECTRUM OF OPEN-BOUNDARY WAVEGUIDING SYSTEMS

Jerry M. Grimm\* and Dennis P. Nyquist  
Department of Electrical Engineering  
Michigan State University  
E. Lansing MI 48823

The general class of open-boundary waveguides, whether microstrip in the MMIC environment or dielectric waveguides for integrated optics, has become an integral part of much of electromagnetic engineering. Due to the complex nature of the fields and geometry, exact analysis of all but the simplest structures was impossible until the advent of inexpensive computational power. Great strides have been made in determining the characteristics of these structures; however, certain fundamental theoretical questions still remain unanswered. Most significant of these is the characterization of the radiation spectrum for open-boundary waveguides. These continuous modes are necessary for a complete modal description of EM wave excitation, coupling, and scattering associated with general open-boundary waveguiding structures.

Full-wave analysis of these structures is accomplished in the axial-transform domain using an EFIE based on Hertzian potentials supported by equivalent polarization currents arising from dielectric contrast, namely,

$$\bar{e}(\bar{\rho}; \zeta) - (k_c^2 + \bar{\nabla} \cdot \bar{\nabla}) \int_{CS'} \bar{g}(\bar{\rho} | \bar{\rho}'; \zeta) \cdot \left[ \frac{\delta n^2(\bar{\rho}')}{n_c^2} \bar{e}(\bar{\rho}'; \zeta) \right] ds' = \bar{e}^i(\bar{\rho}; \zeta)$$

enforced at all points interior to the waveguide cross-section. The background environment is planarly layered, infinite in extent in the axial ( $z$ ) and transverse ( $x$ ) dimensions. The representation of the Green's dyadic obtained is in the form of an inverse Fourier transform on transverse spectral frequencies  $\xi$ . The scalar coefficients depend on the transformed wavenumber  $p_i = [\zeta^2 + \xi^2 - k_i^2]^{1/2}$ , and take the general form of Sommerfeld integrals. Subsequent to the solution of the above equation, an inverse axial transform on  $\zeta$  will be necessary to recover spatial fields. For this inverse transform, trivial as it seems, to exist, a cutting of the  $\zeta$ -plane must be established to ensure analyticity.

This paper will present a rationale for the choosing of a branch point and branch cuts in the  $\zeta$ -plane. Once these are chosen, the remaining cuts necessary to perform the spectral integration over the transverse spectral frequencies are fixed. These are not independent, but rather are related to the  $\zeta$ -plane cutting through the traditional Sommerfeld-plane branch cuts. The implication of this, both in determination of the radiation spectrum and leaky modes, will be discussed for typical structures, both simple and complex.

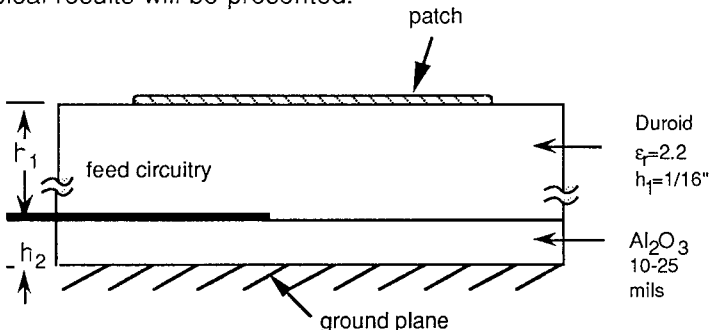
B1-2  
0940

## Integration of Radiating Elements with Hybrid Microwave Integrated Circuits

**Rajan P. Parrikar and K. C. Gupta**  
**Department of Electrical and Computer Engineering**  
**University of Colorado at Boulder**  
**Boulder, CO 80309-0425**

Hybrid microstrip integrated circuits are usually fabricated on high dielectric constant ( $\epsilon_r=10$ ), thin (10-25 mils) substrates. These substrate parameters are not appropriate for designing microstrip patch antennas to be integrated with MICs. A thicker dielectric overlay of lower dielectric constant with a radiating element on the top surface is proposed as a convenient configuration for integration of radiating elements in hybrid MICs. A Multiport Network Model (MNM) approach for modeling and analysis of such integrated circuit-antenna modules is discussed in this paper.

The MNM approach is used to represent the radiating configuration in terms of equivalent sub-networks. The region underneath the patch is modeled as a cavity surrounded by magnetic walls on the sides and electric walls on the top and the bottom. Unlike in the conventional cavity model, the proposed model accounts for field variations in the vertical dimension also. The Schelkunoff Equivalence Principle is used to separate the cavity volume into a source region and a source-free region. The electromagnetic analysis of fields in the source and the source-free regions results in the formulation of two equivalent networks called the Feed Network and the Patch Network. These networks are characterized by a multiport Z-matrix and a multiport hybrid matrix respectively. The external fields (fringing, radiation etc.) are represented by an Edge-Admittance-Network which is combined with the other two networks to obtain an overall network model of the antenna. Network analysis yields equivalent magnetic currents at the edges of the antenna which are used for evaluating the radiation characteristics. Methods of analysis and typical results will be presented.



B1-3 PROPAGATION IN CERTAIN  
1000 MAGNETOELECTRIC SLAB WAVEGUIDES

J.D. Ali and P.L.E. Uslenghi(\*)  
Department of Electrical Engineering and Computer Science  
University of Illinois at Chicago  
Box 4348, Chicago, IL 60680.

Magnetolectric, or bianisotropic, materials obey the constitutive relations

$$(1) \quad \underline{D} = \epsilon_0 \bar{\epsilon} \underline{E} + c_0^{-1} \bar{\xi} \underline{H}, \quad \underline{B} = \mu_0 \bar{\mu} \underline{H} - c_0^{-1} \bar{\eta} \underline{E},$$

where the four dimensionless tensors  $\bar{\epsilon}$ ,  $\bar{\mu}$ ,  $\bar{\xi}$  and  $\bar{\eta}$  may be represented by 3x3 matrices in any given coordinate system, in which the field vectors are 3-element column vectors; here we consider only the rectangular x, y, z coordinate system. Certain bianisotropic materials, e.g. several orthorhombic and tetragonal magnetic crystals, have constitutive tensors of the type (see, e.g., T.H. O'Dell, "The Electrodynamics of Magnetolectric Media", North Holland, Amsterdam, 1970):

$$(2) \quad \bar{\epsilon} = \begin{pmatrix} \epsilon_1 & 0 & 0 \\ 0 & \epsilon_2 & 0 \\ 0 & 0 & \epsilon_3 \end{pmatrix}, \quad \bar{\mu} = \begin{pmatrix} \mu_1 & 0 & 0 \\ 0 & \mu_2 & 0 \\ 0 & 0 & \mu_3 \end{pmatrix}, \quad \bar{\xi} = \begin{pmatrix} 0 & \xi_4 & 0 \\ \xi_5 & 0 & 0 \\ 0 & 0 & 0 \end{pmatrix}, \quad \bar{\eta} = \begin{pmatrix} 0 & \eta_4 & 0 \\ \eta_5 & 0 & 0 \\ 0 & 0 & 0 \end{pmatrix}.$$

We consider guided propagation by a slab of material (1,2) either immersed in air or supported by a metallic substrate. The slab boundaries are planes  $x = \text{constant}$ , propagation occurs in the  $z$  direction, and all field components are independent of the  $y$ -coordinate. In general, propagation in the slab material is in terms of two different transverse wavenumbers for each polarization. The components of  $\underline{E}_z$  and  $\underline{H}_z$  are decoupled, leading to the description of the field as superposition of TE and TM modes. The dispersion relations of these modes are obtained, and a variety of numerical results are displayed for the case of lossless slab material. The cutoff frequencies are examined and compared with those of the biaxial slab without magnetolectric effect ( $\bar{\xi} = \bar{\eta} = \bar{0}$ ).

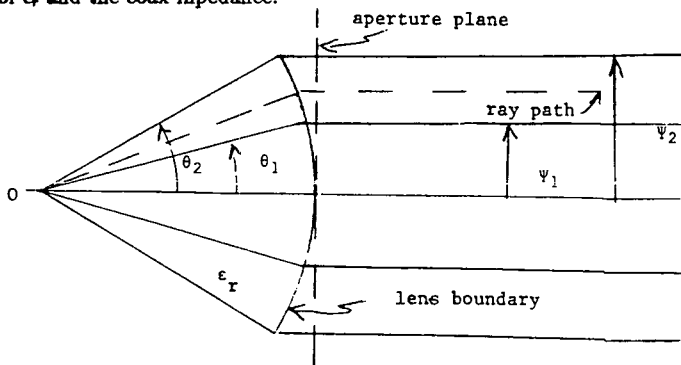
A more general structure consisting of a parallel-plate waveguide partially filled with a magnetolectric slab (1,2) which is sandwiched between two dielectric layers is examined. In particular, the possible existence of a TEM mode in each of the three regions is investigated.

B1-4 A PROLATE SPHEROIDAL UNIFORM ISOTROPIC  
1040 DIELECTRIC LENS FEEDING A CIRCULAR COAX

A. P. Stone  
Department of Mathematics and Statistics  
University of New Mexico  
Albuquerque, NM 87131  
C. E. Baum  
Phillips Laboratory  
PL/WSEA, Kirtland AFB  
Albuquerque, NM 87117

EM lenses for transitioning TEM waves between certain types of transmission lines, without distortion or reflection, may be developed (Transient Lens Synthesis, C. E. Baum and A. P. Stone, Hemisphere Publishing Co., 1991) through an analysis of exact solutions to EM boundary value problems. The key concepts are the matching of impedances at transmission line boundaries and the conservation of transit-times of waves following different paths. Previous work has established exact solutions for certain types of lens problems. The interest here is in approximate solutions which will yield high quality, dispersionless lens designs.

We consider a concentric circular conical uniform isotropic dielectric lens feeding a circular coaxial line as shown below. A transition region (lens) is to be specified so that a wave launched at 0 propagates through the transition region onto the coaxial line with minimum reflection at the boundary between the regions and with minimum distortion. The specification of the lens material (permittivity) and the shape of the boundary constitutes the lens design. In the coaxial line, any path is parallel to the  $z$ -axis and we desire that all transmitted rays arrive at the aperture plane ( $z = 0$ ) at the same time. This equal-time condition determines, at high frequencies, the lens shape. Perfect impedance matching (no reflection at the lens boundary) requires a consideration of local impedance matching along each ray. We may relax this condition and allow a uniform isotropic dielectric lens and a macroscopic impedance matching condition. The boundary angles,  $\theta_1$  and  $\theta_2$ , for the lens region are then determined from the selected permittivity and the characteristic impedance of the coaxial line. In addition, we study the transmission of waves at the lens coax boundary in the high-frequency limit. Snell's law is the governing relation and transmission and reflection coefficients are obtained. The special condition under which no reflection occurs at the lens boundary is the Brewster angle, which is a function of permittivity,  $\epsilon_r$ . One may also define a high frequency transfer function,  $T_v$ , which compares an initial voltage on the coax to a voltage on the conical section with  $|T_v| < 1$ . This quantity is calculated as a function of  $\epsilon_r$  and the coax impedance.



B1-5  
1100**TWO-DIMENSIONAL FIELD ANALYSIS  
AND DESIGN OF ROTMAN LENSES**

C.M. Tsai and K.C. Gupta

Department of Electrical Engineering

University of Colorado at Boulder

Colorado, CO 80309-0425

The classical methods for analysis and design of Rotman type beam forming lens are based on ray optics of electromagnetic waves. However, this approach does not incorporate effects such as mutual coupling between ports and multiple scattering. Thus, the experimental results do not always in agreement with predictions of the theoretical design.

In this paper, a two-dimensional field analysis based on contour integral method is used to analyze Rotman type lenses. This method results in a Z-matrix of multiport model of the lens. The S-matrix is then evaluated from the Z-matrix and the reflection coefficients, coupling between ports and radiation patterns could be found.

The results of this method are in good agreement with the experimental data. It is shown that the coupling between ports could be significant and result in power loss for improper design of the lens. For optimization of the lens configuration, variations on lens geometry and tapered sections at the ports have been tried to investigate their effects on lens performance.

B1-6  
1120 A GRAPHICAL STUDY OF INTENSITY DISTRIBUTIONS AND  
ELECTROMAGNETIC FIELDS IN HIGHER ORDER GAUSSIAN  
BEAMS

Rajendra K. Arora  
FAMU/FSU College of Engineering  
Department of Electrical Engineering  
P.O. Box 2175  
Tallahassee, Florida 32316-2175

A solution of the paraxial wave equation in rectangular  $(x,y,z)$  coordinates yields a family of modes characterized by Hermite-Gaussian variation in the transverse  $(xy)$  plane. Likewise, a solution of the paraxial wave equation in circular cylindrical  $(r,\theta,z)$  coordinates yields a family of modes characterized by Laguerre-Gaussian variation in the transverse  $(r,\theta)$  plane. These modal families each constitute a complete and orthogonal set of solutions of the paraxial wave equation. Any arbitrary amplitude distribution at an "input plane" can be expressed as a superposition of such modes. The circularly symmetrical Gaussian mode is the lowest-order member of these families of modes.

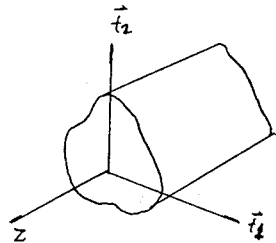
In this paper, the theory of Hermite-Gaussian and Laguerre-Gaussian beam modes is briefly discussed, leading to expressions for the electric and magnetic fields in these modes. The amplitude distributions in these modes in the transverse planes are shown by three-dimensional graphs, from which constant-amplitude contours are derived. Also shown are the electric and magnetic field lines in the longitudinal  $(xz)$  and  $(yz)$  planes. Such plots provide a physical insight into the mechanisms of generation and propagation of such modes, which is important for proper design of experiments utilizing open resonators and beam waveguides.

B1-7 A MATRIX EQUATION TO CALCULATE FIELDS IN  
1140 CYLINDRICAL WAVEGUIDE

Huang Guanghua, 2314 COE# 296, university of Wyoming,  
Laramie, WY 82070

Abstract: A field matrix equation to calculate electromagnetic fields in cylindrical waveguides is presented. Combined with boundary conditions of the fields on metal walls, the method demonstrates calculation directly and impressively.

As shown in the Fig., A cylindrical waveguide with arbitrary transverse cross section has Z direction wave propagation and transverse coordinates  $\bar{t}_1$  and  $\bar{t}_2$ . Electromagnetic fields inside the waveguide must satisfy the Maxwell's equations from which the field matrix equation can be derived and defined



$$\begin{bmatrix} E_{t1} \\ E_{t2} \\ H_{t1} \\ H_{t2} \end{bmatrix} = -\frac{1}{K_c^2} [A] \cdot \begin{bmatrix} \partial E_z / \partial t1 \\ \partial E_z / \partial t2 \\ \partial H_z / \partial t1 \\ \partial H_z / \partial t2 \end{bmatrix}$$

where

$$[A] = \begin{bmatrix} \dot{r}/h_1 & 0 & 0 & j\omega\epsilon/h_2 \\ 0 & \dot{r}/h_2 & -j\omega\epsilon/h_1 & 0 \\ 0 & -j\omega\mu/h_2 & \dot{r}/h_1 & 0 \\ j\omega\mu/h_1 & 0 & 0 & \dot{r}/h_2 \end{bmatrix}$$

$E_z, H_z$  of TE or TM mode can be directly write out according to the boundary conditions

$$\bar{H}_n = 0, \quad \bar{E}_t = 0$$

on metal wall inside cylindrical waveguides with arbitrary cross section.

$E_{t1}, E_{t2}, H_{t1}, H_{t2}$  then can be determined by the field matrix equation.

Reference

Frede Gardiol, " Introduction to Microwaves ", book, 1984

C1-1  
0920

**MULTITAPER SPECTRAL ESTIMATION  
FOR POWER LAW PROCESSES**

**D. B. Percival** Applied Physics Laboratory, University of  
Washington, Seattle, WA

**A.T. Walden** Department of Mathematics, Imperial College,  
London, UK

Given a time series  $X_1, \dots, X_N$  that is a portion of a realization of a stationary process with a spectral density function  $S$  such that  $S(f) = hf^\alpha$  over  $0 \leq f \leq f_c \leq 0.5$ , we consider the problem of estimating the coefficient  $h$  and the exponent  $\alpha$  under the assumption that  $-1 < \alpha < 0$ . One approach (discussed by Mohr, 1981, and others) is to estimate  $S$  using a direct spectral estimate and then to estimate  $h$  and  $\alpha$  using simple linear regression with the log of the spectral estimate as the dependent variable and  $\log f$  as the independent variable. Because the error terms in this regression model have a markedly skewed distribution, Mohr proposed smoothing the direct spectral estimate prior to fitting the regression model. Here we examine the use of multitaper spectral estimation (Thomson, 1982) as an alternative to smoothing across frequencies. This approach has the advantage of producing a spectral estimate with degrees of freedom greater than 2 without introducing bias inherent in smoothing across frequencies. We also consider extensions to this approach for handling nonstationary power law processes ( $\alpha \leq -1$ ).

C1-2  
1040

# Characterization of Diffuse Multipath at Low-Grazing Angles

A. Drosopoulos and S. Haykin

## Abstract

When an electromagnetic signal propagates in a communication channel (e.g. microwave link or radar) a multipath component is generated. This refers to the reflections, diffractions and/or scattering that the signal suffers on its journey from transmitter to receiver. The multipath signal is commonly broken into two separate parts: *specular* and *diffuse*. The former is usually well defined in terms of amplitude, phase and incident direction and can be modeled as a deterministic signal. The latter however, arises out of the random nature of the scatterers and, as such, is non-deterministic. Again, it does not come from a single, well specified direction but from a continuum of directions, making the modeling much more difficult. In fact it is usually neglected. Multipath (both components) degrades the direct signal component and can make information transmission or angle-of-arrival estimation difficult. This is a serious problem in any area based on the propagation and scattering of electromagnetic or sonar signals, particularly at low grazing angles when both direct and specular components are within a beamwidth of each other.

The focus here is in the experimental characterization of the diffuse component at low-grazing angles. A database of X-band signals were collected with a 32-element sampled aperture array at Lake Huron, Canada, during the fall of 1987 [1]. The issues addressed here are:

- The second-order statistics in the wavenumber domain were investigated using the multiple window method (MWM) [2], [3], [4]. As far as the authors are aware this is the first time that a non-parametric estimate of the diffuse component spectrum is obtained. A theoretical model of electromagnetic scattering from a rough surface confirms the importance of shadowing under such experimental conditions.
- There has been renewed interest recently in higher-order statistics [5] and already a scattering model for an ocean surface has appeared [6] that makes use of the surface bispectrum. The bispectrum of the diffuse component of our experimental data in the wavenumber domain is estimated, using again MWM [7], and it is seen that further investigation in higher order statistics is indeed warranted.
- Finally, since diffuse multipath is a form of radar clutter, the recent work on the K-distribution of the amplitude statistics of clutter [8] are verified for our database as well.

## References

- [1] Kezys, V. and Haykin, S.: "Multi-Frequency Angle-of-Arrival Estimation: An experimental evaluation", *SPIE Vol. 975 Advanced Algorithms and Architectures for Signal Processing III*, 1988, 93-100.
- [2] Thomson, D.J.: "Spectrum Estimation and Harmonic Analysis", *Proc. IEEE*, 70(1982)1055-1096.
- [3] Thomson, D.J.: "Quadratic-inverse spectrum estimates: applications to paleoclimatology", *Phil. Trans. R. Soc. Lond. A*, 332(1990)539-597.
- [4] Drosopoulos, A. and Haykin, S.: "Adaptive Radar Parameter Estimation with Thomson's Multiple-Window Method", Chapter 7, in *Adaptive Radar Detection and Estimation*, Haykin, S. and Steinhardt, A. eds., Wiley, 1991.
- [5] Nikias, C. and Raghuveer, M.R.: "Bispectrum Estimation: A Digital Signal Processing Framework", *Proc. IEEE*, 75(1987)869-891.
- [6] Chen, K.S. and Fung, A.K.: "A scattering model for ocean surface", *Proc. of the International Geoscience and Remote Sensing Symposium, IGARSS 91*, 1251-1254.
- [7] Thomson, D.J.: "Multi-Window Bispectrum Estimates", *Proc. of the Workshop on Higher-Order Spectral Analysis*, Vail, Colorado, June 1989, 19-23.
- [8] Jakeman, E. and Pusey, P.N.: "A model for non-Rayleigh sea echo", *IEEE Trans. on Antennas and Propagation*, 24(1976)808-814.

C1-3  
1120**DYNAMIC QUADRATIC-INVERSE ESTIMATES OF  
MAGNETOSPHERIC FLUCTUATION SPECTRA****David J. Thomson**

AT&amp;T Bell Laboratories, Murray Hill, N.J. 07974

It is commonly assumed that, if one excludes diurnal and seasonal structural changes plus discrete events such as storms and  $C_p$  oscillations, magnetospheric fluctuations have a rather featureless power-law spectrum. Recent work by Alpert, Lanzerotti *et.al.* has suggested an alternative model that is almost a continuum of frequency localized modes undergoing a complicated time evolution. The average spectrum agrees with standard theory but a "snapshot" made from data on a short time interval will usually be significantly different.

The statistics of such a process are significantly different from those of a stationary process and require the theory of harmonizable processes. I show that the familiar "dynamic spectrum" gives an estimate of Loeve's generalized spectrum and describe the use of quadratic-inverse spectrum estimates (*Phil. Trans. R. Soc. Lond. A (1990) 332 pp 539-97*) to estimate them. A singular value decomposition of the dynamic spectrum is then used to isolate the dominant characteristics.

SPECTRUM MANAGEMENT IN A CHANGING TELECOMMUNICATIONS ENVIRONMENT  
Chairman: R.D. Parlow, National Telecommunications and Information  
Administration

Organizers: R.D. Parlow and D.J. Cohen, National Telecommunications and  
Information Administration; and G.H. Hagn, SRI International

E1-1 NATIONAL AND INTERNATIONAL SPECTRUM MANAGEMENT  
0840 UPDATE AND CURRENT CCIR ISSUES  
R.D. Parlow, Associate Administrator  
National Telecommunications and Information  
Administration, Room 4099  
U.S. Department of Commerce  
14th & Constitution Avenue, N.W.  
Washington, D.C. 20230

This paper presents information concerning changes that are taking place in the spectrum management community, both in the United States as well as abroad. The National Telecommunications and Information Administration (NTIA) has conducted a year-long study on the future management of the radiocommunications spectrum, the process and associated issues that have both national and international implications. The report titled "U.S. Spectrum Management Policy: Agenda for the Future" recommends ways for the NTIA and the Federal Communications Commission (FCC) to improve their spectrum management systems. Specific proposals and recommendations were made for five areas: (1) Regulatory Process, (2) The Block Allocation System and Flexibility, (3) Market-Based Spectrum Management, (4) Spectrum Use and Efficiency, and (5) Strategic Planning and Forecasting.

In addition, efforts are underway in Canada, the United Kingdom and within the European Community. Information regarding the scope and progress of these efforts will be presented. In the international regulatory community, the International Telecommunication Union (ITU), changes are on the horizon that will change the character, organization and work methods of the Union. A special committee has made recommendations that will prepare the ITU for the future and change the traditional roles of the CCIR and other permanent organs. The implications of these changes will be addressed as well as current technical issues that are being addressed.

E1-2  
0900THE CHANGING TELECOMMUNICATIONS INFRASTRUCTURE  
AND SPECTRUM REQUIREMENTSDale N. Hatfield, Senior Fellow  
Annenberg Washington Program  
Hatfield Associates, Inc.  
4840 Riverbend Road  
Boulder, CO 80301

The telecommunications infrastructure in the United States and throughout the rest of the world is changing rapidly and in fundamental ways. For example, there are well-documented trends toward digital rather than analog transmission and switching, toward increased use of intelligence within the network, toward the use of broadband fiber optic systems in not only the long-haul portion of networks but in the local distribution portions as well, and toward the use of radio for wireless or "tetherless" access to the "wired" networks. These changes have significant implications for spectrum utilization and management. For example, the shift from point-to-point microwave to fiber optic systems in the long-haul portion of networks holds out some promise for freeing up spectrum for other purposes. On the other hand, the increased economic efficiency and convenience associated with tetherless forms of communications has created significant pressures for additional spectrum for these radio based services. These two developments, in combination, raise important questions such as the utility of these microwave bands for mobile/portable communications purposes and the technical and management means that might be adopted to facilitate their use on a shared basis during some transition period.

Another example is the increased use of digital technology that allows more efficient utilization of the spectrum resource, but presents similar technical and management issues as to how they can be introduced into radio bands that are already heavily used. This paper reviews the major technological (and market) trends that are occurring in the telecommunications industry, and then attempts to identify and describe the implications of these changes for spectrum utilization and management. Finally, areas that suggest the need for research attention in the radio scientific community will be noted.

E1-3 WHAT IS SPECTRUM EFFICIENCY  
0920 AND WHO WANTS IT?  
Leslie A. Berry  
2425 Forest Avenue  
Boulder, CO 80304

Spectrum efficiency is regarded as desirable by most members of the radio-using community, but the concept has different meanings for system designers, spectrum managers, regulators, and economists. These different concepts will be discussed. Economic spectrum efficiency can only be attained if there is a free market for spectrum, so this talk will concentrate on technical spectrum efficiency from the viewpoint of the community of users, as represented by the spectrum manager and regulator.

Attempts to define and compute quantitative measures of spectrum efficiency have been hampered by disagreements about specific meanings of some factors in the definition, by lack of adequate data, and by disinterest (or active antagonism) of user groups. Some of the problems encountered will be discussed.

The methods for allocation and assignment of the radio spectrum provide some incentives for spectrum efficiency in the form of equipment standards, imposed operating procedures, congestion in some bands, and peer pressure. There are also dis-incentives, including, among other things, costs, lack of standards or obsolete standards, unnecessarily large protection margins, and problems resulting from allocation of blocks of spectrum to specific services, such as unused spectrum in some bands and hoarding.

Prerequisites for quantitative calculation of technical spectrum efficiency will be identified, and the likelihood of near-term quantification will be estimated.

E1-4  
0940

## NEW TECHNICAL METHODS OF SPECTRUM SHARING

David J. Cohen  
National Telecommunications and Information Administration  
Annapolis, Maryland 21401

A greater use of spectrum sharing is one approach to improve spectrum utilization. This paper describes several new technical methods of inter-service spectrum sharing. These new methods are under study and/or being tested and utilized in the United States and the international spectrum management community.

Inter-service spectrum sharing exists when two or more radiocommunication services effectively utilize the same frequency band. Spectrum sharing is made possible by appropriate separations between equipments. These separations may be in one or a combination of the four dimensions: frequency, time, spatial and orthogonality. The new inter-service sharing methods described will include:

- (1) Spectrum overlays
- (2) Low power consumer electronic devices
- (3) Sharing by constraints
- (4) Flexible use
- (5) Geographic sharing
- (6) Time sharing
- (7) Dynamic variable partitioning

Examples of each these new methods of sharing will be given along with an assessment of some of the advantages and disadvantages of these methods. Several of the above methods apply to or are dependent on new technologies such as digital communications and computerized spectrum management procedures.

Internationally, a new CCIR Study group has been formed (Study Group 12) to study difficult inter-service sharing problems and a CCIR Task Group (TG1/1) is examining new technical methods to share spectrum. The work of these groups will be reviewed.

E1-5  
1000

**SPECTRUM MEASUREMENTS:  
THE TECHNOLOGY OF ASSESSING SPECTRUM CONSUMPTION**  
Robert J. Matheson, ITS.S  
U. S. Department of Commerce  
Institute for Telecommunications Sciences  
325 Broadway  
Boulder, Colorado 80303

The place of spectrum measurements in assessing what portion of a frequency band is available for further assignment has fallen repeated into and out of favor. This is probably because of a lack of understanding of the limitations of the process and the need for considerable interpretation between the raw measurements and the frequency management conclusions.

The traditional objections to the use of measurements to determine spectrum usage is that measurements are:

1. Expensive, time consuming, and fraught with logistics problems.
2. Limited in time, location, and sufficient sensitivity.
3. Difficult to interpret and apply to a given problem.
4. Ignorant of planned future usage, operational duty cycles, and receiver frequencies that need to be protected.

Unfortunately, alternative methods of assessing spectrum usage depend on incomplete and unreliable technical data in frequency listings, unrealistic propagation models, unknown deployment and operational duty cycles, and massive oversimplification. The increasing ability to easily gather massive amounts of accurate raw data suggests that spectrum measurement should remain under consideration as a method for forming realistic opinions about the actual usage of spectrum. Faced with such a choice, the prudent person might decide to use both techniques and try to figure ways to reconcile the differences.

This paper describes some of the interpretation that needs to be performed on raw measured spectrum usage data, illustrating the principles with spectrum measurements made over the years on various signals.

E1-6

CDMA OVERLAYS OF MICROWAVE SYSTEMS-RECENT RESULTS

1040	Donald L. Schilling Dept. of EE CCNY New York, NY 10031	William Biederman Millicom, Inc. New York, NY 10022	Laurence B. Milstein Dept. of ECE U. of CA. San Diego La Jolla, CA 92093
	Raymond L. Pickholtz Dept. of EECS George Washington U. Washington, DC 20052	Marvin Kullback SCS Mobilecom, Inc. Port Washington, NY 11010	Don C. Salerno LOCATE, Inc. New York, NY 10004

This paper describes the Field Tests and summarizes the results obtained when overlaying Broadband-CDMA on the frequency band used by existing point-to-point fixed service microwave systems. Indoor and outdoor measurements are described including: adaptive power control, the use of a notch filter, transmission of x-ray imagery in a hospital, and base station interconnection using PSTS and T1.

It is shown in this paper that using the definitions of spectral efficiency proposed by AT&T and GTE, Broadband CDMA is more than twice as efficient as TDMA or narrowband CDMA systems. In addition, Broadband CDMA can share its spectrum with other users. Furthermore, this system is shown to be fade resistant and allows high quality voice reproduction, thereby providing untetherless, wired-line type performance.

*Japan uses antenna diversity in their cellular  
Cells are 9 mi<sup>2</sup> and 56 users in US  
want to maximize users/mi<sup>2</sup>/Hz*

*First license 1850 to 1950 MHz Houston, Orlando, NY  
I think in spread spectrum*

*32 kbps delta mod after spreading by factor of 750  
w/BPSK no FEC 48 MHz BW*

*Can go up to 45 Mbps*

*all users must be received at equal power at base.  
The base sends a s. grid to user to adapt power control*

*RAKE switched time diversity at base  
Space diversity at base*

<i>users/cell</i>	<i>FDMA</i>	<i>TDMA</i>	<i>B-CDMA</i>
	<i>56</i>	<i>1250</i>	<i>200</i>

E1-7  
1100 ACTS--AN EXAMPLE OF DYNAMIC SPECTRUM SHARING AMONG  
USERS IN THE FIXED SATELLITE SERVICE  
Robert Bauer, ACTS Project Application Engineer  
NASA Lewis Research Center  
21000 Brookpark Road, MS 54-6  
Cleveland, OH 44135  
(216)433-3431

The Advanced Communications Technology Satellite, or ACTS, is NASA's latest project aimed at maintaining communications satellite preeminence in the United States. While the experimental satellite program is being sponsored by NASA, the actual spacecraft is being built by U.S. industry. ACTS is expected to be launched in early 1993 aboard the Shuttle and will have an initial mission life of two years (which may be extended to up to four years provided sufficient interest is presented by the system's users). NASA will make the ACTS communications system available to any interested U.S. organization, that is, from industry, academia, or government, as an opportunity to use and test the new technologies with the intention that sufficient interest will be generated to spur industry to develop an operational follow-on system. An experiments program has been established by NASA to coordinate the users with ACTS operations.

ACTS will fly five new technologies which are too technically demanding, costly, and risky to be left for development by the private sector alone. These technologies are: coverage provided by a multiple hopping spot beam antenna; use of the next higher frequency band (Ka-band, 30/20 GHz) including space and ground component development for this band; development of a baseband processor that incorporates onboard stored-baseband switching of communication traffic; a wide bandwidth microwave switch matrix having three 900 MHz-wide channels; and automatic rain fade compensation that occurs independently on the uplink and downlink and transparently to the user.

Communication satellites using C and Ku bands have an available bandwidth of 500 MHz. Total channel capacity can be increased only if the bandwidth can be increased or reused. ACTS will investigate expanding a satellite's total available channel capacity by having 1000 MHz of available bandwidth at Ka band and by reuse of the frequency. Both spatial and polarization frequency reuse are being employed with ACTS.

In an ideal satellite, maximum spatial isolation from other users would be achieved by using one antenna beam to serve each earth station (T. Pratt, C.W. Bostian, Satellite Communications, 1986, pp. 82-85). This impractical limit is approximated with ACTS by using a multibeam antenna. Taking advantage of the higher frequency Ka band, narrow (nominally 0.25°) highly focused spot beams can be formed with beam forming networks and reasonably sized spacecraft reflectors to provide spatial frequency reuse. The 2.2 m diameter 30-GHz receive reflector and the 3.3 m diameter 20-GHz transmit reflector are inversely scaled with respect to frequency so that each produces spot beams having the same angular size in both frequency bands, and thus having the same ground coverage footprint of approximately 100-miles in diameter on the ground.

The multibeam antenna incorporates two hopping spot beam families and three fixed beams. The spotbeam families (designated East and West) each contain a scan area and a total of 13 isolated spot beams focused on major U.S. metropolitan areas. The two families are discriminated by orthogonal linear polarization thereby providing for frequency reuse. For each family, uplink signals are also cross polarized to downlink signals. This permits the East and West spotbeams to simultaneously transmit and receive. Antenna beam sidelobes are controlled so that any two co-polarized beams will have at least 25 dB of co-frequency isolation when the beam centers are separated by two half-power beamwidths. Cross polarization provides at least 25 dB of co-frequency isolation when simultaneously-active beams are separated by less than two half-power beamwidths (e.g., where two family hopping beams are operating adjacent to a common family boundary; J.C. Graebner, W.F. Cashman, 13th AIAA, paper # AIAA-90-0835-CP, 1990).

E1-8  
1120

# Over-the-Horizon Radars: An Example of Dynamic Spectrum Sharing Across Many Radio Services in the HF Band

E. Lyon III  
SRI International

## ABSTRACT

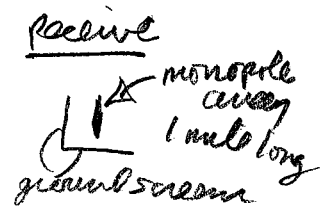
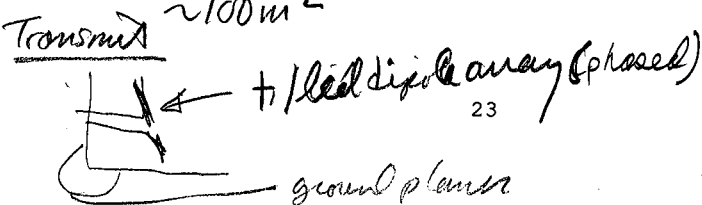
Two examples of Over-the-Horizon Radars (OTHRs) are described, insofar as their frequency requirements and frequency-time operating patterns are concerned. One is characteristic of pulsed OTHR's apparently in operation since the late 1970's in the Soviet Union; the other is characteristic of both the USAF and USN OTHR's which have just completed development and initial deployment.

Of special interest is the frequency spectrum occupancy by other users in which these radars must operate. This is the HF (5-30 MHz) spectrum, and the method by which the US military OTHR's monitor and select operating frequencies to avoid harmful interference with these other users can be used as a model for certain other HF radio services, as well. It is noteworthy that the USAF OTH Radar system in operation in Maine, and the US Navy OTH Radar now operating in Alaska have enjoyed thousands of operating hours with virtually no known instances of harmful interference to others. Part of the credit for this record is due the design of the radar formats and the equipment being used to ascertain spectral occupancy, while the balance is due the operating doctrines in effect at the radar stations.

This type of operation is contrasted with a highly-interfering method which was extant for several years in a pattern of emissions generally attributed to a Soviet OTH Radar system (or systems). This operation reflected neither the emission spectral control nor the operating controls necessary for the HF spectrum sharing required in the modern world.

*Operate OTH radar in polar regions  
Navy has one in Alaska  
and one he talks about here:  
separated transmit & receive sites  
in Maine that look mono sketch  
1000's miles away*

*Transmit 100 MW average power. Targets  
emit 10 uW/m<sup>2</sup> and targets (air planes) are  
~100 m<sup>2</sup>*



E1-9  
1140**SPECTRUM USAGE MEASUREMENTS IN POTENTIAL PCS  
FREQUENCY BANDS**

Jeffery A. Wepman, ITS.S3  
U.S. Department of Commerce  
Institute for Telecommunication Sciences  
325 Broadway  
Boulder, Colorado 80303

This paper discusses spectrum usage measurements that were made in several potential Personal Communication Services (PCS) frequency bands in the 600 to 2600 MHz range in five U.S. cities. The purpose of these measurements was to determine the relative degree of spectrum usage that a PCS system might encounter in each measured frequency band. The issue of interference caused by a PCS system to existing services was not addressed.

Measurements were made using a mobile, computer-controlled radio frequency measurement system that was installed in a mini-van. Geographic dependence (within a city) of spectrum usage was determined for all of the cities. In each city, measurements were typically made at 37 sites with a five mile spacing between sites.

The raw data taken at each site consisted of received signal levels for each frequency measured. These data were processed to provide signal level, measured frequency usage, and measured band usage graphs. The signal level graphs show minimum, maximum, and mean received signal levels at each frequency as measured at all sites in each city. The measured frequency usage graphs display the percentage of sites where received signal levels at each frequency were below threshold during the measurement periods. The measured band usage graphs show the percentage of sites that had a certain percentage or more of the frequencies in the band whose received signal levels were below threshold during the measurement periods.

The highest usage was seen in the 869-894 MHz and the 864-868 MHz bands. The bands showing the lowest usage were the 2400-2483.5 MHz, 1850-1990 MHz, and 901-902 MHz bands. Other bands showing low usage were the 902-928 MHz, 2110-2130 MHz, 2160-2180 MHz, and 614-806 MHz bands.

G1-1  
0900

## THE MORPHOLOGY OF EQUATORIAL F LAYER IRREGULARITIES

### RELEVANT TO THEIR OCCURRENCE

Jules Aarons, Center for Space Physics  
Boston University, Boston, MA 02215

Determining the morphology of F layer irregularities as a function of longitude in the equatorial region is vital for understanding the physics of the development of these irregularities. We aim to lay the observational basis which then can be used to test theoretical models. Theoretical models have been developed, notably in the papers by R.T. Tsunoda (Rev. Geophys. 26, 719, 1988) and by T. Maruyama and N. Matuura (J. Geophys. Res. 89, 10903, 1984). The question is whether the models are consistent with the morphology as we see it. According to our criteria, the data used should be confined to observations taken near the magnetic equator during quiet magnetic periods and at times within a few hours after sunset. Anomaly region data should be omitted for studying the generation mechanism.

The questions to be answered by proposed mechanisms are (1) why do the equinox months have high levels of occurrence over all longitudes and (2) why are there relatively high levels of occurrence in the Pacific Sector in the July-August period and in the 0-75° West Sector in the November-December period (3) why are there very low levels of occurrence in November and December in the Pacific Sector and in July and August in the 0-75° West Sector.

In the paper by Matayuma and Matuura, the authors have taken observations of topside soundings of spread F. With this data set in hand, they conclude: "During the northern winter periods, there is maximum enhancement at the Atlantic longitudes of large westward geomagnetic declination and during the northern summer at the Pacific longitude of large eastward declination." Tsunoda's conclusions from his use of scintillation data is that "scintillation activity appears to maximize at times of the year when the sunset nodes occur". The emphasis of one paper is on the maximum enhancement during the solstices and in the other paper on variations from the equinox as determined by latitude and declination. Each stresses certain characteristics of the morphology. While the two papers explain relatively different morphologies, each makes contributions. However there remain problems to be resolved before certifying a solution as to the physics explaining the longitudinal pattern of F-region irregularities.

Satellite in-situ data, scintillation and spread F observations will be reviewed. The limitation of each data set will be outlined particularly as relevant to the bias produced by the existence of thin versus extended layers of irregularities. A cartoon as to the occurrence pattern, as we see it, as a function of longitude will be shown.

G1-2  
0920

**ALTAIR INVESTIGATIONS OF PLASMA-BUBBLE EVOLUTION**  
**R.T. Tsunoda, Principal Scientist**  
**Geoscience and Engineering Department**  
**SRI International**  
**Menlo Park, California 94025**

Using both coherent backscatter and incoherent-scatter measurements of plasma bubbles obtained with ALTAIR, a fully-steerable radar in the Kwajalein Atoll, Marshall Islands, we are able to determine the time evolution of plasma-bubble development in the nighttime equatorial ionosphere. Evolution characteristics include the background ionospheric conditions, time and location of bubble origin, the seed distribution in east-west direction, bubble growth velocity, and the time dependence of the two-dimensional shape of plasma bubbles. These features are interpreted in terms of equatorial electrodynamic, plasma instability and seeding theories.

G1-3 A STUDY OF VELOCITY FLUCTUATIONS IN EQUATORIAL  
0940 F-REGION USING RADAR INTERFEROMETRY AND  
SCINTILLATION TECHNIQUES

Hale Pinar Zengingönlü, Steven J. Franke, and Erhan Kudeki  
University of Illinois at Urbana-Champaign  
Department of Electrical and Computer Engineering  
1406 West Green Street  
Urbana, IL 61801-2991

Simultaneous radar backscatter and scintillation experiments were conducted during 10-14 October San Marco Campaign at Jicamarca and Huancayo, respectively. Spaced receiver correlation analysis is used on the scintillation data to determine the km-scale irregularity zonal drift,  $V_O$ , and the characteristic velocity,  $V_C$ , which is a measure of random changes in the diffraction pattern that can be related to the fluctuations of the drift velocity. Estimates of  $V_O$  and  $V_C$  computed at 4-minute intervals are compared with the average drift of plasma density irregularities and velocity fluctuations obtained from 50 MHz radar backscatter data, using radar interferometer techniques. The standard deviation of the radar velocities is calculated by employing 4-minute velocity averages for the heights 300-500 km near F-peak. Comparisons between characteristic velocity and the rms velocity fluctuation are made for the three days of the experiment. Due to the lower levels of  $S_4$  index the other days could not be included in the computation process. The rms velocity fluctuations show good agreement with the characteristic velocity calculations for the examined days.

G1-4 THE INTERPRETATION OF SPREAD F,  
1000 FROM DYNASONDE OBSERVATIONS

J. W. Wright  
1915 Spruce Ave. Longmont Colorado 80501.

P. E. Argo  
Los Alamos National Laboratory, Los Alamos  
New Mexico, 87545

We show that most of the echoes of ionogram 'Spread-F' must be interpreted in terms of total internal reflection, thereby contradicting some recent theoretical descriptions of the phenomenon. Neither 'Rayleigh', nor 'Bragg', nor diffuse multiple large-angle refractive scatter can be reconciled with the radio bandwidth-determining details of equatorial and higher-latitude Spread F patterns. The consequences of small-angle refraction and normal-incidence total reflection from Fresnel- (and larger-) scales are, however, consistent with our frequency-dependent echo amplitude and echolocation observations.

Ionograms therefore indicate rather comprehensively the range of irregularity plasma densities within view of the ionosonde. We demonstrate that with modern digital ionosonde observations much can be learned of the spatial structures of plasma density responsible for Spread F at equatorial and auroral latitudes. In particular, several characteristic features of equatorial Spread-F ionograms are shown to be consistent with little-noted attributes of 'plasma bubble' simulations.

G1-5  
1040THE GLOBAL IONOSPHERIC RESPONSE TO A GREAT  
STORM

K. C. Yeh AND K. H. Lin

Department of Electrical and Computer Engineering

University of Illinois at Urbana-Champaign

Urbana, IL 61801-2991

R. O. Conkright

National Geophysical Data Center

National Oceanic and Atmospheric Administration

Boulder, CO 80303-3328

By any measure the magnetic storm beginning with a storm sudden commencement at 0128UT March 13, 1989 must be classified historically as a great storm. Associated with this great magnetic storm is the drastic modification of the normal ionosphere lasting for several days. To study this abnormal behavior ionospheric data collected at 52 ionosonde stations and 12 total electron content observing stations have been analyzed. The global data show a longitudinal dependence on the storm behavior; a pronounced worldwide depression in the diurnal maximum values of  $f_oF_2$ ; the extreme depression of the diurnal minimum in  $f_oF_2$  to a frequency less than 2 MHz at many stations, sometimes accompanied by an unprecedented rise in  $h'F$  to 700 km or more; the presence of traveling ionospheric disturbances; the presence of large scale standing oscillations; the development of hemispheric asymmetry; and the suppression of the equatorial anomaly. These and other unusual phenomena are described in this paper.

G1-6       STUDIES OF MESOSCALE DYNAMICS AND STRUCTURE IN THE  
1100       HIGH LATITUDE IONOSPHERE WITH MAGNETOSPHERIC AND  
          THERMOSPHERIC COUPLING

M.J. Keskinen, P.K. Chaturvedi, and J.A. Fedder  
Space Plasma Branch  
Plasma Physics Division  
Naval Research Laboratory  
Washington, DC 20375-5000

P. Satyanarayana  
Science Applications International Corp.  
McLean, VA 22102

The Naval Research Laboratory ionosphere-magnetosphere mesoscale coupling model has been generalized to include some thermospheric coupling effects. This model combines magnetospheric inertial effects together with ionospheric collisional contributions. We apply this model to study the dynamics and structure associated with some mesoscale phenomena in the high latitude ionosphere, i.e., polar cap patches and sun-aligned arcs.

G1-7  
1120NIGHTSIDE AURORAL ZONE SCINTILLATION  
MORPHOLOGYSu. Basu<sup>1</sup>, S. Basu<sup>2</sup>, and E. MacKenzie<sup>1</sup><sup>1</sup> Institute for Space Research  
Boston College  
885 Centre Street  
Newton MA 02159-1164<sup>2</sup> Phillips Laboratory  
PL/GIS  
Hanscom AFB MA 01731-5000

Long-term scintillation measurements using high elevation ( $>45^\circ$ ) quasi-geostationary satellites transmitting at 250 MHz have been made at three auroral locations namely, Goose Bay, Tromso, and Sondrestrom. Many years of data are available from the first two stations while Sondrestrom measurements are available for the year 1990. All three stations show a minimum nighttime scintillation occurrence in local summer and a diffuse maximum from fall through spring. This seasonal pattern is not observed during low sunspot years when scintillations are observed at a constant low level throughout the nighttime hours. This pattern follows closely that observed deep in the polar cap at Thule and is quite different from that found at the equatorward edge of the oval using low elevation ( $\sim 20^\circ$ ) geostationary satellites. Careful comparison of phase scintillation spectra at Thule and Sondrestrom indicates that the spectral index at Thule is shallower than that at Sondrestrom. The results of these comprehensive polar and auroral scintillation measurements should be incorporated into user oriented scintillation models such as WBMOD.

G1-8      AURORAL DYNASONDE SPREAD F;  
 1140      RADIO AND GEOPHYSICAL  
           INTERPRETATION.

J. W. Wright  
 1915 Spruce Ave. Longmont Colorado 80501.

Frequency spreading on ionograms quantitatively indicates the prevailing plasma density range  $\pm\delta N$  of Fresnel (and larger) -scale irregularities. Dynasonde observations at Tromsø are shown to disclose, furthermore, that this same frequency spreading is arrayed spatially. Taken together, these two related properties suffice to determine a gradient scale length  $L \approx (\delta N/N \cdot \delta x)^{-1}$  where  $x$  is a (signed) spatial coordinate, in practice approximately perpendicular to the magnetic field  $\underline{B}$ . Meanwhile, the diversity of echo line-of-sight Doppler velocities  $V^*$  and the echolocations among the echoes of the Spread F pattern yield a best-fitting vector velocity  $\underline{V}$ . EISCAT comparisons show that  $\underline{V}$  corresponds well with the induced  $\underline{E} \times \underline{B} / B^2$  velocity at least under conditions of moderate to large electric field  $\underline{E}$ .

In this paper I use  $L$  and  $V$  estimated in Tromsø Spread F cases to define an irregularity 'growth-rate',  $\Gamma = V/L$ . According to instability theory, if  $L$  and  $V$  are of like (unlike) sign the irregularities are expected to increase (decrease) in intensity expressed as  $(\delta N/N)^2$ , with an e-folding time  $\Gamma^{-1}$ , typically a few hundred seconds. The procedure chosen for estimating  $L$  does not yet use the dynasonde data in an optimum way, but reasonable agreement with these expectations is found nevertheless. This lends further support to the plasma-interchange instability theories of high latitude ionospheric irregularities. It supports also the interpretation of ionogram Spread F in terms of total reflection from irregularities of Fresnel scale (a few km), and larger, such scales appearing naturally within the spectra determined by theory and numerical simulation. With improved methods for estimating the gradient scale  $L$ , the dynasonde should acquire a capability for real-time single-site prediction of ionospheric irregularity development.

J1-1  
0900 INTERPLANETARY SCINTILLATIONS NEAR THE SUN  
J. W. Armstrong  
Jet Propulsion Laboratory, California Institute of Technology  
Mail Stop 238-737  
4800 Oak Grove Dr.  
Pasadena, CA 91109

Our observational knowledge of the inner solar wind has been gained by an aggregate of UV, optical, and radio remote sensing techniques. Radiowave scattering techniques are particularly useful for studying the velocity and density structures of the inner heliosphere in and out of the ecliptic. Until a *Solar Probe*-class mission is flown, remote sensing techniques will be the *only* way we can obtain information on this dynamically-important region of solar wind.

In this paper I primarily review the observations and secondarily the interpretation of radiowave scattering/interplanetary scintillation (IPS) data taken in the inner heliosphere (defined here as being within about 40  $R_{\odot}$  from the Sun). The paper is organized as follows. First I briefly outline the relationships between IPS observables (e.g., intensity scintillations, phase scintillations, angular broadening, spectral broadening, range delay fluctuations, Faraday rotation fluctuations, dynamic spectra) and the underlying density, velocity, and magnetic field properties of the solar wind plasma. I then briefly summarize the extant observations of scintillations of compact natural radio sources, radar signals backscattered from the inner planets, and coherent spacecraft beacons in and out of the ecliptic plane. Finally, I discuss the quantities usually inferred from these observations, such as the electron density spectrum and near-sun velocity field.

J1-2  
0920THE DETECTION OF CORONAL ALFVEN WAVES  
VIA ROTATION MEASURE FLUCTUATIONSS.R. Spangler and T. Sakurai  
Dept. of Physics and Astronomy  
University of Iowa  
Iowa City, Iowa 52242

Most theories for the heating of the solar corona and the acceleration of the solar wind assume the action of hydromagnetic (Alfven) waves, but there is very little observational evidence for such waves. Perhaps the most compelling evidence was the observation of Faraday Rotation fluctuations of the Helios spacecraft transmitter (Hollweg *et al*, J. Geophys. Res., 87, 1, 1982). Such observations can also be made with linearly polarized extragalactic radio sources, which have a number of advantages in comparison with spacecraft transmitters. In March 1990 we made VLA observations of eight radio sources within about 8 degrees of the sun. Linear polarization measurements were made at 18 and 20 cm. The observations consisted of approximately 9 scans of 5 minutes duration each for every source, as well as extensive calibration observations of sources far from the sun. We find that for sources with greater than about 10 milliJanskys of polarized flux, position angle residuals from the mean are of order 2 to 3 degrees, confirming the power of the VLA for this type of observation. We are in the process of determining how much of these residuals (which are larger than attributable to radiometer noise) are due to coronal rotation measure variations and how much are residual error in polarimeter calibration and ionospheric Faraday Rotation estimation. Of particular interest is our observation of the source 0010+005, which has clearly resolved, polarized structure. This source may serve as a linearly polarized screen with which to detect high resolution spatial variations in the coronal rotation measure.

J1-3  
0940NUMERICAL SIMULATION OF THE INTERPLANETARY  
SCINTILLATION G-MAP TECHNIQUE

D. G. Sime and V. J. Pizzo

High Altitude Observatory

National Center for Atmospheric Research\*

P.O. Box 3000

Boulder, CO 80307

We have investigated the effectiveness of so called interplanetary scintillation g-maps for the description of the large scale structure of the interplanetary medium. These g-maps are whole sky displays of the deviation from average scintillation index measurements made on large numbers of radio sources. The scintillation observations are already a complex and indirect probe of the interplanetary medium resulting from scattering along an extended region of the line of sight. Since interplanetary scintillation also has an unspecified dependency on physical properties of the medium, the g-maps can be difficult to interpret and can display many properties which are at first not obvious.

To investigate these properties, we have constructed a numerical model of the scattering process and have applied it to simplified models of the interplanetary density structure. Even in the case of a simple dependence on density, the appearance of the resulting g-maps is surprising. The simplest plausible geometry, a non-evolving, rotating tilted dipole density distribution results in a g-map in which evidently outward propagating curved fronts appear. This is the appearance which might be expected to arise from a transient disturbance in the medium perhaps associated with a coronal mass ejection. Examination of the model reveals how this and other features arise and provides a basis for clearer insight into the nature of this observing technique. We discuss use of the model to examine several improvements in the technique including an evaluation of the use of different wavelengths. An observational confirmation of our findings will be presented.

---

\*The National Center for Atmospheric Research is sponsored by the National Science Foundation

J1-4  
1000NEARLY INCOMPRESSIBLE TURBULENCE<sup>1</sup>Gary P. Zank and William H. Matthaeus  
Bartol Research Institute  
University of Delaware, Newark DE 19716

Although observations of Kolmogoroff-like density spectra in turbulent plasmas such as the solar wind and ISM have been known for some time, only recently have theoretical descriptions emerged which attempt to explain, among other things, these observations. The models are subject to the assumption that the magnetofluid, at sufficiently low acoustic Mach number, is "nearly incompressible" (NI). The several possible approaches to incompressibility are distinguished both by the plasma beta  $\beta$  and the relative ordering of the pressure, density and temperature fluctuations. For each plasma  $\beta$  regime, two distinct approaches to incompressibility exist, heat fluctuation dominated (HFD) and heat fluctuation modified (HFM). For an HFM fluid, a pseudosound-like relation relating pressure and density fluctuations holds, from which a  $k^{-5/3}$  density fluctuation spectrum is inferred. The HFD model shows that density fluctuations behave like a passive scalar in this regime, leading again to a  $k^{-5/3}$  power law density spectrum. Thus, given the assumptions of NI theory, it would be surprising were the ISM density fluctuation spectrum anything other than Kolmogoroff-like. In particular this conclusion can be obtained somewhat independently of assumptions concerning several plasma parameters that are difficult to measure in an astrophysical environment. In this review, various theoretical NI models are described, possibilities for the further application of NI theory are discussed. Emphasis is also placed upon the effect of  $\beta$  on the "dimensionality" of the underlying incompressible MHD turbulence and the structure of density fluctuations and turbulence spectra in the various cases.

<sup>1</sup>This research supported by the NASA Space Physics Theory Program at Bartol under grant NAG-W-2076.

J1-5  
1040THE GALACTIC DISTRIBUTION OF ELECTRON  
DENSITY TURBULENCEJames M. Cordes  
Astronomy Department and NAIC  
Cornell University  
Ithaca, NY 14853

Dispersion, distance, scattering, and absorption measurements of Galactic pulsars and masers and extragalactic sources are used to model the galactic distribution of free electrons. We model simultaneously the local electron density and microstructure in the density that evidently follows a Kolmogorov law from about 100 km to greater than parsec scales. Most measurements are consistent with an axisymmetric, two-component model, though there is evidence for spiral arm structure and a clear need for clumps of very strong turbulence that enhance the scattering along some lines of sight. The modeling also indicates that either the distribution or the internal structure of ionized clouds is dramatically different in the inner Galaxy compared to the solar neighborhood. In particular, the inner Galaxy must provide not only a larger column density of electrons, but also either the internal variation  $\delta n_e/n_e$  inside clouds must be significantly larger there or the volume filling factor must be much smaller. The implications for radio pulsar searches, radio interferometry at low galactic latitudes, searches for extraterrestrial intelligence and for the structure of the interstellar medium will be discussed.

J1-6  
1100**DYNAMIC SPECTRA OF RADIO PULSARS  
USING THE NRAO SPECTRAL PROCESSOR**

R. S. Foster

National Research Council/NRL Cooperative Research Associate  
Naval Research Laboratory

Code 4210

4555 Overlook Avenue, SW  
Washington, DC 20375-5000

Radio pulsars behind regions of turbulence can be used as interstellar probes. A map of the two dimensional frequency versus time intensity pattern can be used to measure scintillation parameters, including scintillation time scale, decorrelation bandwidth, intensity modulation index, and refractive bending (interstellar fringing). Twenty strong radio pulsars have been observed every two months for one year at 800 and 1330 MHz using the National Radio Astronomy Observatory's 140 foot radio telescope. We present a report on the new spectral processor used to measure the pulsar dynamic spectra and summarize the results after one year of observation. The goals for this program include determining the frequency of "interferometric" fringing, measuring the amplitude of refractive variations along different lines of sight, and measuring secular changes in scintillation patterns.

J1-7  
1120**RESOLVING PULSAR MAGNETOSPHERES  
WITH INTERSTELLAR SCINTILLATIONS**Andrew W. Clegg<sup>1</sup> and James M. Cordes<sup>2</sup><sup>1</sup>Naval Research Laboratory  
Code 4213.10

Washington, DC 20375-5000

<sup>2</sup>Department of Astronomy  
Cornell University  
Ithaca, NY 14853-6801

Interstellar electron density fluctuations diffract the emission from spatially compact emitters such as pulsars. The resultant diffraction patterns impart scintillations in time and frequency of the emission as observed on Earth. The isoplanatic angle (or critical angular size) is less than a micro-arc second, comparable to the sizes of pulsar magnetospheres. Spatial structure in the emission regions of pulsar magnetospheres can be measured or constrained by determining temporal and/or spectral offsets in the projected diffraction patterns produced by spatially offset emission points. By resolving pulsar pulses into many distinct bins and cross correlating the observed scintillation patterns for each bin such spatial offsets can be measured or constrained with regard to particular pulsar beaming models. To this end we have obtained high quality pulse-resolved dynamic spectra for several pulsars at 1400, 430, and 130 MHz using the 305m Arecibo radio telescope. Correlation analysis of the data constrains the altitude of the corresponding emission regions. We will present a new interpretational model from our results and we will compare our constraints on the location of emission regions with those derived from multi-frequency timing data, pulse-width data, and polarization waveforms.

J1-8  
1140**USING IMAGE-WANDER OBSERVATIONS AS  
A PROBE OF INTERSTELLAR TURBULENCE**Robert L. Mutel  
Department of Physics and Astronomy  
University of Iowa  
Iowa City, Iowa 52242

Measurement of the time dependence of angular separation of closely spaced compact radio sources is a powerful method of probing the spatial spectrum of interstellar turbulence. For power-law turbulence ( $P_{\delta n_s} = C_n^2 q^{-\alpha}$ ) the RMS differential angular wander angle can be written as a simple algebraic function of baseline separation, diffraction angle, and screen distance. Recent analyses of image wander by Rickett and Coles (I.A.U. Symp. 129, 287-294, 1988), Cordes, *et al*, (Ap.J., 310,737-767,1986), and Romani *et al*, (MNRAS,220,19-49, 1986) are shown to give identical results aside from a normalization function  $f(\alpha)$ . We discuss the application of this analysis to VLB measurements of closely spaced doubles along highly scattered lines of sight. For the compact double 2050+364, observations at 608 MHz by Fey and Mutel (preprint) find a differential wander  $\Delta\theta = 4 \pm 4$  mas over 4 years. This is consistent with a shallow power-law spectrum with  $\alpha < 3.8$ .

Tuesday Afternoon, 7 January, 1335-1700

Session A-2 1335-Tues. CR2-06

NOISE METROLOGY

Chairman: Sunchana Perera, National Institute of Standards and  
Technology, Boulder, CO 80303

A2-1 ACCURATE NOISE CHARACTERIZATION OF LOW NOISE DEVICES

1340

Martin Grace  
Wiltron Co.  
490 Jarvis Drive  
Morgan Hill, CA 95037

George Vendelin  
Vendelin Engineering

This paper describes the use of the vector corrected noise measurements to determine the noise parameters of low noise HEMT devices. The noise parameters of low noise HEMTs were measured using the Wiltron 360 VNA, 3642A noise figure module, and the 3680 universal test fixture. The noise parameters  $F_{\min}$ ,  $\Gamma_{\text{opt}}$  were determined from error corrected Y factor measurements and the effects of input and output tuners were de-embedded from the device measurements. The noise parameters were derived from Y factor and S-parameter measurements.

Although the 4 noise parameters of a two-port can be derived in many equivalent forms, the use of noise wave concepts is the most applicable to the measurements described in this paper. These representations are either the output noise waves at each port and their correlation, or the two noise waves at the input port and their correlation. These noise waves can be easily converted to the more familiar data sheet representation of  $F_{\min}$ ,  $R_n$ , and  $\Gamma_{\text{opt}}$ . The limitations to the representation of noise parameters will be presented, and also methods of measurement.

A2-2 MILLIMETER-WAVE, CRYOGENICALLY-COOLABLE, LOW-NOISE  
 1400 HFET AMPLIFIERS: STATE-OF-THE-ART AND FUTURE  
 TRENDS

Marian W. Pospieszalski  
 National Radio Astronomy Observatory\*  
 2015 Ivy Road  
 Charlottesville, VA 22903

Recent progress in the development of ultra low-noise, cryogenically-coolable, HFET (heterostructure field-effect transistor) amplifiers for millimeter wavelength receivers is reported. The design, construction and performance of a Q-band (38-45 GHz) amplifier for radio astronomy applications with record-breaking cryogenic performance (noise temperature of less than 30 K at 41 GHz and ambient temperature of 17 K) are discussed in detail.

The validity and usefulness of a recently developed noise model of a FET (HFET), (M. W. Pospieszalski, *IEEE Trans. MTT*, MTT-37, pp. 1340-1350, 1989; M. W. Pospieszalski and A. C. Niedzwiecki, *Proc. 1991 Int. Microwave Symp.*, pp. 1117-1120, Boston, MA), for the computer-aided design of millimeter-wave amplifiers are established. The implications of this model in the search for new low-noise HFET structures are discussed. A model-based prediction of noise performance is compared with recently published data for AlInAs/GaInAs on InP HFET's (K. H. Duh *et al.*, *Proc. 1990 Int. Microwave Symp.*, pp. 595-598, Dallas, TX; S. E. Rosenbaum *et al.*, *Proc. 1991 Int. Microwave Symp.*, pp. 815-819, Boston, MA; P. D. Chow *et al.*, *Proc. 1991 Int. Microwave Symp.*, pp. 1041-1044). A model-based prediction of cryogenic performance shows that cryogenically-cooled HFET receivers should soon be competitive with SIS (superconductor-insulator-superconductor) mixer receivers (A. R. Kerr and S.-K. Pan, *Int. J. Infrared & Millimeter Waves*, vol. 11, pp. 1169-1187, 1990) in the 3mm wavelength atmospheric window.

---

\*The National Radio Astronomy Observatory is operated by Associated Universities, Inc. under Cooperative Agreement with the National Science Foundation.

A2-3 NOISE MEASUREMENT UNCERTAINTY ANALYSIS  
1420 F.X. Xu & M.S.P. Lucas  
Dept. of Electrical & Computer Engineering  
Kansas State University  
Manhattan KS 66506-5105

Measurements are fundamental to the development of science and technology but errors exist in all measurements. Hence, for a measurement system to be truly useful, the user must be able to estimate the system measurement uncertainty. This paper presents a measurement uncertainty analysis of the ATN Microwave Inc., NP5B Noise Measurement System. This complex system is designed to make on-wafer noise parameter measurements of active devices in the 2-26GHz frequency range. However, the analysis technique described is general and can be extended to other measurement systems.

A numerical, multivariate error analysis method was used to determine the NP5B system measurement uncertainty attributed to random errors. The analysis was applied both to the system calibration and device measurements. The device noise parameters are calculated by applying a least squares fit to directly measured observables such as S-parameters, reflection coefficients, temperature, noise power, and system noise parameters obtained from a least squares fit during the system calibration. Therefore, the measurement uncertainty of the device noise parameters is caused not only by measurement errors in the observables but also by the uncertainty of the calculated system noise parameters.

A computer program based upon the multivariate error analysis method was developed to determine the uncertainties in the system calibration and device measurement. The inputs to the program are raw data as measured by the NP5B system and the measurement errors of the directly measured parameters. The results of the program are displayed either in a tabular or graphical form; they show the device noise parameters as a function of frequency with their associated uncertainties. The program was written in Hewlett-Packard Basic 5.13 to provide compatibility with the NP5B operating system.

A2-4  
1440      UNCERTAINTIES IN ULTRALOW NOISE AMPLIFIER  
          NOISE FIGURE/NOISE TEMPERATURE MEASUREMENTS  
          Aksel Kiiss  
          MITEQ  
          Hauppauge, NY 11788-2034

The question is often asked as to how accurately can one determine the noise figure/noise temperature of a low noise amplifier. With the continuous improvement in transistor as well as amplifier design technology the measurement accuracy assumes everincreasing importance. A few years ago when amplifier noise figures ranged from 2-3 dB in L band to 5-6 dB in X band, a 0.2-0.3 dB measurement uncertainty was not too important. But when one talks about a 0.5 dB noise figure, a 0.2-0.3 dB uncertainty is quite unacceptable. In this paper we will attempt to provide a quantitative answer to that question. First, we will investigate the various methods of performing noise figure/noise temperature measurements. We will then study the possible sources of measurement uncertainties, divide them into avoidable errors and unavoidable measurement uncertainties. Under the measurement uncertainties we will study the calibration as well as test equipment uncertainties. Finally, we will present noise figure test data on a variety of ultralow noise amplifiers from L to Ku band by using different commercially available test instruments.

A2-5 ON-WAFER NOISE PARAMETER MEASUREMENTS:  
1520 VERIFICATION, COMPARISON, AND REPEATABILITY  
Jeff Raggio, Member of the Technical Staff  
TRW Measurement Engineering Department  
One Space Park S/2470  
Redondo Beach, CA 90278

The capability to perform on-wafer measurements of semiconductor devices such as HEMTs and MESFETs has rapidly improved during the past few years. As processing enhancements provide higher frequency and lower noise characteristics, S-parameter calibration becomes a critical part of the measurement process. Whether using a commercially-available calibration substrate, in-house calibration elements, or NIST-supported calibration structures, differences in calibration elements and methods often lead to discrepancies in S-parameter measurements. Data from an on-wafer S-parameter round-robin measurement of passive structures will be presented to illustrate operator dependence in these measurements.

Additionally, the calculation of noise parameters is dependent on S-parameter measurements. On-wafer noise parameter measurement systems are presently available operating to 26 GHz. The TRW Measurement Engineering Department contracted Kansas State University to develop an algorithm to independently verify the results from a commercially-available noise parameter measurement system. Plots will be shown depicting the level of agreement between both algorithms based on identical input data.

Finally, the results from an on-wafer noise-parameter round-robin measurement will be presented. The round-robin was coordinated by the TRW Measurement Engineering Department and consisted of two distinct segments. In the user-configuration segment, each participant calibrated their existing system using their customary S-parameter calibration method and calibration artifacts. After calibration, four GaAs MESFETs were measured at specified bias conditions from 2-18 GHz or 2-26 GHz (depending on system capability). In the identical-configuration segment, the participants used provided equipment and calibration elements to recalibrate their systems and remeasure the four devices. The TRW Measurement Engineering Department served as the pivot lab by measuring the devices four separate times during the round-robin. Hence noise parameter measurement repeatability results from the TRW facility will also be presented.

A2-6  
1540**NOISE IN MULTIPLE QUANTUM WELL APD'S**Sai Chong Kwok and Frank S. Barnes  
Department of Electrical and Computer Engineering  
University of Colorado at Boulder  
Campus Box 425  
Boulder, CO 80309-0425

Noise in avalanche photodiode (APD) comes from the randomness in photon arrivals, the randomness in the carrier multiplication, and the dark current noise. APD's utilizing III-V compounds take advantage of the asymmetry of the heterojunction with respect to the conduction and valence band offset and the different mean free paths for holes and electrons to suppress the ionization of one type of the carriers while increasing the other, resulting in a less randomness in the carriers' multiplication and hence a lower multiplication noise. APD's consisting of multiple layers of p-Al<sub>0.45</sub>Ga<sub>0.55</sub>/n-GaAs/p-Al<sub>x</sub>Ga<sub>1-x</sub>As ( $0 < x < 0.45$ ) are investigated experimentally and the results will be presented.

A2-7 NOISE: PRACTICAL CALIBRATION OF RADIO SIGNAL  
1600 MEASUREMENTS

Robert J. Matheson, ITS.S  
U. S. Department of Commerce  
Institute for Telecommunications Sciences  
325 Broadway  
Boulder, Colorado 80303

Noise sources are often not regarded seriously as the "source of choice" for calibrating systems making RF measurements; instead, CW sources will usually be selected. In some situations, however, noise sources have major advantages. This paper illustrates some of the very practical advantages of using noise sources for routine calibration of the Radio Spectrum Measurement System (RSMS).

The RSMS is a .01-18 GHz RF measurement system used for a wide variety of spectrum management and surveillance functions, including band usage measurements, compliance measurements, and EM compatibility testing.

In the RSMS, noise sources are located throughout a tovertop manifold of receiving antennas and signal bandpass filters, and preamplifiers. The use of noise sources has allowed great freedom in reconfiguring the system signal-conditioning structure for specialized measurements, as well as providing a valuable maintenance aid. Notch filters have been added, along with other configuration changes, depending on the local strong signals and measurement requirements. The advantages of noise sources in this application include:

1. Small, lightweight, cheap, low power, broadband.
2. Multiple calibration locations close to antenna terminals.
3. Sufficiently accurate (typically +/- 1 dB)
4. Simple control of calibration source - no tuning routines
5. Arbitrary frequency resolution

There are also some disadvantage of using noise sources, including:

1. Need for good noise figure on receiving system.
2. No frequency check as part of amplitude calibration - frequency image problem
3. Longer integration time needed - slower calibration
4. No calibration through input attenuator - VWSR uncertainties.
5. Credibility - many people do not understand noise calibration.

A2-8 THE MOON AS A NOISE CALIBRATOR FOR LARGE ANTENNAS  
1620 Paul A. Lilie  
National Radio Astronomy Observatory  
Socorro NM 87801

The Very Large Array radio telescope operates with dual polarization in six frequency bands on 28 antennas. Monitoring system noise temperature and injected noise calibration levels by manual methods (e.g., placing absorbers of known temperature in the apertures of the feeds) would be operationally impossible.

Using an astronomical source, it is possible to measure all the antennas simultaneously. The advantages and disadvantages of using the moon instead of a point source will be discussed. (The moon subtends an angle larger than the main beam of the VLA 25m antennas.)

Procedures for tracking the moon, data acquisition, and analysis will be described. Errors in the methods will be discussed and evaluated.

The method is currently used primarily for system monitoring and fault diagnosis. Plans to adopt improved thermal models of the moon to refine its usability as a standard will be discussed.

A2-9 S-BAND SOLAR Y-FACTOR MEASUREMENTS  
1640 IN THE AIR FORCE SATELLITE CONTROL NETWORK  
L. G. Bryans  
Loral Space and Range Systems  
1260 Crossman Avenue  
Sunnyvale, Ca 94089

The U.S. Air Force has nine satellite control network facilities located at sites around the world. Each site has one or more antennas operating at S-Band: 1750 to 1850 MHz transmit and 2200 to 2300 MHz receive. Antennas range from 23 feet to 60 feet in diameter. Solar y- factor data are routinely used to measure antenna transmit gain and receive G/T. Solar y-factor measurement techniques are described. Typical measured transmit gain and G/T data are presented. Expected accuracies are derived and compared to the measured data. Measured results have been good. Plans are in process to utilize these measurement techniques for routine maintenance and performance problem analysis. Refinements in data reduction will increase the measurement accuracy. Accuracy of measurement, simplicity of test equipment, and ease of testing make solar y-factor measurements ideal for S-Band antenna maintenance.

Session A-3 1335-Tues. CR0-30  
NEAR FIELD ANTENNA MEASUREMENTS SESSION

Dedicated to Dr. R.C. Baird

Chairman: Motohisa Kanda, National Institute of Standards and Technology,  
Boulder, CO 80303

A3-1  
1340

PROBE CORRECTION IN SPHERICAL NEAR-FIELD SCANNING

Carl F. Stubenrauch, 813.05  
National Institute of Standards and Technology  
Boulder, CO 80303

The effect of a probe in near-field measurements can be divided into a pattern correction part and a polarization correction part. While the pattern correction is often not significant in spherical scanning measurements, the polarization correction can be significant, especially away from the "E" and "H" planes.

A3-2  
1400**DETERMINING AND CORRECTING FAULTS ON A FLAT PHASED  
ARRAY ANTENNA USING THE PLANAR NEAR-FIELD SCANNING METHOD**

A. G. Repjar, J. R. Guerrieri, D. P. Kremer, N. Canales  
Antenna Metrology Group, Electromagnetic Fields Division  
National Institute of Standards and Technology  
Boulder, CO 80303, U.S.A.

**ABSTRACT**

The Antenna Metrology Group of the National Institute of Standards and Technology (NIST) has recently developed and implemented measurement procedures to locate and identify faults on a flat phased array antenna. Several antennas, all mechanically- and electrically- similar, were measured on the NIST planar near-field (PNF) range. First, measurements were taken on a plane where the multiple reflections between the probe and each antenna under test were minimized. This is important since the PNF method does not directly allow for their effects. The NIST PNF software which incorporates the fast fourier transform (FFT) was then used to determine the antenna's gain and pattern and to evaluate the antenna's performance. Next, the inverse FFT was used to calculate the fields at the aperture plane. By using this technique, errors in the aperture fields due to multiple reflections can be avoided. By analyzing this aperture plane data through the use of detailed amplitude and phase contour plots, faults in the antenna were located and corrected. The PNF theory and utilization of the inverse FFT will briefly be discussed and results shown.

A3-3 NEAR-FIELD TO FAR-FIELD TRANSFORMATION USING  
1420 AN EQUIVALENT MAGNETIC CURRENT APPROACH

Peter Petre  
Tapan K. Sarkar  
Department of Electrical and Computer Engineering  
Syracuse University, Syracuse, New York 13244

## Abstract

A simple, efficient and accurate method is presented for computing far-field antenna patterns from near-field measurements. The method utilizes near-field data to determine equivalent magnetic current sources over a fictitious planar surface which encompasses the aperture of the antenna, and these currents are used to ascertain the far-fields. Under certain approximations, the currents should produce the correct far-fields in all regions in front of the antenna regardless of the geometry over which the near-field measurements are made. An electric field integral equation (EFIE) is developed to relate the near-fields to the equivalent magnetic currents. Method of moment (MOM) procedure is used to transform the integral equation into a matrix one. The matrix may be rectangular or square depending on the number of data points and currents chosen. The equation is solved with the conjugate gradient method (CGM), and in the case of a rectangular matrix, a least squares solution for the currents is found without explicitly computing the normal form of the equation. Near-field to far-field transformation for planar scanning may be efficiently performed under certain conditions by exploiting the block Toeplitz structure of the matrix and using CGM and Fast Fourier Transform (CGFFT), thereby drastically reducing computation and storage requirements. One of the main advantage of the present approach is its numerical efficiency because the EFIE is a decoupled one with respect to the coordinate axes for the planar scanning case. By taking the limiting case of the integral equation, an equivalent magnetic dipole array approximation is also developed where the aperture of the antenna is replaced by an equivalent magnetic dipole array. Numerical results are presented using both equivalent currents and equivalent dipole array approximation for several antenna configurations by extrapolating the far-fields using synthetic and experimental near-field data.

A3-4  
1440

SPHERICAL-WAVE EXPANSIONS OF THE ELECTROMAGNETIC FIELDS  
OF A UNIFORMLY EXCITED CIRCULAR APERTURE

Ronald C. Wittmann, 813.05  
National Institute of Standards and Technology  
Boulder, CO 80303

Analytic spherical-wave expansions will be given for the electromagnetic fields due to uniform surface currents on a circular aperture. The formulas are valid throughout the illuminated hemisphere, and are suitable for efficient and accurate numerical calculation. The uniformly excited circular aperture provides a realistic model source for the evaluation of many near-field measurement techniques.

A3-5  
1520

A SUCCINCT RIGOROUS ESTABLISHMENT OF A COORDINATE SYSTEM TRANSLATION  
THEOREM FOR THE FREE-SPACE DYADIC GREEN'S FUNCTION IN SPHERICAL COORDINATES

Richard L. Lewis  
National Institute of Standards and Technology  
UNITED STATES DEPARTMENT OF COMMERCE  
Boulder, Colorado

In this paper we show that the electric field at any point, as obtained from using a spherical-wave free-space dyadic Green's function formulation, is invariant with respect to translation of the coordinate system origin that is used for expanding the spherical vector-wavefunction solutions of Maxwell's equations. Thus, we establish a translation of coordinates identity for the spherical-wave free-space dyadic Green's function. Although such an identity is intuitively obvious, its rigorous establishment involves, among other things, justifying interchanging the orders of summation of infinite double series. The proof involved in carrying this out is outlined in this paper, which will conclude with a presentation of this mathematical identity, along with a brief description of its use toward rigorously establishing a spherical-wave source-scattering matrix analysis of the interactions between two coupled antennas.

A3-6  
1540

## Fast Near-Field Radiation and Scattering Measurements Via Arrays of Modulated Scattering Probes

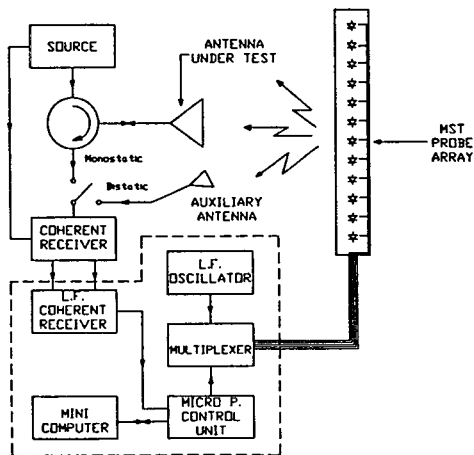
B. J. Cown  
GEMTECH Microwaves, Inc.  
1318 Chandler Court  
Acworth, GA 30101 (USA)

J.P. Estrada  
Georgia Ins. of Technology  
Atlanta, Ga 30332 (USA)

J. Ch. Bolomey  
Ecole Supérieure D'Electricité  
Plateau du Moulon  
91190 Gif-Sur-Yvette, France

G. Cottard and P. Berthaud  
SATIMO (SARL)  
Les Ulis, France

This paper summarizes the results of efforts to utilize arrays of modulated scattering probes to efficiently measure the near-field electric fields radiated by microwave/millimeter wave antennas and/or the fields scattered by radomes, radome materials, composites, and aerodynamic targets of interest. The measurement systems are based on the Modulated Scattering Technique (MST) employing arrays of electrically-small modulated scattering elements. The basic components of "typical" MST measurement systems are illustrated in the diagram. Experimental and numerical results obtained during the research and development efforts involving 2nd and 3rd generation prototypes in the U.S. and France will be presented and discussed for fixed-site and transportable measurement facilities.



A3-7 **BI-POLAR NEAR-FIELD AND ARRAY-FED COMPACT RANGE**  
1600 **DEVELOPMENTS AT UCLA**

Y. Rahmat-Samii  
Electrical Engineering Department  
University of California Los Angeles  
Los Angeles, CA 90024-1594

At UCLA, we are in the process of developing two antenna measurement range facilities. The main objective has been to develop novel concepts which could be used for the antenna near-field measurements and compact range applications in a simple and cost effective manner. Among the many techniques considered, it has been decided to develop the bi-polar near-field measurement technique and the array-fed-reflector compact range technique. Both concepts have several unique features which will be highlighted during the presentation.

Among the topics to be presented for the bi-polar near-field technique are: (a) bi-polar near-field concept, (b) simulation algorithms to verify transformation techniques to the far field, (c) mechanical developments of a unique bi-polar scanner, (d) measurement considerations.

Among the topics to be presented for the array-fed-reflector compact range concept are: (a) array-fed circular-rim parabolic reflector compact range concept, (b) array developments and simulations, (e) quiet zone evaluations and comparison to other concepts, (f) advantages and disadvantages of the concept.

The author would like to acknowledge the contributions of many of his graduate students at UCLA.

A3-8 ANTENNA COUPLING AND NEAR-FIELD SAMPLING  
1620 IN PLANE-POLAR COORDINATES  
Arthur D. Yaghjian  
Rome Laboratory/ERCT  
Hanscom AFB, MA 01731, USA

During the past decade a substantial amount of work has been done and a number of fine articles have been written on the subject of planar near-field antenna measurements in polar coordinates. However, there appears missing from the published literature a rigorous sampling theorem with uniform radial spacing for plane-polar measurements and computations. The rigorous sampling theorem with  $\lambda/2$  data point spacing for plane-rectangular scanning does not apply to the radial eigenfunction expansions of plane-polar scanning. Also, there appears absent from the literature a detailed formulation of probe-corrected plane-polar scanning from first principles directly in polar coordinates. The approach in the past has been to base the plane-polar derivations on the formulas from plane-rectangular near-field scanning. Thus, it is the purpose of this paper to derive, directly in plane-polar coordinates, rigorous formulas for near-field antenna coupling and sampling. (See Proc. 14th ESA Workshop on Antenna Measurements, Noordwijk, Netherlands, May 1991.)

The derivations are based on three fundamental theorems of antenna theory. One, the mutual coupling function between two antennas, which translate with respect to each other without rotation, satisfies the homogeneous wave equation when multiple interactions are neglected. Two, the output of a receiving antenna can be expressed as a linear differential operator converting the incident field and its spatial derivatives at a single point in space to an output voltage. Three, the mutual coupling function expanded in plane-polar as well as rectangular eigenfunctions is virtually bandlimited by the free-space propagation constant if the antennas remain outside their reactive zones.

The first theorem is applied to derive a vector plane-polar transmission formula and related expressions for the fields of the test antenna. The second is applied to determine the effect on the vector output of the probe of rotating the probe antenna with respect to the test antenna, or equivalently, the effect on plane-polar data of rotating the test antenna without co-rotating the probe. The third theorem is applied to derive a rigorous sampling-reconstruction theorem for straightforward evaluation of the plane-polar representation coefficients using  $\lambda/2$  radial data-point spacing.

Comparisons are made with previous plane-polar expressions, and numerical results are presented for a hypothetical uniformly illuminated circular-aperture test antenna. Finally computer run times are discussed for different methods of processing the plane-polar near-field data.

Chairman: W. Stutzman, Bradley Dept. of Electrical Engineering, Virginia Polytechnic Institute and State Univ., Blacksburg, VA 24061

B2-1 1340 **A WIDESCANNING TRI-REFLECTOR SYSTEM WITH AN ELLIPTIC SUBREFLECTOR AND MOVING TERTIARY REFLECTOR**

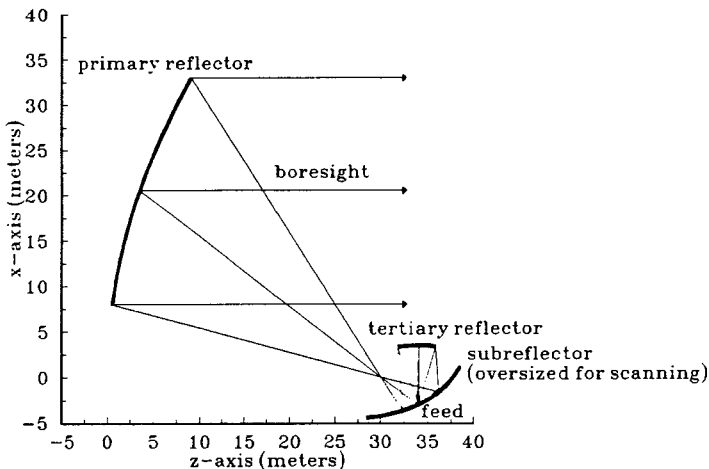
P. Werntz<sup>1</sup>, K. Takamizawa<sup>1</sup>, W. Stutzman<sup>1</sup>, P. Foldes<sup>2</sup>

1. Bradley Department of Electrical Engineering  
Virginia Tech, Blacksburg, VA 24061-0111.

2. Foldes Incorporated, 1131 Radnor Hill Road, Wayne, Pa 19087.

High resolution earth observation from geostationary orbit offers several advantages compared to traditional low earth orbit systems. Among the advantages are decreased time to scan the visible geo-disk and the ability to stare at a particular event. The design of a large high gain reflector system capable of wide beam scanning and suitable for geostationary applications involves a number of constraints which have not been addressed by previous wide scanning reflector configurations. These constraints are: minimization of feed motion; minimization of feed array size; maximization of primary aperture efficiency; and minimization of reflector motion.

A tri-reflector system which meets the above constraints is presented and its principles of operation are explained. The reflector system makes use of an elliptical subreflector which has one focus point near the center of the primary reflector and the other focus point near the center of the tertiary reflector. With this configuration, scanning is achieved by rotation and slight translation of a small tertiary reflector. The method of synthesis and optimization of a 2-dimensional cylindrical model capable of scanning  $\pm 5^\circ$  are discussed. Also discussed are methods of extending the 2-dimensional results to a 3-dimensional structure.



B2-2  
1400A VERSATILE THREE-PARAMETER ( $\mathcal{J}$ - $P$ ) APERTURE  
DISTRIBUTION FOR ANTENNA APPLICATIONS

D. W. DUAN and Y. RAHMAT-SAMII

Department of Electrical Engineering

University of California, Los Angeles

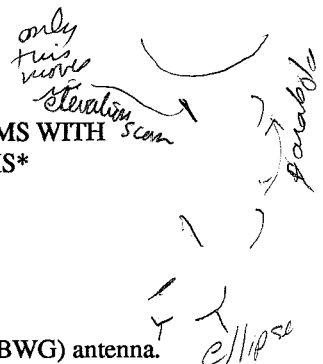
Los Angeles, CA 90024-1594

In the design of aperture type antennas such as reflector antennas and large planar arrays, aperture field distribution models are frequently utilized. This is because one can typically obtain the far field in closed form, which facilitates efficient designs and provides useful physical insights. A novel three-parameter ( $\mathcal{J}$ - $P$ ) distribution is developed in this paper. The  $\mathcal{J}$ - $P$  distribution is versatile in the sense that it is reducible to many familiar aperture distributions such as Hansen's  $1$ - $P$  distributions, the parabolic  $2$ - $P$  distributions and the Bickmore-Spellmire distributions. The radiation characteristics of these existing distributions are substantially improved due to the enlarged parameter space offered by the  $\mathcal{J}$ - $P$  distributions. Additionally, in narrow beamwidth/low sidelobe level designs, the performances of the  $\mathcal{J}$ - $P$  distributions are comparable to those of the Taylor distributions. However, unlike Taylor distributions, the  $\mathcal{J}$ - $P$  distributions are *always* monotonically decreasing toward the edge of the aperture.

An important feature of this newly developed  $\mathcal{J}$ - $P$  distribution is that it is applicable to both *elliptical* and circular apertures. This is made possible by an appropriate parameterization procedure. The  $\mathcal{J}$ - $P$  distribution employs the Lambda function and contains a pedestal term. The pedestal term plays an important role because it gives a more realistic description for edge tapers, and provides the possibility of achieving high taper efficiency.

Radiation characteristics of the  $\mathcal{J}$ - $P$  distributions such as the edge taper, the taper efficiency, the aperture power, the closed form far fields, the side lobe levels, the beam width and the beam efficiency are analyzed. These characteristics are presented in such a way that optimum study and compromise study can be easily conducted. Also derived is an asymptotic expression of the far field, based on which the far angle behavior of the  $\mathcal{J}$ - $P$  distributions such as the far field envelope, the decay rate and the positions of nulls are obtained. The aperture distributions and the far fields are normalized by giving a special attention to the computation of the total power.

The G.O. synthesis approach  
is based on work of  
Miyasawa (?)



B2-3  
1420

**SOLUTIONS TO LOW-FREQUENCY PROBLEMS WITH GEOMETRICALLY DESIGNED BWG SYSTEMS\***

W. A. Imbriale  
Jet Propulsion Laboratory  
California Institute of Technology  
Pasadena, CA 91109

JPL has recently built a new 34-meter beamwaveguide (BWG) antenna. The design of the center-fed BWG consists of a beam magnifier ellipse in a pedestal room located below ground level that transforms a 22-dB gain feedhorn into a high-gain 29-dB gain pattern for input to a standard four-mirror (two flat and two paraboloid) BWG system. The design is based on a Geometrical Optics (GO) criteria (IEEE APS, vol. 32, 844-846, 1973) which guarantees a perfect image from a reflector pair. The system was initially designed for operation at 8.45 GHz (X-band) and 32 GHz and has less than 0.2-dB loss (determined by comparing the gain of a 29-dB gain horn feeding the dual-shaped reflector system with that obtained using the BWG system). Next, S-band (2.3 GHz) will be added.

If a standard 22-dB horn is placed at the input focus of the ellipse, the BWG loss is greater than 1.5 dB, primarily due to the fact that, for low frequencies, the diffraction phase centers are far from the GO mirror focus, resulting in a substantial spillover and defocussing loss. This defocussing is especially a problem for the magnifier ellipse where the S-band phase center at the output of the ellipse is 3 meters from the GO focus. If the input to the paraboloids was focussed, the output defocussing would only cause a 0.3-dB loss. One solution would be to move the high-frequency phase center a the ellipse output to the low-frequency phase center (accomplished at X-band by simultaneously increasing the gain of the input horn to 26 dB and moving the horn phase center 0.5 meters below the input focus) and repositioning the phase centers to the input focus of the paraboloids. This can be accomplished by leaving the ellipse in its original position and increasing the spacing between the paraboloids. With this arrangement, the BWG loss at S-band is only 0.4 dB and the loss at X-band is virtually unaffected. This solution has the disadvantage, however, of necessitating a physical modification of the structure of the BWG system. Another solution is to use a more complex feed system (multiple horns) at S-band. A preliminary design has been developed to provide nearly the same performance as the modified BWG structure.

best approach

One solution was to track distortions all the way thru and use a horn with complex conjugate oper. dist.

\*The research described in this publication was carried out by the Jet Propulsion Laboratory, California Institute of Technology, under a contract with the National Aeronautics and Space Administration.

used this approach

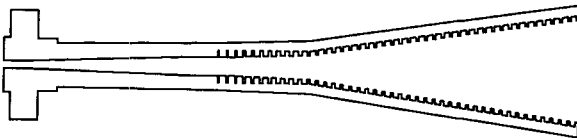
high pass - GO.  
bandpass - Gaussian beam  
(limited bandwidth) 60

B2-4 DESIGN OF CORRUGATED FEED-HORNS FOR  
1440 WIDE-BAND, HIGH-FREQUENCY APPLICATIONS

Xiaolei Zhang  
Radio Astronomy Laboratory and Dept. of EECS  
601 Campbell Hall  
University of California at Berkeley  
Berkeley, CA 94720

The wide-band design of a corrugated feed-horn often requires the simultaneous achievements of wide-band single-mode operation and wide-band, low return-loss impedance-matching. So far no analytical approach was available in the literature to realize the two goals in the same design. The pioneering work of C. Dragone (*Bell System Tech. Journal*, Jul-Aug 1977, pp 835-888), especially those on the understanding of the feed-horn modal fields near the cutoff region, produced a design which has the maximum possible single-mode bandwidth. Unfortunately, the return loss result of his design over most of the bandwidth was not always good. Similar high return-losses are also present in many of the other wide-band designs. In the recent decades, computer simulations of feed-horn performances have been done through calculating the scattering matrix of a series of cascaded cylindrical sections, which make up the grooves and ridges of the horns (e.g. G.L.James, *IEEE Trans Microwave Theory Tech.*, Vol. MTT-29, pp 1059-1066, 1981). These simulations allow the design of certain low return-loss and wide-band mode-launchers through trial and error on the computers. The numerical design approach requires the availability of the simulation softwares, and the result is often not optimum in terms of the widest possible band-width. In this research, a new analytical procedure is developed for the design of the mode-launching region of the corrugated feed-horns, through analyzing the results of the space harmonics calculations for feed-horns with small aperture sizes (which is appropriate for horns at their throat or mode-launching region). Using this approach, we can achieve single-mode operation and low return-loss matching simultaneously over a fractional bandwidth of 50%.

For horns used in the millimeter and submillimeter range, the possible choices of the design parameters are limited by the fabrication and cost concerns. The limiting behavior of the feed-horns, as we vary the groove-coarseness and conical flare-angles, are also investigated in this work through computer simulations. The results of these investigations can be used as guidelines for designs restricted by the manufacturing and cost limitations, especially at very high frequencies.



A model of the corrugated feed-horn, designed according to the above principles, has been fabricated and tested. It displayed excellent performance in terms of wide-band single-mode operation and wide-band impedance-matching. The measured radiation patterns agree well with the theoretical calculations.

B2-5  
1500**A MULTIPOINT NOISE MODEL WITH  
APPLICATIONS TO REMOTE SENSING ARRAYS**R. M. Barts, W. L. Stutzman, and W. A. Davis  
Bradley Department of Electrical Engineering  
Virginia Tech, Blacksburg, VA 24061-0111

Arrays are not often used in radiometers because of losses in the feed network and calibration difficulties. However, arrays offer the advantage of electronic scanning. Especially attractive is the use of a modest sized array as a feed in a large reflector system for electronic scanning of the reflector beam.

A multipoint noise model based on network scattering parameters will be presented. The model was developed to evaluate the noise characteristics of an array antenna and its associated feed network for microwave remote sensing. An accurate noise model for the array and feed network is necessary for array radiometer calibration and evaluation of remote sensing data. Required inputs to the model are the scattering parameters of the array, feed network, and receiver. Additionally, information about the network noise sources and the external noise scene must be specified. For passive feed networks, the network noise sources can be calculated directly from the network scattering parameters. The model calculates the system noise temperature and includes the effects of mutual coupling, feed coupling, and mismatches in the array and feed networks. Applications of the model for various array configurations will be discussed. Results showing the impact of errors in scattering parameter measurements on radiometer temperature measurements will be shown.

## B2-6 A NOVEL APPROACH TO ANTENNA OPTIMIZATION

1540 *Tom* T. S. Angell and R. E. Kleinman  
Department of Mathematical Sciences  
University of Delaware  
Newark, DE 19716, USA  
A. Kirsch  
Institute für Angewandte Mathematik  
Universität Erlangen  
8520 Erlangen  
Germany

A standard approach to many problems of finding current distributions which optimize various measures of antenna performance involves reduction of the problem to a constrained optimization problem e.g. the problem of maximum directivity subject to constraints on input power.

We present here an alternative approach to optimization of antenna performance in which several desirable characteristics are simultaneously optimized as, for example, the simultaneous maximization of main lobe power and minimization of side lobe power. This approach is based in the mathematical theory of multicriteria optimization involving vector valued objective functions.

Numerical results are presented for a problem of simultaneously maximizing signal-to-noise ratio and a quality factor.

*Pareto minimal*

B2-7  
1600GAIN OPTIMIZATION FOR AN ENDFIRE ARRAY OF DIPOLES  
OVER PERFECT GROUND

D. H. Werner

Applied Research Laboratory  
The Pennsylvania State University  
Post Office Box 30  
State College, PA 16804*Julie*J. Huffman and J. K. BreakallThe Department of Electrical and Computer Engineering  
The Pennsylvania State University  
University Park, PA 16802

There are numerous applications for which high gain antennas are required. The detailed pattern shape is frequently not of concern in applications where maximum gain is the primary design requirement. One technique for achieving high gain is to stack individual dipoles above a perfectly conducting ground plane.

A method will be presented for determining the required current excitations which will produce the optimum gain associated with an arbitrarily spaced endfire array of dipoles stacked above and parallel to a ground plane. The success of this technique is based on the fact that the array gain can be expressed in terms of a ratio of two quadratic forms (D. K. Cheng and F. I. Tseng, IEEE Trans. on Antennas and Propagat. AP-13(6), 973-974, 1965). Image theory is used to find an expression for the array factor of the stacked dipole array. This array factor in conjunction with the dipole element pattern are then used to determine the optimum array current distribution and gain. Results will be presented for uniformly as well as nonuniformly spaced arrays.

$$G_{opt} = 4N$$

$$G_{opt} = 6 + 10 \log N \text{ dB}$$

↑ due to ground plane

why isn't this 3 dB?

*Ed Miller*

If mutual coupling was a problem -  
just synthesize currents as would  
w/o coupling and do an extra step  
to find out what voltages are needed  
to produce those currents using  
a MoM code.

## A GENERALIZED EDGE ADMITTANCE NETWORK FOR MODELLING OF RADIATION FROM MICROSTRIP PATCH ANTENNAS

Abdelaziz Benalla and K. C. Gupta

Department of Electrical and Computer Engineering  
University of Colorado, Boulder CO 80309

In the multiport network model (MNM) for radiating microstrip patches on thin substrate (A. Benalla and K. C. Gupta, IEEE AP-36, pp. 1337-1342, 1988), the power radiated by the patch is modelled by defining equivalent edge admittance networks (EAN's) connected to the various edges of the patch. The Y-matrix characterizing these EAN's is a diagonal matrix. If we select  $n$  uniformly spaced ports (each representing a section of length  $W = b/n$ ) along the edge of width  $b$ , the conductance  $G_p$  connected to each of the ports is taken as  $G_r/n$ . The edge conductance  $G_r$  is related to the radiated power  $P_{rad}$  and to the voltage distribution  $f(s)$  along and edge by

$$G_r = \frac{2P_{rad}}{\frac{1}{b} \int_0^b f^2(s) ds} \quad (1)$$

where  $s$  denotes the distance along the edge of the patch. For the computation of  $G_r$  using eqn (1),  $f(s)$  need to be known apriori. However, the calculation of  $f(s)$  requires knowledge of  $G_r$  and hence iterative computations may be needed. For each iteration, the radiated power has to be computed from integration of far field. Hence, the computation of  $G_r$  using (1) is very time consuming.

In this paper, an alternative model for radiation in terms of generalized edge admittance (GEAN) is presented. In this new formulation, an edge is divided into a number of small segments and a GEAN network is connected to this edge. The diagonal terms of the Y-matrix characterizing this network are equal to the self conductance  $G_r = W^2/(90\lambda_0)$  of a magnetic current element of length  $W$ . The off-diagonal terms are equal to the mutual conductance between various segments of the edge (A. Benalla and K. C. Gupta, IEEE AP-37, pp. 148-152, 1989). The modelling of radiation using this formulation does not require apriori knowledge of voltage distribution. The radiated power from the patch is obtained as the power loss in the GEAN network. Hence no integration of far field is required in order to obtain radiated power.

B2-9  
1640

*Douglass*

**FRACTAL RADIATION PATTERN SYNTHESIS**

D. H. Werner\* and P. L. Werner\*\*

\* The Applied Research Laboratory  
The Pennsylvania State University  
P. O. Box 30  
State College, PA 16804

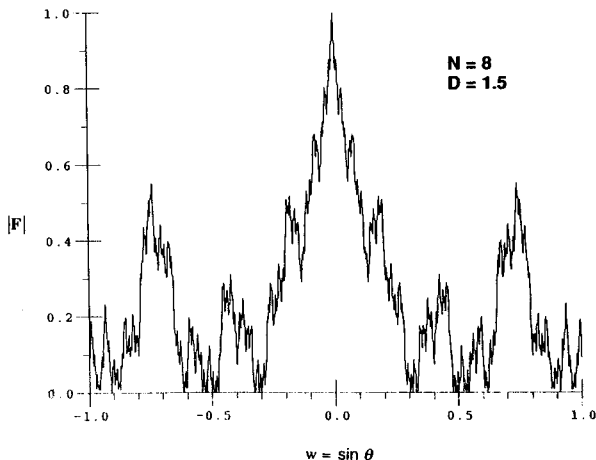
\*\*School of Engineering Technology and  
Commonwealth Engineering  
The Pennsylvania State University  
University Park, PA 16802

One of the important attributes of fractals is that they possess a self-similar structure on all scales (B. B. Mandelbrot, *The Fractal Geometry of Nature*, W. H. Freeman, San Francisco, 1982). A direct consequence of this scale invariance property of fractals is that their derivatives are unbounded. For any fractal resulting from a physical system, scale invariance only exists over a finite range of scales, that is the fractal behavior is bounded from both above and below (H. N. Kritikos and D. L. Jaggard, *Recent Advances in Electromagnetic Theory*, Springer-Verlag, 183-223, 1990). In fractal geometry, the usual concept of Euclidean dimension must be generalized. The fractal dimension  $D$  is a fractional dimension which lies between the integer dimensions of one and two ( $1 < D < 2$ ). Hence, fractal curves occupy the space between one and two dimensions.

$$\sum_{n=1}^{\infty} r^{(n-2)/n} g(r^{n/a})$$

*D = fractal dimension*

The properties of a certain class of functions, known as generalized Weierstrass functions, will be discussed. These functions are everywhere continuous but nowhere differentiable and exhibit fractal behavior at all scales. It will be demonstrated that the array factor for a nonuniformly spaced linear array can be expressed in terms of a Weierstrass partial sum (bandlimited Weierstrass function) for an appropriate choice of array spacings and excitations. The resulting fractal radiation patterns possess structure over a finite range of scales. The range of scales can be controlled by the number of elements in the array. For a fixed array geometry, the fractal dimension of the radiation pattern can be controlled by the array excitation. The figure below shows a normalized radiation pattern with a fractal dimension of 1.5 produced by a 16-element linear array.



C2-1 POWER GRID NEMESIS: GEOMAGNETIC DISTURBANCES

1340 Vernon.D. Albertson  
Department of Electrical Engineering  
200 Union Street Southeast  
University of Minnesota  
Minneapolis, MN 55455

John G. Kappenman  
Minnesota Power  
30 West Superior Street  
Duluth, MN 55802

Severe geomagnetic disturbances can have serious consequences for large interconnected power grids, and for the associated connected power conversion and protective equipment that are critical to its operation. The great magnetic storm of March 13, 1989 provided dramatic proof when it triggered a blackout of the power grid in the entire province of Quebec. The blackout affected some six million people for nine hours; that outage time was minimal because of the ease of starting hydro generation from a "black start". That same storm also resulted in the failure of a large power transformer at a nuclear generating station in eastern United States, and triggered hundreds of other events on power systems in the United States and Canada.

This paper will present the basic mechanisms by which geomagnetic disturbances access and affect power system equipment and operation, and summarize the major events resulting from the March 13, 1989 storm. It will also discuss the most recent research efforts in mitigation of geomagnetically induced currents in power systems, and transformer failure studies for possible correlation with geomagnetic activity cycles. The increasing vulnerability and risks to large power grids and equipment will be covered, as well as the urgent need for a solar wind monitor satellite for accurate alerting of geomagnetic storms, and the status of the effort to launch the satellite.

C2-2 ELECTROMAGNETIC SOUNDING OF THE SEAFLOOR  
1420 Steven Constable  
Institute of Geophysics and Planetary Physics  
La Jolla CA 92093-0225

By measuring the response of the seafloor to an externally applied electromagnetic field the electrical conductivity of the oceanic crust and mantle may be determined. Although the inversion of experimental data to infer conductivity structure is unstable and underdetermined, modern regularized inversion methods provide models that are bounded in some sense, usually by minimizing the 2-norm of the first spatial derivative of the logarithm of conductivity to produce the 'smoothest' model.

The external EM field may be man-made (controlled source, or CS-EM, sounding) or the natural, time varying, external magnetic field of Earth (magnetotelluric, or MT, sounding). In both cases measurements must be made on the seafloor, because the integrated lateral conductance of the ocean is typically 16000 Siemens. This conductive ocean removes almost all the external field in the frequency range of CS-EM (0.1 to 25 Hz), and forces the use of periods longer than about 100 s for MT. The respective depths of resolution for CS-EM and MT are thus about 0 – 30 km and 50 – 500 km, making the two methods highly complementary. Seafloor noise for CS-EM is dominated by the electrodes used to make contact with seawater, so antennas up to 3 km long are employed to maximize the signal for a given pair of electrodes. Noise levels as low as  $1 \times 10^{-13}$  V/m at frequencies of 1 to 10 Hz in a synchronous stacking bandwidth of  $1 \times 10^{-3}$  Hz may be achieved this way. Three CS-EM soundings performed in the eastern Pacific on lithosphere of ages 0, 25 and 40 My show (a) the uppermost mantle to be extremely resistive ( $> 10^5 \Omega m$ ), (b) details of the porosity and melt structure in the uppermost 2 km of a mid-ocean ridge, and (c) that the oceanic crust is electrically anisotropic.

Classic seafloor MT soundings have been thought to require a very conductive region in the mantle at a depth of about 200 km. This region is not compatible with models of temperature and melt distribution in the lithosphere nor with laboratory conductivity measurements on mantle materials. However, because the lateral conductance of the ocean is much larger than the leakage path provided by the resistive upper mantle, MT fields propagate large horizontal distances and are distorted both by coastlines and seafloor topography. It can be shown that the MT soundings are consistent with a more resistive mantle coupled with distortion by the coast effect.

C2-3  
1540**A STATISTICAL STUDY OF "NON-PREDICTABLE"  
INDUCED VOLTAGES ON LONG CABLES****David J. Thomson**

AT&amp;T Bell Laboratories, Murray Hill, N.J. 07974

Geomagnetic induction effects are responsible for numerous problems on long power and communications cables and it is desirable to be able to predict them accurately from magnetometer data. Superficially, analysis of this problem has much in common with the estimation of magnetotelluric transfer functions using natural sources. However, it is well-known that reliable estimation of these transfer functions requires strongly robust methods and that these typically reject 5 to 30 percent of the data. Unfortunately, the rejected portions of the data usually represent storms and other periods when the geomagnetic field is unusually active: that is just those times when induction effects are most serious and prediction most necessary.

This talk reports on an empirical study of the large residuals from robust estimation procedures using data from Transatlantic telephone cables and power lines. It appears that at much of the residual is related to the horizontal fields in a non-linear way.

C2-4 ELECTROMAGNETIC ARRAY PROCESSING: G. Egbert  
1620

F1-1  
1340

**A STATISTICAL ASSESSMENT OF EVAPORATION  
DUCT EFFECTS ON PROPAGATION AT FREQUENCIES  
FROM 3 TO 94 GHz**

Kenneth D. Anderson  
Ocean and Atmospheric Sciences Division, Code 543  
Naval Ocean Systems Center  
San Diego, CA 92152-5000

Radio frequency propagation measurements from a unique multi-frequency over-water propagation experiment made by NATO RSG8 in Lorient, France are compared to accumulated frequency distributions of propagation loss calculated from a climatology of evaporation duct heights for the region. On a 27.7 km length path, propagation measurements were made at frequencies of 3, 5.6, 10.5, 16, 35, and 94 GHz. Transmitters and receivers were located about 8.5 and 10.5 m above mean sea level, respectively. By using the lowest frequency as a gage to eliminate occurrences of surface-based ducting from elevated trapping layers, excellent agreement between theory and observations is found.

An earlier study (H.V. Hitney and R. Vieth, *IEEE T-AP*, 38,794-799, 1990) made similar comparisons for measurements in the Aegean Sea and the North Sea at frequencies from 0.6 to 18 GHz and achieved excellent agreement between theory and observations in most cases. With the addition of higher frequencies from the Lorient measurements, a capability now exists that provides systems designers a method to compute statistical performance parameters, such as signal margins or maximum detection range, for most over-water geographic areas.

F1-2  
1400

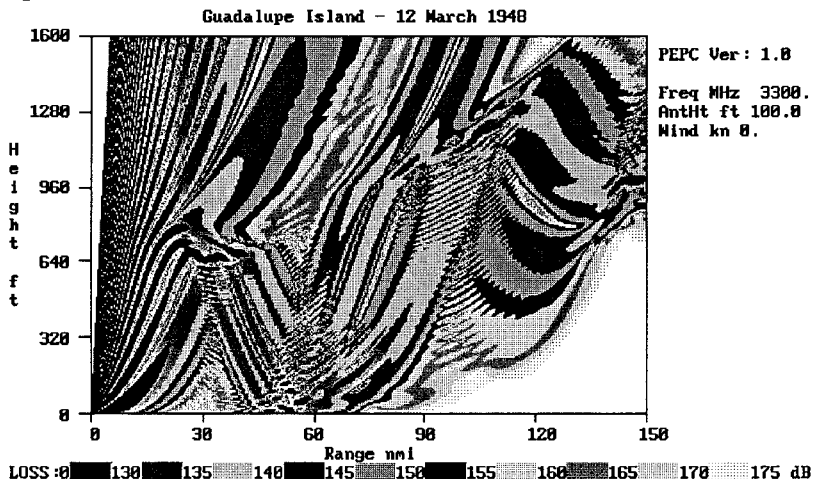
**PARABOLIC EQUATION MODELING IN RANGE-DEPENDENT ENVIRONMENTS**

Amalia E. Barrios  
Naval Ocean Systems Center  
Tropospheric Branch, Code 543  
San Diego, CA 92152-5000

A parabolic equation (PE) model has been developed for tropospheric radiowave propagation over the ocean. The model is based on the method originally developed by Fock ("Electromagnetic Diffraction and Propagation Problems", Chaps. 11-14, 1946) and uses the split-step Fourier method developed by Hardin and Tappert (*SIAM Rev.* 15, p. 423, 1973). A smooth surface and horizontal polarization are assumed. Two methods to model range-dependent environments are investigated. The first method uses linear interpolation in range between vertical profiles. The second is a feature-to-feature interpolation that linearly interpolates a feature from one profile to a corresponding feature in the next profile.

Results from the model are compared to experimental data taken from two experiments performed during the years 1947 and 1948. In one experiment measurements were made on over-water paths from Guadalupe Island to San Diego (*Symposium on Tropospheric Wave Propagation, NEL Rep. 173*, 25-29, July 1949). Measurements from the other experiment were made off-shore toward Wakanui Beach in the South Island of New Zealand (Great Britain Dept. of Sci. and Ind. Res., "Report of Factual Data from the Canterbury Project", Vol. I, II, III, 1951).

Comparisons are made between the two methods of interpolation. The technique of feature-to-feature interpolation is shown to be the better method and gives a reasonably good estimate of the environment between measurements, leading to excellent agreement between the predicted fields and observed radio data, even when vertical refractivity measurements are separated by large distances. The figure below is an example of the PE model applied to a range dependent environment.

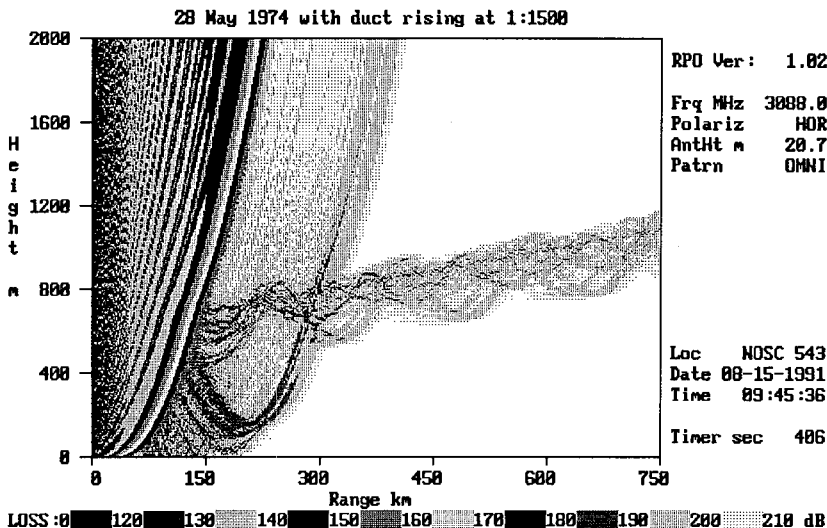


F1-3  
1420**WHISPERING GALLERY EFFECTS IN THE TROPOSPHERE**Herbert V. Hitney  
Tropospheric Branch, Code 543  
Naval Ocean Systems Center  
San Diego, CA 92152-5000 USA

Experimental data that recorded higher-than-expected signals far beyond the horizon at 3088 MHz in the presence of an elevated duct are examined and compared to results from the NOSC Radio Physical Optics (RPO) propagation model. RPO is a range-dependent hybrid model that combines ray optics methods at higher elevation angles with parabolic equation methods at lower altitudes. In the case presented, the transmitter and receiver were 21 and 915 meters above sea level, respectively. Measurements were made to ranges of 700 km.

Previous modeling of this same data by Pappert and Goodhart (*Radio Sci.*, 12, 75-87, 1977) using waveguide methods over-estimated the propagation loss by 30 to 80 dB at ranges far beyond the horizon, where the observed attenuation rate was nearly zero. A re-investigation of the case by Hitney, Pappert, and Hattan (*Radio Sci.*, 13, 669-675, 1978) proposed that the relatively high signals and low attenuation rate might result from very strong evaporation duct effects. The RPO results presented here match Pappert's and Goodhart's results for the range-independent refractivity profile measured at the transmitter location, also over-estimating the propagation loss. However, when the elevated duct is allowed to rise slightly with range, as frequently observed in the San Diego offshore area, the RPO results very nearly match the observed loss values.

It is concluded that the measured data resulted from whispering gallery propagation in an elevated duct. Whispering-gallery, or earth-detached, modes in tropospheric layers were proposed by Wait (*Electron. Lett.*, 4, 377-378, 1968), who suggested that these usually-neglected modes can contribute to the total field in transhorizon propagation. This study appears to confirm his proposal. The figure below illustrates the RPO results for the rising duct assumed in the study.



F1-4  
1440

## CREEPING WAVES OVER A FLATTENED EARTH

H.-M. Lee

Department of Electrical and Computer Engineering  
Naval Postgraduate School (EC/Lh)  
Monterey, CA 93943-5100

The earth-flattening approximation [J.E. Freehafer in D.E. Kerr, ed. *Propagation of Short Radio Waves*, pp. 50-53, Peter Perigrinus, London, 1987] has been widely used for incorporating earth curvature into tropospheric propagation problems while keeping the formulation in a 'flat' coordinate system. Such a framework is desirable because, for microwave propagation, the range of interest rarely goes beyond an extremely small fraction of the circumference of the earth. By restricting their applicable range, the Maxwell equations are converted from the spherical coordinate system concentric with the earth to any one of several familiar cylindrical coordinate systems attached to the earth surface. This procedure replaces the troublesome Mie-type series sum of zonal harmonics with a contour integral from which high frequency effects can be extracted.

Only the smallness of this range-to-circumference ratio is essential to this approximation under which the polar angle in the spherical coordinate system, after being converted to the great circle distance, is transformed into the radial distance of the cylindrical coordinate system. As a result, without further simplification, only the Legendre functions of the polar angle are replaced with their large order asymptotic forms, the Bessel functions. For the idealized problem of the propagation of waves in a homogeneous atmosphere over a spherical earth, the presence of the infinitely many simple poles in the physical sheet of the complex wavenumber plane is in sharp contrast to their absence in the Sommerfeld problem of radio over a truly flat earth [A. Sommerfeld, *Partial Differential Equations in Physics*, Academic Press, New York, 1949]. These poles are the creeping wave modes in the theory of diffraction and, aside from the use of the large order asymptotic form of the Legendre functions, the earth-flattening approximation conforms to the theories of van der Pol and Bremmer [H. Bremmer, *Terrestrial Radio Waves*, Elsevier Publishing, New York, 1949] and V.A. Fock [*Electromagnetic Diffraction and Propagation Problems*, Pergamon Press, New York, 1965].

The properties of the creeping wave modes [F. Ursell, *Proc. Camb. Phil. Soc.* 64, 171-191, 1968] under the earth-flattening approximation are investigated. Their locations relative to the zeroes of the Hankel function of the first kind of order one-third are obtained. These expressions are different from those given by J.B. Keller, et. al. [*J. Math. Phys.* 4, 829-832, 1963] and J.A. Cochran [*Numerische Mathematik* 7, 238-250, 1965].

F1-5            STATISTICAL DISTRIBUTIONS IN THE PROPERTIES OF  
1520            INCOMING RAYS UNDER MICROWAVE MULTIPATH  
                 PROPAGATION CONDITIONS.

Alan R. Webster,  
Department of Electrical Engineering,  
The University of Western Ontario,  
London, CANADA. N6A 5B9.

Results are presented from the operation of a wide-aperture receiving array on a terrestrial microwave communications link of length 51 km. The vertical aperture of 666 wavelengths allows a resolution approaching  $0.1^\circ$  in the identification of individual rays and the system operates continuously with a sample interval of 1 second. The objective of this research is to provide information on the occurrence, amplitude and angle-of-arrival of individual rays under multipath conditions, with a view to improving the modelling of the medium and prediction of the consequences on microwave communications systems.

Previously reported information (A. R. Webster, IEEE Trans. Ant. Prop., 39, 6, 798-803, 1991) concentrated on the basic distribution of the 3 strongest rays in such a multipath situation. Here, the emphasis is placed on conditional statistics referred to the angle-of-arrival (AOA) of the strongest ray and the results from 200 hours of fading data taken in 1989 are presented. These include the amplitude distribution of the strongest ray within  $0.1^\circ$  intervals in AOA of that ray, and the angular distributions of the rays of smaller amplitude conditioned on these same intervals for the strongest. This procedure is carried out for the entire data set and for the data from the worst fading month (July, 1989).

The evidence indicates that the strongest rays are predominantly elevated from the normal AOA, which suggests an origin in elevated layers, although occasions arise where the opposite is true. The distributions of the weaker rays exhibit some dependence on the AOA of the strongest which is suggestive of an overall refractive constraint, while the finer detail shows differences which relate well to high level atmospheric rays, as predicted by ray-tracing, and low elevation rays expected from ground reflections. The median amplitude within each  $0.1^\circ$  interval for the strongest ray is found consistently to be somewhat below that of the direct ray under normal (single path) conditions.

F1-6 REFRACTIVITY PROFILE MEASUREMENTS USING  
1540 A VERTICAL ARRAY OF RAPID RESPONSE  
TEMPERATURE AND RELATIVE HUMIDITY SENSORS  
J.K. Stapleton  
Naval Surface Warfare Center  
Radar Systems Branch Code F42  
Dahlgren, VA 22448

An assessment of the RF propagation environment during radar testing has become vital to later sensor data reduction efforts. One of the most common methods of assessing RF propagation is through the use of refractivity profiles measured versus height. Several different refractivity measurement schemes have been devised and used with variable levels of success. Most of these schemes involve moving a single sensor package, consisting of a temperature sensor, a relative humidity sensor, and a pressure sensor, vertically through the troposphere. During recent testing performed at the NAVSWC Detachment, Wallops Island, VA, a vertical array of seven fixed position temperature and humidity sensors was used to make refractivity profiles. An eighth sensor on a motor driven shuttle was used to provide a drift and offset reference between the fixed sensors. The lower few sensors were more closely spaced than those at the higher positions in order to provide finer height resolution in the evaporative region. The modified refractivity value in M units was calculated using these measurements and plotted against the height of the fixed sensors. An entire profile was measured every five seconds so that the temporal fluctuation of these profiles could be studied. Preliminary analysis of a representative subset of the collected data is presented.

F1-7 SENSITIVITY OF FIELD VALUES TO REFRACTIVE  
1600 INDEX VARIATIONS IN A SURFACE BASED DUCT  
John F. Cavanagh  
Code F405  
Naval Surface Warfare Center  
Dahlgren, VA 22448-5000

The recently developed numerical methods for solving the two dimensional wave equation, known as the Parabolic Equation Method, PEM, is a powerful tool for investigating propagation in surface based ducts. Preliminary results for a simple bilinear duct are presented. Monte Carlo experiments were performed with duct profiles having a small random variation superimposed on an idealized constant gradient. For those cases where several modes are supported, these refractive variations redistribute the energy within the duct but the deep nulls predicted for the constant gradient case are still present with the random variations. In another experiment, the duct height was varied with range. In this case the calculations show little change in the predicted fields. An initial attempt to characterize propagation in ducts on a statistical basis has been made.

F1-8  
1620 CLOUD DISPERSIVE EFFECTS ON DIGITAL  
COMMUNICATION SIGNALS  
G.C. Gerace  
E.K. Smith  
Campus Box 425  
Department of Electrical and Computer  
Engineering  
University of Colorado  
Boulder CO 80309-0425

This paper presents the initial results of a detailed investigation into the dispersive effects of atmospheric liquid water clouds on digital communication signals. Using the Liebe millimeter-wave propagation model as the basis for a cloud "transfer function", signal distortion is numerically computed for AM, FM, and PM digital signals with carrier frequencies up to 1000 GHz.

Since bit error rates (BERs) are highly dependent on coding and detection methods, pulse spreading and mean square phase error rather than BERs are used to characterize cloud dispersive effects on digital signals. Thus the results are general in the sense that they are independent of specific system implementations. In particular, analytic approximations of pulse spreading are compared to numerical results for a gaussian pulse and extensive numerical results are presented for rectangular pulses with the modulation schemes mentioned above.

Cloud dispersive effects are a complicated function of cloud parameters (liquid water content, drop distribution, temperature, cloud extent) and signal characteristics (pulse width, carrier frequency, modulation scheme). The results of this study indicate that there are some fundamental limits on absolute channel bit rates with respect to cloud dispersion.

The current work focused on the coherent signal only. Our on going efforts are concentrating on the non-coherent signal (multipath within the cloud).

G2-1 THERMOSPHERIC TEMPERATURES DERIVED FROM  
1340 DIGISONDE IONOGRAMS

Xueqin Huang and Bodo W. Reinisch  
University of Massachusetts Lowell  
Center for Atmospheric Research  
Lowell, Ma. 01854, USA

Abstract

An attempt is made to derive thermospheric neutral temperatures from the electron density profiles obtained from Digisonde ionograms. Assuming that the layer profile can be represented by an  $\alpha$ -Chapman function with height dependent scale height  $H(z)$ , we calculate  $H(z)$  from the electron density profile  $N(z)$ . The Digisonde profiles are represented with the help of Chebyshev polynomials. Using matrix multiplication the polynomial coefficients are converted to the pressure scale height. Two months of data were analyzed for several mid-latitude stations and the results are discussed. At F2 layer heights the scale heights vary systematically with time of day and season, with median values going from 50 km on a December morning to 125 km at noon in July 1989 for Millstone Hill, Massachusetts. Relating scale height and neutral temperature through  $T [K] = 20 H [km]$  leads to temperature values at  $z \approx 350$  km that are in fair agreement with the simultaneously measured temperatures from the Millstone Hill incoherent scatter radar.

G2-2  
1400

## **IONOSPHERIC MODELLING FOR SMART SSL**

**L.F. McNamara  
ANDREW SciComm  
2916 National Drive  
Garland, TX 75041**

**Determining the location of a long-range HF transmitter requires**

- 1. Measurement of the azimuth and elevation of the incoming wave front.**
- 2. Real-time updating of a synoptic model of the propagation medium (the ionosphere) along the circuit.**
- 3. The tracing of rays through that model back along the path of the incoming wave.**

**This is the Synoptic Modelling And Ray Tracing (SMART) approach to the Single Station Location (SSL) of remote HF transmitters.**

**It is the second step, setting up a reliable model of the ionosphere, which introduces the largest errors. This paper therefore describes the requirements of a reliable synoptic ionospheric model for this purpose, reviews possible techniques for updating the model in real time, and suggests areas where future research is required.**

G2-3  
1420

## FROM OBLIQUE IONOGRAMS TO MID-POINT ELECTRON DENSITY PROFILES

W.S. Kuklinski, B.W. Reinisch and G.S. Sales  
University of Massachusetts Lowell  
Center for Atmospheric Research  
Lowell, MA 01854

Jurgen Buchau  
Phillips Laboratory/LIS  
Hanscom AFB, MA 01731

### ABSTRACT

Oblique ionograms were recorded between Digisondes in Goose Bay and Wallops Island (2060 km) using the end point vertical ionogram as a guide, the oblique ionograms were scaled automatically with software running on a 386 PC. The oblique echo traces are then inverted to mid-point vertical electron density profiles. Quasi-parabolic profile slopes are assumed for the E, F1 and F2 layers. For validation of the automatic inversion process the profiles are compared with the profiles obtained from a mid-point vertical sounder.

The good agreement of the profile parameters derived from oblique and vertical sounding suggests that oblique remote ionospheric sensing can be used on an operational basis as considered in the Phillips Laboratories DORIS project.

G2-4      GENERATING ELECTRON DENSITY MODELS WITH  
1440      CONTINUOUS GRADIENTS FROM DISCRETE DATA  
            Adolf K. Paul  
            7455 Brockway Drive  
            Boulder, Colorado 80303

A new approach to the general mapping problem will be presented. The function fitting the discrete data is a superposition of local functions. The contribution of a local function to the total variation decreases with increasing distance from the center of each such function.

The method can be applied to many kinds of data representation problems, ranging from interpolation of missing or irregularly spaced data in time series analysis to mapping of empirical regular or irregularly spaced multi-dimensional data.

The application of this method will be demonstrated for two ionospheric problems, mapping of standard parameters and ray tracing in an empirical ionosphere.

G2-5  
1520MIDLATITUDE ELECTRON DENSITY PROFILES DERIVED FROM  
IONOSONDE AND INCOHERENT SCATTER RADAR MEASUREMENTSC.F. Chen<sup>1</sup>, B.W. Reinisch<sup>1</sup>, X. Huang<sup>1</sup>  
M.J. Buonsanto<sup>2</sup>, J.L. Scali<sup>1</sup>, R.R. Gamache<sup>1</sup>, B.D. Ward<sup>3</sup>

1. *University of Massachusetts Lowell, Center for Atmospheric Research*
2. *Massachusetts Institute of Technology Haystack Observatory, Westford*
3. *Surveillance Research Laboratory, DSTO, Australia*

ABSTRACT

Incoherent scatter radars and ionosondes are the major instruments used to measure ionospheric electron density profiles. Because the two instruments use different techniques to determine the electron density, it is important to compare the results. Recently, by using a large data base a more detailed foF2 and hmF2 comparison has been carried out. The data were obtained by the Digisonde 256 and the incoherent scatter radar operating at Millstone Hill (lat.=43N, long.=289E), Massachusetts, U.S.A.. Data from different seasons in 1990 were used for the comparison. The electron density profiles generally match well during magnetically quiet times and when a narrow E-F valley exists. Compared to the ISR profiles, the profiles calculated by the DGS ARTIST system usually display lower true heights in the F region. The peak height difference is seasonally dependent. During January (winter) the difference is about 5-10 km, during March, April (spring) it is about 15 km, while during June (summer) the difference is about 25-30km. This suggests that different ionospheric structures dominate during different seasons. Usually the peak height differences between ISR and DGS profiles are smaller during night time than during day time. The possible explanation of this diurnal variation is that the E-F valley problem is not critical at night and the F1-F2 transition (valley) is non-existent.

G2-6  
1540PROCESSING AND ANALYSIS OF  
DIGISONDE ELECTRON DENSITY PROFILESXueqin Huang and Bodo W. Reinisch  
University of Massachusetts Lowell  
Center for Atmospheric Research  
Lowell, MA 01854

## ABSTRACT

There are about 40 Digisondes operating in the world today automatically scaling the important ionospheric characteristics such as critical frequencies, minimum vertical heights etc., and calculating the electron density profiles in real time. These data are generally corrected or "edited" off-line using the ADEP software package, which outputs the data in the URSI (Ionospheric Informatics Working Group) recommended ADEP format.

This paper discusses new processing techniques that determine monthly median profiles, equivalent parabolic layer descriptions, and reduced TEC (up to hmF2), all derived from the Chebyshev polynomial coefficients of the Digisonde profiles. Using the results with all data from the Digisonde network will enhance the development of good ionospheric models by validating the models with measured data.

G2-7  
1600FINITE DIFFERENCE - TIME DOMAIN SOLUTION OF THE  
MAXWELL EQUATIONS FOR THE DISPERSIVE IONOSPHERE

P. M. Franke

University of Illinois

Everitt Lab, Rm. 60H

1406 W. Green Street

Urbana, IL 61801-2991

L. J. Nickisch

Mission Research Corporation

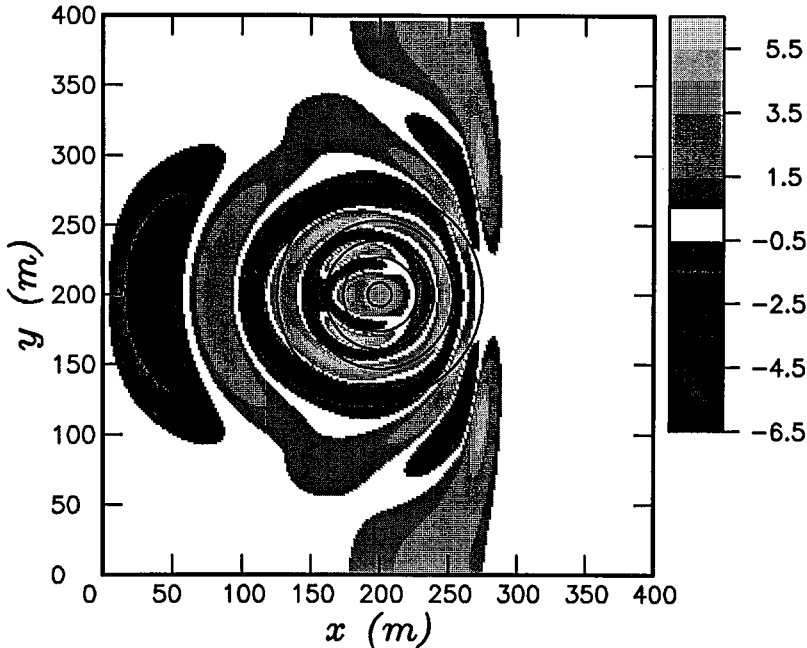
2300 Garden Road, Suite 2

Monterey, CA 93940-5326

The Finite Difference - Time Domain (FDTD) technique is a conceptually simple, yet powerful method for obtaining numerical solutions to electromagnetic propagation problems. The application of FDTD methods to problems in ionospheric radiowave propagation is, however, complicated by the dispersive nature of the ionospheric plasma. In the time domain, the electric displacement is the convolution of the dielectric tensor with the electric field, and this convolution is untractable in the nearest neighbor FDTD approach.

This difficulty can be avoided by returning to the constitutive relations from which the dielectric tensor is derived. By integrating these differential equations simultaneously with the Maxwell equations, dispersion (and absorption) is fully incorporated. The method is shown to be accurate by comparing to a known analytic solution for a special case.

A video will be shown of pulse propagation through various two-dimensional ionospheric structures, including structured random media.



G2-8 APPLICATION OF PSEUDO-DIFFERENTIAL OPERATOR  
1620 METHODS TO THE DERIVATION OF EXTENDED  
PARABOLIC VECTOR WAVE EQUATIONS

By

Ronald Brent  
Department of Mathematics  
University of Massachusetts • Lowell  
Lowell, MA 01854

and

Louis Fishman  
Department of Mathematical and Computer Sciences  
Colorado School of Mines  
Golden, CO 80401

The recent application of pseudo-differential operator and functional integral methods to the factored scalar Helmholtz equation has yielded extended parabolic wave theories and corresponding path integral solutions for a large variety of acoustic wave propagation problems. These known techniques are applied here to the full vector electromagnetic problem resulting in a new first-order Weyl pseudo-differential equation, which is recognized as an extended parabolic wave equation. Perturbation treatments of the Weyl composition equation for the operator symbol matrix yield high-frequency and other asymptotic wave theories. Unlike the scalar Helmholtz equation case, the one-way vector EM equation (and a scalar analogue provided by the Klein-Gordon equation of relativistic physics) require the solution of a generalized quadratic operator equation. While these operator solutions do not have a simple formal representation as in the straightforward square root case, they are conveniently constructed in the Weyl pseudo-differential operator calculus.

G2-9  
1640  
A COMPARATIVE ANALYSIS  
OF HIGH FREQUENCY PARAMETERS  
DETERMINED FROM VARIOUS  
PROPAGATION MODELS  
Greg R. Hand  
U.S. Department of Commerce  
NTIA/ITS.S3  
325 Broadway  
Boulder, CO 80303-3328

A detailed analysis has been undertaken to compare the results of calculations performed using high frequency propagation prediction programs IONCAP, HFBC84 and CCIR91. The purpose of the study was to determine the degree to which the calculated field strength, maximum usable frequency and reliability varied for the different models.

In order to determine field strength and reliability, the CCIR Working Party 10D antenna model and Reports 322-2 and 322-3 noise models were employed.

The results of the analysis will be illustrated by comparing area coverage contours of the basic parameters. It is seen that there exist striking differences between the results calculated by IONCAP, HFBC84 and CCIR91. Variations in the manner in which the above-the-MUF loss is calculated dramatically effects the calculated field strength at all distances within the coverage area. Suggestions for areas where the models can be improved will be offered and suggestions for extending the analysis to include other models will be given.

H1-1 ELECTROMAGNETIC ION CYCLOTRON WAVES  
1400 DRIVEN BY ION BEAMS IN THE MAGNETOSPHERE

D. Winske

X-1, Los Alamos National Laboratory

Los Alamos, NM 87545

N. Omidi

ECE Dept., UC San Diego

San Diego, CA 92093

We discuss a new mechanism for the generation of electromagnetic ion cyclotron waves in the magnetosphere, the electromagnetic ion/ion cyclotron (EMIIC) instability. The instability is driven by the relative streaming of two field-aligned ion beams. In the electrostatic limit it reduces to the well known ion beam driven electrostatic ion cyclotron instability, but for finite beta the instability is enhanced and propagates over a broader range of angles with respect to the magnetic field. Linear theory and one-dimensional hybrid simulations are used to study the characteristics of the instability as a function of beam density, angle of propagation ( $\theta$ ), ion beta, ratio of the streaming velocity to the Alfvén speed, electron to ion temperature ratio, and other parameters. Generally, the one-dimensional calculations show that the instability behaves like its electrostatic counterpart when  $\theta$  is near  $90^\circ$ , saturating at low levels by heating the ions in the perpendicular direction. At smaller angles the instability is dominated by electromagnetic effects, large amplitude waves, and stronger beam coupling. Two-dimensional hybrid simulations show some evidence for coherent effects due to a narrowing of the wave spectrum during the linear growth stage and a more quasi-linearlike heating process in the nonlinear phase, eventually yielding similar asymptotic values for plasma parameters. Applications of the EMIIC instability to ion cyclotron waves in the plasma sheet boundary layer and the low latitude boundary layer are also discussed.

H1-2  
1420EXCITATION OF MAGNETIC PULSATIONS  
IN THE EARTH'S POLAR CUSPC. S. Lin, H. K. Wong and J. D. Menietti  
Southwest Research Institute  
San Antonio, TX 78228

Magnetosheath plasma injected into the polar cusp has been suggested to produce various high frequency waves. Recently ground observations have indicated broadband ULF pulsations and narrowband Pc 3 waves in the cusp region. In this paper the cusp injected plasma is examined for exciting low frequency electromagnetic waves. Our preliminary calculations indicate that the electron distribution injected into the cusp cannot effectively excite low frequency electromagnetic waves because the plasma beta is too small. The injected ion distribution function is therefore modeled for instability analysis. The ion distribution function is assumed to contain a beam and rings in a background of cold ions and hot electrons. A small concentration of  $O^+$  ions is also considered. The electromagnetic dispersion equation for the beam-ring distribution is then solved for frequencies below the proton gyrofrequency. For plasma parameters at the DE-1 altitudes of about 3 earth radii, it is found that ion waves below the  $O^+$  ion gyrofrequency are excited. The ion wave instability growth rate increases with the ion beam energy and the beam density. The propagation of the ion waves and the associated heating of  $O^+$  ions in the polar magnetosphere are discussed.

H1-3  
1440**GENERATION OF WAVES AND PARTICLE HEATING  
IN THE CUSP****R. M. Winglee, C. S. Lin and J. D. Menietti****Department of Space Sciences, Southwest Research Institute, San  
Antonio, TX 78228-0510**

The injection of magnetosheath plasma into the cusp can lead to the heating of ionospheric plasma in association with the generation of intense low frequency waves. The heated ionospheric plasma under the influence of the mirror force and the convection electric field eventually flows out into the magnetosphere. Two-dimensional (three velocity) particle simulations are compared with observations from DE-1 to investigate these processes as a function of the properties of the injected magnetosheath plasma and the strength of the convective electric field. It is shown that the strength of the convective electric field is important in generating differential flows between the injected magnetosheath ions and electrons which can lead to the generation of field-aligned currents and potentials. In addition, the convective electric field in conjunction with the mirror force cause strong velocity filtering of the particle distributions. This velocity filtering leads to the generation of ring and/or beam distributions in different regions of coordinate space. The induced wave emissions vary along and across the field lines due to the development of these different distributions, as does the heating of the ionospheric plasma.

H1-4  
1500SHEAR-DRIVEN BROADBAND ELECTROSTATIC NOISE AT THE  
PLASMA SHEET BOUNDARY LAYER-LOBE INTERFACE\*

P. B. Dusenbery

Department of Astrophysical, Planetary and Atmospheric  
Sciences

University of Colorado at Boulder

Boulder, CO 80309-0391;

G. Ganguli and H. Romero

Observations of the equilibrium structure of the plasma sheet boundary layer-lobe interface indicate that strong density gradients and electron flows are established over scale lengths smaller than the ion gyroradius. The free energy associated with this equilibrium gives rise to a broadband spectrum of electrostatic instabilities. A combined fluid and kinetic approach is used to investigate the features of this broadband spectrum. We find that shear in the parallel flow gives rise to instabilities near the electron plasma frequency. Shear in the perpendicular flow gives rise to the electron counterpart of the inhomogeneous energy density driven instability. In this case, the frequency of the instability is around the electron gyrofrequency. Shear in the perpendicular flow also excites a spectrum around the lower hybrid frequency. Since these instabilities are affected by the Doppler-shift due to the flow velocity, their spectrum is not sharply peaked around any one frequency but has a significant spread similar to that seen in experimental data. We present a detailed study of the electrostatic waves that can be generated in this equilibrium.

\*Work supported by ONR, NASA, and ONT.

H1-5 NONLINEAR STIMULATION OF ELECTROMAGNETIC EMISSION  
1600 BY PARAMETRIC DECAY OF UPPER HYBRID WAVES

T. B. Leyser  
Swedish Institute of Space Physics  
Box 812  
S-981 28 Kiruna  
Sweden

A nonlinear dispersion relation for the parametric decay of an electrostatic upper hybrid (UH) wave, propagating perpendicular to the ambient magnetic field, into an ordinary mode electromagnetic (EM) wave, propagating parallel to the magnetic field, and an electrostatic low frequency wave, has been derived. The low frequency wave can be either a lower hybrid (LH) wave or an high harmonic ion Bernstein (IB) wave. The coherent and resonant wave interaction is considered to take place in a collisionless Vlasov plasma with  $O^+$  ions.

The instability growth rate is computed for parameter values typical of ionospheric modification experiments, in which a powerful high frequency electromagnetic pump wave is injected into the ionospheric F region from ground-based transmitters. The UH wave is assumed to be excited by the electromagnetic pump wave scattering off pump-enhanced stationary geomagnetic field-aligned plasma density striations in the ionospheric plasma.

The instability growth rate is studied for different frequencies of the decaying UH wave. When the UH wave frequency is near the third electron cyclotron harmonic, decay can occur for the case of the low frequency wave being a LH wave, with frequencies slightly above the LH resonance frequency. Both positive and negative group dispersive UH waves can decay, and the instability growth rate is sharply peaked for the case of negative group dispersive UH waves. In the case of the UH wave frequency being near the fifth electron cyclotron harmonic, parametric coupling can also occur to high harmonic IB waves, having frequencies both above and below that of the LH wave.

Thus the excited low frequency wave spectrum, and associated radiated EM wave spectrum, is significantly wider for the higher UH wave frequency, close to the fifth electron cyclotron harmonic, compared to the lower UH wave frequency around the third cyclotron harmonic. This is consistent with experimental results of stimulated electromagnetic emission (SEE) measurements, in which the spectral width of the commonly observed downshifted (DM) emission increases with the pump frequency and the actual width is in agreement with that suggested by the present model.

H1-6  
1620

DISTRIBUTION FUNCTIONS OBSERVED NEAR AN AKR SOURCE REGION

J. D. Menietti, R. M. Winglee and J.L. Burch (Department of Space  
Sciences, Southwest Research Institute, San Antonio, TX 78228-  
0510; 512-522-3210)

The DE-1 satellite flew near the source of auroral kilometric radiation on many passes through the nightside aurora region. We have noted on one of these passes a wide variety of particle distributions including large temperature anisotropies and beams as well as loss cones and trapped particles. It is difficult to determine whether the observed distributions are the source of the radio emission or the product of wave particle interactions. Recent numerical simulations have indicated that the observed distributions may be unstable to AKR and bursty radio emission.

H1-7      SENSITIVITY OF Z MODE WAVE DUCTING TO THE ELECTRON  
 1640      PLASMA FREQUENCY TO GYROFREQUENCY RATIO  
             Robert F. Benson, Code 692  
             NASA/Goddard Space Flight Center  
             Greenbelt, MD 20771

There are a number of ionospheric responses stimulated by topside sounders that appear to be extremely dependent on the ambient ratio of the electron plasma frequency  $f_N$  to the electron gyrofrequency  $f_H$ . For example, the ion spurs observed on the plasma resonance stimulated at  $f_N$  are greatly enhanced when  $f_N/f_H \approx n$  and those observed on the resonances stimulated at  $nf_H$  are most common when  $f_z \lesssim nf_H$  where  $f_z$  is the z wave cutoff at the satellite [Benson, Radio Sci., 10, 173-185, 1975]. In addition, there are a variety of diffuse signal returns stimulated by topside sounders that are observed only when  $f_z \lesssim nf_H \lesssim f_T$ , where  $f_T$  is the upper hybrid frequency, that have been interpreted as signatures of efficient heating of the plasma by the sounder pulse under these ambient conditions [Benson, Radio Sci., 17, 1637-1659, 1982]. In the present paper, it will be shown that the reception of z mode echoes ducted along field-aligned electron density irregularities, which are commonly observed at low altitudes in the topside ionosphere [Benson, Radio Sci., 20, 477-485, 1985], are greatly enhanced when  $f_N/f_H \approx n$ .

J2-1  
1400

**DIFFRACTIVE SPECKLES IN A PULSAR'S  
SCATTERING DISK**

C.R. Gwinn, K.M. Desai, J. Reynolds, E.A. King,  
D. Jauncey, G. Nicholson, C. Flanagan,  
R.A. Preston and D.L. Jones  
Physics Dept.  
University of California  
Santa Barbara, CA 93106

The speckle pattern of the Vela pulsar, as observed with the SHEVE southern-hemisphere very-long baseline interferometry (VLBI) network, provides a new observable for studies of radio-wave scattering the interstellar plasma. The speckle pattern contains full information on the distribution of scattering material, in holographic form. We observe the pattern as variations in the pulsar's intensity with frequency and time, as are familiar from single-dish studies of scintillation in pulsars. The speckle pattern also produces variations of VLBI phase; these variations are far greater than those expected on the basis of the finite signal-to-noise ratio of the pulsar. These phase variations can be interpreted as the variation in position of speckles within the scattering disk. Analysis of the speckles yields information on the distribution of scattering material along the line of sight from the Vela pulsar.

J2-2 PROBING INTERSTELLAR TURBULENCE BY OBSERVATIONS  
1420 OF FARADAY ROTATION IRREGULARITIES

J.H. Simonetti

Department of Physics

Virginia Polytechnic Institute and State University  
Blacksburg, VA 24061-0435

Observations of the difference in Faraday rotation measure toward radio sources seen along closely separated lines of sight yield information on irregularities in the electron density and magnetic field in the interstellar medium. Such observations toward sets of extragalactic radio sources probe the irregularities on typical length scales between approximately 0.01 and 100 pc ( $10^{16}$  to  $10^{20}$  cm). The Very Large Array has been an essential tool in this program. In general, the results suggest the outer scale of either electron density or magnetic field irregularities, or both, extends to at least 1 pc. Interestingly, if one assumes the magnetic field is uniform, the results are consistent with an extrapolation to parsec scales of the power spectrum for the fine scale ( $< 10^{13}$  cm) electron density irregularities that cause the scintillation of high galactic-latitude pulsars. Since the electron density power spectrum inferred from observations of pulsar scintillation is approximately Kolmogorov, it is suspected the irregularities are produced by interstellar turbulence. Thus scintillation studies and observations of Faraday rotation measure irregularities, taken together, suggest interstellar turbulence may extend over a very wide range of length scales.

Observations of Faraday rotation measure irregularities seen through suspected generators of interstellar turbulence (e.g., supernova remnants) may help ascertain the sources of the turbulence. In the case of one supernova remnant (CTA 1), the observations suggest a greater level of turbulence within the remnant, compared to just outside the remnant. However, the level of turbulence is apparently much greater within the unidentified clumps of strong turbulence in the galactic plane that are inferred from observations of the scintillation and scattering of low galactic-latitude pulsars and extragalactic radio sources.

J2-3 SOURCES OF PLASMA WAVES IN THE INTERSTELLAR MEDIUM  
 1440 Katia Ferrière  
 High Altitude Observatory  
 National Center for Atmospheric Research\*  
 P.O. Box 3000  
 Boulder, CO 80307

Direct observations of the interstellar medium provide information on the large-scale ( $\gtrsim 1$  pc) properties of interstellar turbulence; they indicate that the electron density and magnetic field have a random component of the order of their mean value. On the other hand, the observed scintillation of pulsar signals reveal fluctuations in the electron density on scales ranging from  $10^{10}$  to  $10^{13}$  cm. The scintillation data are consistent with a Kolmogorov spectrum ( $F(k) \propto k^{-\frac{5}{3}}$ ), and the extrapolation of this spectrum to large scales is in agreement with direct measurements.

This brought Lee and Jokipii (Lee, L. C. and Jokipii, J. R., *Ap. J.*, 204, 735, 1976) to suggest that interstellar turbulence has a continuous Kolmogorov-type spectrum extending over the entire range  $10^{10}$  -  $10^{19}$  cm. It is tempting to regard such a smooth power-law spectrum as the result of an energy cascade from large to small scales. However, the idea of a turbulent cascade meets with serious difficulties. In particular, there exist various damping mechanisms which dissipate the long waves before they have a chance to transfer much of their energy to shorter waves. Moreover, the irregularity spectrum inferred from interstellar scintillations appears to be clumpy, whereas it should be relatively smooth if it resulted from a cascade.

To avoid the problems inherent to a Kolmogorov cascade, one can imagine that the short-scale electron density fluctuations are directly produced on the scales on which they affect pulsar signals. For instance, cosmic rays streaming ahead of a supernova shock excite resonant Alfvén waves, which, if strong enough, can generate acoustic waves. These acoustic waves peak at a wavelength of a few times the Larmor radius of the lowest-energy cosmic rays ( $\sim 10^{11}$  -  $10^{12}$  cm) and their amplitude is consistent with the observed density fluctuations.

---

\*The National Center for Atmospheric Research is sponsored by the National Science Foundation

J2-4 ROUND TABLE DISCUSSION ON SCATTERING PHENOMENA IN RADIO ASTRONOMY  
1520

JE1-1  
1340

## THE IMPACT OF WARC-92 ON RADIO ASTRONOMY

Thomas E. Gergely  
Electromagnetic Spectrum Manager  
Division of Astronomical Sciences  
National Science Foundation  
Washington, DC 20550

A World Administrative Radio Conference (WARC) will be held in early 1992. The purpose of WARC-92 is to reallocate portions of the radio spectrum to allow the introduction of new services and the expansion of others. The heaviest competition is in the 500-3000 MHz range where Mobile Satellite (MSS), Broadcast Satellite (BCS), Radio Determination Satellite (RDSS), and the Land Mobile Service have combined requirements for several hundred MHz of spectrum. There are additional requirements for new allocations above 12 GHz for High Definition Television, and above 20 GHz for new Space Services.

Even with all this pressure, it is unlikely that frequency bands allocated to radio astronomy will be reallocated to other services. After the WARC, however, regions of the spectrum where observations of redshifted HI or redshifted OH are currently carried out may become inaccessible for astronomical observations. Unless steps are taken to reduce out-of-band and harmonic emissions from satellite transmitters, interference is likely to increase, even in bands that are allocated to radio astronomy. Finally, with the growing competition for spectrum, pressure for sharing is also certain to increase. Radio astronomers must pay more attention to the regulatory process and will, in the longer run, probably have to devote more resources to it as well to preserve their access to the spectrum.

JE1-2  
1400**The Status of Frequency Allocations for Passive  
Microwave Earth Remote Sensing****A.J. Gasiewski**  
School of Electrical Engineering  
Georgia Institute of Technology  
Atlanta GA, 30332-0250

Earth- and spaceborne passive microwave sensors are important elements in a diverse sensor network used to improve near-term weather forecasts and understand potential long-term climate and biogeochemical changes. Channels that are either currently used or projected to be used for Earth observation range from L-band to the sub-millimeter wave region. These channels are located approximately every octave in frequency and at the absorption line centers of the primary atmospheric gases ( $O_2$ ,  $H_2O$ ) and other trace gases ( $O_3$ ,  $NO$ ,  $ClO$ ,  $CO$ ). Many of these channels are also used by radioastronomers.

However, only a few of the more than three dozen radio bands that are either currently in use or potentially useful for Earth remote sensing are allocated for passive service on a primary basis. With ever-increasing demands for spectrum by communications concerns and other active users, the risk that passive microwave Earth remote sensing will be compromised by man-made interference also increases. Potential sources of interference include spread spectrum communications systems and unfiltered high-power broadcast carriers, each of which can produce detectable harmonics. Particularly vulnerable channels are those within the L- and S-bands and the millimeter-wave window frequencies near 10, 18, 37, and 90 GHz. Given the long lead times (5-15 years) involved in the deployment of new satellites, it behooves the passive microwave Earth remote sensing community to periodically assess the impact of emerging communication trends and technologies on their systems. The talk will review the spectral needs, tolerable interference levels, and potential sources of interference for several passive microwave systems.

JE1-3      DISPLAY OF SPECTRUM USAGE DATA  
 1420      R. M. Price  
           Department of Physics and Astronomy  
           University of New Mexico  
           Albuquerque, NM 87131-1156

Spectrum usage data is multidimensional. Among the measured characteristics of interest are channel occupancy as a function of time. This may include peak power and average power received over appropriate time averaging intervals, and with sufficient frequency and time resolution for the specific monitoring task at hand. Direction-of-arrival information may also be needed. Polarization information is sometimes desired.

When monitoring spectrum usage to find interfering signals, especially when considering the passive services, very low received power levels are often of interest. This requires a large dynamic range of signals be considered.

The display of this multidimensional data poses a problem. Typical displays use contours, ruled surfaces, time slices, and other two dimensional forms. Because of the great amount of data to be displayed, and the resolution required, these displays become cluttered and often confusing.

The use of the "data cube" approach has been considered and has applicability to this type of data. In particular, multiple frame "movies" and the use of color to provide an additional dimension is successful in helping understand complex spectrum use data.

The results of monitoring some UHF bands for several months will be shown and discussed.

JE1-4 LIGHT POLLUTION VS. RADIO-FREQUENCY INTERFERENCE  
1440 Patrick C. Crane  
National Radio Astronomy Observatory  
Post Office Box 0  
Socorro, New Mexico 87801

The physical principles underlying the generation, transmission, propagation, reception, and detection of the optical and radio signals responsible for light pollution and radio-frequency interference - in optical and radio astronomy, respectively - are reviewed. In each case the principal mechanism of propagation and the reception pattern of the telescope combine to produce the highest level of interference to the astronomical observations.

Wednesday Morning, 8 January, 0815-1200

0815-Weds. Duane Physics G0-30  
PLENARY SESSION

0815 Introduction: Chalmers Butler

1. 0825 Student Paper Competition: David Chang

0930 Break

2. 0940 Recent Accomplishments in Radio Science—A Panel Discussion

3. 1030 Salient Future Research Tasks in Radio Science—A Panel Discussion

4. 1130 General Discussion

5. 1150 Student Paper Awards

*Wednesday Afternoon, 8 January, 1335-1700*

Session A-4 1355-Weds. CR1-9

MICROWAVE AND OPTICAL METROLOGY

Chairman: Alan Michelson, Univ. of Colorado, Boulder, CO 80309

A4-1  
1400

## **Coupling Mechanisms and Transfer Functions for Optical Fiber Devices**

Shao Yang and Alan Mickelson

Department of Electrical and Computer Engineering

University of Colorado

Campus Box 425

Boulder, CO 80309-0425

**Abstract:** A transfer function approach has been put forward as a solution to the multimode fiber system characterization problem. This approach needs a model of the coupling process from which transfer functions can be derived for different devices. Based on the study of two basic coupling mechanisms, that is, scattering coupling and overlap coupling, transfer functions are derived for such devices as fibers/cables, connectors, splices, and power splitters. Results of experiments on these components and a concatenation of four splices show that the transfer functions are independent of launch conditions.

A4-2  
1420

**WAVELENGTH DEPENDENCE OF LP<sub>11</sub>-MODE LEAKAGE  
LOSS IN COATED DEPRESSED-INDEX CLAD FIBERS**

B.P. Pal,\* R.L. Gallawa, I.C. Goyal\*

National Institute of Standards and Technology  
Electromagnetic Technology Division  
325 Broadway  
Boulder, CO 80303  
USA

**ABSTRACT**

A quantitative investigation of the wavelength dependence of leakage loss of the LP<sub>11</sub> mode in coated depressed index clad fibers is made using a matrix method. The propagation constant and leakage loss of the LP<sub>11</sub> mode can be calculated to a high degree of accuracy using this method. The study reveals oscillations in the loss spectrum due to the finite width of the outer cladding and the presence of the higher refractive index primary coating. These results support experimental observations of oscillations reported in cut-off wavelength measurements. Comparison with published results is given.

\* Guest Researchers on leave of absence from the Department of Physics, Indian Institute of Technology, New Delhi, 110016, INDIA

A4-3 RADAR DEPOLARIZATION IN THE GROUND-BASED  
1440 SYSTEM DUE TO A CHAFF CLOUD

Y.Guo and H.Überall  
Department of Physics  
The Catholic University of America  
Washington, DC 20064

In practical applications it is necessary to analyze radar scattering by a chaff cloud in a ground-based system rather than in the scattering plane-based system. By means of the Stokes-parameter method, a series of expressions of the bistatic radar scattering cross section corresponding to arbitrarily polarized combinations of transmitters and receivers are derived in the ground-based system in the present study. The influence of chaff wires' orientation on the cross section is also studied based on the comparison between the cases of the spherical-randomly oriented wires and the horizontally Gaussian-distribution oriented wires, which may provide a valuable reference for designing various types of chaff as well as transmitter and receiver systems upon different demands.

## A4-4 INFRARED FOCAL PLANE ARRAYS FOR ELECTRIC FIELD DIAGNOSTICS

1520 Ronald M. Sega\*, John D. Norgard\*, Michael G. Harrison\*\*

\*Department of Electrical &amp; Computer Engineering

University of Colorado, Colorado Springs, CO 80933-7150

\*\* Phillips Lab (PL/NTCA), Kirtland AFB, NM 87117-6008

An Infrared (IR) detection technique has been developed to map two-dimensional cross-sectional views of electric field distributions near an emitter or a scattering body. The IR measurement involves the observation of microwave/millimeter wave (mw/mmwave) energy deposited into an electrically lossy detection screen. Joule heating results in IR emissions which can be detected by an IR imaging system. The detection screen material is calibrated such that a given temperature rise (above the ambient temperature of the material) corresponds to a particular electric field intensity level. The dynamic range of the electric field measurement is dependent on the total measurable temperature rise achieved and the lowest detectable temperature rise above the ambient screen temperature.

A limitation to the technique in the past has been the relative lack of sensitivity of IR scanning systems that were available to detect the IR temperature distribution. Now, by using a Focal Plane Array (FPA) for the sensing element, the sensitivity of the system can be increased by a factor of ten. The scanning IR imaging system previously used could distinguish temperature variations of 0.1 K and could achieve 0.02 K with multiple frame averaging. The FPA-based IR imaging system used in this study can distinguish temperature variations of 0.003 K with a 128x128 array of pixels and can provide the same spatial resolution as the scanning system, but accomplishes the data acquisition much more rapidly.

The implication for IR measurements made in the mw/mmwave spectrum is to allow tailoring of the detector screen material to produce minimally perturbing measurements and to lower the thermal mass of the detector screen for pulsed source transient field measurements.

The results of CW antenna near- and far-field pattern measurements and preliminary scattering and coupling studies are presented.

A4-5 POWER DENSITY MEASUREMENTS  
1540 Hubert Trzaska  
ITA, Techn. Univ. of Wroclaw  
Wyśpińskiego 27  
50-370 Wroclaw, Poland

The work deals with the power density measurement error in the near-field measurements while the power density is measured by E or/and H field measurement. Analysis was done for E- and H-type elemental dipoles. It gives results majorising errors in case of any other type of radiation source.

Because of large values of measurement errors, which may appear here, instead of standard definition of error the logarithmic one was accepted. The error estimations were done for E-field measurement, H-field measurement, E+H measurement (arithmetical mean) and E×H measurement (geometrical mean); it is worth to notice that the latter gives modulus of the Poynting vector.

Carried out analysis leads to the conclusion that the power density measurement method may be accepted on frequencies above 300 MHz. Comparative analysis of a half-wave radiators near-field leads to less rigorous conclusion. However, on frequencies below around 150-200 MHz, in majority of cases, the method and based upon it instruments (offered on the market) are useless.

With no regard to the sense of the power density measurement one must remember that to measure it it is necessary to know both the field components and the phase angle between them. Method worked out by RWP King, based upon multiple loaded loop antennas, and proposed by M. Kanda fiber optic use in the measuring set made it possible the precise measurement of the real part of the power density in any conditions; however, the methods have some limitations and they need sophisticated equipment use. As a result of this, there are the most popular radiation hazard monitors and EMI probes in which is applied the oldest way of the power density measurements, the way very true in the far field, ie. E or H measurement and device calibration in power density units. This is really good, simple and inexpensive way, but nowhere its limitations have been discussed nor mentioned.

A4-6 THE ELECTROMAGNETIC SCALE MODEL AS A  
 1600 DEVELOPMENTAL TOOL FOR THE AIR FORCE'S  
 HARDENED ANTENNA TECHNOLOGY PROGRAM (HAT)  
 Raymond S. Kasevich and Stephen L. Price  
 KAI Technologies, Inc.  
 175V New Boston St. Woburn, MA 01801

Electromagnetic scale models were used to investigate the behavior of buried linear single and multi-element antenna arrays for the United States Air Force's Hardened Antenna Technology Program (HAT). Measurements from scale model antenna systems buried in natural earth were used to confirm the analytical (computer) model predictions, to improve the theoretical analysis of the antenna systems, and to provide an independent check between analytical model results and full scale measurements. All work performed was done under Air Force Contract No. F30602-85-C-0282.

In this paper an analysis of the electromagnetic scale modeling program is presented by first reviewing the design of the buried antenna arrays and their scale models and then comparing the results of scale model antenna elevation and azimuth radiation pattern measurements to both analytical model data and full scale measurements. Particular attention is paid to the way in which the scale model systems were designed to fit into an existing laboratory environment. Additionally, areas where scale model data assisted in the design of the analytical model or pointed out its limitations are highlighted.

With the assistance of this scale modeling program both the analytical model (PAT4J), developed by Eyring Research Institute, Inc. of Provo, Utah and the NEC-3I method-of-moments code, developed by Lawrence Livermore National Laboratory were validated for antennas in underground environments. This work also resulted in Eyring's publication of the Antenna Engineering Design Handbook for Buried Linear Arrays for the United States Air Force.

Chairman: Motohisa Kanda, National Institute of Standards and Technology,  
Boulder, CO 80303

A5-1      DESIGN OF BROADBAND RADAR ABSORBING MATERIALS  
1400      (RAM) FOR WIDE RANGE OF ANGLES OF INCIDENCE  
          Prof. (Emeritus) J. Perini  
          Syracuse University  
          5207 S. Atlantic Av. Ap 1221  
          New Smyrna Beach, FL 32169  
          L. Cohen  
          Naval Research Laboratory Code 5332C  
          Washington, DC 20375-5000

Present RAM materials rapidly loose their rated RF absorption when the angle of incidence deviates from normal. It is possible to design a new class of RAM materials that will maintain a fairly constant absorption not only over a wide range of angles of incidence but also over a specified frequency bandwidth. This can be accomplished by covering a lossy dielectric slab (that could be an existing RAM) with several matching dielectric layers. The thickness and dielectric constants of these layers are now determined so that the absorption is nearly constant over the specified angle and frequency ranges. The idea is to bend the rays coming from any of the desired directions so that they will penetrate the lossy layer allways close to normal incidence.

The reflection coefficient of an electromagnetic wave, incident upon an infinite planar multilayer media, can be expressed as a function of the thickness, dielectric constants and conductivities of each layer, for any angle on incidence and frequency (Wait, J.R., Electromagnetic Waves in Stratified Medium, 2nd Edition, Oxford, England, Pergamon, 1970, Chapter 2). A cost function can now be constructed by summing the magnitude square of the reflection coefficients, for N directions of incidence and M frequencies, equally spaced over the ranges of interest. The dielectric constants and thickness (and conductivity if desired) of the matching layers are then found by minimizing this cost funtion, using a conjugate gradient algorithm (Press, W.H., et all, Numerical Recipies, Cambridge University Press 1986, Chapter 10).

A5-2  
1420

## ANALYSIS OF SEMI-ANECHOIC CHAMBERS USING THE FREQUENCY-DEPENDENT TLM TECHNIQUE.

Fethi H. Bellamine\* and Edward F. Kuester  
Department of Electrical and Computer Engineering  
Electromagnetics Laboratory: Campus Box 425  
University of Colorado, Boulder 80309

Electromagnetic anechoic chambers (EAC) are shielded enclosures which simulate empty, endless free space conditions. To that end, the walls of the chamber are lined with absorbing materials that should possess the capability of absorbing electromagnetic striking energy over the widest range of frequencies possible and dissipating the energy incident upon it. This type of chamber offers many advantages such as all-weather operation, security, protection of expensive systems under test and absence of electromagnetic interference. The floor should not be treated in order to reproduce conditions of an open-site measurement where a conducting ground plane exists. Such kind of enclosure where the floor is not covered is called semi-anechoic chambers.

The constitutive parameters of the lossy absorbing materials are frequency dependent. In this paper, the two-dimensional frequency-dependent transmission line matrix (FDTLM) presented in (F. Bellamine, *North American Radio Science Meeting Digest*, pp. 78, 1991) has been extended to three dimensional problems. This method is applied to the computation of the site attenuation of semi-anechoic chambers. FDTLM presents some advantages over some frequency-domain full-wave methods where the evaluation of transcendental functions and poorly converging integrals and the solution of matrix equations that may be poorly conditioned are required. It also provides the possibility of improving the performance of semi-anechoic chambers by investigating different lining materials for different walls.

A5-3           COMPARISON OF RADIATED-FIELD AND DIRECT-DRIVE  
1440           EXCITATION OF MULTICONDUCTOR TRANSMISSION LINES  
              David A. Hill  
              Electromagnetic Fields Division  
              National Institute of Standards and Technology  
              Boulder, CO 80303

Direct-drive excitation (also called current injection) of cable bundles has been used as a means of providing EMC clearance for aircraft to a specified external field environment (N.J. Carter, M. Redman, and P.E. Willis, IERE International Conference on Electromagnetic Compatibility, 117-124, York, 1988). A criticism of direct-drive testing is that the current distributions on the individual cable bundle wires are not necessarily the same as those produced by radiated-field excitation. Recent measurements of individual wire currents excited by direct drive and radiated fields have shown that this criticism is justified (J.W. Adams, private communication). The purpose of this paper is to present a theoretical comparison of the currents excited by the two methods and to determine under what conditions the two methods yield equivalent results.

The theoretical model consists of a multiconductor transmission line located over a ground plane with arbitrary impedance terminations at each end of the line. The excitation can be either an arbitrary external field (C. Paul, IEEE Trans., EMC-18, 183-190, 1976) or a current clamp encircling the entire wire bundle (M.F. Sultan, IEEE International Symposium on Electromagnetic Compatibility, 188-195, 1986). To simulate typical test conditions, the bulk currents on the cable bundle produced by the two excitations are equated at a particular point where a bulk current monitor is located. Current calculations for a variety of cases show that in general the two different excitations produce significantly different current distributions on the individual wires in a current bundle. When the transmission lines are short enough that the results reduce to circuit theory, the two excitations give similar results.

A defense of direct-drive testing is that there is no unique external field configuration for radiated-field testing and consequently no unique set of current distributions on the individual wires. The statistical properties of the current distributions produced by the two excitations are now under study.

A5-4  
1520**A MICROSTRIP RECEIVER PRESELECTOR  
SUITABLE FOR THE MEASUREMENT OF  
EXTREMELY WEAK ELECTROMAGNETIC FIELDS**

Robert T. Johnk and Kenneth H. Cavcey  
Electromagnetic Fields Division  
National Institute of Standards and Technology  
Boulder, Colorado 80303

The National Institute of Standards and Technology (NIST) has been active for many years in the measurement of signals which cause EMC/EMI problems. Since the Fields Interference and Metrology group at NIST is involved in applied research and development of small, non-intrusive probes to measure electromagnetic field quantities, it is necessary to develop high gain receiving instrumentation that can be used with broadband probes that have a low antenna factor. The measurement of weak signals in a noisy environment places stringent demands on the design of the associated receiving equipment.

One of the receiver components that must be carefully designed is the preselector. The preselector limits input noise power, reduces interference, and it provides image rejection. It also determines to a large extent the overall receiver noise figure. In the NIST receiver, the preselector is the "front end"; and it consists of a bank of 16 switched microstrip bandpass filters, which are fed by the probe output, followed by a MMIC amplifier. The filters are switched individually by means of PIN diodes located at the input and output of each filter, resulting in a variable bandpass filter. Each filter has been fabricated using inductively-coupled microstrip lines in conjunction with chip capacitors. The same microstrip geometry is used on each of the filters, which results in compact construction and a uniform design procedure. The use of microstrip allows one to control precisely the self and mutual inductances. The desired bandpass characteristics can be synthesized using any appropriate network synthesis technique.

A5-5  
1540DESIGN OF A 44 GHz TEST RANGE FOR MEASURING FIELDS INSIDE  
ELECTRICALLY LARGE DUCTS

D. Jordan, R. Bansal, and E. DiCarlo

Department of Electrical and Systems Engineering  
University of Connecticut, Storrs, CT 06269

## ABSTRACT

This paper will describe recent experimental work on measuring the fields inside electrically large ducts with or without scatterers. The main topic of discussion will be the design of a suitable test range at 44 GHz. Techniques will be presented to minimize reflections and ensure reproducible measurements. Some experimental results for simple scattering configurations will be compared with known analytical solutions to validate the design of the range. Also, experimental and computed results for several large ducts will be presented.

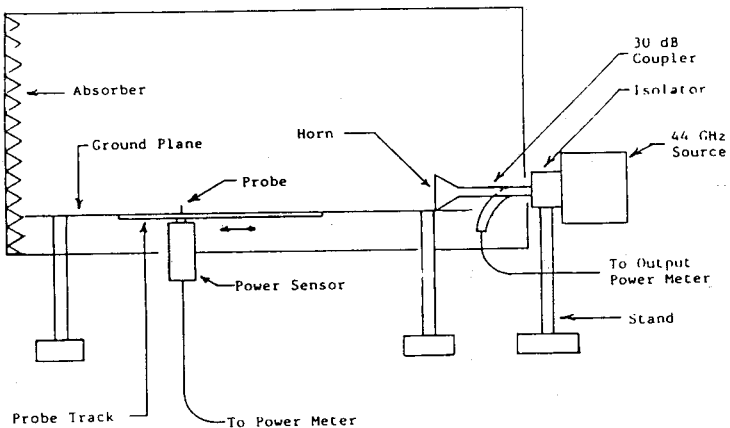


Fig. Experimental setup.

A5-6  
1600

**MEASURED BUILDING PENETRATION LOSS AT  
900 MHZ, 11.4 GHZ AND 28.8 GHZ**  
K.C. Allen, N. DeMinco, and P.B. Papazian  
Institute for Telecommunication Sciences  
325 Broadway  
Boulder, CO 80303

Simultaneous measurements of building penetration loss at 900 MHz, 11.4 GHz, and 28.8 GHz were made in three buildings. The receiving antennas were placed at fixed locations outside of the buildings at a height of about 4.5 m. The transmitting antennas were mounted on a movable cart at a height of about 1.2 m. Commercial Cellular Telephone, vertical-whip antennas were used at 900 MHz. Medium-gain horn antennas with beamwidths of about 30 degrees were used at the receiver for 11.4 and 28.8 GHz. On the transmitter cart, conical antennas, omnidirectional in the azimuthal plane, were used.

Measurements were made with the receiver located at several positions 15-20 m from a re-enforced concrete building while the transmitting cart was moved along many straight-line paths in hallways, offices, and laboratories. Similar measurements were made using a metal sided building (22 by 18 m) consisting of one large room with dividers, tall metal storage shelves, and display shelves. Finally, similar measurements were made using a single level (with basement) ranch style home with brick veneer.

The results can be characterized as showing that penetration loss through solid walls increased with frequency. However, openings such as windows often resulted in less loss at higher frequency.

#### BUILDING PENETRATION LOSS SUMMARY

<u>Walls on path</u>	Mean attenuation in dB		
	<u>900 MHZ</u>	<u>11.4 GHZ</u>	<u>28.8 GHZ</u>
<b>Concrete building</b>			
windowed, outside wall:	9.4	4.1	5.6
2-3 walls:	18.9	26.0	36.2
>3 walls:	28.8	34.4	53.3
<b>House with brick veneer</b>			
windowed, outside wall:	3.2	9.7	8.6
2 walls:	6.6	13.7	14.5
<b>Metal sided building</b>			
windowed, outside wall:	24.3	15.0	17.5

A5-7  
1620 **PRELIMINARY RESULTS OF EMI MEASUREMENTS ON  
NON-MILITARY VESSELS**

**B. R. Dawe, M. Hicks and D. Wells**  
**Canadian Centre for Marine Communications**  
**P.O. Box 8454**  
**St. John's, NF**  
**A1B 3N9**  
**W. R. Lauber**  
**Communications Research Centre**  
**Communications Canada**

The Canadian Centre for Marine Communications recently launched an electromagnetic interference and compatibility (EMI/EMC) program directed toward predicting, identifying, and solving such problems on non-military vessels. The first standards for radiated and conducted equipment emissions. Measurements have been made on a steel hulled government vessel and fishing trawler and compared with International Electrotechnical Commission CISPR standards. Preliminary results indicate that on these vessels radiated emissions do not present a problem. However, in many cases the bridge navigation and communications equipment is exceeding the CISPR limits in the amount of electrical interference it is conducting out onto the ship's power grid.

B3-1 OPTIMIZATION OF THE ELLIPTICALLY POLARIZED  
1340 DIFFUSE POWER SCATTERED FROM A TWO-SCALE  
ROUGH SURFACE

Robert J. Papa  
Rome Lab/ERCE  
Hanscom AFB, MA 01731

Margaret B. Woodworth  
ARCON Corporation  
260 Bear Hill Road  
Waltham, MA 02154

In previous work by the present authors (URSI, June 1989) a technique was presented to optimize the linearly polarized bistatic diffuse power scattered from a rough surface with two scales of roughness. The optimization was accomplished by varying the linear polarization state that could be accepted by the bistatic receive antenna. In this paper the technique is generalized. First, the waves scattered from the rough surface are represented as elliptically polarized and, secondly, the receive antenna can accept elliptically polarized waves.

In the earlier work, the normalized cross section  $\sigma^\circ$  of the rough surface was expressed as the sum of two terms: a cross section  $\sigma_L^\circ$  due to large scale roughness describable by physical optics or geometric optics and a cross section  $\sigma_S^\circ$  due to small scale roughness describable by the perturbation method. In the present paper, Stokes polarization parameters are derived for each scale of roughness in terms of the scattering matrix elements and the surface roughness parameters. Then, assuming the two scales of roughness are entirely statistically independent, the Stokes parameters may be summed to give the polarization characteristics of the composite surface. Also, the Mueller scattering matrix for a rough surface with two scales of roughness is presented. The Stokes parameters may then be used to derive the degree of polarization and the parameters of the polarization ellipse of the scattered waves. Finally, the waves are received at the antenna which is designed to accept elliptically polarized signals.

Results are presented for the amount of polarized and unpolarized diffuse power received by the antenna as a function of antenna polarization parameters, bistatic scattering geometry, surface dielectric constant and surface roughness. Four terrain types are studied: rural dry, rural wet, salty sea and forest canopy. The effectiveness of an elliptically polarized receiver in rejecting clutter is compared to a linearly polarized receiver. The general conclusion is that the minimization technique for elliptically polarized conditions is more effective than that restricted to linear polarization states. Also, a more general technique for optimization is presented which involves varying the polarization of both the transmitter and receiver.

B3-2  
1400

## SCATTERING FROM ROUGH SURFACES

John A. DeSanto

Department of Mathematical and Computer Sciences  
Colorado School of Mines  
Golden, CO 80401

We present computational results for scattering from rough surfaces. All the results are for the Dirichlet boundary value problem and one-dimensional surfaces  $s(x)$ . Electromagnetically this corresponds to TE-polarization.

The first set of results describe the reconstruction of rough-surface profiles from scattered field data. Two methods are presented. Both use the spectral-coordinate approach. The first is based on perturbation theory and is valid when  $|k \cos(\theta_s) s(x)| \ll 1$ , where  $k$  is wavenumber and  $\theta_s$  the scattering angle. The second is based on the Kirchhoff approximation for the normal derivative of the total field on the surface. Using a combination of incident and scattered angles we develop a Fourier transform relation between the scattered data and the surface profile. Both results are FFT-based, and both reconstructions work for only shallow surfaces.

The second set of results is based on ensemble average results for homogeneous Gaussian distributed random surfaces. We illustrate two conclusions. They are (1) the coherent specular intensity is predominantly single scattering even when multiple scattering occurs, and (2) beyond a certain roughness the predominant field in the specular direction is incoherent rather than coherent.

B3-3  
1420

SMOOTHING AND THE COMPOSITE SURFACE MODEL FOR  
ROUGH SURFACE SCATTERING  
Gary S. Brown, Bradley Dept. of Electrical Engineering  
Virginia Polytechnic Institute and State University  
Blacksburg, VA 24061-0111

The composite model for scattering by randomly rough surfaces is the only asymptotic result for surfaces having both small and large wavelength features relative to the incident electromagnetic wavelength. It is essential to understand the importance of both the amplitude and wavelength of the surface height spectral components in this model. The scattering from the long wavelength features of the surface is dealt with using the Kirchhoff approximation while the small wavelength components are assumed to be amenable to boundary perturbation approach. While this basic model has been most useful, it also suffers from some rather serious shortcomings. Most prominent among these is the restriction to small surface slopes, both for the large and small scale features on the surface. Since this constraint may be violated, it is highly desirable to develop a new approach which will overcome this limitation. Such is the goal of the research reported in this paper.

The technique chosen here is the normalized first order smoothing (NFOS) approximation. The essence of the method is as follows. The magnetic field integral equation for the current induced on the perfectly conducting rough surface is first normalized by the height dependent phase factor contained in the Born or source term. This has the effect of eliminating the very high attenuation of the coherent part of the current by this phase factor. As a result, first order smoothing can be used to approximate the fluctuating part of the current and the normalization can be reintroduced after the application of smoothing. Another way to view this normalization scheme is to note that it puts nearly all of the functional dependence in the kernel or propagator in the integral equation for the normalized current. Using the NFOS approximation alone, however, is not sufficient to model all of the desired surface effects. We show how the basic integral equation can be split into the parts that are dominated by the small scale structure and the large scale structure. We then demonstrate that the slopes of the large scale part of the surface can be arbitrary because these slopes only tilt the small scale waves and this tilting has only a geometric effect on the scattering by the small scale structure. It is also shown how shadowing by the large scale surface structure comes into play in this formulation.

B3-4      BREWSTER ANGLES FOR BI-ISOTROPIC  
1440      (NONRECIPROCAL CHIRAL) INTERFACE

I.V. Lindell, A.H. Sihvola, A.J. Viitanen  
Electromagnetics Laboratory  
Helsinki University of Technology  
Otakaari 5A, Espoo SF-02150 FINLAND

Chiral media have raised interest in recent years because of their extra parameter over the isotropic medium, allowing more freedom in the design of man-made materials for electromagnetic purposes. More general, actually most general, isotropic media are called bi-isotropic (BI) or nonreciprocal chiral, whose constitutive equations can be written in the form

$$\mathbf{D} = \epsilon \mathbf{E} + (\chi - j\kappa) \sqrt{\mu_0 \epsilon_0} \mathbf{H},$$

$$\mathbf{B} = \mu \mathbf{H} + (\chi + j\kappa) \sqrt{\mu_0 \epsilon_0} \mathbf{E}.$$

where all medium parameters are real for lossless media. The parameters  $\kappa$  and  $\chi$  have definite physical meaning for a plane-wave propagating in the BI medium. The chirality parameter  $\kappa$  gives the rate of polarization rotation when compared with the phase angle of plane wave propagating in free space. The Tellegen parameter  $\chi$  is related to the angle between linearly polarized electric and magnetic field vectors, which are orthogonal only for  $\chi = 0$ .

In the present paper, reflection and transmission at the air-BI interface is considered in more detail. Reflection and transmission dyadics are determined. From the reflection dyadic we find the eigenpolarizations and eigenvalues. The condition for an eigenvalue to vanish is studied and expressions for the corresponding Brewster angles are derived, which seem to be new even for the special case of air-chiral interface. It is seen that, unlike for isotropic media, there exist two Brewster angles for certain BI media. Also, it can be seen that, for certain BI media, there exist 'cross-polarization Brewster angles' for which one of the cross-polarized reflections vanishes. This effect does not exist for reciprocal chiral (Pasteur) media or nonreciprocal nonchiral (Tellegen) media.

B3-5  
1500**ALGORITHM FOR CHARACTERISTICS THEORY  
SOLUTION OF MAXWELL'S EQUATIONS  
IN ANISOTROPIC MEDIA**E. Bleszynski<sup>†</sup> M. Bleszynski\* and W. Hall\*<sup>†</sup> North American Aircraft, Rockwell International Corporation  
P.O. Box 92098, Los Angeles, Ca 90009\* Science Center, Rockwell International Corporation  
P.O. Box 1085, Thousand Oaks, Ca 91360

*We developed an algorithm for solving Maxwell's equations in anisotropic media within the framework of the theory of characteristics. We constructed general expressions for the fluxes at the interface between two anisotropic media from Riemann invariants.*

One of the approaches for solving time dependent Maxwell's equations in the partial differential form is the method of characteristics. The method is based on representing Maxwell's equations in the curvilinear ( body-fitted) coordinates  $(\xi, \eta, \zeta)$  in the conservation law form (V. Shankar et al., Proc. of the 9-th Computational Fluid Dynamics Conference, Buffalo 1989)

$$\partial |Q\rangle / \partial \tau + \partial |E\rangle / \partial \xi + \partial |F\rangle / \partial \eta + \partial |G\rangle / \partial \zeta = |S\rangle.$$

Here  $|Q\rangle \approx (D, B)$  is the known six dimensional "state vector",  $|E\rangle$ ,  $|F\rangle$  and  $|G\rangle$  are the "fluxes" constructed from the components of  $H$  and  $E$  fields tangential to the  $\xi = \text{const}$ ,  $\eta = \text{const}$  and  $\zeta = \text{const}$  surfaces respectively, and  $|S\rangle$  is the "source" vector. The unknown state vector  $|Q(\tau + \Delta\tau)\rangle$  is evaluated at the center of each computational cell, from the knowledge of the fluxes at the cell interfaces. Hence the accurate evaluation of the fluxes plays an essential role in the algorithm. The interface fluxes are obtained by using the characteristics theory of partial differential equations.

We extended the method of characteristics to solve Maxwell's Eqs. in anisotropic media. The approach can be schematically characterized by the following steps. To evaluate flux  $E$  associated with the interface between two computational cells perpendicular to  $\hat{\xi}$  (analogous procedures hold for the fluxes associated with cell faces perpendicular to  $\hat{\eta}$  and  $\hat{\zeta}$ ), the eigenvalues and the eigenvectors spanning the 6-dim space of the Jacobian operator  $A = \partial |E\rangle / \partial |Q\rangle = \hat{\xi} \times \begin{pmatrix} 0 & -\epsilon^{-1} \\ \mu^{-1} & 0 \end{pmatrix}$ , where  $\epsilon$  and  $\mu$  are permittivity and permeability tensors, are found. Subsequently, the fluxes on each side of the interface are expanded in the space spanned by the eigenvectors. Since two of the eigenvalues are equal 0 and the fluxes do not depend on the eigenvectors corresponding to zero eigenvalues, only four expansion coefficients are needed to determine the flux on each side of the interface. These coefficients are determined by the theory of characteristics as well as by the appropriate boundary conditions. From the theory of characteristics (S. Whitham, Linear and Nonlinear Waves, J. Wiley, 1978) it follows that the expansion coefficients multiplying eigenvectors related to positive (negative) eigenvalues remain constant in a wave propagating in the positive (negative)  $\hat{\xi}$  direction. This property introduces four relations between the expansion coefficients. The remaining four coefficients are determined from the boundary conditions imposed on the tangential components of the fields on both sides of the interface.

B4-1  
1540**ELECTROMAGNETIC SCATTERING BY AN  
ARBITRARILY SHAPED BODY WITH AN  
ANISOTROPIC IMPEDANCE BOUNDARY CONDITION**Allen W. Glisson\*  
Department of Electrical Engineering  
University of Mississippi  
University, MS 38677Mark Orman, Frank Falco, and Donald Koppel  
Riverside Research Institute  
330 West 42nd Street  
New York, NY 10036

The impedance boundary condition (IBC) relates the tangential electric and magnetic fields at the surface of a scatterer through a simple impedance relationship. When the IBC approximation is valid, it can significantly reduce the computational effort required in the numerical solution of electromagnetic scattering problems. The impedance boundary condition has been previously implemented and validated for the electric field integral equation in a version of the triangular-patch code for modeling electromagnetic scattering from arbitrarily shaped bodies.

In this work we present the implementation of the IBC in the triangular-patch scattering code for an anisotropic surface impedance. To facilitate the implementation of the anisotropic IBC, two orthogonal unit vectors  $\hat{a}_1$  and  $\hat{a}_2$  are defined within each triangular face in the patch model. The orientation of the first unit vector may be chosen arbitrarily for each face. The second unit vector is defined by  $\hat{a}_2 = \hat{n} \times \hat{a}_1$ , where  $\hat{n}$  is the outward-directed unit surface normal for the face. The anisotropic IBC surface impedance dyadic may then be written for each face as

$$\underline{Z}_s = Z_{11}\hat{a}_1\hat{a}_1 + Z_{12}\hat{a}_1\hat{a}_2 + Z_{21}\hat{a}_2\hat{a}_1 + Z_{22}\hat{a}_2\hat{a}_2$$

The moment matrix contributions for the anisotropic IBC terms are developed and singularity analyses of these terms are performed to permit the field point to be very near the source triangle.

Numerical results are presented for thin plate and body of revolution geometries. The numerical results are validated through self-consistency checks and by comparison with numerical results obtained with a body of revolution model for the anisotropic impedance boundary condition. A Weston theorem check is also presented for a pyramid geometry having an anisotropic surface impedance with a mean value of unity.

B4-2 SCATTERING BY ROTATIONALLY SYMMETRIC BODIES  
1600 WITH ARBITRARILY VARYING SURFACE IMPEDANCE

S. F. Kawalko, S. R. Laxpati<sup>(\*)</sup> and P. L. E. Uslenghi  
Department of Electrical Engineering and Computer Science  
M/C 154  
University of Illinois at Chicago  
P. O. Box 4348, Chicago IL 60680

The scattering of a linearly polarized and obliquely incident plane electromagnetic wave by a body that is rotationally symmetric along the axis and has an impedance surface is studied in this paper. The impedance on surface is allowed to vary arbitrarily along both the axial and azimuthal directions. Impedance bodies of revolution with axial impedance variation and an axially incident plane wave have been previously studied by Graglia and Uslenghi [IEEE Trans. Antennas and Propagation, Vol. 36, No. 9, pp.1313-17, September 1988.]

The formulation of the problem is in terms of generalized Maue integral equations for the surface currents on the body. Integral equations of both electric and magnetic field type are derived for the vector electric surface current density. These equations are solved numerically via moment method procedure using isoparametric elements.

In the cylindrical coordinates  $(\rho, \phi, z)$ , the generating curve for the scatterer is described in its parametric form by two functions  $\rho(s)$  and  $z(s)$ , where  $s$  is the arc length. This form makes it possible to define uniquely a point on the surface even for a complex shaped body and permits the mapping of the surface of the scatterer into a rectangular region in the  $s$ - $\phi$  plane. This region is then subdivided into smaller rectangular regions (surface patches). The electric surface current density on the patches is represented by two-dimensional Hermitian expansion functions. The choice of the expansion functions allows one to represent surface currents which may be discontinuous or may have discontinuous derivatives. Furthermore, the Dirac delta function as testing function (collocation) may be used in moment method to transform the integral equations into a matrix equation.

The matrix is inverted to obtain the coefficients of the expansion function at each node and consequently the surface electric current density. The far scattered fields are then derived in terms of this current density and the integrals are evaluated numerically. Both back scattered and bistatic fields are calculated in the form of RCS.

The computer code is written in Fortran 77 and structured to allow addition of geometry modules to define a specific scatterer and its surface impedance. The code is tested and validated for several simple shapes such as a sphere, a cone-sphere and a cone-cylinder-sphere with rotationally symmetric impedance boundary and axially incident plane wave, which are available in the literature. Results for some of these geometries and with an obliquely incident plane wave are presented.

B4-3 INCREMENTAL LENGTH DIFFRACTION COEFFICIENTS FOR AN  
1620 IMPEDANCE WEDGE OF ARBITRARY INTERNAL ANGLE

Hasnain H. Syed and John L. Volakis  
Radiation Laboratory  
Dept. of Electrical Engineering and Computer Science  
University of Michigan  
Ann Arbor, MI. 48109-2122

Incremental length diffraction coefficients(ILDCs) are presented for computing the scattering by a finite length impedance wedge of arbitrary angle. These are based on an approximate dyadic diffraction coefficient which was recently constructed from the known skew incidence impedance half plane solution whose faces can satisfy different impedance boundary conditions (Syed and Volakis, 1989 *IEEE/AP-S Symposium Digest*, pp. 1286-1289; also see paper to appear in *Electromagnetics*, 1992). Exact skew incidence diffraction coefficients for impedance wedges are only available for three internal wedge angles and the derived approximate diffraction coefficient has been shown to numerically agree with these specialized analytical solutions before its use in this application.

The derived ILDCs have been implemented in a standard general purpose Physical Theory of Diffraction(PTD) code and results will be presented which demonstrate the accuracy of the formulation for a number of impedance and (dielectrically) coated structures. These will include typical shapes such as plates, finite length cones and cylinders or other more complex hard bodies which have been partially or fully coated. It will be shown that the computed co-polarized scattering patterns are in good agreement with measured and/or numerically obtained data within, of course, the limitations of the first order PTD formulation. In the case of the cross-polarized patterns, some improvements are required which will be discussed along with other additions to the PTD code.

B4-4  
1640

SCATTERING BY DIELECTRIC-COATED SUPER-  
QUADRIC CYLINDERS USING HIGHER-ORDER  
IMPEDANCE BOUNDARY CONDITIONS

D. J. Hoppe and Y. Rahmat-Samii  
Department of Electrical Engineering  
University of California at Los Angeles  
Los Angeles, CA 90024-1594

In this paper scattering by two dimensional PEC cylinders with lossy dielectric coatings is examined. Dielectric coated superquadric cylinders are chosen as representative canonical examples. These cylinders, which include circles, ellipses, rectangles, and squares as special cases, are chosen in order to examine the effects of finite radii of curvature on the accuracy of the approximate boundary conditions. The case of H polarization is considered in detail, the case of E polarization can be handled similarly.

Higher order impedance boundary conditions, (HOIBC), involving derivatives of the tangential field components, are derived for the dielectric coating using a spectral formulation. After exact impedance boundary conditions are derived for each spectral component, the impedance terms are approximated as a ratio of polynomials. These approximate boundary conditions in the spectral domain are then transformed into the spatial domain using elementary properties of the Fourier transform. This formulation, which may be applied to more complicated coatings, such as chiral coatings, ferrite coatings, etc., includes the Simple Impedance Boundary Condition (SIBC), and the Generalized Impedance Boundary Conditions (GIBC), as special cases. It is applicable to three dimensional as well as two dimensional examples.

Differential and integral equations based upon the approximate boundary conditions are derived, and solved by the method of moments. Spline functions are chosen as expansion functions for the currents, and pulse functions for the testing functions. In addition, a rigorous method of moments solution which accounts for the coating exactly is formulated. For this solution Galerkin's method, and triangle expansions are employed.

Both computer programs are validated by considering the special case of dielectric-coated circular cylinders, for which series solutions exist. Next computations of bistatic and monostatic radar cross section, using the approximate boundary conditions, simple impedance boundary conditions, and the rigorous method of moments solution, are presented for a number of superquadric cylinder examples. These examples illustrate the increased accuracy of the higher order impedance boundary conditions relative to the simple impedance boundary conditions. Further examples point out the limitations of the approximate boundary conditions.

C3-1  
1340

BOUNDS FOR CONVOLUTIONAL PROJECTION CODE

Dong Li\*  
Dept. of Elec. Eng.  
City College of New York

Gang Yang  
Dept. of Elec. Eng.  
City College of New York

Donald L. Schilling  
Dept. of Elec. Eng.  
City College of New York

Abstract

Generating function techniques for analyzing the error event and the bit-error probabilities for convolutional Projection code is considered. For a small constraint length convolutional code, one can use Viterbi's state-diagram technique to obtain the generating function. A typical convolutional Projection code has a constraint length of 56. The state-diagram technique cannot be used to obtain the generating function because of the extreme large number of computation involved. A new technique called the state equation calculation is developed to handle such large constraint length convolutional Projection code. Several examples using the new technique to obtain the generating function are presented. A convolutional P3 rate 1/2 code's generating function is calculated by a computer program devised specially for the P3 convolutional Projection code utilizing the new technique. The bit error probability upper and lower bounds are compared with the probability of error obtained by simulation.

---

This research represents a portion of the dissertation submitted to the faculty of the school of Engineering of the CUNY in partial fulfillment of the requirements for the Ph.D in EE.

C3-2  
1400

## **AN ANALYSIS OF THE CPMFSK SCHEME WITH ADAPTIVE THRESHOLD DETECTION (ATD)**

Nader Bolourchi  
Department of Engineering Technology  
New York Institute of Technology  
Old Westbury, NY 11568

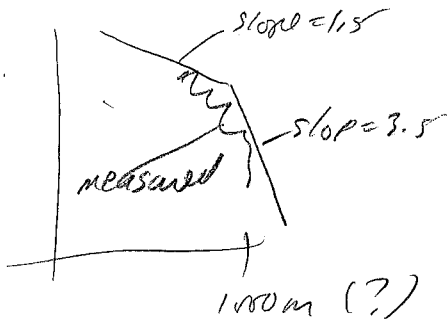
Donald L. Schilling  
Department of Electrical Engineering  
City College of New York  
New York, NY 10031

### **Abstract**

An adaptive threshold detection (ATD) technique for the continuous phase multiple frequency shift keying (CPMFSK) is proposed to compensate for intersymbol interference (ISI) caused by bandlimiting predemodulation filter. The system performance is compared with the conventional CPMFSK demodulation utilizing noncoherent detection. Computer simulation results show significant improvement in the bit error probability (BER)

C3-3 CDMA OVERLAY IN THE 1850-1990 MHz BAND: R. Pickholtz, D.L.  
1420 Schilling, and L.B. Milstein

Somebody from GW filled in  
It works.



Run microwave system as low as power  
as can and set  $10^{-6}$  BER

as long as BER  $> 10^{-5}$  we say no  
interference has occurred.

add CDMA users then  
a notch filter for a co-channel  
narrowband user can be used,

Currently 7 users/cell  
3 mile cells

Suppress carrier during no activity,  
Could have 23, 17, 269 users in  
Houston, Orlando, + NK, resp.

Buildup in NK help

Goes up as add notch filter  
and voice activity detection,

C3-4 STATE TRANSPARENT CONVOLUTIONAL CODES: H.R. Sarrafzadeh and A.K.  
1440 Kakaes

E2-1  
1400

**A UNIFIED TOPOLOGICAL APPROACH TO  
ELECTROMAGNETIC ENVIRONMENTS (EME)  
PROTECTION**

J. Philip Castillo, George Baker, DNA  
Logicon R & D Associates  
P. O. Box 9377  
Albuquerque, NM 87109-9377

This paper presents an approach to the potential unification of protection technology for a wide spectrum of electromagnetic environments (EME). Of particular interest is the development of consolidated protection practices for complex electronic systems. An electromagnetic topological approach will be utilized to develop a consistent shielding protection methodology. Initially, applicable electromagnetic topological techniques will be presented. Next the characteristics of the various EME, for electromagnetic sources both internal and external to the system, will be related. The EME under consideration in this paper include the following:

- EMI/EMC (Electromagnetic Interference/Compatibility)
- LEMP (Lightning Electromagnetic Pulse)
- NEMP (Nuclear EMP)
- HPM (High Power Microwaves)
- UWB (Ultra-Wide-Band)

Existing protection practices will then be discussed. Incompatibilities and suggested remedies among these practices will be included. Finally, a generalized topological approach and the basic technological needs for applying the unified approach will be presented.

E2-2 SPECIAL CONSIDERATIONS FOR  
1420 LIGHTNING HARDENING  
R. L. Gardner, Lt Col  
Phillips Laboratory/WSE  
Kirtland AFB, NM 87117

When compared to other High Power Electromagnetic (HPE) effects, lightning has a high energy density and exerts high voltages over large distance. These characteristics demand special consideration when designing a means of hardening large systems to lightning.

Hardening to lightning effects requires the same topological hardening approach that is typically used for other electromagnetic effects. The outer shield, however, may not be solid for economic reasons. Penetration of that outer shield can occur through several different means. These means include diffusion, breakdown, restrike.

Since high currents phases of lightning last for microseconds magnetic fields can penetrate into shielded enclosures that might be secure for faster effects. Potentials of millions of volts occur regularly in lightning and must be considered in hardening because they can potentially breakdown air and cause currents to flow in interior conductors. Finally, the large, enduring fast rates of rise of lightning currents can produce large voltages that, in turn, can cause the lightning channel to strike the interior of the outer shield.

Quantitative examples of each are presented using a large umbrella-like structure as an example. Such umbrella-like structures are often used as outer shields for lightning protection of large structures.

E2-3  
1440**HIGH FREQUENCY ASYMPTOTIC LIMITS ON EM  
LEAKAGE INTO SHIELDED CABLES**David E. Merewether  
Logicon R & D Associates  
P. O. Box 9377  
Albuquerque, NM 87119-9377

To design systems that are hardened against the deleterious effects of external electromagnetic radiation it is desirable to know an upper bound on the power that could be received by an external conductor, and how much protection is obtained by replacing that conductor with an imperfectly shielded cable of known transfer impedance characteristics. While this is a very difficult prediction problem in general, at frequencies where the cable is much longer than a wavelength, yet still thin, it is possible to derive an asymptotic limit for the coupled power. This paper describes the formulation of the problem and its solution. Results are presented for common coaxial cables.

E2-4 A REVIEW OF MICROWAVE SOURCES ---  
1520 VIRCATORS, BWOs, MILOS, IREBs, AND  
MAGNETRONS  
Albert W. Biggs  
Phillips Laboratory/WSEA  
Kirtland Air Force Base NM 87117

When relativistic electron beams are injected into drift tubes in excess of the space-charge-limiting current, virtual cathodes are formed and electrons are reflected back to the accelerator. The unstable situation leads to electromagnetic radiation. Power levels exceeded 320 MW at 3.5 to 4.5 GHz.

Magnetrons are slow wave devices with interaction between electrons and electric fields in slow wave structures. Several magnetrons have been combined with phase locking techniques. One relativistic version of the linear magnetron is the magnetically insulated transmission line oscillator (MILO), where the magnetic field is created by the beam itself.

Other high power microwave sources are designed with modulated intense relativistic beams (IREBs), where the beams propagate through passive resonant cavities. Interaction between beams and cavities modulate the beams. The modulated beams are shaped by a second cavity. A third cavity extracts the beam energy and converts it into microwave energy.

Backward travelling wave oscillators (BWOs) are described in a discussion of relativistic multiwave Cerenkov generators developed by Bugaev and others.

E2-5        MATCHING MODULATED ELECTRON BEAM TO WAVEGUIDE  
1540        Carl E. Baum  
            Phillips Laboratory/WSEA  
            Kirtland AFB, New Mexico 87117-6008

A classical problem in generating electromagnetic fields in a closed perfectly conducting waveguide involves passing an electron beam modulated at some particular frequency through the guide. This paper discusses this problem in the context of an idealized sheet beam for which one can set up a simple boundary value problem for the  $H_{1,0}$  mode in a conventional rectangular waveguide. This applies to the case of power propagating away from the beam in one or both directions. For comparison to the idealized sinusoidal distribution of the electron beam across the wave guide, other distributions are considered for their relative effectiveness in exciting the lowest order waveguide mode.

The efficiency of conversion of electron-beam power to power in the  $H_{1,0}$  mode is maximized by matching the beam voltage (or electron energy in e. V.) to the line integral of the electric field in the mode while matching the current to the magnetic field. This affects the choice of height to width ratio of the rectangular guide, or equivalently the choice of the beam parameters to match desired waveguide dimensions.

The electron beam, even though with relativistic electron speeds, takes a non-trivial time to propagate across the waveguide height, thereby reducing the effectiveness of coupling to the waveguide mode. This effect can be reduced by introduction of conducting sheets perpendicular to the  $H_{1,0}$  electric field ( parallel to the magnetic field). This can be used to maintain an effective open circuit on one side of the beam (feeding a shorted quarter-wave section). On the other side the guide can be bent to match the phases of the modes on each part of the subdivided waveguide by the different lengths of the subguides.

E2-6 **REFLECTOR ANTENNA CHALLENGES FOR HPM APPLICATIONS**  
1600 Y. Rahmat-Samii, D.W. Duan and B. Hoshmand  
Electrical Engineering Department  
University of California Los Angeles  
Los Angeles, CA 90024-1594

Applications of different antenna systems to produce directive High Power Microwave (HPM) radiations are reviewed. The overall system architecture of a reflector antenna configuration from the source, waveguide, and feeds to the reflector antennas is presented. The key design issues are summarized and, novel synthesis/analysis techniques, based on the applications of the newly developed diffraction optimization synthesis techniques, are highlighted. Representative design concepts are presented for an optimized dual shaped reflector antenna system in order to maximize the antenna performance for a given feed configuration including the air breakdown issues. Additionally, representative results will be shown for the transient behavior of the radiated field by utilizing a novel frequency-domain/FFT algorithm.

F2-1  
1400

## **REMOTE SENSING OF THE EVAPORATION DUCT USING AN X-BAND RADAR**

Kenneth D. Anderson

Ocean and Atmospheric Sciences Division, Code 543

Naval Ocean Systems Center

San Diego, CA 92152-5000

Results from an analytical and experimental effort to assess low-altitude, short-range propagation effects over the ocean are presented. On the experimental side, an X-band radar has been installed at NOSC to measure signal return from a set of calibrated targets which are carried on a high-speed ocean-going boat. In addition, surface and upper air meteorological sensors are used to measure the ducting conditions. On the analytical side, the NOSC Radio Physical Optics (RPO) model is used to predict propagation loss from measured ducting conditions for comparison to the measured propagation loss.

Although the measurement program is in its early phases, results indicate that a correction is needed to the meteorological formalism describing the evaporation duct refractivity profile. This correction is concerned with the refractivity gradients above the evaporation duct height that control the field strength at ranges near the horizon. For example, in a thermally neutral atmosphere, a standard gradient (0.118 M/m) is reached at a height of 17.8 times the evaporation duct height. Radar measurements clearly indicate that the height where the gradient should be near standard is on the order of twice, or less, the evaporation duct height for certain cases.

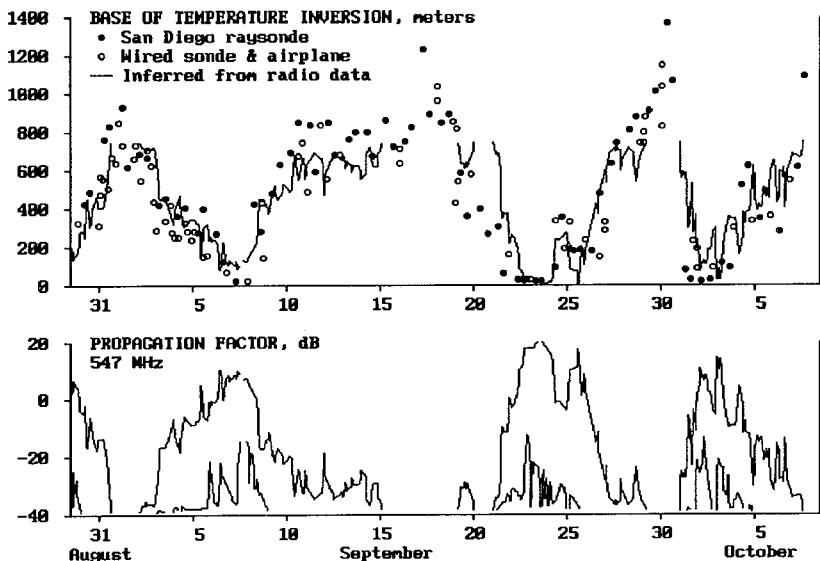
Remote sensing of the evaporation duct with a radar in conjunction with advanced numerical modeling capabilities may lead to a better understanding of atmospheric boundary layer physics.

F2-2  
1420**REMOTE SENSING OF REFRACTIVITY STRUCTURE BY  
DIRECT RADIO MEASUREMENTS AT UHF**Herbert V. Hitney  
Tropospheric Branch, Code 543  
Naval Ocean Systems Center  
San Diego, CA 92152-5000

A method is presented that allows the base of a trapping layer to be determined directly from observations of UHF signal strength on a path in the southern California coastal area. The method uses long-term statistics of trapping layer thickness and refractivity gradient in the area. These statistics are used to compute radio signal strength as a function of the base height of the trapping layer using the Naval Ocean Systems Center (NOSC) Radio Physical Optics (RPO) propagation model. RPO is a range-dependent hybrid model that combines the complementary strengths of ray optics methods at higher angles with parabolic equation methods at lower altitudes.

Refractivity statistics were derived by fitting three linear segments to modified-refractivity-versus-height profiles derived from 261 radiosonde measurements taken at NOSC over a 7 year period. The median thickness and strength of all the trapping layers are 130 meters and 30 M units, respectively.

The radio path is an over-water 148 km path with transmitter and receiver both located 30 m above sea level. The RPO results are used to infer the trapping layer base height directly from observations of received signal strength. This method has been applied to a 40-day period of continuous signal strength recordings during which the trapping layer base height was known to vary from near zero to about 1000 meters. Inferred base height versus time is compared to direct meteorological measurements of the base of the temperature inversion in the area of the measurements, as shown in the figure below.



F2-3 MEASURING HUMIDITY GRADIENTS AND REFRACTIVE INDEX  
 1440 GRADIENTS ALOFT WITH A SURFACE-BASED CLEAR  
 AIR SENSING RADAR--A STATUS REPORT

by

Earl E. Gossard  
 CIRES, Univ. of Colorado, Boulder, CO 80309  
 (303) 492-1113

Theoretically a surface based, clear-air Doppler radar can measure humidity ( $Q$ ) gradients and R.I. ( $n$ ) gradients aloft under stably stratified conditions in the atmosphere. Reliable measurements of backscattered power (to get  $C_n^2$ ) and Doppler spectrum width (to get  $C_w^2$ ) are required, where  $C_n^2$  and  $C_w^2$  are the structure parameters of refractive index ( $n$ ) and the vertical component of turbulent velocity ( $w$ ). In terms of the potential temperature ( $\theta$ ) gradient (measurable with RASS), the theoretical expressions are: (Gossard and Sengupta, 1988):

$$\frac{\partial \phi}{\partial z} = C_r \left( C_1 \frac{g}{\theta} \frac{\partial \theta}{\partial z} \frac{C_n^2}{C_w^2} \right)^{1/2}$$

$$\frac{\partial Q}{\partial z} = \frac{1}{b} \frac{\partial \phi}{\partial z} + \frac{a}{b} \frac{\partial \theta}{\partial z}$$

where

$$\phi = \frac{77.6 P_r}{\theta} \left[ 1 + \frac{7.73 Q}{\theta} \right], \quad \theta = T \left( \frac{P_r}{P} \right)^{0.286}$$

$$a = (77.6 P_r / \theta) (1/\theta + 15.46 Q/\theta^2)$$

$$b = 77.6 P_r (7.73/\theta^2)$$

and where

$\phi = N(P_r/P)^{0.714}$ ,  $N = (n-1) \times 10^6$ ,  $P$  is pressure (mb),  $P_r = 1000$  mb  $C_r = -1$  is the temperature-R.I. correlation coefficient,  $C_1$  is a factor near unity,  $Q$  is specific humidity ( $g \text{ kg}^{-1}$ ),  $\theta$  is potential temperature ( $^{\circ}\text{K}$ ). Using RASS to measure  $\partial \theta / \partial z$  the gradients of  $Q$  and  $N$  may be calculated. The primary obstacles are: 1) lack of controlled tests of the accuracy of  $C_w$  calculated from Doppler spectrum second moments, 2) the difficulty of eliminating contaminating effects of unwanted targets such as insects and especially clouds without going to low frequencies where narrow beams are expensive, 3) the lack of a suitable low frequency ( $\sim 200$  MHz) facility to test the concept adequately.

Gossard, E.E. and N. Sengupta, 1988: Measuring gradients of meteorological properties in elevated layers with a surface-based Doppler radar, *Radio Science*, 23, 625-639.

F2-4  
1520

POLARIMETRIC SIGNATURES IN THE STRATIFORM REGION OF  
A MESOSCALE CONVECTIVE SYSTEM  
D.S. Zrnic, N. Balakrishnan, C.L. Ziegler, V.N.  
Bringi and K. Aydin  
National Severe Storms Laboratory  
1313 Halley Circle

Four polarimetric measurands were collected in the stratiform region of a Mesoscale Convective System. The four are the reflectivity factor, the differential reflectivity, the correlation coefficient between orthogonal co-polar echoes and the differential propagation constant. Most striking is a signature of large aggregates (about 10 mm in size) seen in the differential phase through the melting layer. Another significant feature is an abrupt notch in the correlation coefficient that occurs towards the bottom of the bright band. One dimensional model and aircraft observation are used to explain some polarimetric measurements and to infer the presence of graupel. These unique observations and modeling provide inferences concerning the presence of graupel and the growth of large aggregates in the melting layer.

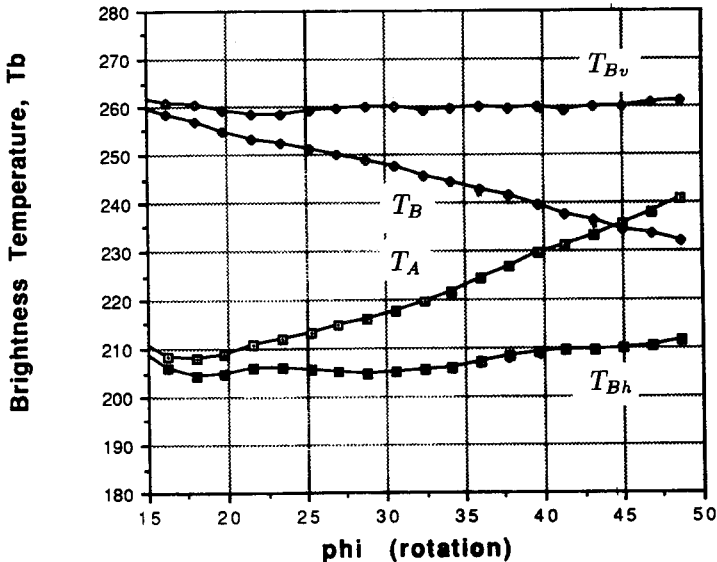
F2-5  
1540

## Laboratory Demonstration of Electronic Polarization Basis Rotation

A.J. Gasiewski, D.B. Kunkee  
School of Electrical Engineering  
Georgia Institute of Technology  
Atlanta GA, 30332-0250

Laboratory observations using a conically-scanned 90-GHz Dicke-switched dual-polarized radiometer have been used to verify the theory and the potential advantages of Electronic Polarization Basis Rotation (EPBR). Using EPBR, an estimate of the vertically and horizontally polarized brightness temperatures ( $T_{Bv}$  and  $T_{Bh}$ ) is derived from two arbitrarily oriented orthogonal linearly-polarized feedhorn modes ( $T_A$  and  $T_B$ ) and a third signal representing the correlation of their in-phase amplitudes ( $T_U$ ). These are the first three Stokes parameters. Inclusion of the correlation channel is paramount for maintaining an accurate estimate of  $T_{Bv}$  and  $T_{Bh}$  over a full scan range, particularly when observing polarized radiation.

Near-Brewster angle scans of a fresh water surface have shown that  $T_{Bv}$  and  $T_{Bh}$  can be accurately recovered over the full range of scan angles. Moreover, the hardware modifications to a dual-polarized radiometer necessary for implementing EPBR are minimal. The correlation signal is derived by summing the phase-equalized IF signals from each feedhorn mode and subsequent square-law detection.



F2-6            MEASUREMENT OF RADIAL VELOCITIES OF  
 1600            OCEAN WAVES WITH TWO-ANTENNA SAR'S  
                  Andrew S. Milman  
                  8655 Warner Rd  
                  Saline, MI 48176  
                  313-429-4302

A synthetic aperture radar (SAR) with two or more antennas can be used to measure the radial velocity of the ocean surface (R. M. Goldstein *et al.*, *Science*, 246, 1282-1285, 1989). The performance of such a system depends, *inter alia*, on the separation of the antennas; there is an optimum separation between the antennas that depends on the speed of the SAR and the coherence time of the surface.

The radar system contains a single transmitting antenna and two receiving antennas that are separated by a distance  $2B$ , with the two antennas displaced in the direction that the radar moves. This is the equivalent of having two different SAR's separated by a distance  $B$  that view a scene at two times separated by  $\tau = B/v$ , where  $v$  is the speed of the radar. If the scene being viewed is stationary, the two SAR images will be the same; if some part moves, its phase will differ in the two images by  $\Delta\phi = u_r\tau/\lambda$ , where  $u_r$  is the radial velocity and  $\lambda$  the electromagnetic wavelength.

The entire surface of the ocean is moving randomly. Let  $z(x,y,t)$  be the height of the surface at position  $(x,y)$  and time  $t$ . As far as SAR imaging is concerned, the surface is decorrelated when

$$\Phi_z(\tau) \equiv \langle [z(x,y,t) - z(x,y,t+\tau)]^2 \rangle^{1/2} \geq \pi\lambda/8,$$

where  $\langle \cdot \rangle$  denotes the average value and  $\lambda$  is the electromagnetic wavelength. Define the correlation time  $\tau_c$  by  $\Phi_z(\tau_c) = \pi\lambda/8$ , which implies an rms phase error at the SAR of  $\pi/4$  radians. When  $\Phi_z \geq \Delta\phi$ , the phase information needed to estimate the radial velocity is lost. Note how  $\tau_c$  depends on  $\lambda$ .

Our analysis shows that the optimal separation of the two antennas is

$$B_{opt} = \frac{v\tau_c}{\sqrt{2\pi}}.$$

Since  $\tau_c$  is proportional to  $\lambda$ , so is  $B_{opt}$ . Increasing the separation beyond this optimum will increase the noise in the radial-velocity measurement exponentially.

G3-1  
1340

**COHERENT OR INCOHERENT SCATTERING  
FROM CHARGED DUST PARTICLES. POSSIBLE  
APPLICATION TO PMSE?**

T. Hagfors  
NAIC, Department of Astronomy  
Cornell University  
Ithaca NY 14853

Observations of enhanced polar mesospheric summer echoes (PMSE) (Röttger et al., *Radio Science*, **25**, 671-687, 1990) has lead to speculations that the cause of these echoes is due to the presence of highly charged dust grains attracting a cloud of electrons each capable of scattering coherently (Havnes et al., *JATP*, **52**, 637-643, 1990).

This note discusses the application of the superposition of dressed particle concept to the problem of the electron density fluctuations in a plasma with embedded, charged dust grains. It is shown that the dressed particle approach breaks down when the dust grain separation  $r_d$  and the charge  $Z$  become large, and that the scattering cross section then may indeed be strongly enhanced. When a large fraction of the charge is carried by the dust grains, and the dust-Debye length is larger than  $r_d$  the usual incoherent scatter formulas for the scattering apply, and the enhancement associated with the dust becomes insignificant.

The criteria for the transition from one regime to the other are established and applied to the specific problem of scattering of electromagnetic waves from the polar mesopause. The calculations show that it is unlikely that the presence of dust grains alone, even when highly charged, can fully account for the observed enhanced PMSE. Some possible mechanisms which may act simultaneously to enhance the scattering are discussed.

G3-2  
1400**PLASMA LINE OBSERVATIONS IN THE AURORAL OVAL:  
STATISTICAL ANALYSIS OF SONDRESTROM DATA**C.E. Valladares  
Institute for Space Research  
Boston College  
885 Centre Street  
Newton MA 02159-1164

During the years 1985-1987 the Sondrestrom incoherent scatter radar made numerous detections of enhanced plasma lines. The bulk of these measurements were associated with auroral arc events. The hardware that was used consisted of a filter bank operating at 8 different frequencies. The filter bank was continuously cycled between the up and down shifted plasma lines. The ion line was also measured and several ionospheric parameters such as:  $N_e$ ,  $T_e$  and  $T_i$  were determined by our standard off-line processing package. Additional plasma parameters, such as the plasma wave temperature (PWT) and the plasma line enhancement level, were deduced after including the plasma line data in the analysis program. A great variety of ionospheric conditions and different characteristics of the precipitating particles (total number flux and peak energy) were observed during the experiments. This fact allowed the binning of data according to the total number flux being deposited into the ionosphere and the construction of altitude profiles of PWT. The altitude profiles of the binned PWT presented an almost exponential increase. The enhancement level of the plasma lines was, on some occasions, up to 200 times the thermal level. A computer model of the plasma line enhancement due to wave-particle interaction set by the flux of secondaries suggests that this mechanism is unable to increase the intensity of the plasma waves up to the level that was observed. Alternative mechanisms which may explain these results will also be discussed.

G3-3 DIGISONDE POLAR CAP CONVECTION STUDIES FOR  $B_z$  NORTH  
1420 AT QAANAAQ, GREENLAND

G. Crowley and B.W. Reinisch  
University of Massachusetts Lowell  
Center for Atmospheric Research  
Lowell, MA 01854

Paul S. Cannon  
Defense Research Agency, Aerospace Division  
Farnborough, Hampshire  
United Kingdom

Jurgen Buchau  
Phillips Laboratory/LIS  
Hanscom AFB, MA 01731

ABSTRACT

Controversy still exists regarding even the average ionospheric polar convection pattern when the IMF has a northward component. The Lowell Digisonde at Qaanaaq ( $87^\circ\text{N}$  CGL) measures the plasma flow in the central polar cap as a function of time. When the  $B_z$  north data are divided into separate data sets for  $B_y$  positive and  $B_y$  negative, flow patterns evolve that suggest a multicell structure. Possible convection patterns that can be synthesized from the Digisonde observations are compared with the convection models of Zhu and Kau (1990), Potemra et. al. (1984), and the Heppner and Maynard (1987) distorted two-cell pattern.

G3-4  
1440

MEASUREMENT OF DRIFT VELOCITIES AT THE DUSK  
SECTOR MID-LATITUDE TROUGH

J.L. Scali and B.W. Reinisch  
University of Massachusetts Lowell  
Center for Atmospheric Research  
Lowell, MA 01854

and

J. Buchau  
Phillips Laboratory/LIS  
Hanscom AFB, MA 01731

ABSTRACT

Drift velocities measured at the high-latitude stations Goose Bay, Argentia and Millstone Hill are used to investigate the formation of the mid-latitude troughs in the dusk sector. The observations cover a period from January to June 1990 and the results indicate the existence of westward drift velocities of magnitudes comparable to the velocity of the earth's rotation, during trough formation. These drifts are part of the two cell convection pattern as implied by the stagnation theory of trough formation.

G3-5  
1520IONOSPHERIC PLASMA LINE MEASUREMENTS USING  
THE CODED LONG PULSE TECHNIQUE AT ARECIBO

Michael P. Sulzer  
Arecibo Observatory  
P. O. Box 995  
Arecibo, P. R. 00613  
Frank T. Djuth  
Geospace Corporation  
550 N. Continental Blvd., Suite 110  
El Segundo, CA 90245

Ionospheric photo-electron enhanced plasma line measurements have usually been made with filter banks or digital equivalents, or more recently with a chirp technique. Measurements made with the filter bank technique have severe altitude-frequency tradeoffs, while the chirp technique gives extremely fast measurements of the plasma frequency and its altitude gradient but only at a single point which matches the transmitted chirp. The limitations of these techniques are overcome by using a modern radar technique, the coded long pulse, and applying it to the plasma line much as one would the ion line, but sampling a much wider bandwidth. Recent improvements and cost reductions in digital sampling, computing and storage technology make it possible to apply this technique to a number of outstanding ionospheric problems. The initial use of this technique at Arecibo shows that it is capable of measuring electron density to an accuracy of .02% in about two seconds in the F region, potentially covering the entire altitude range at once. The technique has immediate applications to the measurement of HF induced irregularities in ionospheric modification experiments, of gravity wave oscillations in the E-region, of accurate electron densities in the F1 region to reduce the number of free parameters when fitting for molecular ions, and, when both up- and down-shifted measurements are made, of currents.

The initial measurements are limited by clutter from other ranges rather than system noise. We show that the clutter has a spectral shape that is wide compared to the signal and thus acts like random noise. The ionospheric gradient is the most important factor in determining the sensitivity of the technique.

G3-6  
1540**APPLICATION OF THE CODED LONG-PULSE  
RADAR TECHNIQUE TO IONOSPHERIC STUDIES AT  
ARECIBO OBSERVATORY**F. T. Djuth<sup>1</sup>, M. P. Sulzer<sup>2</sup>, J. H. Elder<sup>1</sup>, and H. C. Carlson<sup>3</sup><sup>1</sup>Geospace Research, Inc., 550 N. Continental Blvd., El Segundo, CA 90245<sup>2</sup>Arecibo Observatory, Arecibo, Puerto Rico 00613<sup>3</sup>Geophysics Directorate, Phillips Laboratory, Hanscom Air Force Base, MA 01731

Recently, the coded long-pulse radar technique described by Sulzer [*Radio Sci.*, 21, 1033-1040, 1986] was tested at Arecibo Observatory, Puerto Rico using photoelectron-enhanced plasma lines in the daytime ionosphere. The technique immediately proved to be a powerful diagnostic tool for studying natural ionospheric phenomena. Moreover, it can readily be applied to a variety of ionospheric modification experiments. Our initial observations indicate that extremely accurate measurements of absolute electron density (0.01 to 0.03 % error bars) can be achieved with an altitude resolution of 150 m and a temporal resolution of ~2 s. In addition, the technique provides information about electron density structure within a 150-m altitude cell and yields parameters from which the energy spectrum of suprathermal electrons (> 4 eV) can be deduced. Our initial measurements will be used to illustrate applications of the coded long-pulse technique to several aeronomic/ionospheric problems. These include studies of electron-gas thermal balance in the ionosphere, the detection of neutral waves in the lower thermosphere, investigations of ion composition in the F<sub>1</sub> region, determinations of inelastic scattering cross sections, examinations of irregularity processes responsible for radio wave scintillations, measurements of ionospheric currents, and verification of the magnetic field dependence of Langmuir wave damping. The technique is particularly well-suited to auroral investigations where good temporal and spatial resolution is often needed to map out electron density structures and determine electron energy distributions. In addition, it can be used to monitor small-amplitude electron density perturbations generated by Langmuir turbulence in HF modification experiments. The technique is also extremely valuable in chemical release experiments involving alkaline-earth metals (e.g., barium, calcium, and lithium). In the presence of sunlight, these atoms become photoionized thereby producing vast quantities of photoelectrons. The resulting photoelectron-enhanced plasma waves can then be used to probe the rapidly evolving ion cloud.

G3-7  
1600

## SEASONAL VARIATION IN METEOR BURST DIVERSITY GAIN

A.K. Shukla\*. Defence Research Agency, Farnborough, Hampshire, U.K.

The implementation of diversity techniques in meteor burst (MB) communications systems to reduce the effects of signal fading, and increase the signal throughput, has not been exploited to any great extent. This is in contrast to high frequency (HF) communication systems. Any reluctance has partly been due to the lack of experimental evidence quantifying the advantages of particular diversity configurations.

Shukla et al (1) have shown that uncorrelated signals, necessary for the implementation of MB diversity, can be obtained using spaced diversity with an antenna separation of  $10 \lambda$  at 37 MHz. The results showed that 40 % of all signals of duration  $\geq 0.75$  s experienced a correlation value of less than 0.6 after the first 0.25 s of signal decay. Signals not scattered from overdense or underdense trails, which were categorised as not known (NK) were found to be the most uncorrelated and, therefore, of greater potential advantage to a MB system incorporating space diversity. In this paper these results are reviewed.

The paper goes on to present preliminary results from a simulated MB broadcast system incorporating space diversity with a scanning combiner. Data collected in February and June when the occurrence of these NK signals are expected to be at a maximum and minimum respectively are examined as a function of signal threshold and optimum broadcast data block duration. The seasonal variation of the signal throughput improvement obtained using a scanning diversity system is reported.

## References

1. Shukla, A. K., Cannon, P. S., and Lester, M., 1991, "Spaced antenna diversity in temperate latitude meteor burst systems near 40 MHz: Variation of signal cross correlation coefficient with time". Submitted Rad. Sci.

G3-8  
1620**ON THE DERIVATION OF AN IMPROVED PARAMETER  
CONFIGURATION FOR THE DYNASONDE**

L-C Tsai, F T Berkey and G S Stiles (Utah State University, Logan, UT  
84322-4405)

The accuracy and ambiguities of the measurement of ionospherically reflected echoes depend on the transmitted pulse set pattern, the receiving array configuration, and the data analysis scheme. Building on earlier work carried out for the NOAA Dynasonde (Grubb, 1979) by Pitteway and Wright (1991), we use six phase parameters ( $\Phi_o$ ,  $\Phi_x$ ,  $\Phi_y$ ,  $\Phi_v$ ,  $\Phi_p$ , and  $\Phi_d$ ) to derive echo location, Doppler shift, and wave polarization. We use the method of least-squares to determine the accuracy and a 'zero-freedom' technique to derive the ambiguities associated with the phase parameters.

Three criteria can be specified which lead to an optimum design of the system parameters: a) the aliasing of the derived phase parameters must be equal to  $2\pi$ , which represents the minimum ambiguity; b) the relative confidence limit factors of the derived phase parameters should be as small as possible; c) there must be no aliasing of echo location. Various designs have been simulated by varying the array configuration, frequency pattern, the number of pulses per pulse set, and the number of parallel receivers and receiving dipoles, in order to find a configuration with minimal error. For a Dynasonde transmitting four pulses per set and using two receivers, the 'optimum' configuration consists of a square array, with crossed dipoles at each corner, and a transmitted pulse set with four different frequencies, each separated by  $\sim 8$  kHz. This configuration enables the aliasing of the derived phase parameters to be  $2\pi$  and the sum of the relative confidence limit factors of the six phase parameters to be a minimum.

Grubb, R. N., The NOAA SEL HF radar system (ionospheric sounder), NOAA Tech. Memo. ERL SEL-55, Space Environ. Lab., Boulder, CO, 1979.

Pitteway, M. L. V. and J. W. Wright (1991), Toward an optimum receiving array and pulse-set for the Dynasonde, in press Radio Sci.

G3-9  
1640

CAN X-RAY FLARES BE PREDICTED FROM IONOSONDE  
OBSERVATIONS ?

Adolf K. Paul  
7455 Brockway Drive  
Boulder, Colorado 80303

On March 25, 1981 the maximum electron density of the F-layer as observed at Brighton, Colorado dropped suddenly by approximately 25% within 30 minutes. Approximately 45 minutes after the start of the electron density decrease a solar X-ray flare ( X 2.0) occurred. The same relative change of the maximum density was observed simultaneously at White Sands, located approximately 1000 km south of Brighton. At both locations, corresponding changes of the height of the F-layer maximum and the MUF(3000) took place. Details of the observations will be presented and the potential relation to the X-ray flare will be discussed.

H2-1 PLASMA WAVE OBSERVATIONS DURING THE CRRES HIGH  
1400 ALTITUDE CHEMICAL RELEASES  
R. R. Anderson  
Department of Physics and Astronomy  
The University of Iowa  
Iowa City, IA 52242-1479

In January and February 1991 the CRRES project carried out eight releases of barium and lithium in the evening magnetosphere at geocentric distances from 1.5  $R_E$  to 6  $R_E$ . The release conditions ranged from high magnetic field, high plasma density, and cool temperatures deep in the plasmasphere to the low magnetic field, low density, and high temperatures in the outer magnetosphere. One release occurred right at the plasma-pause. A fascinating variety of emissions were detected by the CRRES Plasma Wave Experiment receivers connected to a long-wire electric dipole antenna and a search coil magnetometer. A low-frequency burst of electromagnetic radiation was observed as the leading edge of the expanding ion cloud moved over the spacecraft for all the releases. The Upper Hybrid Resonance Frequency Emissions which the experiment detected allowed us to track the cloud density measured at the spacecraft. Similar to our observations during the AMPTE/IRM releases the free space electromagnetic radiation was excluded by the dense plasma cloud the spacecraft was emersed in. Strong low frequency whistler-mode emissions were observed inside the clouds for the releases done closest to earth. Strong broadband electrostatic emissions were observed when the electron number density in the cloud returned to ambient levels for many of the releases. Remote observations of auroral kilometric radiation during the high altitude releases in the tail indicated possible stimulation of auroral activity. The extremely interesting results obtained from both the AMPTE and CRRES chemical releases indicate the need for additional chemical releases in space in the presence of well instrumented spacecraft making in situ observations.

H2-2  
1420

PLASMA WAVE OBSERVATIONS IN CHEMICAL  
RELEASES IN THE F-REGION IONOSPHERE  
P.Rodriguez, M.M.Baumbach, C.L.Siefring,  
and D.N.Walker  
Code 4785, Space Plasma Branch  
Plasma Physics Division  
Naval Research Laboratory  
Washington, D.C. 20375-5000  
H.C.Koons  
Space and Environment Technology Center  
The Aerospace Corporation  
P. O. Box 92957  
Los Angeles, CA 90009

Strong plasma wave activity has been detected in a series of chemical releases at low altitudes from the CRRES satellite (~ 380 km) and two NICARE rocket experiments (~ 250 km). Plasma wave electric fields have been measured over the frequency range from Hz to several 10s of kHz. Magnetic field fluctuations in the ELF range were measured at several 10s of dB above background in the satellite releases. The ratio of wave magnetic field to electric field amplitudes (proportional to the wave index of refraction) suggests that both electrostatic and electromagnetic waves are generated by the release of barium thermites. Both enhancements and depletions of the electron density have been measured. Plasma density irregularities have also been measured against a background density of  $10^6 \text{ cm}^{-3}$  in the case of electron producing chemicals, such as  $\text{Ba}^+$ , to a few  $10\text{s cm}^{-3}$  associated with electron attaching chemicals, such as  $\text{SF}_6^-$ . Electrostatic ion cyclotron waves have been detected in these releases, including the first detection of negative ion plasma waves in space. A future chemical release experiment involves the CRRES AA-4 rocket which is scheduled to be launched in 1992, from Puerto Rico and to intercept the HF-heater beam of the Arecibo Observatory. AA-4 will deposit an electron attachment chemical in the heater beam in order to create an electron density "hole" which will act as a focusing lens for the HF waves.

H2-3  
1440

DEVELOPMENT OF IRREGULARITIES IN ARTIFICIAL  
PLASMA CLOUDS BY INITIAL VELOCITY DISTRIBUTIONS  
P.A. Bernhardt and W.A. Scales  
Space Plasma Branch  
Code 4780, Plasma Physics Division  
Naval Research Laboratory  
Washington, DC 2037-5000

A recent series of barium releases have been conducted from the Combined Release and Radiation Effects (CRRES) satellite. Releases occurred at altitudes ranging from 350 km to over 32000 km above the earth's surface. A new type of structure was observed for the barium injection that occurred at an altitude of 6200 km in an ambient magnetic field of about 5000 nT. The satellite velocity perpendicular to  $B$  was  $v_{\perp} = 5760$  m/s. The irregularities produced by this release were not field-aligned and had a characteristic scale length equal to  $v_{\perp} / \tau_i$ , where  $\tau_i = 2\pi / \Omega_i$  is the ion gyro period. We have interpreted these observations as "cyclotron bunching" of the initial barium ion distribution deposited along the trajectory of the barium neutral cloud that was being continuously photoionized in sunlight. The optical emissions from the spiraling ions also are affected by Doppler shifts of their resonant fluorescent lines in the solar emission spectra. The irregularities in the barium cloud vanished after 40 seconds when the injected plasma evolved past its initial stage. These processes have been simulated with a three dimensional Vlasov code without electric fields and a two dimensional hybrid code with electric fields.

H2-4 VLASOV EQUILIBRIUM AND EVOLUTION IN A NEGATIVE ION  
 1500 CATION RELEASE EXPERIMENT

G.I. Ganguli, P.A. Bernhardt,  
 W.A. Scales and P. Rodriguez,  
 Space Plasma Branch, Naval Research Laboratory,  
 Washington D.C. 20375

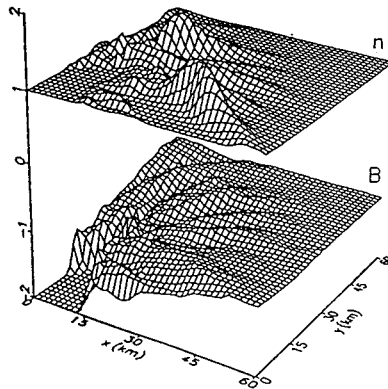
Recent results from two NICARE (Negative Ion, Cation Release) Experiments suggest that initially upon release the electron attachment materials ( $\text{CF}_3\text{Br}$  or  $\text{SF}_6$  in these cases) cause the formation of sharp density drops within about one negative ion gyroradius. At the boundary layer, the negative ion density falls rapidly to zero and simultaneously the electron density rises to the ambient value. Subsequently, waves and density structures appear on the surface of the negative ion cloud. We have developed a Vlasov theory to investigate the equilibrium features of the boundary layer and then have proceeded to study the stability of this equilibrium. Assuming a uniform magnetic field in the  $z$  direction and the density gradient in the  $x$  direction we have identified three constants of motion: (1) the total energy  $E = mv^2/2 + q\Psi(x)$ , where  $v$  is the velocity and  $\Psi(x)$  is the electrostatic potential, (2) the guiding centre position  $X_g = x + v_y/\Omega$ , and (3) the parallel velocity,  $v_z$ . Using these we then constructed an initial distribution function  $f_0(E, X_g, v_z)$ . By imposing quasi-neutrality we found that sharp density drops are supported by a self-consistent electrostatic potential across the magnetic field in the  $x$  direction. Also, cross-field flows and currents were predicted by the model. Detailed properties of these equilibrium features and their stability will be presented.

Results from a 2D electrostatic PIC simulation of a 3 species plasma (i.e.,  $0^+$ ,  $e^-$  and negative ions) will be presented. The simulations show the generation of plasma instabilities at the interface of the negative ion plasma and the background plasma where a shear in the flow velocity exists.

H2-5 WAVES AND IRREGULARITIES EXCITED BY THE CRRES  
 1540 MAGNETOSPHERIC BARIUM RELEASES  
 J.D. Huba  
 Space Plasma Branch (Code 4780)  
 Plasma Physics Division  
 Naval Research Laboratory  
 Washington, DC 20375-5000

Theoretical and computational analyses of the the CRRES magnetospheric barium releases are presented. The focus of this paper is on the structuring of the density and magnetic field during the expansion phase of the releases, and the generation of waves. The simulations use a 2D MHD code which includes the Hall term. This additional term is critical to the dynamics of sub-Alfvénic plasma expansions, such as the CRRES barium releases, because it leads to instability of the expanding plasma. We will present detailed simulation results of the G10 release. The release structured at time  $t \leq 22$  sec and developed scale sizes  $\sim 10 - 15$  km. The structuring allows the formation of plasma blobs which free stream across the magnetic field; thus, the barium plasma can propagate to larger distances transverse to the magnetic field than the case where no structuring occurs. Finally, we also discovered a new normal mode of the system which may be excited at the leading edge of the expanding barium plasma. This mode is a magnetic drift wave which propagates azimuthally around the barium cloud with a frequency  $\omega \approx k_y V_A^2 / \Omega_i L_n$  where  $k_y$  is the transverse wavenumber,  $V_A$  is the Alfvén velocity, and  $L_n$  is the density gradient scale length. We show that the simulation results are consistent with optical data of plasma structuring and jetting, and with in situ magnetometer data of the evolution of the diamagnetic cavity.

Fig. 1) Surface plots of the density and magnetic field for the G10 release simulation study at  $t = 46$  sec.



Research supported by NASA.

H2-6  
1600USING THE CRRES BARIUM RELEASES TO STUDY  
NON-EQUILIBRIUM PLASMAS IN SPACE

M. B. Pongratz, W. B. Clodius, R. A. Roussel-Dupre,

D. J. Simons and J. H. Wolcott

Group SST-7 MS D466

Los Alamos National Laboratory

Los Alamos, NM 87545

The CRRES chemical release experiments provided an opportunity to study the mechanisms that allow non-equilibrium plasmas to approach equilibrium. In the CRRES Caribbean campaign the chemical releases occurred near perigee where the CRRES satellite was moving about 9.5 km/s, essentially perpendicular to the geomagnetic field. Barium ions produced by photoionization had an initial kinetic energy of over 60 eV - hundreds of times greater than the temperature of the ambient plasma. The barium ion plasmas also had considerable momentum perpendicular to  $B$ . Both *in situ* and remote diagnostic techniques were utilized to measure phenomena associated with momentum coupling and velocity distribution relaxation.

Collisional effects complicate the determination of the role of collective plasma phenomena in thermalization. Collision time scales are much longer than plasma time scales, but they are close to the time resolution of the diagnostics. This paper will review Monte-Carlo code predictions of collisional effects.

This paper gives an overview of diagnostics and geometries and summarizes results. Preliminary results indicate that the barium ion plasma skidded about ten gyro-diameters before losing momentum and lost kinetic energy at a rate faster than *via* collisional processes.

## H2-7 TRANSIENT CURRENTS IN THE LOWER IONOSPHERE

1620

Leslie C. Hale

Communications and Space Sciences Laboratory

Penn State University

University Park, PA 16802

Rocket measurements of transient Maxwell currents (curl H) at various altitudes up to 147 km have been performed. On one flight above thunderstorms current transients of similar shape and amplitude were observed at 89, 120, and 147 km. These transients were related to whistler observations and hence were probably lightning-related. They lasted for several milliseconds and attained values of the order of a microampere/m<sup>2</sup>. An explanation is postulated based on the rapid release of excess electrons into the ionosphere when positive ions are "tied up" in the quasi-static field produced by a negative C.T.R. Wilson monopole, indicating positive or intra-cloud lightning. (This model can also explain enhanced coupling observed near the magnetic equator, since the energy is confined to a more localized region by the magnetic field.)

On the same flight three additional current transients of similar magnitude but different duration were observed which lasted for seconds. These transient events were not obviously related to lightning. These may be related to similar events observed on satellites by Voss.

Unlike "parallel" DC electric fields, field aligned transient unipolar charged particle currents which penetrate deeply enough will couple capacitively to lower altitudes as displacement currents, since  $\text{div curl H} = 0$ , by definition. We have observed "bursty" Maxwell currents in the middle-atmosphere increasing with altitude at Poker Flat, indicating a higher altitude source, and decreasing with altitude above a thunderstorm at Wallops Island, as might be expected.

Finally, we performed a vertical Maxwell current measurement in the stratosphere below the Viking satellite which showed a power spectrum similar to that observed in the satellite E-field. We do not regard this one measurement as sufficient proof of "mapping" but suggest that similar measurements be performed, preferably during the observation of more structured spectra, which were observed at different times on both Viking and in the stratosphere.

H2-8  
1640PROBING THE MAGNETOSPHERE BY RADIO SOUNDING  
TECHNIQUESJames L. Green, Shing F. Fung, and James R.  
ThiemanNational Space Science Data Center  
Goddard Space Flight Center  
Greenbelt, MD 20771

The concept that will be discussed is the viability of a space-based active radio transmitter and receiver, stationed on the moon, which will "sound out" remote magnetospheric plasma regions. It will be assumed that the lunar-based radio frequency transmitters would be designed to generate steerable narrow beams of emissions over a wide frequency range (from 9 kHz to 1 MHz) with R-X and L-O mode "free space" wave polarizations. These signals would be reflected and refracted off magnetospheric structures such as the plasmopause, plasmasheet, magnetopause, and the high and low latitude boundary layer. The frequency range of the sounder will depend on the local lunar ionospheric conditions and the region of the magnetosphere that is targeted to be probed.

It will be shown, through ray tracing calculations, that several of the magnetospheric plasma regimes can be remotely sensed by using a range of selected discrete frequencies; this technique could then produce a nearly instantaneous picture of the global magnetosphere. In addition, at times when the active radio experiment is in the solar wind, information can be obtained on the density and speed of streams of particles coming toward the Earth.

By way of example, particular emphasis will be placed on the application of the proposed sounding technique to understanding plasmasphere dynamics. By using the lunar-sounder, it is believed that the filling rate, the plasmopause position, the formation and motion of a detached region, and the intensity of local current systems very near the plasmasphere could be accomplished within a few frequency sweeps of the instrument.

J3-1  
1340

AN OPTICAL TELESCOPE POINTING SYSTEM FOR THE 12M  
RADIO TELESCOPE

P.R. Jewell, T. W. Folkers, and D. T. Emerson  
National Radio Astronomy Observatory  
949 N. Cherry Ave., Campus Bldg. 65  
Tucson, AZ 85721-0655

We will describe an auxiliary optical pointing system used to refine the pointing properties of the 12 m radio telescope mount. The system consists of a small optical refractor mounted at the apex of the 12 m feed support legs. Images are acquired with a CCD camera and a digital frame grabber. The system is used mainly at night, but can also be used in the daytime with an IR low-pass filter. Data acquisition and full pointing runs are entirely automated. In addition to a discussion of the equipment and observing techniques, we will describe how we use the optical data to refine the mount pointing equations, how we combine optical and radio pointing data, and the techniques used to identify and diagnose pointing anomalies.

J3-2  
1400

**POINTING ACCURACY OF THE OVRO 10 METER  
TELESCOPES AND THE USE OF TILTMETERS FOR  
REAL-TIME POINTING CORRECTION**

D. P. Woody and S. L. Scott  
Owens Valley Radio Observatory  
California Institute of Technology  
Big Pine, CA 93513

Achieving the pointing requirements of high gain radio telescopes becomes more difficult as their size increases and the useable wavelength decreases. The beam widths of the largest millimeter and submillimeter telescopes are much less than one arcminute. Full utilization of these telescopes thus requires absolute pointing accuracy of a few arcseconds. One of the major limiting factors for pointing of these large structures is the tilting of the azimuth axis and distortion of the mount structure as a function of temperature changes and wind loading. This problem is further compounded for transportable telescopes which are moved periodically to different locations.

The Owens Valley Millimeter Array consists of three 10.4 meter diameter telescopes (two more are under construction) operating in the frequency range from 80 to 300 GHz. An optical telescope mounted on the antenna backing structure is used for determining the pointing constants. The offset of the radio beam from the optical beam is determined by observing the few brightest radio quasars. Electrolytic bubble levels are used for real-time correction of the tilt of the azimuth axis. They successfully compensate for tilt changes as large as one arcminute.

The telescopes in the Owens Valley Millimeter Array have proven to be particularly well behaved in that the tiltmeters provide an accurate measure of the orientation of the azimuth axis relative to vertical and only seven pointing terms corresponding to the mechanical errors that can occur in making an alt-az mount are required. The achieved pointing accuracy is 4 arcsec with the exception a factor of two larger excursions associated with sunrise and sunset. The pointing constants are stable over long time scales and the absolute pointing accuracy is obtained immediately after moving the telescopes by simply using an optical target on a nearby mountain to determine the new azimuth zero.

*Tilt meters work very well  
Based on an article by Westphall*

J3-3 POINTING AND SURFACE ACCURACY OF THE NEW BIMA ANTENNAS  
1420 W. J. Welch, D. D. Thornton, M. C. H. Wright,  
M. Flemming, W. Hoffman, and J. R. Forster  
Radio Astronomy Laboratory  
University of California  
Berkeley, Cal. 94720

New six meter diameter antennas are being built for the millimeter wavelength array of the Berkeley-Illinois-Maryland-Association at Hat Creek, California. The antennas are equipped with Inductosyn (magnetic) encoders with stable digitizing electronics and stiff roller drives. First pointing tests on stars show excellent accuracy and repeatability.

The antenna surfaces are intended to provide excellent performance at one millimeter wavelength. The backup structures are stiff with a small homologous gravitational deformation. The panels are machined aluminum castings with surface errors of the order of 5 microns. The panel setting is by holography. Tests of the holographic method show excellent repeatability.

J3-4  
1440

## The Effect of Atmospheric Fluctuations on the Pointing of Radio Antennas

Colin R. Masson  
Harvard-Smithsonian Center for Astrophysics

Since the discovery of so-called "anomalous refraction" at the IRAM 30 m telescope in Spain, it has been recognized that atmospheric fluctuations in refraction can have significant effects on the pointing of radio antennas. These fluctuations have previously been measured directly at the 30 m telescope and at the JCMT in Mauna Kea.

Recently the SAO has been carrying out a survey of atmospheric stability with a small interferometer on Mauna Kea in Hawaii. This interferometer has a baseline of 100 m, but analysis of the temporal fluctuations in measured phase allows us to estimate the effect on the pointing of single dishes of diameters less than 100 m.

We present an analysis of the interferometer data, and estimates of the pointing fluctuations for high-resolution single-dish antennas. Under bad atmospheric conditions, the atmospheric irregularities provide a significant contribution to the wavefront error of such antennas. Since the atmospheric fluctuations are dominated by large-scale effects, the irregularities show up primarily as random pointing shifts. The timescale of these shifts is proportional to the antenna diameter divided by the wind speed, with typical values of a few seconds for antennas of approximately 10 m diameter.

J3-5  
1500**LEAST SQUARES ANALYSIS FOR ACCURATE  
ESTIMATION OF POINTING ERROR SOURCES FOR  
THE NASA/JPL DEEP SPACE NETWORK ANTENNAS**Leon Alvarez  
Jet Propulsion Laboratory  
4800 Oak Grove Drive  
Mail Stop 144-201  
Pasadena, California 91109

A systematic pointing error model that is used to calibrate antennas in the NASA/JPL Deep Space Network is presented. Experience has shown that the majority of beam pointing errors, defined here as the difference between the antenna axis position transducers and the true antenna boresight, are systematic and are incurred by mechanical misalignments and structural deformations. The parameters in the error model are obtained empirically, by fitting pointing measurements from during spacecraft or radio star observations. The parameters are then used by the mechanical control system to generate pointing corrections to accurately point the antenna.

This paper will develop the theory of the parameter estimation and demonstrate the effectiveness of the pointing error modeling process. The estimation of the parameters results in a least squares problem which may have poor numerical conditioning. This occurs when measurement sets incorporating inadequate sky coverage are used, hence resulting in unsatisfactory estimation accuracy. The specific approach used to assess the numerical condition of the least squares measurement distribution matrix as a function of a single or multiple source trajectories will be discussed here. A key feature of the analytical method is its predictive capability, that is the accuracy of the systematic error parameter estimates may be predicted from measurement distribution before actual pointing calibrations, thus allowing for an efficient scheduling of sources to track. This effectively minimizes measurement redundancy and required antenna pointing calibration time.

J3-6  
1540

## Precision Control of Large Structure Antenna

Ralph Goddard, George Sevaston, Noble Nerheim,  
Dan Eldred, Robert Scheid, and Ken Lau

Jet Propulsion Laboratory  
California Institute of Technology

### Abstract

Future technology upgrades are generating requirements for more stringent control of large structure antenna. This paper presents a survey and highlights of the research at NASA's Jet Propulsion Laboratory which is directed at solving the various aspects of precision antenna pointing and wavefront control.

Inertial instrumentation mounted directly on the primary structure provides blind pointing direction in an inertial frame. Much of the uncertainty in flexure and structural misalignments are thus bypassed. An instrument consisting of optical gyros, accelerometers, and an inclinometer is proposed. A minimum-variance estimator combines measurements to obtain pointing attitude.

Metrology technology research is directed at detecting changes in the shape of the primary and secondary reflectors for both pointing and wavefront compensation. The JPL Spatial High Accuracy Position Encoding Sensor (SHAPES) is capable of simultaneously measuring the 3-D position of multiple targets at a 10 Hz update rate with submillimeter accuracy. The distance measuring function of SHAPES is a time-of-flight laser ranging sensor which measures ranges from one or more optical heads to retroreflector targets placed at selected locations on the primary reflector. The SHAPES detector is a streak tube camera operated with a sinusoidal drive voltage and equipped with a CCD detector, and the optical head consists of an array of small transmitting lenses. The Precision Segmented Reflector (PSR) project for space-based telescopes utilizes an optical truss metrology system to measure the relative positions and alignments of the telescope segments through the use of a fiber coupled, discrete beam, superheterodyne interferometric laser yielding 1-5 nanometers accuracy.

A generalized predictor-corrector is described to compute real-time pointing bias commands; compensating for environmentally induced deflections of the primary and secondary reflectors. Outputs of a metrology system are compared to the predicted reflector deflections obtained from a finite element model and the error produces a correction in the form of real-time bias commands for pointing control. A ten-to-one reduction in pointing uncertainty is achieved under nominal uncertainty conditions.

The PSR project includes figure maintenance control function achieved through the use of a "wavefront compensation" technique, rather than a traditional panel state compensation algorithm. Each segment is positioned along three degrees of freedom to minimize the RMS wavefront error. The segment positioning system is composed of DC brushless motors, lead screw actuators and local sensors to achieve .1 micron positioning accuracy and an overall submicron RMS wavefront error.

J3-7 The Pointing and Metrology Systems for the Green Bank Telescope  
1600

J. M. Payne  
National Radio Astronomy Observatory  
Tucson, Arizona

The Green Bank Telescope, presently under construction and due for completion in 1995, will be equipped with a deformable primary mirror. A metrology system will continuously measure the shape of the primary mirror, thereby enabling correction of thermal and gravitational deformations. The metrology system will consist of three rangefinders lying in a reference plane. Two thousand points on the surface will be located with respect to this plane by three-dimensional trilateration. The position of the reference plane with respect to fixed points on the ground may also be determined by accurate range measurements and in this way accurate pointing information may be derived.

The necessary instrumentation for this metrology system has been developed and will be described.

*No show ?*

J3-8  
 1620

**DIRECT MEASUREMENT AND ADJUSTMENT OF THE SURFACE OF THE 10.4 METER CSO TELESCOPE**

D. P. Woody and A. Schinckel  
 Caltech Submillimeter Observatory  
 California Institute of Technology  
 Pasadena, CA 91125

Achieving good performance from a large submillimeter telescope requires more than just a stiff or homologous structure and accurate panels. You must also be able to measure and adjust the surface to the required accuracy. A major step in achieving the desired surface accuracy can be accomplished by using the telescope's altitude-azimuth mount as a rotary table and a measuring fixture to determine the deviations from rotational symmetry. This is a simple way to obtain the high spatial resolution measurements which are so hard to obtain any other way. The radial deviations from the desired shape must be obtained using some other method such as holography or direct survey techniques. This is now essentially a one-dimensional measurement problem and does not require high spatial resolution.

Bob Leighton and Ken Young of Caltech first developed this method using a wheel on a linear transformer attached to a light weight frame. One end of the frame was mounted on a bearing at the vertex and the other end rested on a horizontal plate attached to the telescope dome structure. With the feedlegs removed, the dish was rotated and the deviations from azimuthal symmetry measured. Verification of the initial assembly of the Caltech Submillimeter Observatory (CSO) telescope was checked using this method.

This technique has been improved by using 16 non-contacting Capacitec™ transducers. Additionally, data from a sensor measuring the end-play of the frame relative to the dome and the electrolytic tiltmeters in the mount were used to correct for the lateral and tilting motion of the dish as it was rotated. This greatly improved the measurement speed and accuracy. An accuracy of better than 10 microns was achieved in a measurement time of 30 minutes. The same measurement system was then used to monitor the adjustments to the panels as they were being made. This eliminated the usual problems of backlash and hysteresis in the adjustment screws and allowed us to monitor the effect of changing one panel corner on the nearby surface in real-time. A series of measurements and adjustments of the surface of the CSO carried out over a period of a few days reduced the deviation from the desired azimuthal shape from 23 microns to less than 15 microns RMS.

change is measured (not absolute)

Need holography to get absolute curve

$$10 \mu\text{m} = 0.01 \text{ mm} \frac{1}{25.4 \text{ mm}} =$$

85 panels (hexagonal) with adjustments at corners (both adjacent panels move together)  
 Use an HP Laser Interferometer to get initial parabolic shape 10 μm accuracy



J3-9 MICROWAVE ANTENNA HOLOGRAPHY: ERROR SIMULATIONS AND  
1640 APPLICATIONS

D. J. Rochblatt<sup>1</sup> and Y. Rahmat-Samii<sup>2</sup>

Jet Propulsion Laboratory<sup>1</sup>  
California Institute of Technology  
Pasadena, California 91101

Department of Electrical Engineering<sup>2</sup>  
University of California, Los Angeles, Ca 90024

Microwave holography has proven to be a powerful tool for various evaluations, diagnostics, and RF performance improvements for reflector antennas. The technique utilizes the Fourier Transform relation between the complex far-field radiation pattern of an antenna and the complex aperture field distribution. Resulting aperture phase and amplitude distribution data can be used to precisely characterize panel alignment, subreflector position, aperture illumination, directivity at various frequencies, and gravity deformation.

In order to properly assess the ultimate achievable holographic performance improvements, attention must be given to detailed system error evaluation. The effects of measurement errors appearing during the implementation of the microwave holographic technique are investigated and many representative results are presented based on computer simulations. In the simulations, the receiver front-end noise and architecture are modeled as well as a known distortion signature of the antenna. These results provide the system designer with the tools to specify receiver parameters and signal source requirements.

Numerical and measurement results are presented for the NASA's Deep Space Network antennas including the newly built NASA/JPL 34-m beam waveguide antenna. Preliminary results showing the limitation of the technique in determining in-orbit, spacecraft antenna deployment status, and comparison with phase retrieval holography will be presented.

J3-10 EXPERIENCE WITH PHASE-RETRIEVAL AND COHERENT  
1700 HOLOGRAPHY AT THE NRAO 12M TELESCOPE  
D. T. Emerson, Assistant Director  
National Radio Astronomy Observatory  
949 N. Cherry Ave., Campus Bldg. 65  
Tucson, AZ 85721-0655

At the N.R.A.O. 12m telescope on Kitt Peak, a combination of coherent and phase-retrieval holography has been used to improve the high frequency efficiency of the telescope.

Coherent holography was used with a prime-focus receiver to give a relatively high resolution measurement of surface errors of the primary reflector. These observations used the LES8 satellite operating at 38 GHz. From these measurements, a high precision shaped sub-reflector was machined, designed to compensate for the measured errors of the primary reflector. A significant increase in telescope efficiency resulted, although even higher gain had been anticipated. This work was carried out with the help with Dr. John Davis at the University of Texas, and Dr. Charlie Mayer from the University of Alaska.

With the shaped sub-reflector installed, phase-retrieval measurements were later made at frequencies of 90 GHz and 230 GHz, using natural emission from planets. These observations were made and analyzed with the assistance of Dr. Dave Morris from I.R.A.M. Some corrections to the data were necessary to allow for the angular extent of the planets. Although of much lower resolution than the earlier coherent holography measurements, the results indicated significant large-scale residual errors in the combination of primary mirror and its matching error-correcting secondary.

Independent mechanical measurements of the machined sub-reflector showed large-scale machining errors which match the residuals shown by the phase-retrieval holography. The errors may result from a flaw in the bearing of the numerically controlled milling machine used to cut the sub-reflector. A new shaped sub-reflector avoiding these imperfections is now planned.

This combination of independent coherent and phase-retrieval radio holography measurements is presented as a powerful technique for telescope efficiency optimization. Some pros and cons of the two techniques are discussed.

A6-1  
0840

**WIDEBAND DATA ACQUISITION AND  
INFORMATION PROCESSING IN RADIO SCIENCE**

**E. K. Miller**  
Group MEE-3, MS J580  
Los Alamos National Laboratory  
Los Alamos, NM 87545  
**T. K. Sarkar**  
Department of Electrical Engineering  
Syracuse University  
Syracuse, NY 13244

Both computation and measurement provide data to the radio scientist for a wide variety of observables and purposes. The uses to which these data may be put essentially involve determining the properties of a radiating source, a scatterer, or some intervening medium through which the fields have propagated. The sought-for properties cover a wide spectrum, ranging from solving true inverse problems where detailed spatial, angular, temporal or spectral information is the goal, to more aggregated representations, such as reducing the number of degrees of freedom in the description of some electromagnetic phenomenon. These goals of acquiring and processing data are encountered in the activities of all URSI Commissions. Although some aspects will be unique to specific applications, there is a core of closely similar, if not common, methods that span the activities of two or more Commissions. It is the purpose of this Special Session to bring together at a common forum researchers knowledgeable and active in the separate URSI Commissions so that they may discuss problems and solutions, especially where there might be some shared commonality with other activities.

In this introductory discussion, we briefly survey some of the kinds of observational data of interest in radio science and methods used for its processing. Emphasis will be on applications, specifically with respect to estimation of physical parameters and properties. Our goal is to set the stage for the remainder of the session and to provide a unifying theme for subsequent discussion. Overall, we hope to show that the various Commissions have a great deal in common with respect to information processing and its underlying mathematical structure, and thereby that there is much to gain by exchanging information and ideas.

A6-2 IONOSPHERIC TOMOGRAPHY  
0900 Paul F. Fougere  
Geophysics Directorate  
Phillips Laboratory  
Hanscom AFB MA 01731-5000

The general 2-D tomographic reconstruction technique uses path integrals of an unknown density to infer the distribution of density inside a two-dimensional region. In the ionosphere, the density is that of electrons in the ionospheric plasma, and the integral is called the total electron content (TEC). It will be shown that when the continuous density is replaced by values averaged over relatively small plane areas, the reconstruction easily can be set into the form of a linear inverse problem, which however may be badly underdetermined. At this point the Maximum Entropy technique comes to the rescue and yields a unique reconstruction, which is conservative in the sense that artifacts are suppressed and only features strongly supported by the data are expressed. Results of simulation runs will be shown to indicate the power of the method and some real ionospheric data will also be used. Results will be compared with ionospheric density data obtained directly from an incoherent scatter radar facility.

A6-3      VERY LONG BASELINE INTERFEROMETRY  
0920      M. J. Reid  
            Smithsonian Astrophysical Observatory  
            60 Garden Street  
            Cambridge, MA 02138

Radio astronomers often use arrays of antennas to produce images of the sky. Simultaneous observations with antennas widely spaced on the earth (Very Long Baseline Interferometry) are most conveniently made by using wide-band digital tape recordings and by employing hydrogen-maser frequency standards at each antenna. By using VLBI techniques astronomers have succeeded in making interferometric images with angular resolutions of nearly 0.0001 arcseconds ( $5 \times 10^{-10}$  radians).

Images of extraordinary clarity have been produced from VLBI observations by adaptive calibration techniques and powerful deconvolution algorithms, even though the interferometer has sparse sampling of the fringe visibilities. In addition to observations of sources of continuum emission in many radio bands, images have been produced for spectral-line sources via Fourier transforms of interferometer cross-correlation functions. Also, by cross-correlating signals of opposite circular polarization among the antennas of the interferometer array, images in all Stokes parameters have been made.

A6-4      IDENTIFICATION AND MEASUREMENT OF TRANSIENT  
0940      AND LOCALIZED IONOSPHERIC DISTURBANCES  
            IN VERY LOW FREQUENCY RADIO DATA

Umran. S. Inan

Space, Telecommunications and Radioscience Laboratory  
Stanford University, Stanford, California 94305

Transient and localized disturbances of the lower ionosphere caused by lightning discharges are identified in very low frequency (VLF) radio data by means of their characteristic temporal signatures (typically  $< 2$  s onset followed by 10-100 s recovery). The association of these signatures with lightning is typically based on the simultaneous analysis of other time series data, such as measurements of broadband VLF amplitude in which radio atmospherics due to lightning appear as impulsive spikes. Due to the inherent variations of the ionospheric signatures and the non-periodic nature of the phenomena time domain analysis is still the only efficient means of studying these events. Through such time domain correlation analysis the characteristic temporal features of the phenomenon of lightning-induced electron precipitation has been extensively studied, and, a new phenomenon of lightning-induced heating of the lower ionosphere has been uncovered. Examples of phenomena and analysis techniques will be discussed.

A6-5  
1020**SIGNAL PROCESSING IN HF CHANNEL  
MEASURING SYSTEMS****Paul E. Argo  
T. Joseph Fitzgerald  
Los Alamos National Laboratory  
Group SST-7, MS D466  
Los Alamos, NM 87544**

We have designed digital systems for measuring the HF propagation channel, and changes therein. One system, a channel probe, sends a phase-modulated, pseudo-random sequence through the channel and searches for that sequence in the received data. This is most efficiently done in the frequency domain. Changes in the width of the cross-correlation function describe group and phase path variations of the channel.

The second system uses a spatial array of antennas, and spaced CW frequencies to define the channel. The time-lagged, cross-coherence functions between various antennas and frequencies are compared, as a radio interferometer, and angle-of-arrival and slowness diagrams are used to describe the channel and its time evolution.

A6-6  
1040SOME DATA CONSIDERATIONS  
IN  
ULTRA-WIDEBAND  
TARGET IDENTIFICATION*D. G. Dudley*Electromagnetics Laboratory  
ECE, Building 104  
University of Arizona  
Tucson, AZ 85721, USA

Dating from studies involving the singularity expansion method (SEM) in the early seventies, it has become evident that any dramatic successes in monostatic radar target identification are going to depend on the compilation and analysis of ultra-wideband data. This situation arises because the monostatic characteristic assumes that the data taker has given up all three degrees of spatial freedom in obtaining the data. Therefore bandwidth (or temporal resolution) has become an important consideration in gaining back some of what has been given up.

It is well known that in one-dimensional profiling in geophysical applications, it is possible to trade off the spatial variable with frequency. This result is contained, under the Born approximation, in a Fourier transform relationship between space and wavenumber. All ultra-wideband monostatic radar studies necessarily assume that trading off *three* spatial variables with frequency can produce at least a partially successful identification.

In this paper, we examine the basic space-frequency tradeoff. In addition, we comment on problems that arise because of bandwidth limitations on equipment and noise in data.

A6-7      AQUISITION AND PROCESSING OF RADAR PROFILER  
1100      DATA  
          R. G. Strauch and K. P. Moran  
          Wave Propagation Laboratory  
          NOAA/ERL  
          Boulder, CO 80303

Sensitive pulse Doppler radars are able to measure vertical profiles of horizontal and vertical wind throughout the troposphere and into the lower stratosphere, vertical profiles of virtual temperature in the lower troposphere with the Radio-Acoustic Sounding System (RASS), profiles of precipitation drop size distributions, and other information on various scattering mechanisms in the lower atmosphere. The basic data acquisition and processing methods used are the same for all these radar observations--time domain integration of the video signals from each range resolution cell, spectral analysis, spectral averaging, moment calculations, moment averaging and outlier editing. The techniques used will be described and illustrated, and new processing concepts will be presented.

A6-8  
1120

## TIME-DOMAIN ANTENNA CHARACTERIZATIONS

Oliver E. Allen  
University of Colorado at Boulder  
Boulder, Colorado 80309  
and the  
Naval Air Warfare Center  
Patuxent River, Maryland 20670  
(301) 863-4681

David A. Hill  
Electromagnetic Fields Division  
National Institute of Standards and Technology  
Boulder, Colorado 80303  
(303) 497-3472

Arthur R. Ondrejka  
Electromagnetic Fields Division  
National Institute of Standards and Technology  
Boulder, Colorado 80303  
(303) 497-3309

The standard method of describing an antenna's transmit and receive response is through the many well defined and accepted frequency-domain antenna characterizations. The frequency-domain characterizations are based on the antenna being excited by a monochromatic signal. When an antenna is designed to transmit and receive signals whose frequency content extends over a wide band, these characterizations become much more cumbersome. A set of time-domain characterizations which can efficiently describe such wide band antennas is proposed in this paper. The experimentally measured responses of a transverse electromagnetic horn antenna is used to evaluate the utility of these characterizations. Comparisons are made between each antenna's frequency-domain response and their time-domain characterizations. The comparisons show that the time-domain characterizations can provide significant insight into the antenna's behavior as well as providing a means to accurately compare two or more different antennas.

B5-1  
084

# Generation of Accurate Broadband Information from Narrowband Data using the Cauchy Method

**T.K.Sarkar and R.S.Adve**

Department of Electrical Engineering  
Syracuse University  
Syracuse, NY 13210, USA

## **Abstract**

The Method of Cauchy has been used to extrapolate a desired parameter over a broad range of frequencies. This information is generated using some information about the parameter over a narrow band of frequencies or at some discrete frequency points.

The approach is to assume that the parameter, as a function of frequency, is a ratio of two polynomials. The problem is to determine the order of the polynomials and the coefficients that define them.

This method can be coded as a stand alone program or incorporated as part of a larger program. This technique has yielded accurate results while in use in conjunction with a Method of Moments program and as an independent program in filter analysis.

B5-2  
0900APPLICATION OF THE FAST FOURIER TRANSFORM TO  
THE COMPUTATION OF SOMMERFELD INTEGRALS

Steven L. Dvorak  
Department of Electrical and Computer Engineering  
University of Arizona  
Tucson, AZ 85721

In 1909, Sommerfeld formulated exact integral representations for the fields due to a vertical electric Hertzian dipole over a homogeneous half-space. Since that time, a number of authors have developed various techniques for the efficient evaluation of these so-called Sommerfeld integrals. Numerical integration can be used to evaluate Sommerfeld integrals when the observation location is in the near-zone. However, for intermediate- and far-zone computations, the integrand becomes highly oscillatory, thereby degrading the accuracy and efficiency of the numerical integration. The steepest descent technique can be used to obtain a far-zone asymptotic approximation for the Sommerfeld integral (the reflection coefficient method) and intermediate-zone results can be obtained by applying a numerical integration along the steepest descent path (Y. Rahmat-Samii, R. Mittra, and P. Parhami, *Electromagn.*, vol. 1, pp. 1-28, 1981). However, since both of these methods involve a contour deformation, the pole and branch-cut contributions must be accounted for. This task can be very complicated when multi-layer structures are considered or when transient results are desired.

In this presentation, the fast Fourier transform is used in conjunction with analytical techniques to obtain an approximate expression for the Sommerfeld integral associated with a vertical electric dipole above a half-space. The resulting expression, which is an analytic function of the source and observation locations, can be used in lieu of a numerical integration of the Sommerfeld integral. It can be used in either the near-zone or the far-zone, and it can even be applied for observation angles close to grazing. Since this technique involves no contour deformation, one only needs to worry about the poles and branch points which are on the original path of integration. The accuracy of the expansion directly depends on the number of terms used in the fast Fourier transform. Results obtained using the expansion are compared with those obtained both from a direct numerical integration of the Sommerfeld integral and the reflection coefficient method.

B5-3 AN ALTERNATE VERSION OF THE CONJUGATE GRADIENT METHOD  
0920

Tapan K. Sarkar and Peter Petre  
Department of Electrical and Computer Engineering  
Syracuse University, Syracuse, New York 13244

The conjugate gradient method (CGM) has found a wide variety of applications in electromagnetics and in signal processing, especially for the solutions of large matrix equations. The major limitations of solving dense large systems of complex matrix equations are computer memory and speed. However, the speed is not only gauged by how fast the computations are done, but also what is the numerical stability for direct methods and on convergence rates for iterative methods of solving systems of equations. Since on the average roughly  $\log_{10} N + 0.7$  digits are lost in solution of large systems, an iterative method is preferred over direct methods of solving large systems of equations. The CGM was developed as an efficient way to solve a self-adjoint matrix equation  $AX=Y$  in an iterative fashion. The advantage of this iterative method unlike others, is a theoretical guarantee of convergence in a finite number of steps. The algorithm was later modified to solve  $AX=Y$  for an arbitrary matrix  $A$ , by converting it to the form  $A*AX=A*Y$ . The disadvantage is that the condition number is squared. There are various versions of the conjugate gradient method depending on whether it minimizes the residuals or the error in the solution. Here, an alternate version of the conjugate gradient method is presented which may not have the drawbacks of the earlier methods. Specifically a method is presented, where the square of the residuals and the error in the solutions may be minimized simultaneously. Also from a computational point of view, this new method may be more efficient as only one sweep over all the matrix elements need be made per iteration for an arbitrary matrix. The alternate method does not square the condition number of the original matrix equation. However this is achieved at the expense of doubling the number of unknowns. Numerical examples, i.e. electromagnetic scattering from a straight thin wire antenna and near-field to far-field transformation using an equivalent magnetic currents approach are presented to compare the efficiency of the alternate version of the CGM with the earlier methods.

B5-4  
0940**METHODS FOR FAST CONVERGENCE OF ITERATIVE SOLUTIONS IN COMPUTATIONAL ELECTROMAGNETICS<sup>1</sup>**W.D. Murphy<sup>†</sup>, V. Rokhlin\*, and M. S. Vassiliou<sup>†</sup>  
(*alphabetical*)<sup>†</sup>Rockwell International Science Center, 1049 Camino Dos Rios, Thousand Oaks, CA 91360

\*Dept. of Computer Science, Yale University, New Haven CT 06520

The numerical solution of electromagnetic scattering problems described by the Magnetic Field Integral Equation (MFIE) involves the solution of a linear system. Iterative methods constitute an attractive approach to solving such systems, but they can be plagued by convergence problems because of large condition numbers in the discrete matrix. Large condition numbers affect the accuracy as well as the speed of solutions. One reason for large condition numbers is resonance, and this is a particular concern for electrically large scatterers.

The difficulty can be alleviated via a simple and effective technique that we call "complexification and extrapolation." The technique, based on the mathematical Principle of Limiting Absorption, involves introducing an imaginary part to the real wave number and solving the problem, then repeating with a different imaginary part, and extrapolating the solutions linearly back to the real axis. For higher-order extrapolations, we use additional complex wavenumbers. We have tested the method on a number of closed 2-D conducting scatterers, using the MFIE discretized by Nyström's method and solved by the Fast Multipole Method. We use a variant on the conjugate gradient (CG) method that we call the Pseudo-Conjugate-Gradient (PCG) method. The PCG method as we employ it performs only 1.2 matrix-vector products on average per iteration, as opposed to 2 for the standard CG. The technique of complexification is not limited to the Fast Multipole Method, and should be of broad applicability in the numerical solution of scattering problems described by the MFIE. It should work well with the Method of Moments.

Complexification gives excellent results. Solutions are fast and accurate. The condition number of the discrete matrix is asymptotically bounded for a given problem as the number of points per wavelength increases. The empirical evidence we have gathered thus far also suggests that the condition number is essentially asymptotically bounded as the electrical size of the scatterer increases, holding the number of points per wavelength fixed. Thus the technique has great potential in the solution of scattering from electrically large objects.

<sup>1</sup>*This work was partially supported by Air Force Office of Scientific Research Contract Number F49620-89-C-0048*

B5-5  
1000

**A NEW FAST CONVOLUTION ALGORITHM  
FOR SOLVING ELECTROMAGNETIC SURFACE  
INTEGRAL EQUATIONS  
WITH UNIFORM DISCRETIZATION**  
M. Bleszynski\* and T. Jaroszewicz†

\* Science Center, Rockwell International Corporation  
P.O. Box 1085, Thousand Oaks, Ca 91360

† Physics Department, UCLA, Los Angeles, Ca 90034  
P.O. Box 92098, Los Angeles, Ca 90009

*We describe a new fast convolution algorithm for solving Maxwell's equations in the integral form, applicable to boundary value problems with strongly singular kernels. The method combines the efficiency of fast convolution algorithms, employing uniform rectangular discretization grid, with high accuracy achieved through the application of the boundary-element methods to the singular, short-range components of the integral kernel.*

We analyze the convergence properties of the uniform discretization methods applied to solving Maxwell's equations for surface scattering problems in terms of integral representations involving weakly and strongly singular kernels. An important advantage of uniform discretization schemes is their immediate adaptability to the fast convolution algorithms (with  $O(n)$  performance ( $n$  being the number of computational elements) based on spectral techniques ( $k$ -space and other representations employing discrete fast Fourier transform method for fast matrix operations). While the spectral technique can provide an accurate description of volumetric scattering problems, its applications for surface scattering problems has not been successful due to the staircasing errors which occur when objects surfaces do not conform to the grid lines.

We construct a discretization scheme which overcomes the above difficulty of the spectral technique and provides an accurate description of surface scattering problems for an arbitrary surface shape and surface impedance without losing the  $O(n)$  character.

We carried out several self-consistency tests of the method, by solving the same scattering problems involving objects with and without edges in terms of magnetic (MFIE), electric (EFIE) and the combined field integral equations (CFIE), and by rotating and shifting the object with respect to the grid.

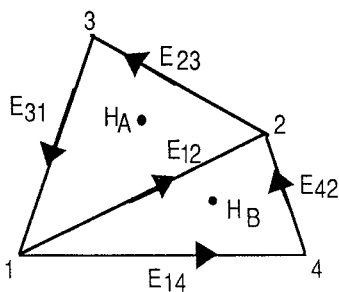
Our approach eliminates the essential difficulty of the spectral techniques: an inaccurate modelling of surface scattering, known as staircasing. In particular, we show that, for surface integral equations with strongly singular kernels (either compact, as in MFIE's, or noncompact, as in EFIE's) the conventional spectral techniques do *not* lead to a convergent discretization scheme.

B5-6 A GENERALIZED FINITE-DIFFERENCE TIME-DOMAIN METHOD FOR  
 1040 MAXWELL'S EQUATIONS WITH IRREGULAR TRIANGULAR CELLS IN  
 TWO DIMENSIONS

Richard C. Booton, Jr. and David C. Chang  
 Center for Microwave/Millimeter-Wave Computer-Aided  
 Design  
 Department of Electrical and Computer Engineering  
 University of Colorado  
 Boulder, CO 80309-0425

Time domain solutions of Maxwell's two curl equations usually approximate the time derivatives by a finite-difference approximation and update E and H values alternately. The usual finite-difference time-domain method updates with a set of explicit equations based upon spatial finite-difference approximations but is restricted to field values defined upon a rectangular grid. A limited amount of work has been performed with equilateral-triangle cells in two dimensions. Time-domain finite-element methods are applicable to non-rectangular cells but require solution of a set of algebraic equations for each update. This paper develops an algorithm similar to the finite-difference method but utilizing irregular triangles. The approach used is based upon a hybrid finite-element representation using both nodal and edge expansions.

The method is illustrated in two-dimensions where the variables are  $E_x$ ,  $E_y$  and  $H_z$ . Consider the two triangles A and B shown in the figure. The E-field is approximated by an expansion using constant tangential values on the sides (edges) of the triangles. The H-field is defined at the center of gravity of the triangles. Maxwell's curl equation for the time derivative of H can then be used to update H without the requirement for solution of algebraic equations. If the triangles are unsymmetrical, algebraic equations still need to be solved for the E-field updates.



Application of this approach to rectangular cells yields the usual FDTD equations. The sometimes desirable situation of mixed use of rectangular and triangular cells can easily be accommodated and requires algebraic-equation solution only for the triangular cells. Furthermore, the interpretation in terms of equivalent network representation can be easily established.

B5-7  
1100 NUMERICAL CONVERGENCE OF VARIOUS EDGE ELEMENTS  
FOR THREE-DIMENSIONAL SCATTERING  
J. W. Parker, R. D. Ferraro, P. C. Liewer  
M/S 198-231  
Jet Propulsion Laboratory,  
California Institute of Technology  
Pasadena, California, USA 91109

Accurate solution of the frequency-domain curl-curl equations with finite elements requires element formulations which are immune to vector parasites (spurious modes) and represent field variations to moderately high order. The first requirement is satisfied by edge elements, in which the unknowns represent the tangential field component along edges of the mesh. The second implies the desirability of generalized edge elements that include higher-order polynomial representations of vector components.

A test bed for a variety of edge elements is devised for scattering problems, including a wave-absorbing boundary limiting the near-field domain. Three varieties of edge elements are included: zero-order Whitney edge tetrahedra, so-called Higher-Order Tangential tetrahedra (J.F. Lee, Int. J. Numer. Methods, December 1990), and a novel weighted Whitney element which approximates the tangential components to arbitrary polynomial order (currently orders 1 and 2 are implemented). All appear to be free of vector parasites. Calculations of near-fields and RCS from spherical scatterers (diameters of the order of a wavelength) with known solution demonstrate the empirical rates of convergence to the correct solution as the mesh is systematically refined. The cost for each solution is represented as the total nonzero entries in the system matrix, as appropriate for iterative solutions.

B5-8  
1120INTERACTION OF EM WAVES WITH A  
DISCONTINUITY IN A GROUNDED  
DIELECTRIC SHEET

Shigeo Ohnuki

Department of Electrical Engineering  
Tokyo National College of TechnologyJiming Song, Dennis Nyquist, Kun-Mu Chen and Edward  
RothwellDepartment of Electrical Engineering  
Michigan State University  
East Lansing, MI 48824

The two-dimensional problem of plane wave interaction with a dielectric discontinuity in an infinite grounded dielectric sheet is considered. An electric field integral equation (EFIE) for TE illumination has been derived based on the Green's function for the field produced by induced polarization sources in the discontinuity region. The EFIE is solved using Galerkin's method -- the rectangular cross-section of the discontinuity is subdivided into rectangles and the resulting field tested by a constant within each subdivision.

The electric field Green's function is expressed in terms of an inverse Fourier transform over spatial frequency (Sommerfeld integral). Computation of the inverse transform has been performed both by integrating along the real axis and by deforming the integration contour into the complex plane and using Cauchy's integral theorem. The latter approach takes fewer computer resources and allows a separation of fields into bound surface modes and radiation modes.

Once the induced sources have been found, the radiation field is calculated using a steepest descents method. Results will be shown for rectangular discontinuities in both perfect and in lossy dielectric slabs.

B5-9  
1140**AN EFFICIENT COMPUTATION OF THE  
EFFECTIVE LENGTH OF A DIPOLE WITH A  
FINITE, OPEN-CIRCUITED GAP**Robert T. Johnk and Motohisa Kanda  
National Institute of Standards and Technology  
Boulder, Colorado 80303

The National Institute of Standards and Technology (NIST) has been engaged in the measurement and calibration of standard electromagnetic fields for many years. A parameter that is heavily used in standard-field measurements is the effective length which relates the magnitude of an incident electric field component parallel to a receiving dipole to the induced open-circuit gap voltage. Discrepancies between theoretical calculations of the effective length and experimentally measured values have been consistently observed for a large number of cases over the years. If the effective length can be accurately and efficiently computed, the results might very well help to resolve these discrepancies.

The approach that is used in our computation of the effective length is to solve the scattering problem of a plane wave that is incident on the broadside of a dipole of length  $L$  that has a symmetrically placed gap of width  $G$ . This scattering problem is formulated in terms of an electric field integral equation (EFIE) in conjunction with a thin-wire approximation. The unknown dipole current in the EFIE is found using a Galerkin procedure that employs piecewise-sinusoidal basis functions. Once the antenna current has been determined, the total electric field is found by means of a straight-forward integration process. The gap voltage is then found by evaluating a line integral of the electric field along a prescribed contour.

The first evaluation of the gap voltage utilizes a direct line integration across the gap of width  $G$ . For this contour, the gap voltage does not converge, even for a very large number of basis functions. This can be attributed to the slow convergence of the current cell values in the immediate vicinity of the gap. In order to circumvent this difficulty, an alternative closed contour is employed for the evaluation of the gap voltage. The electric field along this contour is no longer dominated by the current cells near the gap, but it is influenced more heavily by the rapidly converging current cells that are located away from the gap. The result of using this alternative contour is a gap voltage that converges rapidly, even with relatively few basis functions. The effective length results obtained from this procedure are then compared to those of an antenna with a gap with an infinitesimal width. This comparison enables one to assess the loading effects of a finite gap.

D1-1 CHARACTERISTICS OF  $\text{In}_x\text{Ga}_{(1-x)}\text{As}$  MIXER DIODES  
0840 FOR TERAHERTZ APPLICATION\*

R. J. Mattauch, Udayan Bhapkar, and Theresa Brennan  
Semiconductor Device Laboratory,  
Department of Electrical Engineering  
University of Virginia, Charlottesville VA  
22903-2442, USA

As has been reported earlier (Mattauch, Brennan, and Bhapkar, 1991 North American Radio Science Meeting, London, Ontario Canada June 1991), sufficiency of local oscillator power for space-based heterodyne receivers operating in the submillimeter wave range is a continual problem. One method of easing this requirement is the employment of sub-harmonic mixing. This technique reduces the frequency of LO power needed by a factor of two but requires a mixing element which exhibits a centrally symmetric  $I(V)$  curve. Since the mixer element of choice for such applications is a Schottky barrier diode, the necessary  $I(V)$  characteristic is commonly achieved by an antiparallel arrangement of two such diodes. The applied LO power necessary for minimum conversion loss must be sufficient to drive each element into the high conductivity region of operation once each cycle. Since such an antiparallel device is difficult to bias a large amount of LO power can be required. This shortcoming can be eased by reduction of the "turn-on" voltage of each diode. Such a reduction can be realized by formation of the diode on a ternary material such as  $\text{In}_x\text{Ga}_{(1-x)}\text{As}$ . In this case the material energy gap and thus diode forward turn-on voltage decrease with increasing indium mole fraction,  $x$ .

Computer modeling of the diode  $I(V)$  characteristic as a function of indium mole fraction has been carried out using a quantum mechanical approach. The result of this analysis was used in a mult-port mixer analysis developed Siegel and Kerr and has shown minimal conversion loss degradation with respect to values measured for comparable GaAs mixer elements. In this paper we report on fabrication technologies used to form test mixer elements, low frequency  $I(V)$  relations and their relation to theoretical predictions, and preliminary RF performance.

\*This work was supported in part by NASA through the University of Michigan Space Terahertz Technology Center under grant Z-25251, and by the National Science Foundation under grant ECS-91131232

D1-2  
0900

**A 200 GHz TRIPLER USING SINGLE BARRIER VARACTORS**  
 M. A. Frerking, P. Batelaan, D. Choudhury  
 Jet Propulsion Laboratory, California Institute of Technology  
 Pasadena, CA 91109

The non-linear device most commonly used for submillimeter-wave harmonic generation is the GaAs Schottky varactor diode. Output power adequate to serve as a local oscillator source for SIS tunnel junctions has been demonstrated with whisker-contacted GaAs Schottky varactor multipliers in waveguide mounts up to about 800 GHz (cf. B.L.A. Rydberg, B.N. Lyons, U.S. Lidholm, Proc. Sec. Symp. Space THz Tech., 212-225, 1991). In this paper we discuss two new multiplier devices the single barrier varactor (SBV) (A. Rydberg, H. Gronquist, E. Kollberg, IEEE Elect. Dev. Lett., 373-375, 1990) and the back-to-back BNN (bbBNN) (U. Lieneweg, T. Tolmunen, M. Frerking, J. Maserjian, Proc. Sec. Symp. Space THz Tech., 270-284, 1991). These new varactors have potential advantages such as stronger non-linearities or special symmetry, which make them attractive for submillimeter-wave frequency multiplication.

We have measured the performance of a tripler using a SBV over an output frequency range from 186 to 207 GHz. Peak output powers of 0.4 mW were achieved. The SBVs reported here were fabricated at Chalmers University of Technology and MIT Lincoln Laboratory. A capacitance-voltage characteristic is shown in Figure 1. The varactors are mounted in a crossed waveguide mount shown schematically in Figure 2. We are currently fabricating bbBNN devices and will test them in the tripler mount.

We have calculated the theoretical performance of these devices using a large signal analysis. One of the major losses in the mount was found to be the output backshort. A comparison to measured results and a discussion of various losses in the mount and the varactor will be presented at the conference.

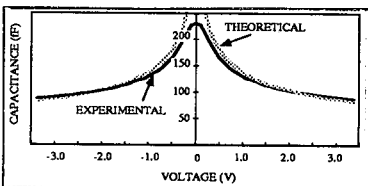


Figure 1: C-V characteristic of SBV

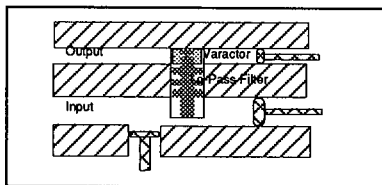


Figure 2: Waveguide tripler mount

**ACKNOWLEDGEMENTS:** The research described in this paper was performed by the Center for Space Microelectronics Technology, Jet Propulsion Laboratory, California Institute of Technology and was sponsored by the National Aeronautics and Space Administration, Office of Aeronautics, Exploration, and Technology.

D1-3  
0920

## THE CHARACTERISTICS OF QUASI-OPTICAL FET OSCILLATOR USING A SLOT ANTENNA

Shigeo Kawasaki and Tatsuo Itoh  
Department of Electrical Engineering  
University of California  
Los Angeles, CA 90024

This paper describes some characteristics of a circuit with 2 quasi-optical oscillators in order to obtain fundamental data for the spatial power combiner. The structure of each quasi-optical oscillator makes use of both sides of the dielectric substrate by adopting a modified slot antenna in a ground plane of the circuit. Due to this structure, a monolithic quasi-optical oscillator can be realized through simple modification on a monolithic microwave integrated circuit. In order to easily design and fabricate circuits and to use a null point of the antenna pattern for measurement rather than its peak point, we design a circuit with a difference antenna pattern. Two negative resistance oscillator circuits are symmetrically fabricated on one side of the dielectric substrate. Ideally, they should have the same characteristics under the same DC voltages, if the two FETs have the same characteristics. On the other side, there is a  $2\lambda$  modified slot. Its metal part works as a ground plane to oscillator circuits in the opposite side. Feed points are located at the  $\lambda/2$  points from both ends of the slot. In order to de-couple each oscillator, it has a high impedance section with width of  $\lambda/2$  at the center of the slot. Due to this high impedance section, each oscillator circuit works as two quasi-optical oscillators with slot antenna length  $1\lambda$ . Under this configuration, we measured the locking frequencies and antenna patterns.

First, we measured the characteristics (the oscillation frequency, receiving power,  $V_{DS}$  and so on) of each oscillator. Under the same  $V_{DS}$  and  $V_{GS}$ , they have almost the same characteristics except oscillation frequencies. Difference is about 110 MHz. When they are operated at the same time, they are locked and generate a difference antenna pattern. Null points were obtained around the broadside direction, if both FET oscillators were operated under the same  $V_{DS}$  and  $V_{GS}$ . However, under the different values of  $V_{DS}$ , the antenna pattern were modified so as to increase the difference between two peak values in antennae pattern. According to the theoretical consideration, this results from the smaller phase difference (e.g.  $135^\circ$ ) between the two feed points of the array compared to the difference antenna pattern condition ( its phase difference is  $180^\circ$  ). Its tuning range was about 30 MHz, when  $V_{GS}$  was changed. In order to obtain a broadband characteristic, one of the oscillation frequencies was changed. The new locking frequency was higher than the lower frequency of the two independent oscillation frequencies by about the two-thirds of their difference. The total radiation power was degraded in this case. However, about a 110 MHz tuning range was obtained by adjusting  $V_{GS}$ .

We investigated the phase shift and the tuning range of the 2 element array of a quasi-optical oscillator circuit. By controlling the applied DC voltages, the antenna patterns were modified. Meanwhile, by adjusting the oscillation frequencies independently, the tuning range was broadened.

D1-4  
0940

## A Quasi-Optical Bow Tie MESFET VCO

Scott C. Bundy      Thomas B. Mader      Zoya Basta Popović

Department of Electrical and Computer Engineering  
University of Colorado, Boulder, CO 80309

A planar grid oscillator is a quasi-optical power-combining source consisting of hundreds of active devices ("A 100-MESFET Planar Grid Oscillator," Z.B. Popović *et al.*, MTT-39, 193, 1991). Such an oscillator can be controlled externally by a planar varactor diode grid which has an electrically variable impedance. In this work, we present a 4 by 6 quasi-optical VCO around 5 GHz. The oscillator is fabricated on an electrically thin ( $\lambda/80$ ) substrate with Fujitsu C-band GaAs MESFETs. The varactor tuning surface is fabricated with Metelics diodes, and the two substrates are positioned back-to-back, as shown in Figure 1(c). The unit cell of the grids is a bow-tie antenna  $0.125\lambda$  long at 5 GHz. We are using a bow-tie grid to achieve maximum tuning range, since the bow-tie element is broadband ("Grid Mixers," Hacker, *et al.*, submitted to IEEE Trans. MTT, 1991). The VCO exhibits 0.486 GHz tuning range at 4 GHz, a 10% tuning bandwidth with only 2 dB change in power over the entire tuning range. An equivalent circuit model and experimental results will be presented.

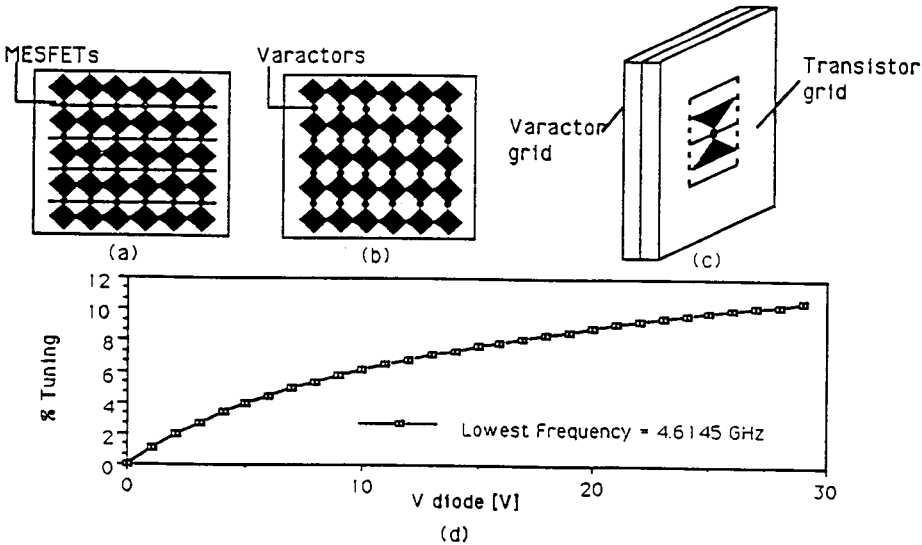


Figure 1: (a) The MESFET grid oscillator and (b) varactor grid tuning element make (c) a quasi-optical VCO. (d) The tuning range is 10% at 4.8 GHz with only 2 dB of change in power.

D1-5  
1020

A SPECIAL FET/HMET MOUNT STRUCTURE FOR  
WAVEGUIDE AMPLIFIERS IN OR ABOVE 12 GHz BAND

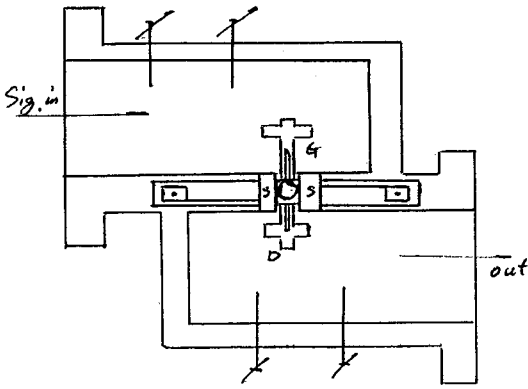
Huang Guanghua, 2314 COE# 296, University of  
Wyoming, Laramie, WY 82070

Abstract: A special FET/HMET mount structure for waveguide amplifiers in or above 12 GHz band is presented. The structure is especially suitable for developing amplifiers through 12 GHz to sub-millimeter or even millimeter wave band due to the significant lower loss of waveguide.

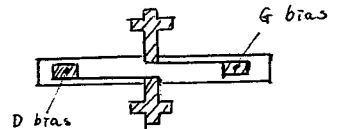
Several two stage amplifiers in 12 GHz band with 500 MHz bandwidth for LNB of satellite receiver are developed. Typically only 0.2-0.4 db noise figure increase between the noise figure of the amplifiers and the FET noise figure within 500 MHz bandwidth (  $NF_{am}$  2.0 db by using two NE 67383 FET which noise figure are 1.6 - 1.8 db in 12 GHz band ).

One stage structure is shown in the Fig. for waveguide amplifier. The main significance of the structure is that microwave signal is coupled directly into/out FET for reducing the loss in input/output matching networks.

No reference.



One stage amplifier



FET mount structure

D1-6        MILLIMETER-WAVE, CRYOGENICALLY-COOLABLE, LOW-NOISE  
 1040        HFET AMPLIFIERS: STATE-OF-THE-ART AND FUTURE  
              TRENDS

Marian W. Pospieszalski  
 National Radio Astronomy Observatory\*  
 2015 Ivy Road  
 Charlottesville, VA 22903

Recent progress in the development of ultra low-noise, cryogenically-coolable, HFET (heterostructure field-effect transistor) amplifiers for millimeter wavelength receivers is reported. The design, construction and performance of a Q-band (38-45 GHz) amplifier for radio astronomy applications with record-breaking cryogenic performance (noise temperature of less than 30 K at 41 GHz and ambient temperature of 17 K) are discussed in detail.

The validity and usefulness of a recently developed noise model of a FET (HFET), (M. W. Pospieszalski, *IEEE Trans. MTT*, MTT-37, pp. 1340-1350, 1989; M. W. Pospieszalski and A. C. Niedzwiecki, *Proc. 1991 Int. Microwave Symp.*, pp. 1117-1120, Boston, MA), for the computer-aided design of millimeter-wave amplifiers are established. The implications of this model in the search for new low-noise HFET structures are discussed. A model-based prediction of noise performance is compared with recently published data for AlInAs/GaInAs on InP HFET's (K. H. Duh *et al.*, *Proc. 1990 Int. Microwave Symp.*, pp. 595-598, Dallas, TX; S. E. Rosenbaum *et al.*, *Proc. 1991 Int. Microwave Symp.*, pp. 815-819, Boston, MA; P. D. Chow *et al.*, *Proc. 1991 Int. Microwave Symp.*, pp. 1041-1044). A model-based prediction of cryogenic performance shows that cryogenically-cooled HFET receivers should soon be competitive with SIS (superconductor-insulator-superconductor) mixer receivers (A. R. Kerr and S.-K. Pan, *Int. J. Infrared & Millimeter Waves*, vol. 11, pp. 1169-1187, 1990) in the 3mm wavelength atmospheric window.

---

\*The National Radio Astronomy Observatory is operated by Associated Universities, Inc. under Cooperative Agreement with the National Science Foundation.

D1-7 8.8 GHz HIGH TEMPERATURE SUPERCONDUCTING  
1100 COPLANAR WAVEGUIDE RESONATOR

A. R. Blemker and G. J. Valco  
Department of Electrical Engineering  
Ohio State University  
Columbus, OH 43210

K. B. Bhasin  
National Aeronautics and Space  
Administration, Lewis Research Center  
Cleveland, OH 44135

Laser ablation has been used to form  $\text{YBa}_2\text{Cu}_3\text{O}_{7-x}$  thin films on  $\text{LaAlO}_3$  substrates. These films have been patterned into several 8.8 GHz coplanar waveguide resonators. A resonator of identical geometry was also fabricated with a gold film. The reflection coefficients of the resonators have been measured as a function of frequency at temperatures from just above their critical temperatures to 20 K. Additional test structures were patterned adjacent to the resonator on each substrate to allow measurement of critical temperature, critical current density and normal state resistivity. These measurements were performed at DC.

Unloaded quality factors were extracted from the reflection coefficients. Values as high as 1250 at 77 K and 1700 at 20 K were obtained. The value at 77 K is approximately seven times larger than that measured for the gold resonator at the same temperature. A correlation between the critical temperatures of the films and the quality factors of the resonators was observed. The correlation was not perfect in that some films with high critical temperatures exhibited poor microwave performance. Optical and scanning electron microscopy suggest that this is a result of poorer morphology in those films.

The films with the higher unloaded quality factors had critical current densities greater than  $10^6$  A/cm<sup>2</sup> at 77 K. The details of the microwave and DC results will be presented and the observed relationships between the microwave properties of the films and their critical temperatures, morphologies, critical current densities and normal state resistivities will be discussed.

D1-8 HYBRID Y-Ba-Cu-O SUPERCONDUCTING MICROWAVE FILTER/GaAs  
1120 LOW NOISE AMPLIFIER CIRCUIT

S. S. Toncich\*, K. B. Bhasin\*, C. M. Chorey\*\*,  
R. R. Bonetti\*\*\* and A. E. Williams\*\*\*

\* National Aeronautics and Space Administration  
Lewis Research Center, Cleveland, Ohio 44135

\*\* LeRC Group, Sverdrup Technology, Brook Park, Ohio  
44142,

\*\*\*COMSAT Laboratories, Clarksburg, MD 20871

High performance microwave systems require low noise, high gain, low loss devices and circuits. The integration of high Tc superconducting passive devices with GaAs active circuits operating at liquid nitrogen temperatures has the possibility to meet these requirements. We have hybridized and characterized a superconducting two pole microstrip bandpass filter and a GaAs low noise amplifier(LNA) at 77K and compared its performance to a hybrid gold filter/LNA circuit operating at the same temperature.

A two-pole microstrip bandpass filter was fabricated using laser ablated Y-Ba-Cu-O superconducting films on lanthanum aluminate substrate with a center frequency at 7.5 GHz. An identical filter using gold film was also fabricated. The superconducting filter showed a lower insertion loss than the gold filter at 77K by 2 dB. Gain and noise figure characteristics of a commercially obtained X-band LNA (Avantek) was obtained at 77K and below. Gain and noise figures improved by 1 and 2 dB respectively at 77K as compared to 300K.

The LNA was then connected to a gold filter and the hybrid circuit was characterized at 300K and 77K. The gain and noise figure characteristics of the hybrid superconducting filter/LNA circuit were also obtained. While the gold hybrid showed improved characteristics at 77K when compared to 300K, the superconducting hybrid showed higher overall gain at 77K.

D1-9 INVESTIGATION OF INTERFACES BETWEEN HIGH TEMPERATURE  
1140 SUPERCONDUCTING MATERIALS, METALS AND SEMICONDUCTORS

Z. Zhang, F.S. Barnes

Department of Electrical and Computer Engineering

University of Colorado at Boulder

Campus Box 425

Boulder, CO 80309-0425

The high  $T_c$  superconducting materials could react, interdiffuse or be inert with metals and conventional semiconductors, thus forming different kinds of junctions at the interface. These junctions provide linear or nonlinear characteristics which are useful as microwave or optical detectors as well as utilizing superconductive interconnections.

High quality epitaxial Yttrium Barium Copper Oxide ( $Y_1Ba_2Cu_3O_{7.8}$ ) thin film has been manufactured on various substrates by laser deposition in our laboratory. Good Ohmic contact has been achieved by evaporating silver and gold on  $Y_1Ba_2Cu_3O_{7.8}$  thin film and the junctions are electrically characterized.  $Y_1Ba_2Cu_3O_{7.8}$  thin film has also been successfully grown on yttrium-stabilized zirconia buffered silicon substrate.

The investigation of the interfaces will be extended to other metals and semiconductor materials and results will be presented.

F3-1  
0840

## **RADIO REFRACTIVITY PROFILES DEDUCED FROM AEROSOL LIDAR MEASUREMENTS**

H.G. Hughes, M.R. Paulson and J.H. Richter  
Ocean and Atmospheric Sciences Division, Code 54  
Naval Ocean Systems Center  
San Diego, CA 92152-5000

A technique is presented for estimating radiowave ducting conditions from aerosol lidar measurements. A 1.06  $\mu\text{m}$  lidar is used to measure the power backscattered from aerosols. On individual days, relative humidity profiles measured with radiosondes launched simultaneously with vertical lidar shots were highly correlated with the range-compensated lidar profiles. However, the relationship between the lidar power returns and relative humidity profiles changed from day to day, indicating an air mass dependence on the aerosols' optical parameters. Using a combined data set of thirteen days, a linear relationship (correlation  $\rho = 0.73$ ) was determined between the relative humidity at a given altitude and the range-compensated power received by the lidar from the same altitude. While the magnitudes differed in most cases, the gradients in modified refractivity calculated using standard vertical lapse rates of temperature and pressure with the experimentally determined relationship were in close agreement with those calculated using the radiosonde measured parameters.

Examples of radio signal coverage based on lidar returns are presented and compared with those calculated from the radiosonde data for both elevated and ground-based ducting conditions.

F3-2 Measurement of Extinction Profiles with an Aureole Lidar  
0900

Wm P. Hooper  
Atmospheric Physics Branch<sup>1</sup>  
Space Science Division  
Naval Research Lab  
Washington DC 20375-5000

While a single wavelength, laser radar (lidar) provides detailed range-resolved profiles of atmospheric aerosol structures, an inability to distinguish between backscatter and scattering losses severely limits this instrument's ability to sense important optical parameters. The newly developed aureole lidar (operating in a down-looking mode from an aircraft) circumvents this restriction by measuring photons which reflect off the oceans surface and interact with atmospheric aerosols, determining the light loss from the laser beam, and finally deriving an extinction profile from the lidar return. In this presentation, the instrumental design, measurements, and limitations will be discussed.

---

<sup>1</sup> Current address Infrared/Optics/Radio Sensors Branch, Center for Advanced Space Sensing, Naval Research Laboratory.

F3-3  
0920**EVALUATION OF AN AUREOLE LIDAR TECHNIQUE FOR ESTIMATING EXTINCTION PROFILES USING AEROSOL SPECTROMETER MEASUREMENTS**

D. R. Jensen

Ocean and Atmospheric Sciences Division,  
Code 543

Naval Ocean Systems Center

San Diego, CA 92152-5000

W. P. Hooper

Atmospheric Physics Branch

Space Science Division, Code 4112

Naval Research Laboratory

Washington, DC 20375

An aureole lidar technique for estimating extinction profiles has been developed at the Naval Research Laboratory, Washington, DC (W. P. Hooper, NRL Memorandum Report 6623, 1990). This technique has been evaluated by making nearly simultaneous measurements of atmospheric extinction profiles using the NRL airborne aureole lidar platform and aerosol spectrometers. Profiles of measured aerosol-size distributions were used to calculate extinction coefficients and were compared with the aureole lidar estimations. Aureole lidar deduced extinction coefficient profiles are similar in structure to the aerosol spectrometers measured profiles and agreed reasonably well in extinction magnitude. When the near surface aircraft aerosol measurements are averaged over a longer period of time, excellent agreement exists between the aureole lidar and the measured values.

F3-4  
0940**LIDAR REMOTE SENSING TECHNIQUES FOR DEVELOPING AND EVALUATING ATMOSPHERIC AEROSOL MODELS**

D. R. Jensen

H. G. Hughes

M. R. Paulson

Ocean and Atmospheric Sciences Division,  
Code 543

Naval Ocean Systems Center

San Diego, CA 92152-5000

A technique is presented by which lidar returns from aerosols can be used to adjust simultaneously observed/modeled aerosol size distributions to represent existing atmospheric conditions. Examples are presented, using this technique, for the evaluation of the Navy Oceanic Aerosol Model (NOVAM) and the Navy Aerosol Model (NAM) for number densities near the ocean surface for low wind speeds. The evaluation of NOVAM indicated that, when scaled to visibility, good agreement exists between the lidar scaled extinction and backscatter coefficients and the predicted profiles. While adjustments of the NAM aerosol number densities can be made to match the modeled profiles to those measured by lidar, the large adjustments for low wind speeds indicate that the modeled aerosol size distribution shape near the ocean may not be correct.

F3-5  
1000**REMOTE SENSING OF AEROSOL EXTINCTION USING  
SINGLE-ENDED LIDARS**

J.H. Richter, H.G. Hughes and M.R. Paulson  
Ocean and Atmospheric Sciences Division, Code 54  
Naval Ocean Systems Center  
San Diego, CA 92152-5000

Aerosol extinction is one of the primary factors limiting the performance of systems which rely on visible or infrared radiation in the atmosphere. Lidars have been used to measure the backscattered radiation from aerosols in an attempt to determine extinction. However, techniques for inverting the power returned to a single-ended lidar to obtain range-dependent extinction coefficients requires a knowledge of the relationship between the backscatter and extinction coefficients along the path. If the aerosol distribution in the atmosphere is horizontally homogeneous, the need for knowing the relationship between backscatter and extinction can be eliminated by comparing the powers received from each altitude along two or more different elevation angles, and the extinction coefficient variation in the vertical direction can be determined.

A review is presented of past efforts to determine atmospheric extinction from single-ended lidar measurements and the assumptions made concerning backscatter/extinction relationships. The degree to which aerosols within the convectively mixed atmosphere can be expected to be horizontally homogeneous is also discussed. The conclusion is, that the accuracy of extinction coefficients determined by a single-ended lidar cannot be assured unless the extinction/backscatter relationship is known or the atmosphere is horizontally homogeneous over the propagation path.

GH1-1  
0840**HIGH-RESOLUTION OBSERVATIONS OF HF IONOSPHERIC MODIFICATIONS****F. T. Djuth, J. H. Elder, K. L. Williams**

Geospace Research, Inc., 550 N. Continental Blvd., El Segundo, CA 90245

**M. P. Sulzer**

Arecibo Observatory, Arecibo, Puerto Rico 00613

**P. Stubbe, H. Kohl**

Max-Planck-Institut für Aeronomie, Postfach 20, D-3411 Katlenburg-Lindau, FRG

**M. T. Rietveld**

EISCAT Ramfjordmoen, N-9027 Ramfjordbotn, Norway

**J. A. Fejer**

Department of Electrical Engineering and Computer Sciences, University of California, San Diego, La Jolla, CA 92093

Langmuir and ion oscillations excited by a powerful, high-frequency (HF) radio wave reflecting in the F-region have been studied in detail at Arecibo, Puerto Rico and at Ramfjordmoen, Norway. Observations have been made using the 80-MW effective radiated power (ERP) HF facility located near Arecibo Observatory, and with the new 1.2-GW ERP facility at Ramfjordmoen, Norway. The principal plasma diagnostics are the 430 MHz incoherent scatter radar at Arecibo, and the 224 MHz and 933 MHz EISCAT radars at Ramfjordmoen. Exceptionally good temporal and spatial resolution highlight the radar backscatter measurements. Currently, height-resolved spectral information is available from both facilities. Recent observations made at Arecibo clearly illustrate the inadequacy of several theoretical approaches employed in the past. Efforts to apply strong turbulence theory to the Arecibo measurements have met with some success, particularly in the early time plasma environment (tens of ms following radio wave turn-on in the ionosphere). At later times ( $> 50$  ms after turn-on), spectral features similar to those expected from the weak turbulence approximation are evident in the measurements, but a more complete theory is required to explain observational details. Ultimately, a plasma state exhibiting unexpected richness of complex structure is realized in the Arecibo ionosphere. Analyses of data acquired with the new facility at Ramfjordmoen, Norway reveal some similarities with Arecibo results, but, more importantly, there are striking dissimilarities. This is particularly true of the evolutionary path of the turbulence. The late-time development of the turbulence (e.g. altitude structure, hysteresis effects, HF power dependences) appears to be distinctive in the Norwegian experiments. Our current observations will be discussed within the context of caviton formation in the plasma over short time scales ( $< 100 \mu\text{s}$ ) following HF turn-on, the coexistence of parametrically excited waves and cavitons in the plasma, and the disruptive influence HF-induced geomagnetic field-aligned irregularities may exert on the late-time development of cavitons.

GH1-2 RADAR OBSERVATIONS OF IONOSPHERIC LANGMUIR  
0900 TURBULENCE DRIVEN BY PULSED HF TRANSMISSIONS  
M. P. Sulzer, Arecibo Observatory  
Box 995, Arecibo, PR 00613  
J. A. Fejer, Department of Electrical and  
Computer Engineering, University of California  
San Diego

Spectra of 430 MHz radar backscatter from Langmuir turbulence were obtained every millisecond from heights 150 m apart. The turbulence was driven by 5.1 MHz HF transmissions of 80 MW ERP with pulsing sequences of either 50 ms on 950 ms off or 10 ms on 990 ms off. The purpose of the observations was the study of the early time evolution of the spectrum of Langmuir turbulence, starting from an unperturbed ionosphere.

Observations with the 10 ms on 990 ms off HF pulsing show the development of a spectrum of about 10 kHz width, almost symmetrical about the pump frequency of 5.1 MHz within 1 ms after the start of the 10 ms long HF pulse. This spectrum is interpreted in terms of scattering of the pump by thermal level ion acoustic waves and is expected to occur at the 'matching height' on theoretical grounds.

After another ms or two a broad strongly asymmetric spectrum appears, extending to about 100 kHz below the pump frequency, at a height about 1 km above the matching height near the reflection height of the pump wave. In addition to the broad spectrum below the pump frequency there is a sharp peak (the free mode peak) above the pump frequency. Near the end of the 10 ms HF pulse the free mode peak is also observed down to 600 m below the reflection height but without the broad spectrum at those 4 lower heights. The broad spectrum at the reflection height is quenched within less than 1 ms after the end of the 10 ms pulse but the free mode peaks are only damped at the rate of about 3 db / ms, suggesting collisional damping.

Observations with the 50 ms on 950 ms off HF pulsing show similar development during the first 10 ms of the on-period; later the free mode is no longer seen and a Langmuir wave cascade develops close to the matching height. After the end of the 50 ms pulse the broad spectrum at the reflection height is again quenched in less than 1 ms while the Langmuir wave cascade spectra are damped much more slowly by (Coulomb) collisions.

The relation of these results to existing theories is discussed briefly.

GH1-3  
0920PRECONDITIONING EFFECTS IN RADAR OBSERVATIONS  
OF IONOSPHERIC LANGMUIR TURBULENCE DRIVEN BY  
POWERFUL HF TRANSMISSIONS

J. A. Fejer, Department of Electrical and  
Computer Engineering, Mail Code R-007  
University of California San Diego  
La Jolla, CA 92093  
M. P. Sulzer, Arecibo Observatory  
Box 995, Arecibo, PR 00613

It has been known for some time (Morales et al., Radio Sci. 17, 1313, 1982) that after powerful HF transmissions of sufficiently long duration much less HF power is needed to produce Langmuir turbulence than before. More recently (Fejer et al. J. Geophys. Res., in press, 1992) it was shown that after HF transmissions with about 40 MW ERP for a duration of 20 seconds, strong 430 MHz radar backscatter from Langmuir turbulence was observed with only 3 MW ERP for over a minute from near the reflection height of the HF pump wave; later only below threshold type spectra from a height lower by about 1 km (the 'matching height') were observed. The temporal resolution of those observations was only half a minute.

In the present observations height-integrated spectra were obtained every second; height discrimination was sacrificed for improved resolution in time. It was found that preconditioning effects were not observed for transmissions with increased power lasting for less than 10 s and for values of the increased power less than 10 MW ERP. After transmissions with increased power in the O-mode strong above threshold type spectra were observed for about 4 minutes intermittently before the spectra reverted to the weak below threshold type permanently. Before that time weak below threshold spectra alternated with strong above threshold spectra.

After transmissions with increased power (40 MW ERP) in the X-mode followed by weak (2.5 MW) transmissions in the O-mode, strong above threshold spectra were not observed for about the first 4 minutes; after that 'waiting period' strong above threshold spectra again alternated with weak below threshold ones for over 5 minutes.

The theoretical implications of the observations will be discussed. The fact that preconditioning is observed with the strong HF transmissions in the X-mode, suggests that thermal self-focusing is responsible for the generation of the irregularities that make preconditioning possible. Ionospheric drifts would then have to bring the irregularities from the region illuminated by the X-mode transmissions to the region illuminated by the O-mode transmissions and by the radar.

GH1-4 ANTI-STOKES LANGMUIR MODES PRODUCED BY HIGH POWER  
0940 HF WAVES AT ARECIBO, PUERTO RICO  
M.C. Lee, K. Velice, K.M. Groves  
Massachusetts Institute of Technology  
Cambridge, Massachusetts 02139  
S.P. Kuo  
Polytechnic University  
Farmingdale, New York 11735

Ionospheric heating experiments were conducted recently at Arecibo, Puerto Rico to investigate the anti-Stokes Langmuir modes (also referred to as free modes in the literature) produced by high-power HF waves. These Langmuir modes have frequencies higher than the heater wave frequencies by tens of kilohertz depending upon the heater wave frequencies. The frequency difference between the anti-Stokes Langmuir waves and the heater wave was found to be inversely proportional to the heater wave frequency, indicating that these induced anti-Stokes Langmuir waves are propagating normal modes. Our observations support the source mechanism (Kuo and Lee, 1991) we propose to generate the anti-Stokes Langmuir modes by ionospheric heating. These frequency up-shifted Langmuir waves can result from the nonlinear scattering of the PDI (parametric decay instability) excited field-aligned Langmuir waves off the background lower hybrid density fluctuations. This process of nonlinear scattering produces upgoing and downgoing Langmuir waves with both upshifted and downshifted frequencies. However, the intensities of the frequency upshifted Langmuir waves are much larger than those of the frequency downshifted Langmuir waves because the former are resonant modes while the latter the nonresonant modes. Quantitative analyses show that even in the presence of weak background lower hybrid waves, the proposed nonlinear scattering process can produce the anti-Stokes (i.e., frequency upshifted) Langmuir waves with large intensities (radar cross-sections). All the observed characteristics of the anti-Stokes Langmuir modes can be reasonably understood in terms of the proposed source mechanism, such as their frequencies, intensities, and temporal evolution.

GH1-5 **Space and Time Distribution of Langmuir Turbulence Excited by**  
1020 **HF Modification of the Ionosphere**

D. F. DuBois, Alfred Hanssen\*, and H. Rose  
Los Alamos National Laboratory, Los Alamos, NM 87545  
(\* Permanent address: Univ. of Tromsø, N-9000 Tromsø, Norway)

The predictions of strong Langmuir turbulence (SLT) theory will be compared with recent altitude and temporally resolved observations of the turbulence induced in a non-preconditioned ionosphere, by powerful hf waves. Near reflection altitude, the theory predicts (upshifted) plasma line power spectra consisting of a broad "caviton continuum" for  $\omega < \omega_{HF}$  and a free mode peak at  $\omega > \omega_{HF}$ . Such spectra are consistently observed at Arecibo at early times in the heating pulse, and agree with predictions in quantitative detail. At lower altitudes and later into the heating pulse, parametric decay cascade type spectra are observed. These are also consistent with SLT predictions as far as the limited number of cascade lines, the shape of the ion line power spectra and the continuous background underlying these spectra are concerned. However, these spectra are not always observed to arise at the required matching altitudes. An explanation of this altitude discrepancy will be offered which involves the self-consistent modification of the electron density profile by the ponderomotive force of the narrow layers of turbulence coinciding with the "Airy" maxima of the heater wave. This mechanism can act on the time scales of  $\sim 100$  ms in which the cascade-like spectra is observed to developed at Arecibo.

GH1-6  
1040**Altitude and Heater Power Dependence of HF Generated  
Langmuir Turbulence From the 1D Modified Zakharov Model**Alfred Hanssen<sup>(1,2)</sup>, D. F. DuBois<sup>(2)</sup>, H. A. Rose<sup>(2)</sup>, and E. Mjølhus<sup>(1)</sup>

(1) Univ. of Tromsø, N-9000 Tromsø, Norway

(2) Los Alamos National Laboratory, Los Alamos, NM 87545

By modifying the 1D Zakharov model so as to include a long wavelength driving term, a frequency mismatch term, and damping operators, we can model the altitude and heater power dependence of the excited turbulence in ionospheric heating experiments. We will demonstrate that there is a continuous distribution of turbulence from broad collapse type energy spectra close to the reflection height, to cascade spectra at lower heights, and that there exist an intermediate coexistence layer with signatures of both types of turbulence in between. We will present well resolved power spectra from these solutions, which shows a remarkable resemblance with well resolved spectra from Tromsø and Arecibo, at early times in cold start experiments. Our model also contains information about the stimulated electromagnetic emissions (SEE) induced by the Langmuir turbulence, and we will present height resolved SEE spectra, as well as integrated spectra, as computed from our version of the 1D Zakharov model. Finally, a demarcation diagram, showing the global distribution of cascade and collapse type turbulence, as a function of height and pump strength, will be proposed.

GH1-7  
1100METHODS FOR ANALYSIS OF  
STRONG TURBULENCE IN PLASMA PHYSICS  
Simon Goodman  
Swedish Institute of Space Physics, S-755 91 Uppsala, Sweden

An outstanding problem in ionospheric heating and other areas of plasma physics is to understand strong turbulence. The post-parametric status of knowledge is limited to unmagnetized and fluid type Langmuir turbulence. Analytic methods are limited to a qualitative understanding of singularities and collapse of wave packets in fluid plasma. Inclusion of realistic kinetic effects, such as Landau damping, makes the problem of plasma turbulence extremely difficult and only accessible to supercomputer number crunching.

In this work we present a study of an attempt to put strong turbulence on a kinetic basis and to present an attempt to develop a method of studying some aspects of the turbulent process in a way which should be general enough to attack a wide class of problems including those of magnetized plasmas and ones where realistic Landau damping can be treated simply and analytically. We treat Langmuir turbulence with Landau damping as our central example. In Langmuir turbulence, the free energy becomes increasingly negative and singularities develop. The process is non-stationary and non-equilibrium. If a suitable damping, e.g. Landau damping, is implemented, then the free energy has a minimum and the process leading to the development of a singularity slows down—we are then motivated to treat the problem as being one of a "quasi-equilibrium" state, and to use the path-integral approach to statistical field theory. This method allows us to handle complex damping terms exactly and to handle quartic nonlinearities exactly, at the energy minimum.

We have calculated the average electric field energy at the point of the onset of burnout of collapsing cavitons and our results agree with particle in cell simulations as well as numerical solutions to the Zakharov equations.

GH1-8 WAVE BREAKING DURING IONOSPHERIC  
1120 MODIFICATION

D.R. Nicholson, Jin-gen Wang, and G.L. Payne  
Department of Physics and Astronomy  
University of Iowa  
Iowa City, IA 52242-1479

Enhanced airglow during ionospheric modification (A. Biondi et al., J. Geophys. Res. **75**, 6421-6424, 1970) is believed to be due to accelerated electrons. If the electron-plasma waves involved in modification are only weakly nonlinear, as in weak turbulence processes (J. Fejer and Y.-Y. Kuo, Phys. Fluids **16**, 1490-1496, 1973), then it is often suitable to use quasilinear theory (D. Nicholson, J. Geophys. Res. **82**, 1839-1845, 1977) to treat electron acceleration. More intense waves require the application of resonance-broadening (J. Weinstock, J. Geophys. Res. **80**, 4331-4345, 1975) and particle trapping (J. Fejer and K. Graham, Radio Sci. **9**, 1081-1084, 1974) theories.

It is possible (V. Petviashvili, Sov. J. Plasma Phys. **2**, 247-249, 1976; J. Weatherall et al., J. Geophys. Res. **87**, 823-832, 1982; D. DuBois et al., J. Geophys. Res. **95**, 21,221-21,272, 1990) that three-dimensional spatially collapsing Langmuir solitons accelerate electrons via wavebreaking at their centers (V. Zakharov et al., Sov. Phys. JETP **69**, 334-341, 1989). We have initiated a systematic study of this possibility (Jin-gen Wang et al., submitted to Phys. Fluids) and present one-dimensional numerical results which follow accelerated electrons up to and beyond wavebreaking in undriven and driven cases.

GH1-9  
1140THE INSTABILITY RESPONSIBLE FOR HFPLS  
OBSERVED IN THE ARECIBO HEATING EXPERIMENTS\*S.P. Kuo and J. Huang  
Weber Research Institute, Polytechnic University, Route  
110, Farmingdale, NY 11735M.C. Lee  
Plasma Fusion Center, Massachusetts Institute of  
Technology, Cambridge, MA 02139

In the Arecibo heating experiments, observations show that HF heater-induced plasma lines (HFPLs) originate from a height near the HF reflection height which is about one kilometer higher than the matching height determined by the location of the photon enhanced natural plasma lines (D. B. Muldrew and R. L. Showen, JGR, 82, 4783, 1977). This observation has been further confirmed by the radar detection with a much improved spatial resolution in the more recent Arecibo heating experiment (J. Fejer, M. Sulzer and F. T. Djuth, JGR, 96, 15985, 1991). Moreover, the observations (S. Nobel and F. T. Djuth, JGR, 95, 15195 1990) have shown the correlation between HFPLs and short scale (3m) field-aligned irregularities (SFAIs). It is generally believed that SFAIs are generated by the Langmuir waves which are excited by the HF heater through the primary parametric decay process. A secondary parametric instability which excites HFPLs and SFAIs simultaneously is considered in the present work.

The pump of the considered instability process is the field-aligned Langmuir waves which are excited by the HF heater near the HF reflection height via the parametric decay process. Four wave interaction whereby the Langmuir pump excites two daughter Langmuir waves together with a purely growing field-aligned density irregularity is then analyzed. This is essentially the filamentation instability of Langmuir waves in a magnetized plasma (S. P. Kuo, B. R. Cheo and M. C. Lee, JGR, 88, 417, 1983). The threshold and the growth rate of the instability are determined. The results show that a broad spectrum of ionospheric irregularities including the 3m line can be produced simultaneously with a large angular distribution of Langmuir waves including the 40<sup>0</sup> line (HFPLs). The considered instability process occurs at a height about 1.1 kilometer higher than the matching height determined by the dispersion relation of HFPLs for 5.1 MHz pump. Hence, the experimental observation of height difference at Arecibo can be explained successfully by the proposed instability process.

\* Work supported by NSF Grant No. ATM-9024827

Session J-4 0835-Thurs. CR2-26

IMAGE PROCESSING AND COMPUTERS

Chairman: Ronald J. Allen, Space Telescope Science Institute,  
Baltimore, MD 21218

J4-1  
0840

**THE AIPS++ PROJECT - A NEW GENERATION  
OF SOFTWARE FOR RADIO ASTRONOMY**

R. M. Hjellming and G. Croes  
National Radio Astronomy Observatory

A consortium of the NRAO and other radio observatories around the world (WSRT, AT, DRAO, Jodrell, ...) are joining in an effort to develop a new software system that will replace and expand upon the capabilities of the Astronomical Image Processing System (AIPS). It will be implemented in C++ using the techniques of object-oriented programming, and has been named AIPS++. The purposes and development plan for this project, which begins with a concentrated design phase, involving all consortium members in Charlottesville in Jan.-June 1992, will be discussed.

J4-2 MOSAICING METHODS IN RADIO SYNTHESIS IMAGING  
0900 Mark A. Holdaway  
National Radio Astronomy Observatory  
Array Operations Center  
Socorro, NM 87801

Until recently, radio imaging has been artificially divided between imaging of very large objects at low resolution with single dishes and imaging smaller objects at higher resolution with interferometers. At millimeter wavelengths, this dichotomy severely limits science as an interferometer's field of view may be only a few arcminutes while many prime target sources are several degrees across.

The formalism of the mosaicing image reconstruction methods unifies single dish and interferometric imaging. Given data from any number of instruments (total power data, interferometer data) and any number of sky positions, mosaic solves the inverse problem of what brightness distribution gives rise to these varied data sets. Hence, mosaic image reconstruction can faithfully reproduce all spatial frequencies (out to the maximum measured spacing) of arbitrarily large celestial objects.

The mosaic formalism and its relation to the short spacing scheme of Ekers and Rots will be summarized. The homogeneous array concept will be presented. Several different mosaicing techniques will be discussed with conditions for their use. An error analysis of mosaic will be carried out for pointing errors, primary beam model errors, antenna surface accuracy, and atmospheric gain fluctuations. New VLA radio continuum mosaic images of NGC253 will be presented.

J4-3 MULTICHANNEL IMAGE PROCESSING USING  
0920 THE MIRIAD SOFTWARE  
Melvyn Wright  
Radio Astronomy Laboratory  
University of California  
Berkeley, CA 94720

This report summarizes the use of the MIRIAD software for Multichannel Image Reconstruction, and the Interactive Analysis and Display of images and aperture synthesis data. The software is designed to run efficiently on high performance workstations and supercomputers and is currently used to process data from the BIMA millimeter wavelength array. MIRIAD was designed so that it is easy to add new algorithms, and examples of imaging multichannel data including the selfcalibration and mosaicing of multiple images are shown.

J4-4 A SYSTEM FOR TAMING SOFTWARE  
0940 THAT CONTROLS HARDWARE  
J. R. Fisher and M. H. Clark  
National Radio Astronomy Observatory  
P.O Box 2  
Green Bank, WV 24944

Modern computer control of hardware is bridging larger and larger gaps between the user's language and the parameters required by the hardware. The user-to-hardware language translation can involve very complex interdependencies between user and hardware parameters and between user parameters themselves. This paper presents a framework that reduces the design effort for large control software systems and provides safeguards against illegal parameter dependencies. Other features include automatic ordering of parameter calculation sequence, minimum recalculation for new parameters, parameter hierarchy reporting, control of manual parameter override, isolation of parameter calculation code, and a fill-in-the-blanks parameter insertion template. Object-oriented language concepts such as polymorphism, inheritance, and operator overloading are central to the framework design but generally invisible to the implementer. Our particular example, used to control an FFT spectrometer, is built with C++.

J4-5       SEARCHING FOR PULSARS WITH (SUPER) COMPUTERS  
1020       Alex Wolszczan  
          National Astronomy & Ionosphere Center  
          Arecibo Observatory  
          Box 995  
          Arecibo, PR 00613

Modern pulsar surveys, particularly those designed to detect millisecond pulsars, involve a CPU-intensive analysis of large volumes of data (>64 Mb per sky position in large scale surveys and >1 Gb per integration in targeted searches). Consequently, a supercomputing power is necessary to process data at the rates similar to those achieved during data acquisition. The most commonly used search algorithm uses Fourier transform and harmonic folding techniques to detect the periodic signature of a pulsar in the period-dispersion-orbital acceleration space. Various versions of this scheme have been implemented on supercomputer-class machines in the last few years and have led to important millisecond and binary pulsar discoveries in globular clusters and the galactic disk.

J4-6  
1040

MAGELLAN PROJECT PROGRESS REPORT  
T.W.Thompson  
Jet Propulsion Laboratory  
California Institute of Technology  
Pasadena, California 91109

The Magellan spacecraft was placed into orbit around Venus on 10 August 1990 and started full-up data acquisition on 15 September 1990. Since then, Magellan has completed mapping over 1 1/2 rotations of the planet (as of mid-October 1991). Synthetic aperture radar (SAR), altimetry and radiometry observations have covered 85 percent of the surface during the first mission cycle from mid-September 1990 through mid-May 1991. Operations since then have emphasized filling the larger gaps (the south polar region and a superior conjunction) from that first cycle. Total coverage midway through cycle 2 was 90 percent; expected coverage at the end of cycle 2 will be 94 percent of the planet. Magellan data products such as the SAR images, altimetry and radiometry data are becoming available via the National Space Science Data Center (NSSDC) at the NASA Goddard Space Flight Center (GSFC) in Greenbelt, Maryland.

The mission plan for the next few years is:  
Cycle 3 (mid-January to mid-September 1992)

- Perform gravity measurements over Artemis.
- Collect radar data with a left-looking stereo look-angle-profile to yield stereoscopic measurements of areas imaged in Cycles 1.

Cycle 4 (mid-September 1992 to mid-May 1993)

- Perform an orbit trim to lower periapsis in order to enhance gravity measurements.
- Acquire gravity observations for 360 degrees of longitude.

Cycle 5 (mid-May 1993 to mid-January 1994)

- Aerobrake to circular orbit.

Cycle 6 and 7 (Mid-January 1994 to Mid-May 1995)

- Perform high resolution and gravity observations with emphasis on the polar regions.

J4-7 HIGH-PERFORMANCE COMPRESSION  
1100 OF ASTRONOMICAL IMAGES  
Richard L. White, JILA/STScI  
Campus Box 440  
University of Colorado  
Boulder, CO 80309

A new method for image compression has been developed for use in the distribution of the digital sky survey constructed by the Guide Star group at the Space Telescope Science Institute. The technique is based on the H-transform (Fritze et.al. 1977, Astr. Nachr. 298, 189), which is a simple two-dimensional wavelet transform. The method may be used for either lossless or lossy compression. Most astronomical images can be compressed to less than 1.5 bits/pixel with no significant losses in the images either under visual inspection or under quantitative analysis (e.g. astrometry or photometry.) Other compression methods, including the JPEG image compression standard and other wavelet-based techniques, are significantly inferior to our method for astronomical images.

This compression method would be ideal for compression of VLA images, especially if it were coupled with CLEAN. The technique can be easily extended to higher dimensions, so that it could also be used to compress data cubes. The method has been designed to be computationally efficient: compression or decompression of a 512 x 512 image requires only 4 seconds on a Sun SPARCstation 1.

J4-8      IMAGE RESTORATION FOR THE  
1120      HUBBLE SPACE TELESCOPE  
            R. J. Hanisch and R. L. White  
            Space Telescope Science Institute  
            3700 San Martin Drive  
            Baltimore, MD 21218

The spherical aberration of the primary mirror of the Hubble Space Telescope has seriously reduced the sensitivity and degraded the resolution of images and spectra from the instruments on the satellite. In this paper we describe the nature of the aberration problem and the resulting point-spread functions for both the imaging and spectrographic detectors, and contrast the HST image restoration problem with that in radio interferometry. A number of image restoration algorithms have been evaluated for use on HST data, including both linear and non-linear techniques, and sample results are shown. The best prospects for obtaining improvements in the restored images are likely to derive from developing techniques for adaptive regularization.

J4-9  
1140

EARLY SCIENTIFIC RESULTS FROM  
THE HUBBLE SPACE TELESCOPE  
R. J. Allen  
Space Telescope Science Institute  
3700 San Martin Drive  
Baltimore, MD 21218

The Science Verification program on the Hubble Space Telescope (HST) is nearing completion. This program, intended to test all features of each science instrument on HST, has been extended to include studies of the effects of the spherical aberration of the primary mirror. In spite of this aberration, HST continues to produce images and spectra of remarkable clarity, a sampling of which will be shown on a variety of interesting astronomical objects.

Data is pouring into the HST archive system at the rate of 0.5 GByte/day, and regular operation of the first orbiting optical observatory available to the general international scientific community has begun.

Thursday Afternoon, 8 January, 1335-1700

Session A-7 1335-Thurs. CR2-06  
TIME DOMAIN METROLOGY

Chairman: Sedki M. Riad, Virginia Polytechnic Institute and State Univ.,  
Blacksburg, VA 24061

A7-1 HIGH-SPEED ELECTRICAL PULSE MEASUREMENT  
1340 CAPABILITIES AT NIST  
W. L. Gans  
Electricity Division  
National Institute of Standards and Technology  
Gaithersburg, Maryland 20899

We at NIST offer a Special Test service to government and industrial clients for a number of parameters related to high-speed electrical pulses. All of these parameters are measured on a NIST-developed Automatic Waveform Analysis and Measurement System (AWAMS).

The AWAMS consists of a commercially available sampling oscilloscope and a desktop computer for signal processing and oscilloscope control by means of the IEEE 488 bus. The sampling oscilloscope has three normal equivalent-time sampling channels, each with a sampling gate duration of 17.5 ps. This gate duration translates into an effective -3 dB bandwidth of 20 GHz. A fourth sampling channel is available with a built-in 45 ps pulse generator for time-domain reflectometry. The input impedance of each sampling channel is nominally 50  $\Omega$  and the input connectors are 3 mm precision coaxial connectors. Under computer control, electrical pulse waveforms of up to 1024 points with up to 2048 sample averages per point may be acquired. The voltage dynamic range is  $\pm 500$  mV and the smallest available waveform time epoch is 100 ps, yielding a maximum time resolution of about 0.1 ps.

These Special Test services offered by NIST fall into three categories: fast electrical pulse parameters, pulse delay interval, and impulse spectrum amplitude. Where possible, terms, definitions, and measurement techniques are used for the first two categories which adhere to both international standards (IEC Pubs. 469-1 & 469-2, Geneva, 1974) and IEEE standards (IEEE Stds. 181-1977 & 194-1977, New York, 1977). For the case of impulse spectrum amplitude, definitions and techniques are taken from the CISPR Specification for Radio Interference Measuring Apparatus and Measurement Methods (IEC/CISPR Pub. 16, Geneva, 1977). A brief description of these services is contained in the NIST Calibration Services Users Guide (Special Pub. 250, Gaithersburg, MD, pp. 170-173, 1989).

This presentation will include descriptions of the AWAMS, and each of the three Special Test service categories. Also, plans for future measurement capability development at NIST will be discussed.

A7-2 "FIELD EXTRACTION COEFFICIENTS FOR FIELD PROBES  
1400 AND BROAD BAND MEASUREMENTS."

T.J.F.Pavlasek, T.I.Al-Mahdawi, P.Boisvert  
Electrical Engineering, McGill University,  
Montreal, Quebec, Canada

Determination of vectorial E and H field components is considered in the context of immediate field measurements. Probe output voltage is related to the measured field by an ill-posed Fredholm integral equation of the first kind. For certain measurement surfaces, this reduces to an algebraic form, allowing the extraction of the amplitude and phase of spacial field modes.

The above leads to the definition of 'vector measured voltages', giving rise to a "Field Extraction Coefficients" concept. The 'FEC's' enable the calculation of the measured field in vectorial form and are defined for wire and aperture probes. In a source-free region, two cross-polarized probes are sufficient to obtain the total three component vector field, using the divergence equation.

The "wire" and "aperture" FEC's are duals. Using both either for wire or aperture probe measured data, yields the E and H fields.

Experimental results are shown applying the FEC concept. Truncation of spacial harmonic components is used to eliminate fields from interfering scatterers, which is reminiscent of similar techniques used in time domain methods.

An experimental probe for broad-band E.M.I./E.M.C. high intensity field measurements is also described. The tri-axial "BOTES" probe is an evolution of the Kanda "BIRES" probe and is intended for indoor measurements in confined quarters for the determination of temporal and spacial behaviour of the e.m. environment in areas housing susceptible broad band equipment. The BOTES probe has been evaluated in 50 - 1000 MHz e.m. environment field tests, in comparison with 'standard' probes.

A7-3  
1420**ULTRAFAST OPTICAL SAMPLING EXPERIMENTS  
IN TIME-DOMAIN****Robert O. Grondin and Samir M. El-Ghazaly**  
Center for Solid State Electronics Research  
Arizona State University  
Tempe, AZ 85287

Ultrashort laser pulses, on the order of few femtoseconds, are generated and used to excite carriers in semiconductor materials and devices. The free carriers are sometimes accelerated by an applied electric field. Other laser beams are applied to the device-under-test. Information regarding the reflected, transmitted, or absorbed beams are collected. The collected data are analyzed to understand the physics of the semiconductor transport phenomena on a subpicosecond scale. Several types of these experiments are routinely being done. The analysis of the collected data, however, is not straightforward.

In this paper, some of the time domain optical sampling experiments are reviewed. The information that can possibly extracted from every experiment are presented. The theoretical models used to correlate the collected experimental-data to the physical parameters of interest are analyzed. The advantages and limitations of the various models and their ability to accurately model the semiconductor transport on the subpicosecond scale are discussed.

A7-4  
1440

## TRANSIENT SCATTERING MEASUREMENTS

J. Ross, E. Rothwell, D. Nyquist, K.M. Chen and J. Nathan  
Department of Electrical Engineering  
Michigan State University  
East Lansing, MI 48824

There is considerable interest in accurate measurement of the transient scattering characteristics of complicated structures. This interest stems from the use of transient data in target discrimination schemes using the E/S pulse method and the future use of ultra-wide band radar in target detection and identification.

To achieve accurate transient measurements, the measurement system impulse response must be deconvolved from the raw measurements. For direct time domain measurements the deconvolution of the system response is difficult due to the limited dynamic range, stability, and power output of most measurement systems. One way around some of these difficulties is to perform the measurements in the frequency domain using an automated frequency-stepping vector network analyzer. The measurements are performed over a wide band of frequencies and the transient response is synthesized via the Inverse Fourier Transform. The resulting transient response is equivalent to the direct time domain measurement provided the system and target are linear and time invariant. Modern network analyzers however provide much greater dynamic range, power, and stability than most current time domain systems and allow for improved results when applying the deconvolution procedure.

This paper will discuss the calibration procedure used to remove clutter and the system impulse response from raw measurements. The effectiveness of frequency domain measurements in synthesizing transient target responses will be demonstrated using both a sphere and a thin wire as calibration standards. Theoretical results and direct time domain measurements corrected using a similar procedure will be presented to substantiate the synthesized transient responses for simple structures as well as several complicated targets.

A7-5  
1520

CONFIGURATIONS OF TEM FEED FOR AN IRA  
Carl E. Baum  
Phillips Laboratory  
Kirtland AFB, New Mexico 87117-6008

This paper considers some of the design options for an antenna consisting of a parabolic reflector with a terminated TEM feed. With a fast-rising (step-like) source, this gives an approximate impulse radiating antenna (IRA). Design options include cable networks for driving the TEM feed, including polarization. Adjustment of the feed-termination impedance at low frequencies can balance the electric- and magnetic-dipole moments. Special media near the feed apex can aid in launching fast, high-voltage pulses in the TEM mode.

A7-6 **A NEW CALIBRATION METHOD FOR TIME DOMAIN SYSTEM**

1540

*Wansheng Su and Sedki M. Riad*

The Bradley Department of Electrical Engineering  
Virginia Polytechnic Institute and State University  
Blacksburg, VA 24061-0111

Today, in time domain measurements, proper calibration of time domain measurement instruments remains a problem. Some researchers have published some work on modeling sampling oscilloscopes and others on modeling pulse generators. This paper introduces a new approach to the calibration problem, using commercially available frequency domain standards and well known calibration techniques applied to time domain measurement instruments.

A practical calibration example which calibrates an HP 54120 20GHz TDR/sampling oscilloscope is presented to illustrate the calibration concept and procedures. The high order modes in coaxial transmission line and their effects to time domain system are also discussed.

A7-7 **AN ENHANCED TIME DOMAIN SYNTHESIS TECHNIQUE**  
1600

K. M. Fidanboylu, S. M. Riad\*  
and A. Elshabini-Riad  
Electrical Engineering Department  
Virginia Polytechnic Institute and State University  
Blacksburg, VA 24061-0111

This paper presents an enhanced time domain synthesis technique which has several applications in microwave measurements and material characterization. Using the proposed technique, an equivalent network model consisting of a cascade of  $N$  lossy transmission lines is obtained for a device under test (DUT) based on its time domain reflectometry (TDR) response waveform.

The synthesis starts by splitting the TDR response waveform of a DUT into  $N$  equal time intervals of length  $\Delta T$ . The first segment of the TDR response waveform is synthesized by a lossy transmission line having a propagation function of  $\gamma_1$  and characteristic impedance of  $Z_1$ . The unknown parameters,  $\gamma_1$  and  $Z_1$  are determined by using an iterative, constrained, non-linear least squares optimization technique to fit the simulated TDR response waveform to the experimental one. The optimization is performed in the time domain by minimizing the error function due to the difference between the two waveforms in the time interval  $0 < t < \Delta T$ . Later, the second segment of the TDR response waveform is synthesized by a lossy transmission line having a propagation function of  $\gamma_2$  and characteristic impedance of  $Z_2$ . For this case, the unknown parameters,  $\gamma_2$  and  $Z_2$  are determined by minimizing the error function due to the difference between the simulated and experimental TDR waveforms in the time interval  $\Delta T < t < 2\Delta T$ . The process continues in this fashion until the last segment is synthesized by a lossy transmission line having a propagation function of  $\gamma_N$  and characteristic impedance of  $Z_N$ .

The paper presents both experimental and simulated results as a verification for the proposed technique.

A7-8 MODEL BASED PARAMETER ESTIMATION  
1620

T. K. Sarkar  
Department of Electrical Engineering  
Syracuse University  
Syracuse, New York 13244

E. K. Miller  
Group MEE-3, MS J580  
Los Alamos National Laboratory  
Los Alamos, New Mexico 87545

The objective of this presentation is to illustrate the use of model based parameter estimation to analytically continue both theoretical and experimental data. This involves not only data extrapolation but also interpolation and compression. Hence, it is possible to efficiently analyze large volumes of theoretical and experimental data in reasonable time.

This talk will survey the various model based parametric estimation techniques. The various techniques discussed are Prony's Method, Matrix Pencil Method and Cauchy's Method. The first two technique involves approximating a function by a sum of complex exponentials whereas the second technique is essentially a generalization of the Pade Approximation. The techniques will be applied to both theoretical and experimental data. It will be shown that typically a 9:1 bandwidth extrapolation/interpolation is possible for commonly used electromagnetic systems.

B6-1 ANALYSIS OF RADIATION AND SCATTERING FROM NARROW  
1340 SLOTS BY MEANS OF THE MODIFIED DIAKOPTIC THEORY

Paul D. Mannikko and Chalmers M. Butler  
Clemson University, Clemson, SC 29634-0915

The modified diakoptic theory (MDT) is applied to narrow slot antenna and scattering problems. The structure of interest is a curved, narrow slot in an infinite conducting plane separating two homogeneous half spaces. Several artificial ports are strategically introduced at points along the contour of the slot allowing one to compute the n-port short-circuit admittance (y-)parameter representation of the "diakopted" slot. The rank of the short-circuit admittance system matrix is typically much smaller than that of a method of moments representation for the same problem. Furthermore, this short-circuit admittance matrix can, but need not, be efficiently computed given one has a knowledge of the method of moments matrix. From the y-parameter system, one can obtain the tangential component of electric field in the slot.

To determine the y-parameters, a stationary expression is derived which expresses these parameters in terms of equivalent magnetic currents. These so-called short-circuit magnetic currents (the magnetic current in the slot due to excitation at a port with all other ports short-circuited) are computed via an efficient iterative scheme identical in nature to that used in the MDT for wire antennas. From this stationary expression, the MDT for slot antennas is shown to be equivalent to the method of moments subject to the constraints that the expansion and testing functions are chosen to be the normalized short-circuit magnetic current distribution. Results are given which enable one to compare the magnetic current distributions in the slot as determined from conventional method of moments techniques with distributions computed with the MDT. Also a comparison is made of the times required to solve a conventional method of moments system of equations with the Linpak Gaussian elimination subroutines and the corresponding times with the MDT. Plane-wave scattering problems are considered too.

B6-2 SCATTERING FROM LOADED STRIPS  
 1400 Randy L. Haupt  
 Department of Electrical Engineering  
 United States Air Force Academy, CO 80840

Large sidelobes result in the bistatic scattering and backscattering patterns when edge-loading a perfectly conducting strip with constant resistive sheets that are a half-wavelength or more wide. The resistive sheets tend to reduce sidelobes in the scattering patterns of perfectly conducting strips but have areas of high sidelobes due to the discontinuity in the induced current. These high sidelobes or grating lobes are reminiscent of the grating lobes in array theory. In fact, the grating lobes in the scattering patterns have predictable heights and locations just as in array theory.

The approximate locations for the grating lobes can be derived from physical optics and are

$$\text{bistatic RCS:} \quad \cos\phi_g \simeq \frac{2\pi n}{kb} - \cos\phi_o, \quad n = \pm 1, \pm 2, \dots, \pm b/\lambda$$

$$\text{backscattering RCS:} \quad \cos\phi_g \simeq \frac{\pi n}{kb}, \quad n = \pm 1, \pm 2, \dots, \pm 2b/\lambda$$

where  $b$  is the width of the resistive load and  $\phi_o$  is the angle of the incident field. At the grating lobe locations the approximate height of the grating lobes are

$$\sigma_{(E)}^{(H)}(\varphi_g) \simeq \left( \frac{\sin^2\phi_o}{\sin^2\phi} \right) \frac{kb^2}{\pi^2 n^2}$$

This equation applies to bistatic and backscattering RCS. The difference is that for the E-polarization bistatic RCS the  $\sin^2\phi_o$  term is a constant, while for the H-polarization bistatic RCS,  $\sin^2\phi$  is a variable and the backscattering RCS has  $\sin^2\phi_o \simeq nd \sin^2\phi$  as variables.

As an example, consider the bistatic RCS ( $\phi_o=0^\circ$ ) of a strip with  $a=3\lambda$  ( $2a$ =width of perfectly conducting portion of the strip),  $b=3\lambda$ , and normalized resistivity=0.5 as shown in Figure 1 below. Grating lobes occur at  $u=\cos\phi=.333$ , .667, and 1.0 and the corresponding heights of the grating lobes are 7.58, 1.56, and -1.96 dB. The backscattering pattern for this strip is shown in Figure 2.

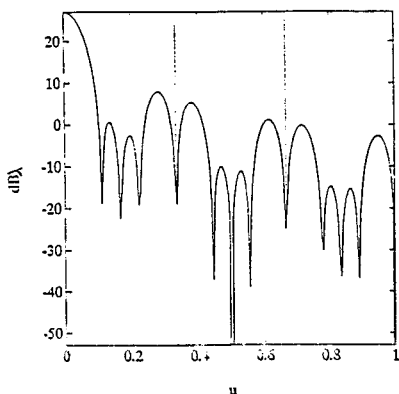


Figure 1. Bistatic RCS.

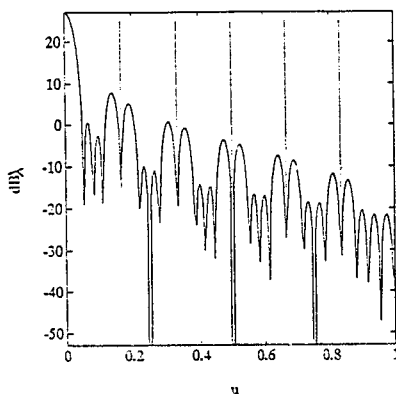


Figure 2. Backscattering RCS.

## B6-3 THE FAR FIELD SCATTERED BY INDENTED SCREENS

1420

J. S. Asvestas  
M/S A02-26  
Grumman Corporate Technology  
Bethpage, NY 11714-3580  
R. E. Kleinman  
Center for the Mathematics of Waves  
University of Delaware  
Newark, DE 19716, USA

New expressions are presented for the far field scattered by an indented perfectly conducting plane screen illuminated by a time harmonic incident wave. The far field is expressed as an integral of the current on the surface of the indentation only. No integrals along fictitious surfaces or the plane screen appear. This is a continuation of previous work in which we derived boundary integral equations for this problem involving integrals only on the surface of the indentation (Asvestas and Kleinman, New Integral Equations for Scattering from an Indented Screen, National Radio Science Meeting, Boulder, CO, 1989; Integral Equations for Electromagnetic Scattering from an Indented Screen, National Radio Science Meeting, Boulder, CO 1990). Results are given for the full  $3D$  electromagnetic problem as well as the  $2D$  problem for both  $TE$  and  $TM$  polarizations. These expressions are valid for all frequencies. The low frequency limits are also derived and shown to be consistent with recent  $2D$  low frequency results (Hansen and Yaghjian, Low Frequency Scattering from Two-Dimensional Perfect Conductors, IEEE APS/North American Radio Science Meeting, London, Ontario, 1991).

B6-4 1440 DIFFRACTION BY PERFECTLY CONDUCTING NARROW  
CYLINDRICAL BUMPS AND DENTS  
Thorkild B. Hansen and Arthur D. Yaghjian  
Rome Laboratory/ERCT  
Hanscom AFB, MA 01731, USA

In two recent papers (Hansen and Yaghjian, IEEE AP-S Symposium Digest, London, Ontario, Canada, 794-801, June 1991) we showed how three-dimensional incremental length diffraction coefficients can be found directly from the corresponding two-dimensional far-fields for cylinders of arbitrary cross section using a direct substitution procedure. No integration, differentiation, or specific knowledge of the current on the conductor is needed. These incremental length diffraction coefficients can be used, for example, to determine the scattering contribution from curved ridges and channels in conductors.

We also showed that the exact expressions for the leading terms in the low-frequency far fields diffracted by arbitrarily shaped perfectly conducting cylindrical bumps and dents are given by

$$TM: E_z^d \sim -(kd)^2 e^{-j\pi/4} \sqrt{\frac{2}{\pi}} C \sin \phi \sin \phi^i \frac{e^{-jkr}}{\sqrt{kr}} \quad (1)$$

$$TE: H_z^d \sim -(kd)^2 e^{-j\pi/4} \sqrt{\frac{2}{\pi}} \left[ \pm \frac{A}{d^2} + C \cos \phi \cos \phi^i \right] \frac{e^{-jkr}}{\sqrt{kr}} \quad (2)$$

where  $A$  is the area of the bump or dent,  $d$  is a characteristic dimension, and the plus and minus signs are used for the bump and dent, respectively. The constant  $C$  depends only on the shape of the cross section of the bump or dent and it is found from the solution to either an electrostatic or magnetostatic problem. Once the value of the constant  $C$  is determined for a certain bump or dent, the three-dimensional incremental length diffraction coefficients for the corresponding narrow ridge or channel are immediately obtainable using the direct substitution procedure.

In the present paper numerical evaluations of the constant  $C$  are presented for a number of bumps and dents of different cross sections. Furthermore, we confirm the low-frequency expressions above by comparing them to low-frequency results obtained from exact time-harmonic solutions. Specifically, we confirm the expressions in the cases of the semi-circular bump, the knife-edge bump, and for the semi-circular dent for which an exact time-harmonic solution was recently obtained in (Hinders and Yaghjian, IEEE Microwave and Guided Wave Letters, 1, 239-242, September 1991). Finally, we will compare the low-frequency solutions with exact time-harmonic solutions to find the frequency range in which the low-frequency expressions are good approximations.

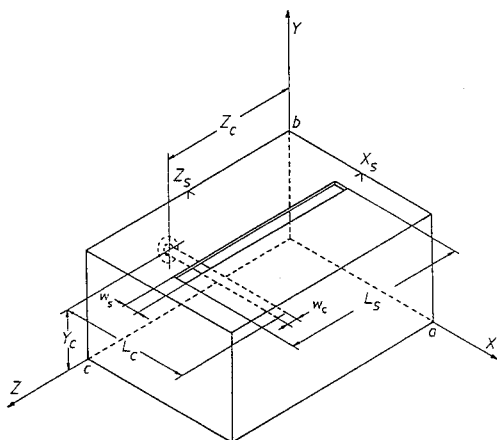
B6-5  
1520

## EXPERIMENTAL AND THEORETICAL STUDIES OF STRIP-FED CAVITY BACKED SLOT RADIATORS

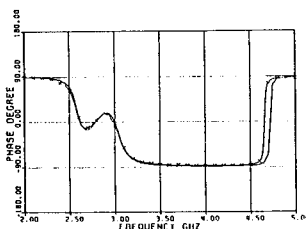
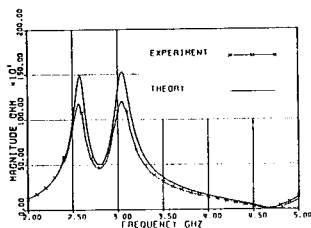
Shahrokh Hashemi-Yeganeh  
Department of Electrical Engineering  
Arizona State University  
Tempe, Arizona 85287-7206

Arrays of cavity backed slot radiators can be effectively made to synthesize a desired power pattern with adjustable side lobes. To achieve this, knowledge of self and mutual impedances of cavity backed slot elements at their input terminals are essential. The aim of the present analysis is the development of a theoretical model for determining the impedance values of the single element or pair of elements as a function of cavity, slot, and strip dimensions.

Coupled integral equations are set up and solved, using the Method of Moments, to compute approximately the slot aperture electric field and the surface current distribution on the strip. The computed current and electric field are used to determine the input impedance and the radiated power of the element. Experimental data are presented to verify the analysis.



Strip-Fed Cavity Backed Slot Radiator



Self impedance of the simple Strip-fed Cavity Backed Slot radiator:  $a=4.953cm$ ,  $b=3.048cm$ ,  $c=6.285cm$ ,  $Y_c=b/2$ ,  $Z_c=2.54cm$ ,  $L_c=4.39cm$ ,  $w_c=0.13cm$ ,  $X_s=a/2$ ,  $Z_s=c/2$ ,  $L_s=5.3cm$ , and  $w_s=0.315cm$ .

B6-6  
1540

## NUMERICAL MODELING OF PASSIVE CIRCUITS IN COPLANAR WAVEGUIDE AND COPLANAR STRIPLINE

Stephanie Petrakos, David Jahn, Edward F. Kuester and David  
C. Chang

Dept. of Electrical and Computer Engineering  
MIMICAD Center: Campus Box 425  
University of Colorado at Boulder  
Boulder, CO 80309

In previous work, the MIMICAD research center at the University of Colorado at Boulder has developed a flexible numerical modeling program (PMESH) for the prediction of scattering parameters of passive microstrip circuits. The program is based on Galerkin's method applied to the mixed potential integral equation for the electric current on the strip conductor of the microstrip circuit. Piecewise linear basis functions are used to represent the current on each cell, with constraints imposed such that currents flowing normal to a cell boundary are constant along each side of the cell, allowing easy imposition of the requirement of continuity of this normal current.

In this paper, we present extensions of this formulation to the cases of coplanar waveguide (CPW) and coplanar stripline (CPS) circuits. The CPW version is in fact able to handle circuits containing both CPW and slotline elements together. The modifications necessary include the calculation of different Green's functions, and (in the CPW/slotline case) the use of slot electric field instead of strip electric current as the unknown function to be solved for. Wave variables and propagation constant are extracted from the numerically determined unknown current or field distribution by a three-point de-embedding scheme used in PMESH, with the additional feature that both even and odd symmetry modes must be separately considered in the CPW case, and a group of radiation modes exists in the CPS case that behaves nearly like a true mode and must also be treated with care. An approximate handling of ground bridges is used in order not to greatly increase the size or slow down the speed of the program. Numerical examples will be presented that demonstrate the accuracy and versatility of the program.

B6-7  
1600

# Analysis of a Wide Rectangular Radiating Slot in the Ground plane of a Microstripline

Masoud Kahrizi, Tapan K. Sarkar and Zoran A. Maricevic

Department of Electrical Engineering  
Syracuse University  
Syracuse, NY 13210, USA

## Abstract

An analysis of a wide rectangular radiating slot excited by a microstrip line is described. Coupled integral equations are formulated to find the electric current distribution on the feed line and the electric field in the aperture.

The solution is based on the method of moments and using the space domain Sommerfeld type Green's function. The information about the input impedance or reflection coefficient is extracted from the electric current distribution on the microstrip line utilizing the matrix pencil technique. The theoretical analysis is described and data are presented and compared with other theoretical and experimental results.

B6-8 **HOMOGENIZATION ANALYSIS**  
1620 **OF STRIP GRATING ANTENNAS**

Ronald R. DeLyser and Edward F. Kuester  
Dept. of Electrical and Computer Engineering  
MIMICAD CENTER: Campus Box 425  
University of Colorado at Boulder  
Boulder, CO 80309

This paper addresses the application of equivalent boundary conditions (derived using the method of homogenization) to analyze a periodic microstrip structure using the method of moments. The structure chosen is called a "strip grating antenna" (SGA) and consists of a square microstrip patch which has been modified by a periodic placement of narrow gaps at a specified angle with respect to the sides of the square.

A microstrip structure is analyzed with arbitrary current source using the spectral domain technique, and then equivalent boundary conditions are applied for the SGA in order to derive integral equations for the unknown zero and first order antenna currents. The integral equations are then solved using the method of moments.

The advantage of using this method of analysis is that use of equivalent or average boundary conditions allows a structure like this antenna to be discretized without regard to its fine details. Thus, homogenization analysis may require less memory for storage of the numerical data that accompanies analysis using the method of moments. The computer program, PMESH, has been shown to be very effective for the analysis of microstrip patch antennas and was easily modified to accomplish the numerical analysis of the SGA.

The SGA was chosen for two principal reasons. (1) Since the homogenization analysis is valid for an infinite periodic structure, a reasonably large physical structure is required so that edge effects can be ignored. (2) A possible benefit of the SGA is that it could turn out to be a wide-band antenna because of the differing lengths of the individual strips. If they resonate at slightly different frequencies, the combined effect could be an overall wider bandwidth than that of a solid patch.

Comparisons of the results of the numerical analysis to those of experiments on several different configurations of the strip grating antenna are given. Analysis of these structures was done using two methods: (1) PMESH was used to analyze some of the configurations directly, and (2) the modified PMESH program, HOMAN, was used to analyze the antennas using the homogenization technique.

B6-9 SPECTRAL DOMAIN ANALYSIS OF SCATTERING  
1640 FROM PLANAR COATED STRIP AND INFINITE STRIP GRATING

Peter Petre and Tapan K. Sarkar  
Department of Electrical and Computer Engineering  
Syracuse University, Syracuse, New York 13244

Gyula Veszely and Laszlo Zombory  
Department of Microwave Telecommunication  
Technical University of Budapest

The problem of electromagnetic scattering from planar flat strip and infinite strip grating with thin homogeneous material coating arises in many physical contexts. The problem of electromagnetic scattering from non-periodic two- and three-dimensional structures consisting of both dielectrics and conductors has been studied extensively, and the literature on the subject is vast. The other types of problem however, i.e., electromagnetic scattering from planar infinite strip grating with thin homogeneous material coating, as far as the authors know, have been analyzed only by the authors. Combined-field integral equation (CFIE), based upon a surface/surface formulation is developed here for analyzing electromagnetic scattering from planar flat strip and infinite strip grating with thin homogeneous material coating. The surface equivalent principle is used to replace all conductor strips by equivalent surface electric currents and all dielectrics by equivalent surface electric and magnetic currents. Enforcing the respective boundary conditions a CFIE is developed for the unknown currents. According to the periodicity of the structure, the operator equation, that pertains to the EFIE is constructed in the spectral domain using the Fourier transforms of the integro-differential operators. The generalized BiConjugate Gradient-FFT (BiCG-FFT) method with subdomain basis functions is used to solve the operator equation numerically. The superiority of this iterative method is also shown. Both periodic and non-periodic structures are treated by the same manner utilizing the sampling theorem. Numerical results which are the reflection coefficients for the coated infinite strip grating problem, and which are the monostatic radar cross sections for the single coated strip problem are presented for various geometries for both transverse electric (TE) and transverse magnetic (TM) polarization and are compared with other published data.

- D2-1 POWER COUPLING AND TIME DEPENDENT  
1340 RADIATIVE TRANSFER IN GUIDED WAVE SYSTEMS  
M.J. Yadlowsky, D.R. Hjelme and A.R. Mickelson  
Department of Electrical and Computer Engineering  
University of Colorado at Boulder  
Boulder, CO 80309-0425

Radiative transfer can be used to simplify the problem of propagating low coherence optical fields through scattering and absorbing media where a full electromagnetic analysis would be intractable. One reason why radiative transfer greatly simplifies such a problem is that it does not explicitly account for interference. In order to determine the conditions under which the intensity or power dependent scattering of radiative transfer could be applied to waveguide systems, a time domain derivation of the time dependent equation of transfer has been done. For systems in which there is little time averaged mode coupling over the distance that it takes the pairwise differences in the modal group delays to exceed the source temporal coherence time, the time averaged modal powers exhibit no interference. The net amount of power transferred between modes is only a function of the time averaged modal powers themselves. The rate at which power is transferred between modes is described by the power coupling coefficients. This derivation shows how the effective power coupling coefficients representative of a particular waveguide depend not only on the perturbations driving the power transfer, but also on the propagation coefficients of the modes, the group velocities of the modes, and the autocorrelation function of the source.

D2-2  
1400

## Faster Computation of Z-Matrices for Triangular Segments in Planar Circuits

Sung Hwan Lee, A. Benalla and K.C. Gupta  
Electrical and Computer Engineering Department  
University of Colorado, Boulder, Colorado 80309-0425

Two dimensional planar approach for the analysis of microstrip and stripline discontinuities such as bends and Y-junctions requires the evaluation of Z-matrices for planar triangular segments. One of the approaches to compute the impedance matrix elements is based on the Green's function for these geometries (Chadha and Gupta, "Green's Functions for Triangular Segments in Planar Microwave Circuits", IEEE Trans. Microwave Theory Tech., Vol. MTT-28, No. 10, October 1980).

The currently available formulations (Maramis and Gupta, "Planar Analysis and Optimization of Microstrip Discontinuities", Tech. Rept. No.1 MIMICAD Center, Univ. of Colorado at Boulder, March 1988) to compute impedance matrix elements for the  $30^\circ - 60^\circ - 90^\circ$  and the equilateral triangular segments use double series expression for Green's function. The present paper reports the development of a method for faster computation of the impedance matrix elements for  $30^\circ - 60^\circ - 90^\circ$  and equilateral triangular segments.

The method of images and currently available single series formulation of a rectangular planar segment have been applied to speed up the computations of impedance matrix elements of  $30^\circ - 60^\circ - 90^\circ$  and equilateral triangular microstrip segments used in planar microwave circuits. For an equilateral triangular segment, the elements of Z-matrix are obtained by using the results for two  $30^\circ - 60^\circ - 90^\circ$  triangular segments, one of which has all magnetic walls and in the other segment, one of the magnetic walls is replaced by an electric wall. The present formulations have been verified by comparison with the previously available double series formulations.

The proposed algorithms increase computational efficiency considerably. For example in case of an equilateral triangular segment (side length= $3mm$ , substrate height= $0.79mm$ ,  $\hat{\epsilon} = 2.2 - j0.0022$ , and freq= $7.5GHz$ ) for 0.8 % error, the double series formulation needs 817.6 seconds whereas the proposed method takes less than 71 seconds (on HP9000/375 workstation).

D2-3  
1420

## Characterization of Coplanar Waveguides With Various Dielectric Layers

Lori E. Primas and Alan R. Mickelson  
Department of Electrical and Computer Engineering  
University of Colorado  
Boulder, Colorado 80309

Coplanar waveguides are becoming increasingly popular in the design and fabrication of microwave/optical devices. The use of coplanar waveguides allow higher packing densities of circuit elements, less parasitic coupling between layered circuits and higher depth of modulation of electro-optic devices than do microstrip waveguides. As more work is done in the area of coplanar waveguides, new materials that can be used as the inter-layer between the electrodes and the substrate or between various interconnect layers must be examined. We propose to study the properties of various materials and by using standard TRL and S-parameter measurements determine the dielectric constant for frequencies up to 20 GHz.

The dielectric constant of various inter-layer materials such as photosensitive polyimides and negative photoresists over a wide frequency range will be examined. The approach will be to build standard coplanar waveguide samples with known dielectrics, buffers, substrates and 50 ohm electrodes. The S-parameters and impedance of the lines will be determined using a high frequency probe station and a network analyzer. From these calibration standards, the dielectric constants of other materials can be determined.

The thickness variation and temperature sensitivity of the inter-layer materials will also be determined. Once these simple coplanar waveguides have been characterized, the effect of the thickness of the electrodes on the frequency response will be measured. Electro-optic sampling techniques will be used to measure the parasitic coupling between multi-layer dielectrics.

D2-4 EXTRACTION OF ELECTRICAL PARAMETERS  
1440 FROM OPTICAL SAMPLING MEASUREMENTS

Dag R. Hjelme, Vesna Radišić

Alan R. Mickelson, and Zoya B. Popović

Department of Electrical and Computer Engineering  
University of Colorado at Boulder  
Boulder, CO 80309-0425

Electrooptic sampling measurements ("Voltage Calibration of the Direct Electrooptic Sampling Technique," accepted for publication in the IEEE MTT, D. Hjelme, A. Mickelson) give us a distribution of the voltage across a microwave GaAs circuit. In this work we concentrate on coplanar waveguide (CPW) circuits, which enables us to measure the voltage distribution under the conductors, as well as in the gaps. From the measured voltages and the quasi-static Green's function for a dielectric slab, we find the charge distribution on the electrodes. From the obtained charge distribution, the electric field components can be extracted. Modelling discontinuities from measurements is shown on the example of a right angle bend, Figure 1. The voltages are measured in the region of the discontinuity between planes A and B. The charge distribution in this region is found, and other electrical quantities, such as the current and scattering matrix can be obtained.

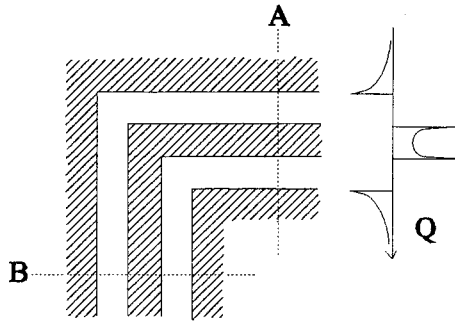


Figure 1. A right angle bend discontinuity in a coplanar waveguide.

D2-5 DE-EMBEDDING SUBSTRATE VARIATIONS FROM  
1520 ELECTROOPTIC SAMPLING MEASUREMENTS MADE  
ON MICROWAVE/MILLIMETER WAVE CIRCUITS  
D.R. Hjelme, M.J. Yadlowsky and A.R. Mickelson  
Department of Electrical and Computer Engineering  
University of Colorado at Boulder  
Boulder, CO 80309-0425

With the development of Monolithic Microwave Integrated Circuit (MMIC) technology, a strong need has evolved for accurate on-wafer probing of microwave/millimeter waves. Electrooptic sampling (EOS) provides a means of making ultra high-speed, non-invasive, on-wafer measurements. In direct EOS, the circuit substrate becomes part of the measurement system and any non-uniformities in the substrate can adversely effect measurements. Therefore, the optical properties of the substrate, and microwave-optical interaction in the substrate must be investigated in detail. We have developed a model for EOS, which describes the effects of the substrate properties on the measured electrooptic signal (D. R. Hjelme and A. R. Mickelson, "Voltage calibration of the direct electrooptic sampling technique," submitted for publication in IEEE Trans. on Microwave Theory and Tech).

The theory presents two calibration factors, one of which can be neglected if all polarization losses are removed from the measurement system. The remaining calibration factor describes the effect of substrate variations on measured electrooptic data. This factor has been used in conjunction with with the localized, time averaged reflectivity of the wafer to remove the effect of substrate variations from 2-D voltage distribution measurements.

D2-6 SOLVING WAVEGUIDING PROBLEMS USING A  
1540 TIME-DOMAIN, FINITE ELEMENT TECHNIQUE

David C. Chang, Cheok Thng and Richard C. Booton, Jr.  
Center for Microwave/ Millimeter-Wave Computer-Aided  
Design

Department of Electrical and Computer Engineering  
University of Colorado  
Boulder, CO 80309-0425

MMIC chips are often packaged together inside a metallic casing; as such package resonance often creates unwanted cross-talk among circuit elements on the same chip, or with circuit elements on a different chip. In this work, our interest is to find a general numerical method which would enable us to find the resonant frequencies of a package with a complex cross-sections. Specifically, we are interested in finding a robust time-domain method which would give us all the guided modes for a given propagation constant, or phase velocity in the longitudinal direction. Because we start by assuming a known variation in the longitudinal direction, our solution process reduces from a truly 3-dimensional one to one which is 2-dimensional in nature, but with a coupled TE- and TM-field.

The method we employed basically can be classified as a time-domain, finite-element method using linear elements of  $E_z$  and  $H_z$  fields in a triangular cell or bi-linear elements in a rectangular cell. At each node, the nodal  $E_z$ - and  $H_z$ -elements are coupled to the weighted average of all transverse  $H_t$ - and  $E_t$ -fields through the four Maxwell equations in each cell sharing the same common node. The time derivatives involved in the Maxwell equations then allow us to update the nodal  $E_z$ , or  $H_z$ -field from the weighted average of the transverse  $E_t$ - or  $H_t$ -field, and to update the transverse  $E_t$ - or  $H_t$ -field from both nodal  $E_z$  and  $H_z$  fields.

Numerical results have been obtained for packages of complex shape. While this method can give extremely accurate results for waveguide modes of fast wave nature, it fails to provide numerically stable result whenever one encounters modes which exhibit at least partially the behavior of a surface-wave nature. Explanation for such a limitation will also be given.

D2-7 AN OPTICALLY DRIVEN PHASED  
1600 ARRAY ANTENNA UTILIZING  
HETERODYNE TECHNIQUES

M.R. Surette, D.R. Hjelme, and A.R. Mickelson  
Department of Electrical and Computer Engineering  
University of Colorado at Boulder  
Boulde, CO 80309-0425

A novel optically driven phased array antenna system is proposed. The proposed system utilizes heterodyne techniques to generate the microwave carrier frequency and phases. The heterodyning at each antenna element requires three injection locked lasers. The microwave carrier frequency is determined by the order of the modulated sideband used in the injection locking scheme. A design for an integrated optical fast Fourier transform is also presented. Using this device, the necessary phase processing for both beam steering and detection of arrival angle can be performed optically. The knowledge of the noise properties of injection locked semiconductor lasers is applied to the proposed antenna system. The effect of noise on the gain, signal to noise ratio, and the bandwidth of the antenna system is examined. We show that the performance degradation of the system, due to the noise in the lasers, is minimal, and therefore the bandwidth promise of optical drive could well be achieved with the use of heterodyne laser locking techniques.

D2-8  
1620

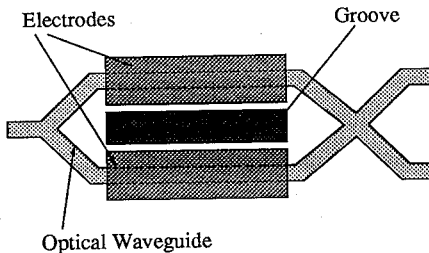
FULL-WAVE ANALYSIS OF THE  
MICROWAVE CHARACTERISTICS OF A  
TRAVELING-WAVE OPTICAL MODULATOR  
WITH AN ETCHED GROOVE

A. G. Engel, Jr. and P. B. Katehi  
NASA Center for Space Terahertz Technology  
Department of Electrical Engineering and Computer Science  
The University of Michigan  
1301 Beal Ave.  
Ann Arbor MI 48109-2122

A traveling-wave optical modulator uses an electric field at microwave frequencies to control the permittivity of two optical waveguides. Accurate prediction of the modulator's performance therefore relies on accurate microwave characterization of the structure. Typically, quasi-static techniques are employed for this characterization, but, as the frequency of the microwave signal is increased, accurate results are obtainable only from full-wave techniques.

Well-established full-wave methods such as the spectral domain technique are easily applicable to many simple modulator structures, but these methods are not well-suited for the analysis of more complicated modulators. A full-wave technique which has been recently developed is applicable to these structures and can accurately determine microwave characteristics such as the microwave refractive index and characteristic impedance. One such complex modulator structure (shown below) has an etched groove, which improves the bandwidth and decreases the coupling between the two optical waveguides (for example, Haga *et al*, *IEEE J. of Quantum Elec.*, pp. 902-6, 1986).

The structure is analyzed with an integral equation-mode matching technique (Engel and Katehi, *IEEE Int. Microwave Symp. Dig.*, pp. 135-8, 1991). The technique is applied by modeling a modulator structure as a rectangular waveguide with rectangular step-inhomogeneities. The waveguide is divided into adjacent sections of layered parallel-plate waveguide. The Green's function is determined by replacing the electrodes with a delta-function excitation and employing mode-matching to apply the boundary conditions at the interfaces between the parallel-plate waveguides. The boundary conditions on the electrodes are then enforced by solving the electric field integral equation with the method of moments. The effective refractive index is determined from the resulting homogeneous system of linear equations and the characteristic impedance is determined from a power-current definition.



D2-9  
1640**ELECTRICALLY INDUCED CONTROL OF CHIRALITY IN ISOTROPIC CHIRAL LIQUID CRYSTALS: EXPERIMENTAL RESULTS**Kathleen B. O'Brien  
General Electric Company  
Morristown, New Jersey  
andLuz J. Martinez-Miranda and Nader Engheta  
The Moore School of Electrical Engineering  
University of Pennsylvania  
Philadelphia, Pennsylvania 19104

Chirality in electrodynamics and chiral materials have gained renewed attention in recent years mainly due to their fundamental electromagnetic characteristics and their potential applications in microwave, millimeter-wave, and optical devices and components. Moreover, possibility of constructing chiral materials for the microwave and millimeter-wave frequency regimes and their potential use for anti-reflection thin coatings have brought increasing interest in this area. It is well known that these materials, which are characterized by  $\mathbf{D} = \epsilon_c \mathbf{E} + i\xi_c \mathbf{B}$  and  $\mathbf{H} = i\xi_c \mathbf{E} + \mathbf{B}/\mu_c$ , exhibit circular birefringence, and possess two refractive indices for right- and left-circularly polarized waves.

Most of the novel applications of chiral materials are conceived based on additional degrees of freedom afforded by the chirality admittance  $\xi_c$ . If this parameter can be changed and controlled in real time due to some external excitation such as temperature, pressure, electric or magnetic fields, one can introduce a variety of novel devices that would operate on this principle. Motivated by this possibility, we studied the effect of external electric field on a class of isotropic liquid crystals which exhibit chirality (optical activity) in the optical regime. In this talk, we present the results of our experimental study on variation of the optical activity as a function of an applied electric field on 70 $\mu\text{m}$  films of the chiral liquid crystal W7, which exhibits an isotropic-smectic A transition at approximately 40°C. We measure the chirality by recording the rotation of the plane of polarization of a probe beam provided by a He-Ne laser. The applied electric field is parallel to the direction of the incident beam. We find that at 41.6°C, the plane of polarization shifts from -2.3° for an applied voltage of 30V to a maximum of -8.1° at 70V. These shifts are in the direction of the smectic A phase and are in general larger than those observed as a function of temperature. The shifts per applied voltage increase as a function of decreasing temperature. The underlying physics of this phenomenon is discussed and its potential applications to optical devices are also mentioned.

E3-1  
1340

## **HISTORY OF RADIO NOISE MODELS**

A.D. Spaulding  
Institute for Telecommunication Sciences  
National Telecommunication & Information Administration  
Boulder, CO 83030

G.H. Hagn  
Information and Telecommunications Sciences Center  
SRI International  
1611 N. Kent Street  
Arlington, VA 22209

This paper will review the history of the development and evolution of empirical and analytical models for radio noise. Models for both natural and man-made noise are included. The history of CCIR Report 322 (atmospheric, galactic and quiet rural), CCIR Report 258 (man-made) and CCIR Report 670 (worldwide minimum) noise models will be emphasized. Specialized models (e.g., quasi-minimum noise, HFBC-84 noise, etc.) also will be discussed.

E3-2 RECENT MAN-MADE RADIO NOISE MEASUREMENTS  
1400 David B. Sailors  
Ocean and Atmospheric Sciences Division  
Naval Ocean Systems Center  
San Diego, CA 92152-5000

Comparison of man-made noise models against recently acquired man-made noise data measured on circular disposed antenna arrays (CDAA) at the receive sites of communication stations at Adak, AL; Diego Garcia; Guam; Honolulu, HI; San Diego, CA; and Stockton, CA is reported. These measurements were made by the Naval Electronics Engineering Activity, Pacific (NEEAP) on their Automated Noise Measurement System (ANMS). Baseline noise data were provided by NEEAP for the forenamed sites measured by the ANMS for the local noon period. Local noon was chosen as the most likely time of day man-made noise would most likely be present.

The data for Guam was compared to other measured results (Shepherd et al., "MF and HF Man-made Radio-Noise and Interference Survey--Guam," Final Report, SRI Project 3328, Stanford Research Institute, 1974). There was a large difference between these two measurements partially due to the measurements by NEEAP being made on a CDAA type antenna rather than on a standard short vertical rod. Using conversion factors obtained by Hagn in Iceland (Hagn, G.H., "Calibration of Nine-foot Rod Antenna for MF and HF EMC Measurements and Comparison with AN/FRD-10 Antenna; Volume I: Groundwave," Final Report, SRI Project 6792, Stanford Research Institute, 1978), the noise data was converted to that of a nine foot vertical rod. The results of this conversion are presented along with curves for rural, quiet rural, and galactic noise.

E3-3  
1420**THE AMBIENT BACKGROUND HF NOISE LEVEL NEAR  
TOK, AK, COMPARED TO THE CCIR NOISE MODELS**

G.H. Hagn and L.O. Harnish

Information and Telecommunications Sciences Center  
SRI International1611 North Kent Street  
Arlington, VA 22209

The ambient background HF noise level was measured on 5 MHz near Tok, Alaska, in August 1988 and in April and May 1989 using three different techniques: a tuned RF voltmeter with an RMS detector, a scanning spectrum analyzer with a fast scan time to permit viewing the ambient background between locally-generated pulses of HF noise, and a fast-Fourier transform (FFT) spectrum analyzer used at the output of a cesium-controlled HF receiver. For all three systems, the daytime ambient background noise level ( $F_a$ ) could only be measured when low-noise preamplifiers and adequate antennas (30-ft and 40-ft vertical monopoles in 1988 and 1989, respectively) were employed. This paper will describe the equipment and its calibration, the results and their comparison with CCIR noise model predictions. The data collected with the various techniques yielded consistent  $F_{am}$  values of  $9.3 \text{ dB (kT}_0) \pm 3.0 \text{ dB}$ . This is 24.3 dB below the CCIR Report 322-3 and CCIR Report 258-5 model predictions for a quiet rural area. It also is several dB below the CCIR Report 322-3 atmospheric noise predictions for the median level of the effective antenna noise figure ( $F_{am}$ ) at 5 MHz during summer mornings (0800 to 1200 hours local time). The measured values also are well below the worldwide minimum levels specified by A.D. Spaulding and G.H. Hagn, at the 1983 Ionospheric Effects Symposium and reproduced in CCIR Report 670. These findings indicate that CCIR Report 670 may require a caveat for high latitudes in the northern hemisphere. Noise measurements at other high latitude location are recommended to verify independently the low levels observed at Tok.

E3-4 A COMPARISON OF MEASURED 32 kHz RADIO  
1440 NOISE AMPLITUDES WITH CCIR MODEL  
PREDICTIONS

M.M. Bowen and A.C. Fraser-Smith  
STAR Laboratory, Stanford University,  
Stanford, California 94305

For some years Stanford University has been conducting a survey of ELF/VLF (10 Hz – 32 kHz) radio noise at selected locations around the world, including three locations at polar latitudes. In this paper we compare the noise amplitudes measured at 32 kHz during the one year period December 1986 through November 1987 with the corresponding amplitudes predicted by the model adopted by the Comité Consultatif International des Radiocommunications (CCIR).

To make this comparison, measurements of the 32 kHz rms noise amplitudes from seven of the Stanford ELF/VLF radiometers were averaged in six four-hour time blocks (0000 – 0400 UT; .. ; 2000 – 2400 UT) for the four three-month seasons defined by the CCIR, thus ensuring that the time blocks for the measurements corresponded to those used by the CCIR noise model.

As might be expected, there was often good agreement between the measurements and the model predictions, but there were some occasions when there were substantial differences. The best agreement was observed at middle to low latitudes. The greatest discrepancies between the measured and predicted amplitudes were observed at our two northern high latitude stations (Søndrestrømfjord and Thule, Greenland), where on some occasions the predicted values were nearly five times greater than the measured values. On the other hand, there was moderately good agreement between the measured and predicted values at our southern high latitude station (Arrival Heights, Antarctica).

E3-5      **A LONG WAVE TE/TM NOISE PREDICTION MODEL**  
1500      C.R. Warber and E.C. Field, Jr.  
            Pacific-Sierra Research Corp.  
            12340 Santa Monica Blvd.  
            Los Angeles, CA 90025

Both vertical and horizontal polarizations are used for communication links between airborne terminals in the VLF/LF bands. Thus, the performance analysis of such communication systems requires knowledge of the naturally occurring noise in each polarization. There is good data on naturally occurring vertical noise; however, data on horizontal noise is extremely sparse. Therefore, based on a theoretical understanding of the physical processes that cause noise, we have developed a computer model that predicts both horizontally and vertically polarized noise in the ELF to LF band (10 Hz - 60 kHz).

Since naturally occurring radio noise in this band is produced by lightning in the lower atmosphere, and propagates to the receiver via the waveguide formed by the earth and the ionosphere, the model starts with the average lightning flash density (flashes/km<sup>2</sup>/s) as a function of season, time of day, and geographic location. The model then turns this data into radiated power density functions (watts/km<sup>2</sup>/s) for horizontal and vertical noise using experimentally known frequency spectrums for those components of a lightning flash that radiate strongly in the long wave band. Adjustments are made to the radiated power to account for experimentally seen seasonal and latitudinal differences in the lightning processes. This noise power density is then integrated over fairly large geographic areas into horizontal and vertical equivalent noise transmitters. The power radiated from each of these transmitters is then propagated to the receiver location using standard anisotropic long wave propagation algorithms and well-known models of the earth-ionosphere waveguide.

From the received power, the model predicts RMS noise, standard deviation, voltage deviation  $V_d$ , and the amplitude probability distribution of the noise for both vertical and horizontal polarizations. Since the model is based on theory, it can also predict these parameters under disturbed ionospheric conditions such as solar proton events.

The model agrees well with experimental data over the entire frequency range treated by the model. We will describe the physical basis of the model, and demonstrate its agreement with a wide range of noise measurement data.

E3-6  
1540

**THE NATURAL BACKGROUND LEVELS  
OF 50 Hz / 60 Hz RADIO NOISE**  
A.C. Fraser-Smith and M.M. Bowen  
STAR Laboratory, Stanford University,  
Stanford, California 94305

Measurements of the amplitude of 50 Hz and 60 Hz power line magnetic fields are often compared with the amplitude of the earth's steady magnetic field (which lies in the range 0.23–0.67  $\mu\text{T}$ ). Although this comparison can be meaningful and useful, it also has the potential to be misleading because (1) the earth's magnetic field is a dc field, whereas the other fields are not, (2) the amplitude of the earth's field is usually large compared with the amplitudes of the power line fields, which gives the impression that the power line fields are small, and (3), insofar as possible biological effects are concerned, mankind has evolved in the presence of the earth's magnetic field, whereas the power line fields have only been present within the last century. A more meaningful comparison is between the measured fields and the natural background fields at the same frequencies and locations, and the purpose of this communication is to report measurement of the natural background levels of 50 Hz and 60 Hz radio noise to facilitate these comparisons.

The measurements were made by Stanford University ELF/VLF radiometers located at various sites around the world. They were made on the magnetic fields of the noise using loop antennas, and they cover the first three harmonics of the power line frequencies (frequencies in the range 50–180 Hz). Due to the likelihood of contamination from local electrical power systems, or even from non-local systems, the measurements at each power line frequency were made at adjacent frequencies and the desired noise amplitudes obtained by interpolation. We show that the amplitudes of the natural noise typically lie in the range 20–600  $\text{fT}/\sqrt{\text{Hz}}$ , or, taking the 50/60 Hz frequencies specifically, in the range 150–600  $\text{fT}/\sqrt{\text{Hz}}$ . These amplitude ranges should be typical for most locations on the earth's surface and for most seasons. Although we cannot rule out a solar cycle variation, our measurements and those of others suggest that it is likely to be small.

In general, power line and electric appliance magnetic fields are much greater than these natural background levels. For example, an illustrative 60 Hz magnetic field amplitude inside the right of way for a 765 kV EHV power transmission line is 2  $\mu\text{T}$ , which is roughly  $10^6$ – $10^7$  times larger than the natural background amplitudes (we assume a 1 Hz bandwidth for the noise measurements) (and in this case roughly 10 times larger than the earth's steady magnetic field). A typical amplitude for the 60 Hz magnetic field fluctuations near an operating household appliance is 10  $\mu\text{T}$ , which is over  $10^7$  times greater than our largest estimated natural magnetic field amplitude, and under some circumstances the 60 Hz appliance fields can be over  $10^9$  times stronger than the corresponding natural 60 Hz magnetic fields.

E3-7  
1600**THE ELECTROMAGNETIC ENVIRONMENT OF  
POWER LINES****Robert G. Olsen****School of Electrical Engineering and Computer Science  
Washington State University  
Pullman, WA 99164-2752**

In recent years, concern has been expressed about possible health effects associated with the ELF electromagnetic fields of electric power lines. In this paper, the methods commonly used by power engineers to calculate the electromagnetic fields near power lines will be reviewed. These methods will be used to illustrate results of recent research to redesign power lines to minimize the impact of the fields. Following this will be an examination of several issues raised by electromagnetics specialists about the methodology used by power engineers. More specifically, questions about ignoring radiation, assuming that the electric and magnetic fields are uncoupled and ignoring the traveling wave nature of the fields will be discussed.

E3-8  
1620

ELF/VLF SPECTRUM MEASUREMENTS  
M.G. Laflin, Member, Technical Staff  
U.S. Department of Commerce  
National Telecommunications and Information  
Administration  
Institute for Telecommunication Sciences  
325 Broadway  
Boulder, CO 80303-3328

A 16-bit digital spectrum analysis system was designed and built to provide measurement capabilities not currently available in commercial systems. The system provides the wide dynamic range necessary to observe very weak signals in the presence of strong signals. Large sample size allows for high frequency resolution. System outputs include spectral densities, amplitude probability distributions, diurnal amplitude variations, and time domain plots. Magnetic flux density is measured using a calibrated loop antenna. Antenna response encompasses a range from 10 Hz to 10 kHz.

Measurements were made to characterize the signal and noise environment in a sampling of office buildings. These include the New York Stock Exchange, the World Trade Centers, and two Denver office buildings. Measurements were made over 24-hour periods and include business day and weekend coverage.

Results reveal a complicated signal environment. Associated with the power distribution frequencies were strong third harmonics with higher harmonics evident into the kilo hertz range. Many off powerline signals also were observed; several of these likely associated with computer monitors and printers.

E3-9            **DIRECTIONAL MEASUREMENTS OF MULTI-SOURCE**  
1640            **SIMULTANEOUS RADIO NOISE EMISSIONS**

R. L. Johnson  
Electromagnetics Division  
Southwest Research Institute  
San Antonio, TX 78228

A problem in determining the source location of radio noise is that there are frequently multiple sources emitting signals simultaneously. During the past two decades, superresolution wavenumber techniques have been developed to decompose a multi-component wavefield into its constituent parts, thus enabling one to perform radio direction finding for each signal separately. Three eigen based techniques of particular interest in this study are MUSIC, ROOT-MUSIC and ESPRIT.

The objective of our experiment was to evaluate the relative performance of the three techniques using conventional off-the-shelf hardware similar to that routinely installed in modern radio direction finding systems. Our study differs from other reported investigations in that this effort was based on empirical data as opposed to computer simulations. To minimize the number of receiver channels, we constructed a minimum redundancy antenna array of nine monopoles. Two mobile radio transmitters were moved to various angular separations relative to the antenna array, and experimental data were acquired and analyzed.

The MUSIC algorithm provided best overall DF performance, but it was computationally more intense since it has no closed form solution. The ESPRIT and ROOT-MUSIC techniques provided a closed form solution, and the ESPRIT method evidenced slightly better performance than the ROOT-MUSIC. These results are somewhat different from previous studies done by others which compare performance for a filled linear array.

F4-1  
1340      **DIFFUSE, INCOHERENT RADAR CROSS SECTIONS FOR  
RANDOM ROUGH SURFACE WITH HEIGHT-SLOPE  
CORRELATIONS INCLUDED**

Ezekiel Bahar  
Electrical Engineering Department  
University of Nebraska-Lincoln  
Lincoln, NE 68588-0511

The principal motivation for the present investigations is to examine the relationships between the full wave solution and the corresponding specular point and small perturbation solutions when the simplifying assumptions regarding the statistical characterization of the random rough surface cannot be made a priori. In order to consider problems that are numerically tractable (using minicomputers) in this paper, only one dimensionally rough surfaces are considered. In order to compare the full wave solution with the often quoted specular point solution of Beckmann, the rough surface, which is assumed to be homogeneous, is characterized by a Gaussian four dimensional joint surface height and slope probability density function. In these cases, it is shown that the full wave solutions for the bistatic scattering cross sections (which intrinsically account for the self shadowing), can be reduced to three dimensional integrals over the slopes at two points and the distance variable. If, in addition, self-shadowing effects are ignored for surfaces with small slopes, these three dimensional integrals can be further reduced to one dimensional integrals over the distance variable.

In this work, where the correlations between the surface heights and slopes at two points are accounted for completely for random surfaces with Gaussian characteristics, it is possible to compare the full wave solutions with the specular point solution and to examine the conditions of the coalescence of the full wave solutions with the specular point solutions. For surfaces with small heights and small slopes, the full wave solutions for the diffuse incoherent scattering cross sections reduce to Rice's polarization dependent solution. Numerical examples are presented to illustrate these comparisons and the consequences of totally ignoring the effects of shadowing are also examined.

The full wave solutions are based on complete expansions of the electric and magnetic fields and the imposition of exact boundary conditions. In addition, on employing the full wave analysis, the questions regarding convergence are rigorously addressed by avoiding term-by-term differentiation of the field expansions. Thus, problems related to convergence of the small perturbation solutions will also be examined. It is also shown in retrospect that Rice's first order solutions contain all the fundamental elements of a general single scatter theory. Thus on performing a phase correction and a coordinate transformation, the small height and small slope restrictions of Rice's first order small perturbation solution can be removed without adopting a two scale model.

F4-2  
1400BISTATIC SCATTERING CROSS-SECTIONS  
OF A RANDOM ROUGH SURFACESaba Mudaliar  
Rome Laboratory  
Hanscom AFB, MA 01731

Perhaps the most commonly used method in the study of scattering from random rough surfaces is the Kirchhoff method. Inherent in this procedure is the notion of illuminated region and shadowed region. Sancer [IEEE Trans. Ant. Propagat., AP-17, 577-585, 1969] has considered this problem and has derived 'shadow corrected' scattering cross sections. However, we observe that this method leads to certain discontinuities in the bistatic scattering cross sections. This is indeed unphysical. We therefore derive in this paper an expression for the 'shadow corrected' scattering cross-section which is devoid of the above-mentioned defect.

Sancer has found that the shadow-correction is effected by a function which is the conditional probability that an arbitrary point on the surface is simultaneously visible to both transmitter and receiver. We first derive this 'visibility function' for our bistatic geometry assuming that the surface height is normally distributed. Attention is focussed particularly to the case when the angles of incidence and observation are large.

We then consider a composite rough surface which is generated by superposing a small scale rough surface on the above-discussed large scale rough surface. Since the scattering from a composite surface may be obtained by employing a perturbation scheme to the underlying large scale rough surface it is apparent that the shadow-correction to the composite rough surface involves the same visibility function. Bistatic scattering coefficients of a composite rough surface has been obtained by Barrick and Peake [Report BAT-197a-10-3, Columbus Labs., Ohio, 1967]. This work completely ignores shadowing effects. However their results in conjunction with our visibility function provide the desired shadow corrected scattering cross sections.

F4-3  
1420ELECTROMAGNETIC WAVE SCATTERING FROM  
A TWO-LAYER ANISOTROPIC RANDOM MEDIUMSaba Mudaliar  
Rome Laboratory  
Hanscom AFB, MA 01731

Electromagnetic wave scattering from a general anisotropic random medium is no longer merely a topic of theoretical interest. The need for such a study occurs in several important areas such as microwave integrated circuits, optical devices, waveguides, remote sensing, radomes etc. Among the few earlier works in this topic attention is restricted to media with uniaxial symmetry.

In this paper we have a general anisotropic random medium layer with permittivity  $\bar{\epsilon}(\bar{r})$ . The principal coordinate system of this anisotropic medium have arbitrary orientation with respect to the geometry of the layer. Further the fluctuating part of  $\bar{\epsilon}(\bar{r})$  is assumed to be small. The medium above the layer is free space while the medium below is homogeneous and isotropic. We have an electromagnetic plane wave incident from above the random medium layer and our objective is to find the bistatic scattering coefficients.

Based on the assumption of small permittivity fluctuations the scattered field is obtained using the Born approximation. Our calculation requires the asymptotic form of the Green's function  $\bar{G}_{10}$ . This is obtained by applying the reciprocity theorem and the method of stationary phase to the Green's function obtained in an earlier paper [S. Mudaliar and J. K. Lee, AP-S/URSI Symposium, Ontario, 1991]. We proceed to calculate the mean intensity and hence the scattering coefficients. The result is expressed in a compact and meaningful form so that the various scattering processes are readily identified. This also enables us to point out the additional scattering processes involved in the case of backscattering. Finally our results are compared with those of a corresponding uniaxial problem.

F4-4  
1440

WEAK TRANSVERSE LOCALIZATION OF LIGHT  
DIFFUSELY SCATTERED FROM A RANDOMLY ROUGH VACUUM-  
METAL GRATING SURFACE A.R. MCGURN, West. Mich.  
Univ., and A.A. MARADUDIN, Univ. of Calif., Irvine.

We consider the diffuse scattering of light from a metal surface which is randomly rough in one-dimension. Specifically, we treat light whose plane of incidence is parallel to the axis of translational symmetry in the surface and which is also perpendicular to the mean surface. The diffusely scattered light is found to occur in a cone whose axis of rotation is the axis of translational symmetry of the surface and which contains the specularly reflected beam. Scattering anomalies associated with weak localization are observed in both polarized and cross polarized scatterings. Results are presented for the scattering of visible light from both silver and gold surfaces.

F4-5  
1500

ENHANCED BACKSCATTERING OF LIGHT FROM THE SURFACE OF A LIQUID METAL, A.A. Maradudin, Univ. of Calif., Irvine and A.R. McGurn, West. Mich. Univ.

We have calculated the amplitude of the scattered light to second order in the surface profile function when p- and s-polarized light is incident on the surface of a liquid metal that is randomly corrugated by surface riplons. The result is used to calculate the mean differential reflection coefficient for in-plane, cross-polarized scattering. Enhanced backscattering is present in the angular dependence of the intensity of the incoherent component of the scattered light for both polarizations of the incident light. Numerical estimates of the size of the effect are present for liquid mercury.

## IONOSPHERIC MODIFICATION-I

Chairman: M.C. Lee, Massachusetts Institute of Technology

GH2-1 HIGH FREQUENCY ACTIVE AURORAL RESEARCH PROGRAM (HAARP)  
1340 P. A. Kossey (PL/PGID) R. G. Brandt (ONR)  
Geophysics Directorate 800 N. Quincy Street  
Hanscom AFB, MA 01731 Arlington, VA 22217

As part of a Joint Services (Navy/Air Force) research program to investigate the potential for exploiting ionospheric modification technology, the Ionospheric Effects Division of the Air Force Phillips Laboratory and the Office of Naval Research are developing a new, high frequency (HF), ionospheric heating instrument in Alaska. The heater, along with a comprehensive complement of diagnostic instruments, will be used to conduct basic and exploratory research to improve the fundamental understanding of the physical processes of heating of the ionosphere by very high power HF radio waves. The planned heater will be capable of providing sufficient energy densities in the ionosphere to enable investigations to be conducted in such diverse areas as the generation of Extremely Low/Very Low Frequency (ELF/VLF) waves in the auroral region, electron acceleration, plasma instabilities, and other phenomena triggered by very high power RF heating of the ionosphere. Research is planned to assess the efficiency of ELF/VLF wave generation in the auroral region including the characterization of the radiation patterns of such generated waves; to identify the mechanisms of generation of plasma instabilities and field aligned ionization, including potentially the controlling of such processes; to quantify optical and other emissions associated with electron acceleration in the ionosphere; and, to characterize the bulk parameters of the ionosphere under both ambient and heated conditions. To conduct such research a new ground based heater having effective radiated powers (ERP) of 1 gigawatt (90 dBW) or more over about the 3-10 MHz band is envisioned, having such features as HF frequency tuning and beam steering agility as well. This paper will briefly describe the progress and plans of the HAARP program.

GH2-2 REVIEW OF RECENT SOVIET RESEARCH  
1400 STUDIES OF IONOSPHERIC MODIFICATION  
BY HIGH-POWER RADIO WAVES

L. M. Duncan  
Dept. of Physics and Astronomy  
Clemson University  
Clemson, SC 29634-1911

A summary is provided of the major research results and discussions from the 3rd Suzdal International Symposium on Ionospheric Modification by High-Power Radio Waves. This meeting was held September 9-12, 1991 in Suzdal, USSR, attended by approximately two dozen scientists from the West and one hundred Soviet scientists. The symposium provides a unique opportunity for Western scientists to meet and interact with Soviet colleagues, many of whom have not had the opportunity to travel outside of the USSR. The substantial Soviet research programs in ionospheric modification have produced a number of interesting theoretical and experimental results in the investigation of HF-induced artificial turbulence, influence of induced disturbances on telecommunications, oblique ionospheric heating, and triggered geophysical phenomena. We also will describe the performance parameters and general operating characteristics of the principal Soviet experimental facilities. In addition, we will discuss future opportunities for collaborative ionospheric modification research.

GH2-3 A COMPUTER SIMULATION OF THE EFFECTS OF HF  
1420 RADIO WAVE HEATING ON THE LOWER  
IONOSPHERE

M.J. Freeman  
Department of Physics  
Clemson University  
Clemson, SC 29634-1911

G.M. Milikh  
Department of Astronomy  
University of Maryland  
College Park, MD 20742

A one-dimensional, self-consistent computer code was written to predict the effects of high-power, high-frequency radio wave heating on the electron temperature and density in the lower ionosphere. In the simulation, which is based upon kinetic-corrected fluid theory, a model background ionosphere was modified by high-frequency (HF) radio waves from the Arecibo heating facility and from the proposed HF Active Auroral Research Program (HAARP) facility under a variety of conditions. Simulations were conducted in the continuous and pulsed regimes. Results from the code show that during the daytime at Arecibo, heating is most effective near 80 km with the electron temperature reaching 700 K. Daytime heating at the proposed HAARP facility produces a peak temperature of 900 K at 70 km. The results of the code will be used to predict the behavior of the polar electrojet in response to an amplitude modulated HF wave, related to the stimulation of very low frequency (VLF) radiation. Also, the code will be used to predict the electron temperature changes induced by various heating schemes such as power shaped pulses, chirped pulses, and coded pulse trains.

GH2-4      LABORATORY SIMULATION OF BRAGG REFLECTORS PRODUCED  
1440      BY THE IONOSPHERIC HEATING PROCESSES  
            S.P. Kuo and Y.S. Zhang  
            Polytechnic University  
            Farmingdale, New York 11735  
            M.C. Lee  
            Massachusetts Institute of Technology  
            Cambridge, Massachusetts 01239  
            P.A. Kossey  
            Air Force Phillips Laboratory  
            Hanscom AFB, Massachusetts 01731  
            R.J. Barker  
            Air Force Office of Scientific Research  
            Bolling AFB, DC 20332-6448

A set of parallel plasma layers is generated by two intersecting microwave pulses in a chamber containing dry air at a pressure comparable to the upper atmosphere. The dependence of breakdown conditions on the pressure and pulse length is examined. The results are shown to be consistent with the appearance of tail erosion of microwave pulse caused by air breakdown. Bragg scattering experiments, using the plasma layers as a Bragg reflector are then performed. Both time domain and frequency domain measurements of wave scattering are conducted. The experimental results are found to agree very well with the theory. Moreover, the time domain measurements of wave scattering provides an unambiguous way for determining the temporal evolution of electron density during the first 100 us period. A Langmuir double probe is then used to determine the decay rate of electron density during a later time interval (1 ms to 1.1 ms). The propagation of high power microwave pulses through the air is also studied experimentally. The mechanisms responsible for two different degrees of tail erosion have been identified. The optimum amplitude of an 1.1 us pulse for maximum energy transfer through the air has been determined.

GH2-5 THE INVESTIGATION OF CHANGES IN THE IONOSPHERE CAUSED  
1520 BY HIGH POWER OBLIQUE HF TRANSMITTERS

Yuming Huang, Gary S. Sales, Ian G. Platt, D. Mark Haines  
University of Massachusetts Lowell  
Center for Atmospheric Research  
450 Aiken Street  
Lowell, MA 01854

John L. Heckscher, Paul Kossey  
Phillips Laboratory, Geophysics Directorate  
Hanscom AFB, MA 01731

## ABSTRACT

Three experimental campaigns to modify the F-region of the ionosphere from a distance of 1200 km from a high power (90 dBW) HF radio transmitter, have been carried out. A low power (500 W) diagnostic signal (probe signal) was transmitted along the same path as the high power wave, passing through the heated region. This probe signal was received on an array of three vertical monopole antennas at a site 2400 km from the transmitter. On-site signal processing yields amplitude, Doppler frequency shift and arrival angles of the received probe signal. In addition, a vertical incidence digital ionospheric sounder, located at the midpoint of the oblique path, provided ionospheric profiles for real-time frequency and elevation angle management.

Extensive processing and analysis of the large data base has been carried out to detect changes in the F-region of the ionosphere caused by a 10 minute periodic modulation of the high power oblique HF heater transmitter. Analysis techniques, including contour plotting of the Doppler frequency vs. time, superimposed epoch analysis, statistical analysis, including amplitude and elevation angle distributions, correlations and Fourier analysis have all been applied to process the amplitude, elevation angle and Doppler frequency of the received probe signal. Heating effects are detected and results of these analyses are presented. Three dimensional ray tracings are used to model the heated region and the interaction of the heated region with the probe signal.

GH2-6 INVESTIGATIONS OF SEE AT THE ARITHMETIC MEAN FREQUENCY  
1540 OF TWO HF PUMP WAVES

M. Waldenvik, B. Thidé, T. B. Leyser, and E. Veszelei  
Swedish Institute of Space Physics, S-75591 Uppsala, Sweden  
S. M. Grach, A. N. Karashtin, V. L. Frolov, D. S. Kotik, and G. Komrakov  
Radiophysical Research Institute, Nizhny Novgorod, Russia

During joint Swedish Institute of Space Physics, Uppsala (IRFU)/Radiophysical Research Institute, Nizhny Novgorod (NIRFI) ionospheric modification campaigns in 1991 the so called "arithmetic mean peak" (AMP) was investigated. This SEE component is generated by two HF pump waves operated at slightly different frequencies. During this experiment the transmitter feeding one part of the antenna array were held at a fixed frequency while we were able to control the frequency of the transmitter feeding the other part from the receiving site. We were thus able to vary the frequency in small steps to investigate the AMP dependence on the difference frequency, as well as the dependence on the pump frequency. We found that the dependence on difference frequency was strong, and more complex than expected. There is also a strong dependence on whether the pump frequency is close to a cyclotron harmonic frequency or not.

GH2-7      STIMULATED ELECTROMAGNETIC EMISSIONS FROM  
1600      MAGNETIZED AND INHOMOGENEOUS PLASMA  
Simon Goodman  
Swedish Institute of Space Physics, S-77591 Uppsala, Sweden

We model the radio emission spectrum for an electromagnetically pumped, magnetized and inhomogeneous plasma and compare the results to observations of upper sideband features of stimulated electromagnetic emissions (SEE) in ionospheric heating experiments when the heater frequency,  $\omega_0$ , is near harmonics of the ionospheric electron cyclotron frequency,  $\Omega_e$ . Our model involves solving the equations of motion for electrons in an electromagnetic pump wave and geomagnetic field to calculate, for an inhomogeneous plasma, a current which excites electron Bernstein and lower hybrid waves. We reinsert this current into the equations of motion and continue in an iterative manner. The result is a current which depends on density gradients across the geomagnetic field. The current intensifies with decreasing density gradient scale. It has a frequency  $\omega = 2\omega_0 - p\Omega_e$ , where  $p$  is an integer and is resonant for  $\omega_0 \approx p\Omega_e$ . There is a cutoff in the spectrum which depends on  $p$ . The power radiated is about 80 decibels below the pump. Our results agree with observations made in SEE experiments.

GH2-8 REVIEW OF STIMULATED ELECTROMAGNETIC EMISSION RESULTS  
1620 OBTAINED DURING JOINT IONOSPHERIC MODIFICATION EXPERI-  
MENTS AT THE "SURA" FACILITY

B. Thidé, T. B. Leyser, M. Waldenvik, S. Goodman, and E. Veszelei  
Swedish Institute of Space Physics, S-755 91 Uppsala, Sweden  
S. M. Grach, A. N. Karashtin, V. L. Frolov, D. S. Kotik, A. Babichenko,  
and G. Komrakov  
Radiophysical Research Institute, Nizhny Novgorod, Russia

We present a review of stimulated electromagnetic emission (SEE) results obtained during joint Swedish Institute of Space Physics, Uppsala (IRFU)/Radiophysical Research Institute, Nizhny Novgorod (NIRFI) ionospheric modification campaigns in 1990 and 1991. The experiments were carried out at the NIRFI ionospheric modification facility "Sura", named after the Volga tributary Sura and located at the NIRFI field station (geographical coordinates: 56.13°N, 46.10°E), 7 km outside the village of Vasil'sursk about 100 km east of the city of Nizhny Novgorod, Russia. The transmitter section of the "Sura" installation consists of three commercial "Vyuga" PKV-250 transmitters, each capable of outputting 250 kW of HF power. The antenna system is a 300×300 m<sup>2</sup> array consisting of three individual steerable ( $\pm 40^\circ$ ) subsystems with four 12 element linear arrays of wideband "turnstile" dipoles, covering the 4.5–9.5 MHz band. When operated in parallel the maximum effective radiated power (ERP) is about 250 MW.

Accurate real-time measurements of the amplitude, phase, and power spectral density of the stimulated emissions and the reflected pump revealed that the evolution of the stimulated electromagnetic emissions proceeds through a number of rather distinct steps. This discovery was possible because in these experiments we were able, for the first time, to operate the HF pump and the SEE detector phase coherently and to have complete control of the pump frequency and timing from the diagnostic site.

The experiments carried out include:

- detection of extremely sharp resonances in the so called "Downshifted Maximum" SEE feature when the pump was operated near high harmonics of the ionospheric electron cyclotron frequency
- analysis of the so called "Broad Upshifted Maximum" SEE feature
- analysis of the dynamic change of the SEE associated with short probing HF pulses in the presence and absence of a continuous heating wave
- study of the arithmetic mean SEE components generated by two pumps operated at slightly different frequencies
- tentative discovery of beat wave excitation of SEE generated by two pumps, separated in frequency by the plasma frequency
- usage of the heater at about 9 MHz as a radar to detect MST scatter as well as coherent scatter from magnetospheric turbulence at about 5 000 km altitude in the auroral region

GH2-9  
1640SPECTRUM OF ELECTROMAGNETIC EMISSION STIMULATED  
BY A POWERFUL RADIO WAVE IN THE IONOSPHERET. B. Leyser, B. Thidé, S. Goodman, M. Waldenvik, V. L. Frolov, S. M.  
Grach, A. N. Karashtin, G. P. Komrakov, and D. S. Kotik

Swedish Institute of Space Physics

Box 812

S-981 28 Kiruna

Sweden

A powerful high frequency electromagnetic pump wave in the ordinary mode vertically injected into the ionospheric F region from ground-based transmitters stimulates the emission of electromagnetic radiation, which can be detected on the ground. We present new and detailed experimental results concerning the spectrum of the stimulated electromagnetic emission (SEE) as it appears on long time scales, more than 100 ms after the pump wave has been turned on. The experiments were performed in September/October 1990 and 1991 at the Sura ionospheric modification facility near Vasilsursk in the USSR.

We emphasize the significant dependence of the SEE spectrum on the pump frequency in relation to harmonics of the F region electron cyclotron frequency, for pump frequencies ranging from below the fourth cyclotron harmonic to above the seventh harmonic. This concerns all commonly observed spectral features in the sidebands of the pump wave, such as the, so called, continuum, downshifted maximum (DM), and broad upshifted maximum (BUM) emissions. There are systematic variations in the SEE spectrum for different pump frequencies between the cyclotron harmonics as well as for pump frequencies near a cyclotron harmonic.

Session J-5 1335-Thurs. CR2-26  
POLARIZATION: TECHNIQUES AND OBSERVATIONS  
Chairman: C. Read Predmore, Dept. of Astronomy, Univ. of Massachusetts,  
Amherst, MA 01003

J5-1        LINEAR POLARIZATION MEASUREMENTS AT THE  
1340        HIGH-FREQUENCY LIMIT OF A RADIO TELESCOPE

G. Novak, Dept. of Physics, Princeton University  
Princeton, NJ 08544

and

C.R. Predmore and P.F. Goldsmith  
Five College Radio Astronomy Observatory  
U. of Massachusetts, Amherst, MA 01003

Several years ago, we began a program of dust emission polarimetry using the 14 meter telescope of the Five College Radio Astronomy Observatory. We detected a linear polarization of 2-3 percent in the 230 GHz continuum emission from the Kleinmann-Low Nebula in the Orion Molecular Cloud. We published this measurement in 1990 (*Ap. J.*, vol. 355, p. 166).

During these and subsequent observations, we detected a spurious linear polarization effect. We studied this effect under a variety of conditions, and at several frequencies in the 100-230 GHz range. We have determined that it is due to the telescope optics. It is produced primarily by thermal and gravitational deformations of the primary reflector. Spurious polarization can also be produced by misalignment of the feed horn axis with respect to the subreflector.

The spurious polarization is most clearly observed when the center of the telescope's beam is pointed towards the half-power point of a source, but we have also detected spurious polarization with the beam centered on a flux peak.

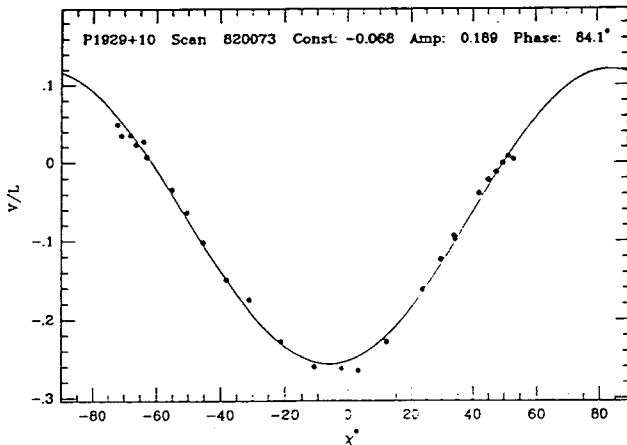
Polarimetric observations made at frequencies near the high-frequency limit of any telescope will benefit from a proper understanding of these effects, and this paper is intended to help promote such an understanding.

J5-2  
1400POLARIZATION CROSS-COUPLING AND  
RADIO SPECTROSCOPYJ. A. Phillips  
Radio Astronomy 105-24  
California Institute of Technology  
Pasadena, CA 91125

Zeeman splitting of spectral lines is an important tool for measuring interstellar magnetic fields. The effect has been detected in neutral hydrogen lines from cold atomic clouds, in galactic OH masers, and possibly from OH megamaser galaxies. Zeeman experiments are usually conducted with dual-circularly polarized antenna systems. One observes the difference between two circular polarizations (Stokes parameter  $V$ ) in order to detect the  $\sigma$  Zeeman components. This procedure is sensitive to magnetic fields parallel to the line of sight. For normal interstellar magnetic fields, the frequency shift between polarizations is much smaller than the total width of the spectral line. The Zeeman-split  $V$  spectrum is proportional to the frequency derivative of the line intensity profile ( $V(\nu) \propto dI(\nu)/d\nu$ ). Simple gaussian line profiles should therefore exhibit an  $S$ -shaped  $V$  spectrum with a zero crossing near the maximum of  $I(\nu)$ .

In practice the "circular" polarization of a radio antenna is only nominal — the true polarization is elliptical. The major axes of the left- and right-handed ellipses may be orthogonal, coincident, or somewhere in between depending on the phase and amplitude of voltage cross-talk between the two polarization channels. The figure below shows 1665 MHz calibration observations of a linearly polarized source (PSR 1929+10) obtained at the Arecibo observatory. The ratio  $V/(Q^2 + U^2)^{1/2}$  varies as a function of parallactic viewing angle  $\chi$  because of  $\sim 10\%$  cross-coupling between polarization channels. The Arecibo 1665 MHz feed is an orthogonal, elliptically polarized system.

A simple model of polarization cross-coupling shows that the characteristic  $S$ -shaped Zeeman spectrum can be mimicked by instrumental effects. If the spectral line is linearly polarized, it is necessary to measure *all four Stokes parameters* ( $I$ ,  $Q$ ,  $U$ , and  $V$ ) to properly calibrate the polarization data. Traditional methods of Zeeman calibration (e.g., periodic switching of IF lines and amplifiers during observing) may not entirely remove important cross-coupling effects.



J5-3  
1420POLARIZATION CHARACTERISTICS OF THE GREEN BANK  
TELESCOPE

S. Srikanth

National Radio Astronomy Observatory\*

2015 Ivy Road

Charlottesville, VA 22903

Detailed design of a new radio telescope to be constructed for the National Radio Astronomy Observatory at its facility in Green Bank, West Virginia, is under way. The telescope is scheduled for completion by the end of 1994. The major design specifications laid out are full-sky coverage, low sidelobes, low system temperature, high efficiency and good spectral lines. To meet the specifications, a 100-meter offset design with unblocked aperture has been selected for the Green Bank Telescope (GBT). The telescope operates at prime focus for frequencies below 1.15 GHz.

When fed by a linearly-polarized prime focus feed, the asymmetrical main reflector introduces cross-polarization lobes which are about -23 dB below the main co-polarized beam for the chosen parameters of the GBT. By use of special purpose prime focus feeds (B. K. Watson *et al.*, *Proc. of 8th EMC*, pp. 183-187, Paris, France, 1978), the cross-polarization can be reduced by about -15 dB over limited bandwidths. In the secondary focus mode, double offset configuration is used. Here, an asymmetrical subreflector cancels the cross-polarization component of the main reflector when the Mizugutch *et al.* condition (equation 1, Y. Mizugutch *et al.*, *Int. IEEE/AP-S Symp. Digest*, pp. 2-5, 1976) is satisfied.

There are certain requirements for the telescope where the Mizugutch *et al.* condition is not met. For instance, while providing multiple beams, the feeds which are not on axis have to be tilted for maximizing gain. Another example is pairs of feeds that are used for the purpose of beam switching. Under this condition, the cross-polarization levels deteriorate. Results of theoretical analysis of these effects will be presented.

---

\*The National Radio Astronomy Observatory is operated by Associated Universities, Inc. under Cooperative Agreement with the National Science Foundation.

J5-4  
1440

CIRCULAR STOKES VECTORS FOR TERRESTRIAL  
PLANETS: 3.54 CM RADAR  
R.F. Jurgens, M.A. Slade, and T.C. O'Brien  
Jet Propulsion Laboratory, MS 238-420  
4800 Oak Grove Drive  
Pasadena, CA 91109

Dual circularly polarized masers and receivers were installed in the Goldstone radar system during the upgrade in 1986. Since then many CW observations have been made of Mercury, Venus, and Mars, and for many of these the complex voltage samples were recorded. This permitted the computation of the Circular Stokes vectors in post processing. In some cases, the Stokes vectors were computed in real time, averaged and recorded to reduce the data volume. Unfortunately, until recently, little was known about the phase stability of the the masers and receivers. However, recent modifications of the X-Band system incorporated directional couplers ahead and behind the masers, and a coherent reference generator was added to the system. Preliminary tests indicate that the phase of the receiving system is adequately stable to form averages for a few minutes. Longer averages would require some scheme to continuously calibrate for phase drifts.

Radar observations of Mars made during the 1990 opposition indicate that some energy is observed in the complex cross power averages. The magnitude of these spectra often resemble the quasi-specular signature and might indicate leakage between the polarizations. The strength of the signature is larger than predicted based on the known leakage properties, and the quasi-specular leakage is not seen in the "Same Sense Circular" (depolarized) spectra. A few very simple scattering models that predict similar and different spectral shapes will be presented. A considerable new effort may be required to connect these observations with realistic physical models.

J5-5 POINT SOURCE POLARIZATION CALIBRATION OF A  
1500 PHASED ARRAY  
M. M. McKinnon  
Department of Physics  
New Mexico Institute of Mining and Technology  
Socorro, New Mexico 87801

The analytical representation of the signals produced by a multiplying polarimeter is derived for the polarized point-source radiation received by a phased array of radio telescopes. Instrumental cross-coupling between the right and left circularly polarized feeds is included in the derivation. The equations derived for the polarimeter signals are simplified by a series of assumptions which are designated as the "single antenna approximation". The simplified equations representing the polarimeter signals are then used to derive expressions for the measured Stokes parameters. The behavior predicted by the expressions for the measured Stokes parameters is confirmed by Very Large Array phased array observations of the polarization calibrator 3C286 and the pulsar PSR 0329+54. The vector of measured Stokes parameters is written as the product of an instrumental matrix and the vector of true Stokes parameters. The instrumental matrix is separated into time-dependent and time-independent matrices. The physical significance of all the elements in the time-independent matrix is discussed. Once the elements of the instrumental matrix are determined by polarization calibration, the true Stokes parameters of an observed source of unknown polarization may be calculated with simple linear algebra. The single antenna approximation allows the polarization calibration scheme to be applied to single antenna observations.

J5-6    **Feed Pattern Measurements in Radio Telescopes**  
1540        **Using the Phase-Amplitude Technique**

*R.J. Smegal, D. Routledge, J.F. Vaneldik (Electrical Engineering Department, University of Alberta), T.L. Landecker (Dominion Radio Astrophysical Observatory, National Research Council of Canada)*

A phase-amplitude antenna measurement system based on a modern vector network analyzer can perform feed polarization measurements in a simple and inexpensive outdoor range with a minimum of specialized mechanical devices. The system provides high reliability by keeping the critical calibration and complex data analysis stages of the measurement separate from the data collection which becomes operationally simple. Since scheduling such measurements is difficult and set up is labour intensive, measurement reliability is important. Complete antenna field information (amplitude, phase and direction) is obtained during collection. This data is passed to post measurement processing software that applies calibration and extracts quantities of interest such as gain and polarization ratio. Depending on the sophistication of the software and the amount of data collected, measurement errors resulting from noise or range reflections can be reduced and contributions from components such as quarter wave plates separated from those of the feed aperture. This technique was employed successfully to obtain gain, phase and polarization patterns of feeds during a measurement program at a radio observatory. The goal of the program is to acquire a good understanding of the antenna properties to permit wide field polarization mapping. This range is described, together with calibration, data collection and data analysis steps of the measurement.

J5-7      **MEASURING THE ZEEMAN EFFECT IN**  
 1600      **INTERSTELLAR CLOUDS**

A. A. Goodman  
 Astronomy Department, University of California  
 Berkeley, CA 94720

Measurement of the Zeeman effect in the spectral lines of OH (1.7 GHz) and HI (1.4 GHz) provides a powerful technique for studying the role of magnetic fields in the support and dynamics of molecular clouds.

In interstellar clouds of density  $10\text{-}10^4\text{ cm}^{-3}$ , the Zeeman splitting due to weak magnetic fields is much smaller than the Doppler-broadened line width. So, the splitting is detected by differencing opposite senses of circular polarization and searching for an S-like pattern caused by the frequency difference between oppositely polarized Zeeman components.

My collaborators (R. Crutcher, C. Heiles, I. Kazès, P. Myers, and T. Troland) and I have now carried out such experiments at several observatories, investigating a range of interstellar conditions, and the results are summarized below. The field strengths we measure are consistent with equipartition between the kinetic energy of the gas and the magnetic field energy. For gravitationally bound clouds in virial equilibrium, the magnetic energy is also comparable to the gravitational energy.

Telescope	Observations	Density Traced	Fields Measured
Hat Creek 85-foot	HI emission and self-absorption in diffuse, dark, and high-latitude clouds	$10\text{-}100\text{ cm}^{-3}$	3-20 $\mu\text{G}$
Green Bank 140-foot	OH emission in dark clouds and absorption against HII regions	$10^3\text{-}10^4\text{ cm}^{-3}$	10-100 $\mu\text{G}$
Effelsberg 100-m	OH emission in dark clouds	$10^3\text{-}10^4\text{ cm}^{-3}$	TBA
Arecibo 1000-foot	OH emission in dark clouds and absorption against HII regions	$10^3\text{-}10^4\text{ cm}^{-3}$	10-60 $\mu\text{G}$

J5-8  
1620

## POLARIZATION OF INTERSTELLAR MILLIMETER EMISSION LINES

D. C. Lis

Downs Laboratory of Physics 320-47  
California Institute of Technology  
Pasadena, CA 91125

Theoretical calculations (P. Goldreich and N.D. Kylafis, *Ap. J. (Letters)*, **243**, L75-L78, 1981; P. Goldreich and N.D. Kylafis, *Ap. J.*, **253**, 606-621, 1982; N. D. Kylafis, *Ap. J.*, **267**, 137-150, 1983; S. Deguchi and W.D. Watson, *Ap. J.*, **285**, 126-133, 1984) predicted that interstellar millimeter emission lines may possess a significant degree of linear polarization, and the polarization direction may be either perpendicular or parallel to the projection of the magnetic field on the plane of the sky. Observations of polarized millimeter line emission were thus suggested as a possible tracer of the magnetic field direction inside interstellar molecular clouds which are opaque to radiation at shorter wavelengths.

I discuss results of observational searches for linear polarization of millimeter emission lines in interstellar molecular clouds with a wide range of physical conditions (P.G. Wannier, N.Z. Scoville, and R. Barvainis, *Ap. J.*, **267**, 126-136, 1983; R. Barvainis and A. Wooten, *Astr. J.*, **93**, 168-171, 1987; D.C. Lis, P.F. Goldsmith, R.L. Dickman, C.R. Predmore, A. Omont, and J. Cernicharo, *Ap. J.*, **328**, 304-314, 1988) No polarized emission was unambiguously detected in any of these searches, with  $3\sigma$  upper limits of a few %. I discuss possible explanations for the discrepancy between the theory and observations.

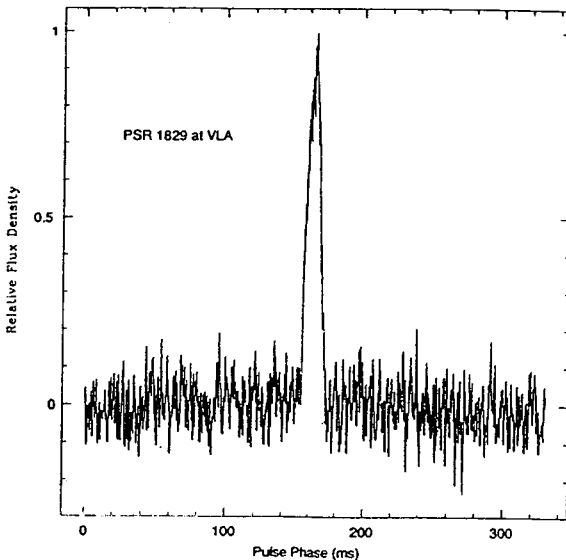
I also discuss observational measurements of linear and circular polarization of the HCN maser emission in the circumstellar envelope CIT 6 (P.F. Goldsmith, D.C. Lis, A. Omont, S. Guilloteau, and R. Lucas, *Ap. J.*, **333**, 873, 1988; D.C. Lis, P.F. Goldsmith, and C. R. Predmore, *Ap. J.*, **341**, 823, 1989). The high degree of linear polarization detected ( $\sim 20\%$ ) confirms the presence of maser amplification. If the polarization is produced by magnetic fields, its observed magnitude and direction are consistent with predictions based on the source geometry derived from the optical polarization data. The HCN maser line was determined to be circularly unpolarized with a  $3\sigma$  upper limit of  $\sim 3\%$ .

J5-9 VLA POLARIMETRY OF THE PULSAR PSR1829-10:  
 1640 TESTING THE PLANET HYPOTHESIS

J. A. Phillips, S. R. Kulkarni, G. Vasisht, and S. E. Thorsett  
 Radio Astronomy 105-24  
 California Institute of Technology  
 Pasadena, CA 91125

Periodic timing residuals in PSR 1829-10 have been attributed to the existence of a planet-mass object around the pulsar (Bailes, Lyne, and Shemar 1991, *Nature*, 352,311). If this interpretation is correct it marks the first definitive detection of a planet outside our own solar system. There are serious theoretical difficulties with a planet around a neutron star. How did it survive the supernova blast? Why is its apparent orbit so nearly circular? If the planet condensed from post-shocked gas, why don't many other pulsars possess detectable planets? Given these questions, it is necessary to consider alternate explanations for this phenomenon before accepting the planet hypothesis. We can test a whole class of alternative models via polarization observations of PSR 1829-10. Temporal changes in the shape of the pulsar radio beam can translate to variations in the apparent arrival time. Precession of the neutron star spin axis or changes in the topology of the stellar magnetosphere could produce such an effect. If the pulsar wobbles due to some form of precession, we should detect changes in the polarization position angle on a timescale of six months (the putative orbital period of the planet). Some pulsars exhibit quasi-periodic "mode changes," which are accompanied by polarization fluctuations. Time scales for such fluctuations are known to range from minutes to days. Polarization observations are required to test whether PSR 1829-10 presents a case of slower-than-usual mode changing.

In September 1991 we began a program to monitor the polarization of PSR 1829-10 once a month using the VLA as a phased array. The observations are expected to continue for 12 months and should provide an important test of the planetary hypothesis.



J5-10 PULSAR POLARIMETRY USING  
1700 COHERENT DEDISPERSION TECHNIQUES

S. E. Thorsett  
Radio Astronomy 105-24  
California Institute of Technology  
Pasadena, CA 91125

The importance of polarization measurements to pulsar research was established in 1969, when Radhakrishnan and Cooke (*Ap. Lett.*, **3**, 225) observed a smooth S-shaped swing of the plane of linear polarization across a number of pulsar profiles and attributed it to the changing projection on the plane of the sky of dipolar magnetic field lines fixed to a rotating neutron star. Since then, observations of significant circular polarization in some pulsars, and of two orthogonal linear modes of emission in others, have set important constraints on proposed radio beam production processes. Recently, high precision polarimetry of pulsars has been used to search for geodetic precession in binary pulsars, and a number of new tests of fundamental gravitation theory based on polarization measurements have been proposed (Damour and Taylor, 1991, preprint).

Polarimetry of the burgeoning class of millisecond pulsars, as well as high precision polarimetry of ordinary pulsars, is significantly complicated by the effects of dispersion in the ionized interstellar medium, which smears the pulsar signal over a significant fraction of a pulse period. The introduction of hardware-based coherent dedispersion techniques (Ryba, 1991, Phd Thesis, Princeton) and the construction of a simple baseband multiplying polarimeter have allowed the straightforward, real-time computation of the Stoke's parameters of pulsar radiation with no dispersion smearing.

The new polarimeter has been used for a variety of observations, including a multifrequency study of the polarization of several millisecond pulsars (Thorsett and Stinebring, 1990, *Ap. J.*, **361**, 644). Polarization properties of millisecond pulsars were not found to differ considerably from those of their slower counterparts, despite rotation rates up to three orders of magnitude faster and magnetic field strengths up to three orders of magnitude smaller. These observations have also led to new limits on certain classes of non-symmetric gravity theories (Klein and Thorsett, 1990, *Phys. Lett. A*, **145**, 79), and on the magnetic fields around the companion of the first eclipsing binary pulsar (Thorsett *et al.*, 1989, Proc. 14th Texas Symp., N.Y. Acad. Sci., 420). The equipment has recently been used for preliminary observations of a pulsar in a high-mass binary system, which may lead to new tests of general relativity (Phillips, Wolszczan, Taylor, Arzoumanian, unpublished work).

Coherently-dedispersed polarimetry can also be used to study the properties of "microstructure" in individual pulses from strong pulsars. Many pulsars emit a significant fraction of their radio flux in intense bursts, with typical timescales of  $10\mu\text{s}$ -1ms (e.g., Hankins, 1971, *Ap. J.*, **169**, 487). Two phenomenological models have been proposed for these bursts: temporally limited flashes which fill a significant portion of the emission cone, and spatially limited tubes of flux which sweep rapidly past the observer's line of sight. The polarization properties of a single "micropulse" could help distinguish between these two models; preliminary observations of single pulses using the coherent dedispersers and polarimeter will be briefly described.

J5-11  
1720MILLIARCSECOND POLARIZATION PROPERTIES  
OF COMPACT RADIO SOURCESDavid H. Roberts  
Department of Physics  
Brandeis University  
Waltham, MA 02254

The linear polarization of a number of compact extragalactic radio sources has been determined by Very Long Baseline Polarimetry using global VLBI arrays at 5 GHz. These observations provide information on the orientation and order of the magnetic field, the thermal particle environment, and the kinematics of the relativistic jets often found in the nuclei of active galaxies. In this paper we discuss the superluminal quasars 3C 273 and 3C 345, for which we have data at a total of nine epochs.

In 3C 273 ( $z = 0.158$ ), *a*) the outermost visible knot is highly polarized ( $m \approx 26\%$ ) and has an inferred magnetic field parallel to the jet axis, *b*) the degree of polarization varies rapidly in the inner few milliarcseconds, *c*) the electric vector position angle changes rapidly with core-knot distance in this inner region, and *d*) the polarization of the inner region changed significantly in eight months, while the total intensity structure was essentially constant.

In 3C 345 ( $z = 0.595$ ), *a*) as components emerge from the core (radial distance from the core satisfying  $r(\text{mas}) \lesssim 1$ ), the position angles of their electric vectors swing rapidly with time, *b*) while the components move along the gently curving middle part of their path ( $1 \lesssim r \lesssim 5$ ), the electric vectors stay aligned with the local jet axis, *c*) in the most distant knot visible at 5 GHz ( $5 \lesssim r \lesssim 8$ ), where the jet appears to bend more sharply to the north, the electric vectors swing dramatically in the counter-clockwise direction, and *d*) preliminary estimates of the fractional polarization *between* the knots shows that it may be significant, suggesting a model in which a plane shock wave compresses jet plasma that contains both longitudinal (ordered) and random magnetic field components.

These sources possess a number of common characteristics. *a*) The polarization of the cores is very small (typically  $m \lesssim 1\%$ ), *b*) the polarization of the knots ranges from modest (a few percent) to very high (near the theoretical limit for incoherent synchrotron radiation,  $m_{\text{max}} \approx 75\%$ ), *c*) the fractional polarization increases with distance from the core, and *d*) the inferred magnetic field in the knots is predominantly along the jet axis, but varies from position to position in the jet. These data suggest that the magnetic field is random near the core, and becomes increasingly ordered as the plasma flows away from the nucleus. The role of the Faraday effect in determining the apparent orientation of the magnetic field cannot be determined without further observations, at a variety of frequencies and at more frequent intervals, that will be possible with the advent of the NRAO Very Long Baseline Array. These will determine the role of Faraday rotation and depolarization in the inner few parsecs of these sources, and thus shed new light on the properties of the "narrow line region" of active nuclei.

Friday Morning, 10 January, 0835-1200

Session A-8 0835-Fri. CR1-42

METROLOGY FOR MATERIAL CHARACTERIZATION

Chairman: Sedki M. Riad, Virginia Polytechnic Institute and State Univ.,  
Blacksburg, VA 24061

A8-1      **WIDEBAND AND MICROWAVE MATERIAL CHARACTERIZATION**  
0840

S. Riad, W. Davis, A. Elshabini-Riad, K. Fidanboylu,  
M. Andrawis, C. Bunting, and W. Su  
Electrical Engineering Department  
Virginia Polytechnic Institute and State University  
Blacksburg, VA 24061-0111

D. Amey, J. Curilla, J. Lyles, A. Murphy,  
and T. Poulin  
DuPont Electronics, Wilmington, DE 19898

This paper presents an overview of material characterization techniques developed by both Virginia Tech and DuPont researchers using both frequency and time domain approaches. The material properties of interest are the dielectric constant and loss tangent over the wide band of frequencies from near low RF to microwaves. The materials considered in this study were DuPont dielectrics for use in thick film and other multilayer electronic circuits. Other manufacturer materials also were considered at times for demonstration and verification purposes.

The developed methods were used in conjunction with empirically and analytically based models to determine the material properties from the measured data. The results of this work have enabled improved high frequency characterization of the dielectric constants and loss tangents of DuPont materials using these independent techniques. The work involved the application of the following methods: The wideband dielectric filled cavity (WDFC), frequency-domain modeling and measurement using the Thru-Reflect-Line calibration on a network analyzer, time-domain modeling and measurement, stripline cavity resonators including linear, ring, and T-shaped resonators, and low-frequency capacitors. These methods have been used for measuring DuPont thick-film materials with different conductor pastes, DuPont Pyralux®, and DuPont Green Tape™.

A8-2  
0900

**ELECTROMAGNETIC CHARACTERIZATION OF MATERIALS USING STRIPLINE/MICROSTRIP FIELD APPLICATOR**

G. Hanson, Dept. of Elect. Eng. and Comp. Sci., Univ. of Wisconsin, Milwaukee, WI 53201;

D. Nyquist, B. Kzadri, J. Grimm and M. Thorland, Dept. of Elect. Eng., Michigan State Univ., East Lansing, MI 48824;

L. Frasch, Boeing Defense & Space Group, Seattle, WA 89124

The broadband measurement of electromagnetic constitutive parameters of materials, which may be only large-scale homogeneous and/or anisotropic, requires the interrogation of large field volumes by an applicator which maintains essentially uni-directional electric and magnetic fields. If broadband measurements are to be implemented using a single field applicator, then it should support TEM or at least quasi-TEM waves. A dual-mode stripline/microstrip field applicator which satisfies these requirements, and provides a flexible measurement methodology to accommodate material samples of various types, has been designed and implemented for use with an automatic network analyzer.

The field applicator consists of a strip conductor located between, and parallel to, a pair of conducting ground plates. Tapered transition regions connect the coaxial applicator terminals to the uniform strip region in which material samples are placed. Both ground plates are present in the stripline mode, and the sample is placed between them and the strip conductor. In the microstrip mode, the upper plate is removed and the sample is located as a substrate between strip and lower plate or as a superstrate above the strip conductor. The transition regions were designed to minimize ambient reflections. A method was devised to measure the scattering parameters of those transition regions between coaxial terminal ports and the front and back terminal planes of the sample region. Scattering parameters of the sample region are subsequently de-embedded from the measured coaxial-terminal parameters using the measured transition-region network model. This de-embedding scheme was found to be very effective, and is believed to be new.

Measured scattering parameters of the sample region are processed to determine phase constant  $\beta_m$  and characteristic impedance  $Z_{cm}$  of the sample-loaded transmission region. If analytical relations for  $\beta(\epsilon, \mu)$  and  $Z_c(\epsilon, \mu)$  are available, then the pair of equations  $\beta(\epsilon, \mu) - \beta_m = 0$  and  $Z_c(\epsilon, \mu) - Z_{cm} = 0$  can be solved simultaneously for the complex constitutive parameters. This can be accomplished analytically when the applicator is operated in the stripline mode, and measurements have been implemented for frequencies over the band of 130-2000 MHz. A full-wave theory for the microstrip-mode phase constant and characteristic impedance renders the above equations transcendental, and they must be solved numerically by a 2-D root search. Results for the complex  $\epsilon$  of a non-magnetic material have been obtained, and the root search was found to be stable. Extensive numerical results will be presented.

## DIELECTRIC LOSS DETERMINATION USING PERTURBATION

*M. Y. Andrawis\*, W. A. Davis, S. M. Riad, and A. Elshabini-Riad*  
*Virginia Polytechnic Institute and State University*  
*Bradley Department of Electrical Engineering*  
*Blacksburg, VA 24061-0111*

A dielectric filled cavity structure is currently being used to estimate the dielectric constant and loss factor of dielectric materials which fill the cavity structure over a wide range of frequencies [M. A. Saed, "Dielectric Characterization Using a Wideband Dielectric Filled Cavity", Ph.D. Dissertation, Virginia Tech, Nov. 1987]. Using the reflection coefficient measurements of the cavity structure and its geometrical dimensions, a full field analysis is used to compute the complex permittivity of the sample material. The method has previously been used successfully to measure the dielectric constant of materials, but limitations in the method have created difficulties in accurate determination of the dielectric loss factor. The measured loss in this method yields an estimate of the total cavity loss, including both the dielectric loss and that of the cavity conductor walls.

In this paper a perturbation approach is used to separate the conductor loss from the total loss. The loss free full analysis solution of the previous work is used to determine the electric current at the conductor boundaries, and thus the current flow in the conductor. This current distribution is then used to evaluate the perturbed power dissipated in the cavity walls based on known conductor properties. By subtracting the loss due to the conductor walls from the total loss measured in the structure, the dielectric loss, and thus the dielectric loss factor, may be estimated.

Measurements are presented for sample dielectric materials. The dielectric loss tangent computed using this new technique provides improved estimates in the microwave frequency range.

A8-4  
0940**Modelling of Broadband Dielectric Sensors***Christopher Sibbald*Department of Electrical Engineering  
University of Ottawa, Ottawa, Ontario, Canada

and

*Stanislaw S. Stuchly*Department of Electrical and Computer Engineering  
University of Victoria, Victoria, British Columbia, Canada

In order to achieve accurate broadband measurements of the permittivity of materials using open-ended waveguide and open-ended transmission line probes, an accurate aperture admittance model is required. This paper presents a novel technique for determining simple, accurate, broadband admittance models for apertures radiating into homogeneous, lossy dielectrics.

The technique exploits the physical and mathematical properties of the driving point admittance of passive, one-port networks to obtain polynomial expressions for the normalized aperture admittance. It is shown that, for suitably restricted ranges of frequency and material permittivity, the aperture admittance is accurately approximated by a polynomial in two variables:

$$Y(s, \epsilon) \approx \sum_{n=1}^N \sum_{m=1}^M a_{nm} s^n (\sqrt{\epsilon})^m$$

where  $Y$  is the aperture admittance of the probe in contact with a material characterized by the permittivity  $\epsilon$ ,  $s$  is the Laplacian variable ( $s = \sigma + j\omega$ ), and  $a_{nm}$  are the model parameters which depend upon the geometry of the feed guide and aperture. These parameters are easily determined for any given structure by a two dimensional least squares fit to a relatively small number of computed admittances. This computed data is obtained via a full-wave moment method solution and, hence, includes the effects of radiation and energy storage in the evanescent waveguide modes and external medium.

The general theory of obtaining these approximating functions, and the resulting range of validity, is discussed. In addition, the solution of the inverse problem, a brief uncertainty analysis, and recommendations on the optimum choice of probe are given. Finally, these concepts are illustrated by applying the method to the open-ended coaxial line geometry: Numerical and experimental results are shown. This talk is an extension of the work presented at the 1991 North American Radio Science Meeting in London, Ontario.

A8-5  
1020

NONDESTRUCTIVE TESTING WITH A COAXIAL  
PROBE  
James Baker-Jarvis and Richard G. Geyer  
Electromagnetic Fields Division  
MS 813.02  
National Institute of Standards and  
Technology, Boulder, CO 80303

The open-ended coaxial probe is commonly used to measure permittivity. Recently, the use of the open-ended coaxial probe as a non-destructive testing device has been considered by a number of researchers.

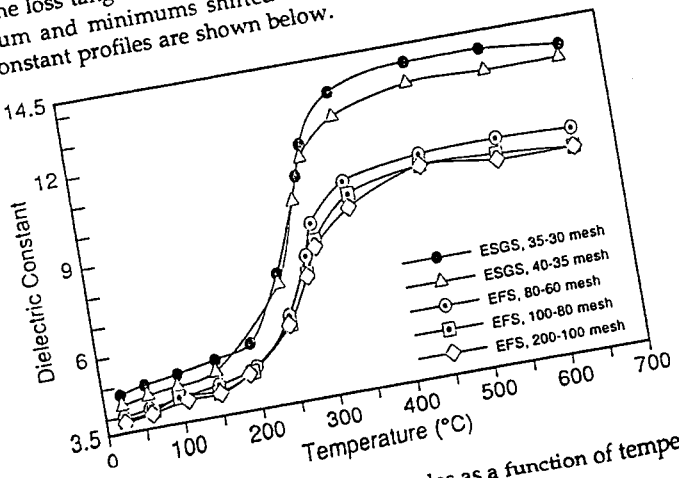
The operation of an open-ended coaxial probe for non-destructive testing depends critically on lift-off, sample permeability and permittivity, and sample thickness. A theoretical model for magnetic and nonmagnetic materials has been developed for probe operation that includes the effects of lift-off of the probe from the sample surface. The theory predicts the effects of both permittivity and permeability on input admittance. The solution separates into a lift-off term and an effective medium term. Results are obtained for cases of finite and semi-infinite domains and for the case of a short-backed sample.

As an application we considered the detection of density variations in alumina in the "green-state". In the manufacturing process it is necessary to monitor pre-fired alumina with a precision of 1-2 %. Measurements were made on "green state" alumina with the coaxial probe in order to detect variations in density. In order to simulate plant conditions, a set of samples were prepared with a broad distribution of density. These samples were then measured with the coaxial probe and again with a precision X-band cavity resonator. The theoretical results were compared with experimental measurements in order to study the sensitivity of the probe admittance to sample density.

# DIELECTRIC PROPERTIES OF HIGH PURITY POLYCRYSTALLINE SILICON AT HIGH TEMPERATURES

A. Baysar and J. L. Kuester  
Center for Solid State Science  
S. M. El-Ghazaly  
Center for Solid State Electronics Research  
Arizona State University  
Tempe, AZ 85287

The utilization of microwaves as the energy source for production of semiconductor grade polycrystalline silicon in fluidized bed reactors has been studied recently. The studies reveal that high purity silicon production by microwave heating is a potential alternative to currently used conventional heating methods. High purity silicon, in the form of particles, may be produced in fluidized bed reactors via chemical vapor deposition at about 700°C with microwave heating. Heating efficiency of a dielectric material depends on its dielectric properties (dielectric constant and loss factor). However, the dielectric properties of particulate silicon with temperature can not be predicted. Therefore, heating efficiency of silicon as a function of temperature behavior of high purity silicon as a function of temperature. A frequency-tuned rectangular cavity operating in the TE<sub>101</sub> mode was used to measure the dielectric properties of silicon obtained from two sources as a function of temperature (23°-650°C) and particle size (75-600 μm range). The measurements were taken at frequencies between 977-995 MHz. The dielectric constant of silicon increased sharply between 150°C and 350°C. Above 350°C, no significant change was observed for all samples. The loss factor initially increased with temperature and reached a maximum in the 240°C and 280°C range, depending on the source of the silicon samples. At higher temperatures, the loss factor decreased for all samples and went through a minimum in the 460°C and 470°C range for large particle size samples. The loss tangent samples followed a similar trend as the loss factor but the maximum and minimums shifted down 30°C to 40°C. Typical results for dielectric constant profiles are shown below.



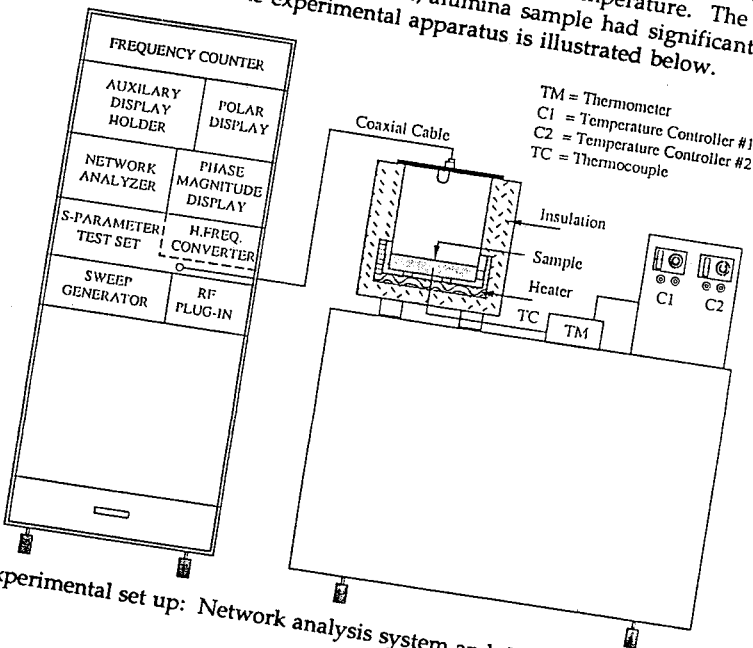
Dielectric constant of ESGS and EFS samples as a function of temperature

# A FREQUENCY TUNED RECTANGULAR CAVITY FOR DIELECTRIC PROPERTY MEASUREMENTS AT HIGH TEMPERATURES

A. Baysar and J. L. Kuester  
Center for Solid State Science  
Arizona State University  
Tempe, AZ 85287

Dielectric properties (dielectric constant and loss factor) of materials in the literature are usually reported at room and/or low temperatures. Hence, the measurement devices are designed for low temperature measurements. In this study, a rectangular stainless steel cavity capable of operation at high temperatures for dielectric property measurements was designed. The knowledge of dielectric properties is essential for predicting the heating efficiency and behavior of materials for high temperature processing. Therefore, the dielectric property information can be used to determine the heating ability of materials for chemical processing. The cavity fabricated for high temperature measurements was operated in the TE<sub>101</sub> mode.

In this paper, the dielectric properties of some materials of interest (alumina, cobalt/alumina catalyst, dolomite and sand ) used in fluidized bed processing are reported. All samples were in particulate form ranging from 53 to 425  $\mu$ m size. The dielectric properties of particulate materials were measured in the frequency range of 925-995 MHz and between room temperature and 610°C. The dielectric constant and loss factor of all samples, except the cobalt/alumina catalyst sample were approximately constant with temperature. The dielectric constant and loss factor of the cobalt/alumina sample had significant increase with temperature. The experimental apparatus is illustrated below.



Experimental set up: Network analysis system and the cavity assembly

A8-8  
1120

# GALLIUM-ARSENIDE PERMITTIVITY MEASUREMENTS AT ROOM TEMPERATURE FROM 8-12 GHz

Eric J. Vanzura, Electronics Engineer  
Broadband Microwave Metrology Group, 813.02  
National Institute of Standards and Technology  
325 Broadway  
Boulder, CO 80303-3328

Complex permittivity ( $\epsilon^* = \epsilon' - j\epsilon''$ ) of Gallium-Arsenide has been measured at room temperature in the 8-12 GHz range. This helps NIST to accurately specify the permittivity of GaAs wafers on which MMIC coplanar-waveguide calibration standards will be produced and distributed. Three 2mm-thick, 60mm-diameter disks were taken from the middle and near both ends of a GaAs boule. From this boulevy wafers were also produced.

The samples were placed flat on one endplate of a cylindrical, mode-filtered  $TE_{01n}$  cavity resonator in order to measure dielectric constant ( $\epsilon'_r = \epsilon'/\epsilon_0$ ) and loss tangent ( $\tan \delta = \epsilon''/\epsilon'$ ). In this configuration the electric field is circularly polarized and tangent to the plane of the disk. Measurement results for the three samples are shown below. From 8-12 GHz  $\epsilon'_r = 12.95 \pm 0.06$  and  $\tan \delta$  varies between 0.000800 at 8 GHz to 0.000450 at 12 GHz. Estimated  $\tan \delta$  accuracy is  $\approx \pm 0.000090$ . These measurements agree with previous results quoted in (J.S. Blakemore J. Appl. Phys. 53, (10), R123-R181, Oct. 1982), and have slightly better accuracy. Permittivity of the three disks agree well-within estimated uncertainty bounds. Repeatability of these results is currently being investigated.

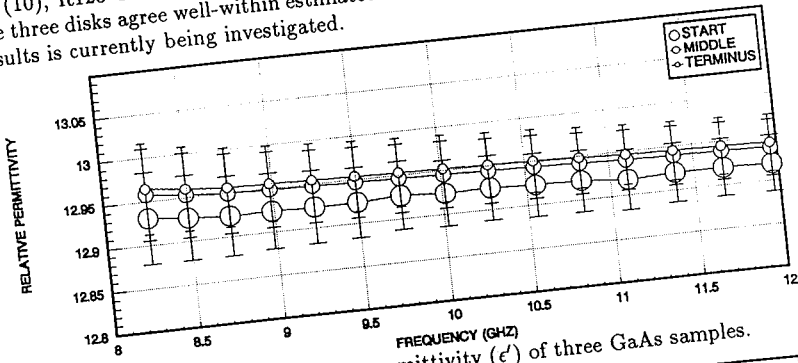


Figure 1: Measured relative permittivity ( $\epsilon'$ ) of three GaAs samples.

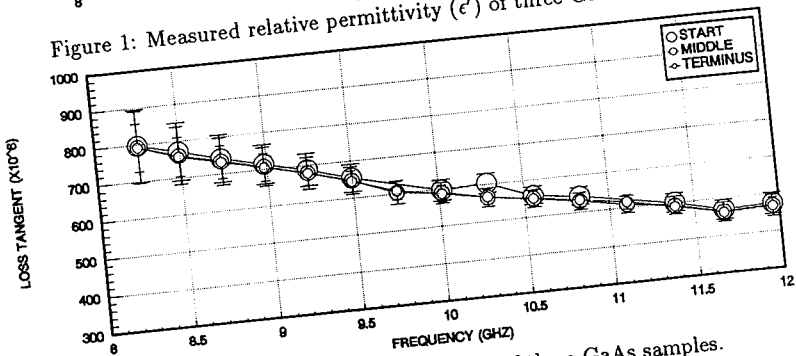


Figure 2: Measured loss tangent ( $\epsilon''/\epsilon'$ ) of three GaAs samples.

Session B-7 0835-Fri. CR2-28  
TRANSIENT AND RESONANT SCATTERING  
Chairman: Don Dudley, Dept. of Electrical and Computer Engineering,  
Univ. of Arizona, Tucson, AZ 25721

B7-1  
0840

**TRANSIENT SCATTERING FROM  
DIELECTRIC CYLINDERS —E-FIELD,  
H-FIELD, AND COMBINED FIELD SOLUTIONS**  
Douglas A. Vechinski and Sadasiva M. Rao  
Department of Electrical Engineering  
Auburn University, Auburn, AL 36849

In this work, the problem of transient scattering by arbitrarily shaped two-dimensional dielectric cylinders is solved using the marching-on-in-time technique. The dielectric problem is approached via equivalence principle. Three different formulations *viz.* the electric field integral equation (EFIE) formulation, the magnetic field integral equation (HFIE) formulation, and the combined field integral equation (CFIE) formulation are considered. Numerical results are presented for two cross sections *viz.* a circle and a square, and compared with inverse discrete Fourier transform (IDFT) techniques. In each case, good agreement is obtained with the IDFT solution.

B7-2  
0900

TRANSIENT FIELDS WITHIN DIELECTRIC SPHERES  
 D. Q. Chowdhury, S. C. Hill†, and P. W. Barber  
 Clarkson University, Potsdam, NY 13699-5720

Dielectric spheres exhibit strong resonant spectra. The  $Q$  of the resonances can be large - measured  $Q$ 's of  $10^6$  are common and calculated theoretical  $Q$ 's can exceed  $10^{40}$ . Imperfections and absorption account for the reduction in magnitude of the theoretical  $Q$ 's to the lower values which are measured. Nevertheless, the electric field within a sphere can be orders of magnitude greater than the incident electric field when the incident frequency is on or near a resonant frequency of the sphere.

Nonlinear optical processes have been observed in spherical liquid droplets and resonant electric fields play a major role in initiating and sustaining these processes. The temporal profile of the field strongly affects the time development of the nonlinear processes.

For an incident pulse containing many oscillations of the incident frequency  $\omega_0$ , the time dependence of the pulse envelope at an internal point  $\mathbf{r}$  is obtained from

$$\hat{\mathbf{E}}^{int}(t, \mathbf{r}) = \mathcal{F}^{-1}(\hat{\mathbf{E}}^i(\omega) \mathbf{E}^s(\omega - \omega_0, \mathbf{r}))$$

where  $\mathcal{F}^{-1}$  is the inverse Fourier Transform,  $\hat{\mathbf{E}}^i(\omega)$  is the Fourier Transform of the envelope of the incident pulse, and  $\mathbf{E}^s(\omega - \omega_0, \mathbf{r})$  is the (shifted) transfer function (the Fourier Transform of the impulse response) at the internal point  $\mathbf{r}$ . The transfer function is found by calculating the continuous-wave response at all frequencies of interest. Our specific interest is in the transient nature of the internal fields when the sphere is excited with a pulse having a Gaussian time dependence and a center frequency on or near a resonance of the sphere.

The time dependence of the electric field is shown to strongly depend upon the spatial location within the sphere. When illuminated at a center frequency corresponding to a resonance, the fields at positions where the resonant fields are negligible generally follow the time dependence of the incident pulse. The time dependence of the electric field at resonant locations is determined by the relation between the incident pulse duration and the lifetime of the resonant mode. When the pulse duration is short relative to the lifetime, then the internal electric field at resonant locations has little time to build, and decays exponentially (at a rate inversely proportional to the lifetime) after the incident pulse has gone. When the pulse duration is long relative to the lifetime, then the internal electric field at resonant locations can build to very high values.

† US Army Atmospheric Sciences Laboratory  
 White Sands Missile Range, NM 88002

# COMPLEX ELECTROMAGNETIC RESONANCES OF DIELECTRIC OBJECTS AND THEIR PHYSICAL INTERPRETATION

Douglas J. Taylor  
Herbert Überall  
Physics Department  
The Catholic University of America  
Washington, D.C. 20064

## ABSTRACT

Dielectric objects display a rich resonance spectrum that has been the subject of inquiry by many researchers, both theoretical and experimental. A mathematical model for complex electromagnetic resonances based on phased matched circumferentially propagating surface waves has provided a physical basis for further work with penetrable dielectric objects. The properties of these surface waves has been explored by computing their phase velocities,  $C_l$ , using the following relation,

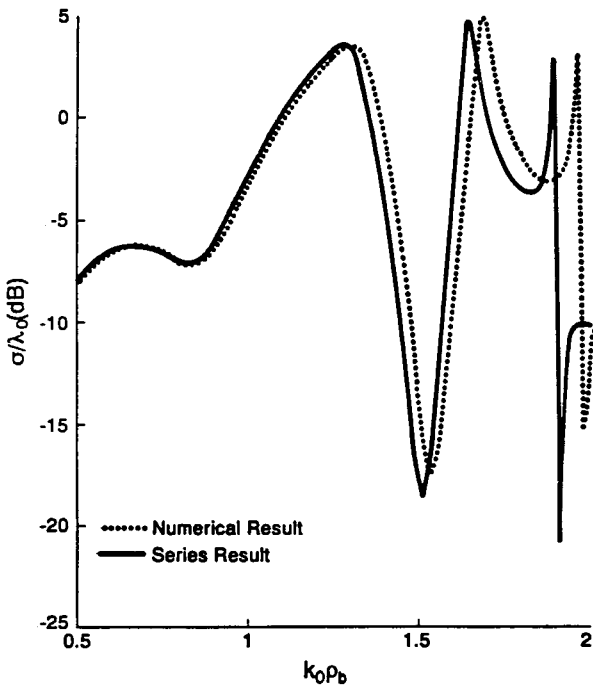
$$C_l/C_0 = \frac{x_{nl}}{n+1/2}$$

where  $C_0$  is the speed of light, and  $x_{nl}$  is the real part of the  $n^{\text{th}}$  complex resonance of  $l^{\text{th}}$  family. The easily calculable complex resonances of spherical and cylindrical canonical geometries were used, computations were based on both lossless and lossy dielectrics to examine the effect of media loss on resonance 'Q'. The TM and TE surface wave families both display a dispersive phase velocity as a function of frequency, modes associated with penetration or 'trapping' of energy in the dielectric are found to possess similar low frequency cutoff and high frequency asymptotic behaviour. The spherical TM family displays a unique non-dispersive region which does not appear in the TE family, in this non-dispersive region the phase velocity hovers at a value very close to  $C_0$ . Similar features have been observed in scalar acoustic resonance scattering analysis but never before in electromagnetic resonance analysis. A physical model based on simple geometrical constructions has been successful in explaining the low frequency 'waveguide' like cutoff behaviour and the TM non-dispersive transition region while being consistent with traditional high frequency total internal reflection models for high Q resonances.

B7-4  
0940ON RESONANCE EFFECTS IN SCATTERING FROM  
HOLLOW NONCONDUCTING OBJECTS

G.L. Hower, R.G. Olsen, and J.E. McPherson  
 School of Electrical Engineering and Computer Science  
 Washington State University  
 Pullman, WA 99164-2752

Calculated scattering from a nonconducting hollow cylinder, using both a series solution and a method of moments computer code, shows great variability to small changes in the material or geometric parameters within certain ranges of these parameters. The observations are explained by a resonance phenomenon in which the operating frequency is found to lie close to a complex natural frequency of the scattering object. The existence of such resonances requires additional care when interpreting computed results for scattering from similar nonconducting objects having electric and/or magnetic properties. More specifically, the scattering cross section of the hollow cylinder calculated using the hollow cylinder computer code with  $.1\lambda$  cell size and using the series solution give results which are offset in frequency as shown in the figure. It does not appear that there is a simple method to compensate for the error in the numerical results such as the "equal area method" used for perfectly conducting objects.



B7-5            TRANSIENT SCATTERING LENGTH AND CROSS SECTION  
1000            Carl E. Baum  
                 Phillips Laboratory/WSEA  
                 Kirtland AFB, New Mexico 87117-6008

By generalizing the use of complex vector magnitude for incident and scattered fields to norms, scattering in time domain can be similarly scalarized. The associated norms of the scattering operator give the maximum possible scattering length for transient scattering. This in turn allows one to optimize transient incident fields for maximum scattering. One can define a scattering efficiency ( $\leq 1$ ) for various waveforms, and various examples are considered.

The concept of a natural norm is introduced based on certain symmetries in the scattering and measurement processes. Among this restricted set there are two norms of particular interest, the 2-norm and the m-norm. The 2-norm is related to the energy in the pulse. In this case it is shown that the maximum scattering length is achieved by an incident pulse dominated by frequencies near the frequency of maximum frequency-domain scattering length with polarization given by the eigenvector associated with the maximum eigenvalue of the Hermitian form of the scattering operator as appears on using the Parseval Theorem in expressing the 2-norm in frequency domain.

The m-norm or maximum norm is based on the maximum magnitude for all time of the incident electric field. The physical significance here concerns electrical-breakdown limitations at the transmitting antenna. The associated operator norm can be bounded for arbitrary incident waveforms. This bound can be shown to be tight (achieving equality) for the case of scatterers with certain symmetries.

B8-1  
1020

## INVERSION OF FOCUSED NEAR-FIELD EM DATA

A. Q. Howard, Jr.,

SCHLUMBERGER WELL SERVICES

Houston, Texas 77252-2175

The multiple depths of investigation available with a multi-array induction logging tool are used to estimate the radial conductivity profile induced by the invasion process. The raw unfocused data consists of 28 channels. This rich data base is key to extending in a realistic way the industry standard three parameter invasion resistivity model of  $R_t$ ,  $R_{xo}$  and diameter of invasion  $D_i$ . Major emphasis however, remains on the ability to accurately estimate the formation resistivity  $R_t$  beyond the invaded zone since this is the quantity that is directly proportional to the volume of hydrocarbon in pay zones. Therefore, at the possible expense of loss of generality obtainable with model free estimation, the method herein assumes a region by region maximally flat profile, which is also smooth (all order derivatives exist).

The simplest example of this type of profile has four parameters, and then it is monotonic and has the shape of a Butterworth filter as defined for example in digital filter design text books. This choice of profile type increases the accuracy of the true formation conductivity estimate  $\sigma_t$ , and prevents spurious overshoots which often occur in least mean square estimation methods. The model parameters are computed by minimizing a  $\chi^2$  cost function of the squares of differences between measured and modeled apparent conductivity. The minimization is based upon a new dynamically constrained Levenberg-Marquardt algorithm. The algorithm drives the ratio of the constraint to  $\chi^2$  fit equal to an a-priori value in the main loop of the Marquardt iteration. This results in a better conditioned Hessian matrix which allows the  $\chi^2$  variable to become orders of magnitude smaller. This yields an improved match to the input channel median curve data when the data fits the parametric model.

The new method automatically adjusts the weight of the constraint to account for typical four order of magnitude variation in signal level. Numerical results are given for both specific synthetic data invaded bed examples in one and two dimensions, and field logs. CPU time for a typical radial profile at one log depth is on the order of 200 ms on a VAX 6400 series minicomputer.

**SIMULTANEOUS INVERSION OF PERMITTIVITY AND  
CONDUCTIVITY PROFILES USING TIME-DOMAIN DATA †**M. Moghaddam<sup>1</sup> and W. C. Chew<sup>2</sup><sup>1</sup> Jet Propulsion Laboratory  
California Institute of Technology  
Pasadena, CA 91109<sup>2</sup> Department of Electrical and Computer Engineering  
University of Illinois at Urbana-Champaign  
Urbana, IL 61801**ABSTRACT**

For an inversion algorithm to be of practical use, it must be capable of incorporating the effect of loss in the objects and media under study. The nonlinear two-dimensional problem of inverting conductivity and permittivity profiles simultaneously from time-domain scattering data is solved here using an iterative algorithm. In this method, called the Born iterative method, both the forward and inverse problems are solved once during each iteration. The forward problem is solved using the finite-difference time-domain algorithm. The inversion is carried out through a regularized optimization. Since the problem is defined in the time domain, or over many frequencies, it is not possible to simply invert the complex permittivity profile and extract the conductivity information from the imaginary part. Hence, the inverse problem is formulated as a double-criterion optimization for two independent unknowns. The method proves to be computationally and experimentally efficient. Several results are presented and the limits of applicability of the algorithm are discussed. It is shown that accurate results are obtained within a few iterations for cases where the first-order Born approximation is severely violated.

---

† This work was supported by the Army Research Office through a grant to the University of Illinois Advanced Construction Technology Center, and by the National Science Foundation. The computation time was provided by the National Center for Supercomputing Applications at the University of Illinois through the Cray Research and Development grant.

B8-3  
1100THE RENORMALIZED STIE APPROACH APPLIED TO  
INVERSION OF SOIL MOISTURE PROFILES

J. Xia, T.M. Habashy \*, R.T. Shin and J.A. Kong

Department of Electrical Engineering and Computer Science  
and Research Laboratory of Electronics

Massachusetts Institute of Technology

Cambridge, MA 02139

\* Schlumberger-Doll Research

Old Quarry Road, Ridgefield, CT 06877

In this paper an inversion technique is presented for remote sensing applications. A recently developed inversion method referred to as the renormalized Source-Type Integral Equation (STIE) approach (T.M. Habashy, E.Y. Chow and D.G. Dudley, IEEE Trans. Antennas and Propagat., Vol. AP-38, pp.668-682, May, 1990) is applied to the profile inversion problem of the complex permittivity for soil. The soil moisture profiles are described by the underground permittivity and conductivity distributions. The unknown profiles are inverted based on the electromagnetic responses above the ground. In this work the STIE formulation is also extended to a general background medium which consists of two different regions.

There are a number of apparent advantages to the STIE approach: (i) it is based on an exact inversion equation; hence, if approximations are to be made they will occur in the numerical methods employed in the solution of this inversion equation, (ii) it has an explicit dependence on the unknowns to be inverted for; this allows one to compute the derivatives of the response with respect to these unknowns in a closed form, (iii) by pre-storing the elements of the inversion equation (which depend only on the background media and are independent of the unknown profile), the method does not require the solution to the full forward problem repeatedly as in the case of the Distorted Born approach and is therefore faster in implementation, and (iv) it allows, in some cases, the rigorous study of the degree of non-uniqueness involved in the inversion, which is a point of great importance in the design problem.

An algorithm is formulated for simultaneously inverting the unknown planar stratified permittivity and conductivity profiles. We will demonstrate the inversion scheme for the case where the exciting source is of the dipole type that generates only transverse-electrically polarized waves. The data are assumed to be given at various locations on the ground surface at a number of frequencies. Several profiles are inverted as numerical examples.

B8-4  
1120ON SYNTHETIC REFLECTION COEFFICIENT  
IN INVERSE SCATTERING THEORY

J. Xia

Department of Electrical Engineering and Computer Science  
Massachusetts Institute of Technology

Cambridge, MA 02139

A.K. Jordan

Center for Advanced Space Sensing

Naval Research Laboratory, Washington DC 20375

By applying the Gel'fand-Levitan-Marchenko (G-L-M) quantum inverse scattering theory, closed-form solutions of scattering potentials may be obtained for certain rational reflection coefficients. In using these results for electromagnetic inverse scattering, some important differences between the quantum inverse scattering and the electromagnetic inverse scattering are pointed out. The wave equation in quantum scattering, the Schrodinger equation, and the wave equation in electromagnetic scattering are usually in different forms. Wave propagation and reflection in inhomogeneous dielectric media are analyzed with the Riccati equation. Two types of the Riccati equation in the literature are derived and distinguished. For synthesis problems, the conditions on the frequency-domain reflection coefficient  $r(\omega)$  are given. The allowed region for the poles and zeros of a special rational function  $r(\omega)$  is derived. Inversion results of synthetic reflection coefficients will be shown. The procedure for synthesizing a reflection coefficient in design problem is discussed.

B8-5 WAVE FIELD SPLITTING, INVARIANT IMBEDDING,  
1140 AND PHASE SPACE METHODS IN DIRECT AND  
INVERSE SCATTERING

Louis Fishman

Department of Mathematical and Computer Sciences

Colorado School of Mines

Golden, CO 80401

Due to the extremely large size of realistic three-dimensional electromagnetic propagation problems, there is an understandable desire to incorporate marching methods into the solution algorithm for the inherently elliptic (frequency-domain) problem. Recognizing that typical electromagnetic propagation problems are essentially scattering problems in terms of a transition region and transversely inhomogeneous asymptotic half-spaces, wave field splitting, invariant imbedding, and phase space methods reformulate the problem in terms of an operator scattering matrix characteristic of the transition region. The subsequent equations for the reflection and transmission operators are first-order in range, nonlinear (Ricatti-like), and, in general, nonlocal. The system is well-posed, but stiff. The reflected and transmitted wave fields can be computed in a very efficient manner, while the wave field in the transition region (if desired) can be computed by essentially a layer-stripping algorithm. In principle, the transition region can be divided into subregions, allowing for parallel computations and subsequent recombination. The reflection and transmission operator equations provide the framework for constructing inverse algorithms based on, in principle, exact solution methods. This is directly applicable to the electromagnetic tomography problem where the features to be reconstructed are confined to the transition region and the sources and receivers are located in the half-spaces. Rotating the formulation by 90 degrees makes it appropriate for the reflection seismology problem. Algorithms based on this approach have been developed and successfully implemented in the time-domain formulation of the electromagnetic problem in one spatial dimension.

GH3-1 INVESTIGATION OF THE CHARACTERISTICS OF THE HIGH-  
0900 LATITUDE IONOSPHERE FROM H.F. HEATING  
EXPERIMENTS

P. L. Werner\*, A. J. Ferraro\*\*, and D. H. Werner\*\*\*

\* School of Engineering Technology and Commonwealth Engineering  
The Pennsylvania State University  
Dubois, PA 15801

\*\* The Electrical and Computer Engineering Department  
The Pennsylvania State University  
University Park, PA 16802

\*\*\*The Applied Research Laboratory  
The Pennsylvania State University  
State College, PA 16804

This paper reports on a series of ionospheric modification heating experiments conducted at the High Power Auroral Simulation (HIPAS) heating facility near Fairbanks, Alaska, over a period of 2 years from June 1987 to August 1989. Particular emphasis is devoted to the study of the mapping of the polar electrojet current from the E region down through the D region; it can then be modulated by the heater beam. D-region modification can be used to study the D-region electron density and the polarization of the electric field of the obliquely downgoing generated ELF/VLF electromagnetic waves generated by irradiation of the heated volume.

The behavior of these ionospheric currents can be deduced from a comprehensive study of the ELF signals received on the ground. A finite difference solution to the electrojet mapping problem is presented in which arbitrary conductivity profiles can be specified. Results indicate that for an electrojet flowing at an altitude of 110 km with a scale size in excess of 100 km, the mapping of the horizontal current density can be completely characterized in terms of the Pederson and Hall conductivities.

The study of the polarization was done by choosing a simple slab model for the D-region to solve the Booker quartic which is used to compute the wave path and direction. The ELF/VLF source is simulated by two horizontal current sources: one in the east-west direction, and one in the north-south direction due to modulation of the mapped down currents from the electrojet source. The waves resulting from these two orthogonal sources are superimposed on the ground to give the tilt angle and ellipticity of the incoming waves which are the parameters being measured. Monitoring the polarization ellipse provides information on the presence of an electrojet or pulsations.

The D region electron densities were derived from the ELF received signals on the ground. A class of exponential density models was used to create a catalog of transmission coefficients deduced from the full wave theory. The electron density profiles were estimated by searching the catalog with the transmission coefficient extracted from the locally received ELF signals and selecting the best fit model to the observations.

Most results reported in this paper were local measurements, i.e., almost directly under the heated region. Some remote measurements were made at a few hundred kilometers distance and these will be briefly discussed.

GH3-2      PARAMETRIC EXCITATION OF LOWER-HYBRID AND UPPER-  
0920      HYBRID WAVES IN OBLIQUE IONOSPHERIC HEATING EXPERI-  
            MENTS

S.P. Kuo

Polytechnic University  
Farmingdale, New York 11735

M.C. Lee

Massachusetts Institute of Technology  
Cambridge, Massachusetts 02139

A great deal of attention has been paid to vertical ionospheric heating which can excite various parametric instabilities near the reflection heights of the o-mode pump waves. By contrast, it was thought that the conditions for parametric instabilities could not be satisfied in the oblique ionospheric heating processes. We note, however, that near the reflection height, the obliquely transmitted o-mode pump wave still has a finite wave number. Thus, the wave field of the o-mode pump does not orientate toward the direction of geomagnetic field and exist a perpendicular wave field component near the reflection height. This wave field component can potentially become a driving force to excite hybrid plasma modes via the parametric instabilities. The conditions for the excitation of parametric instabilities are examined for the oblique ionospheric heating, including the range of wave frequency, the elevation angle, and the threshold field intensity. The threshold field is a function of the wave frequency and the incident angle, the magnetic dip angle, the scalelengths of the instabilities, the collision frequency, and the plasma frequency. Following these conditions, one can selectively modify the ionospheric region with the obliquely injected high power radio waves.

GH3-3 IN-SITU EXPERIMENTS OF THE HF-MODIFIED  
0940 IONOSPHERE  
P.Rodriguez, C.L.Siefring, M.M.Baumbach,  
D.G.Haas, and P.A.Bernhardt  
Code 4785, Space Plasma Branch  
Plasma Physics Division  
Naval Research Laboratory  
Washington, D.C. 20375-5000

We report on the concept and plans for a series of new-generation in-situ experiments of the HF-heated ionosphere using rockets and satellite. The scientific payload for the in-situ experiments includes instruments for measuring the in-situ electric fields and plasma densities, to obtain detailed profiles on nonlinear plasma wave interactions stimulated by the HF heating of the ionospheric plasma. The objectives include the detection of localized, intense electric field oscillations (cavitons). The electric field is to be measured with several scale sensitivities from about 10 cm to several meters, over the frequency range of 10 MHz to several kilohertz. Plasma densities from  $10^6$  to a few  $10^8$   $\text{cm}^{-3}$  will also be obtained. The AA-4 rocket is scheduled to be launched in 1992, from Puerto Rico and to intercept the HF-heater beam of the Arecibo Observatory. The experiment involves the deposition of an electron-attachment chemical in the heater beam in order to create an ionospheric "hole" which will act as a focusing lens for the HF waves. The CHAMPION satellite experiment, scheduled for launch in mid-1993, will be placed in a polar orbit with perigee of 195 kilometers by apogee of 1500 kilometers. Overflights of the CHAMPION experiment are being planned with existing HF modification facilities in order to conduct coordinated heating experiments. These facilities include Arecibo, HIPAS, Tromso, Sura, and the planned HAARP facility. These in-situ experiments will lead to a proposed series of interactive rocket-HAARP modification experiments.

GH3-4  
1020

## THEORETICAL STUDY ON THE BROAD SYMMETRIC STRUCTURE IN STIMULATED ELECTROMAGNETIC EMISSION SPECTRUM\*

J. Huang and S. P. Kuo

Weber Research Institute, Polytechnic University, Route  
110, Farmingdale, NY 11735

During the heating campaign at Tromso in Nov. 1989, a new feature of Stimulated Electromagnetic Emission Spectrum (SEE) was found when the heater frequency was close to the third harmonic of the local electron cyclotron frequency in the interaction region (P. Stubbe et al., *Phys. Rev. Lett.* **65**, 183, 1990). The observed SEE spectrum consists of a pair of broad maxima symmetrically located around  $f_0$  at  $|\Delta f| \sim 15\text{--}30$  KHz. Theoretical understanding of this Broad Symmetrical Structure (BSS) is still at a rather moderate level. The present work investigates the physical mechanism of the BSS phenomenon and develops a theory that can explain the experimental results.

Two parametric processes near the upper hybrid resonance layer are considered simultaneously. The first one is the parametric decay of the heater wave into a lower hybrid wave and an electron Bernstein wave. The second process consists of the parametric excitation of a purely growing density irregularity together with a pair of electron Bernstein sidebands. The electron Bernstein wave generated in the first process ( with  $f_{B1}=f_0-f_{LH}$  ) then can be mode converted into EM emission through the scattering off the short scale irregularity excited in the second process. The emission forms the down shifted side of BSS ( with  $f=f_0-f_{LH}$  ). Similarly, the EM emission responsible for the up shifted side of BSS ( with  $f=f_0+f_{LH}$  ) can also be generated by scattering off the electron Bernstein side bands (  $f_{B2}=f_0$  ) of the second process by the density perturbations of the oppositely propagating lower hybrid waves (  $f_{LH}$  ) generated in the first process. Thus, a symmetric spectrum structure with the shift-frequencies of the order of the lower hybrid wave frequency can be obtained.

In our theoretical analysis, coupled mode equations and dispersion relations for both instability processes are derived. Threshold fields, lower hybrid wave frequencies and growth rates are calculated. The results show that the above mentioned processes can indeed be excited over a range of wavelength whose corresponding lower hybrid wave frequencies are consistent with the experimentally observed  $\Delta f$ 's. The dependence of BSS on heater wave frequency around the 3rd harmonic electron cyclotron frequency is also studied. A good agreement with the observations is found.

\* Work supported by NSF Grant No. ATM-9024827

GH3-5 A NONLINEAR OSCILLATOR IN THE IONOSPHERE:  
1040 BEAM SNAPBACK DURING RF HEATING  
H.L. Rowland and P.A. Bernhardt  
Space Plasma Branch, Plasma Physics Division  
Naval Research Laboratory, Washington, DC 20375-  
5000

During intense RF heating experiments at Arecibo, Puerto Rico (P.A. Bernhardt, L.M. Duncan, and C.A. Tepley, *Science* 242, 1022, 1988; P.A. Bernhardt, L.M. Duncan, and C.A. Tepley, *JGR* 94, 7003, 1989) and SURA, USSR (P.A. Bernhardt, Wayne A. Scales, D.S. Kotik, S.M. Grach, and A.N. Keroshtin, *GRL* 18, 1477, 1991), optical measurements have shown that if the ionosphere is drifting, the density cavities that are created by the rf radiation are not smooth and continuous but localized and quasiperiodic. The horizontal position of the beam at the critical layer is observed to drift with the ambient plasma and then rapidly snapback to zenith. We have developed a computer simulation model that treats the radiation as simulation particles and shows good agreement with the observations. When the radio frequency energy is large enough to strongly modify the ambient density ( $\delta n/n = 10-20\%$ ), the density modifications are not continuous but separate into individual cavities that drift with the plasma. The electromagnetic beam is captured and bent by the drifting cavity. When the beam is bent so far to the side that there is no heating and cavity formation above the heater, the beam quickly snaps back to zenith where another cavity is formed. The process is described by a relaxation oscillator. Small periodic plasma density perturbations which can be caused by gravity waves can entrain and modulate the beam motion.

GH3-6 IONOSPHERIC MODIFICATION USING VLF WAVES  
1100 Umran. S. Inan, J. V. Rodriguez, and S. Lev-Tov  
Space, Telecommunications and Radioscience Laboratory  
Stanford University, Stanford, California 94305

The first observation of the VLF version of the 'Luxemburg effect' [Inan, 1990] provided definitive experimental evidence of significant heating of the lower ionosphere by VLF radiation from ground-based transmitters. In this paper, we provide further experimental data on the occurrence of VLF heating and in particular its detectability by means of subionospheric VLF probe waves. Controlled VLF wave-injection experiments carried out with the 28.5 kHz NAU transmitter (100 kW radiated power) over two different 2-month periods provide the basis of occurrence statistics. A detectable heating effect is observed approximately once or twice a week and no clear dependence is found on geomagnetic activity or on ambient D-region conditions as inferred from the unperturbed VLF transmitter signal levels. Quantitative estimates of VLF probe signal changes in response to transmitter-induced heating are obtained using a new three-dimensional model of subionospheric propagation in the presence of localized disturbances. Calculations are made for the case of the reported observation involving the VLF path from Cutler, Maine (NAA transmitter) to Palmer Station Antarctica with a disturbance located along the path at Puerto Rico (28.5 kHz NAU transmitter used as the heater), and for some other VLF transmitter and VLF probe wave configurations that might be used in future experiments. The heating estimates are obtained using a model similar to that used by Inan [1990] but also including self absorption of the VLF wave.

GH3-7  
1120NONLINEAR INTERACTIONS OF VLF WAVES WITH IONOSPHERIC  
PLASMAS

M.C. Lee, K.M. Groves, Y. Dalkir  
Massachusetts Institute of Technology  
Cambridge, Massachusetts 02139  
S.P. Kuo  
Polytechnic University  
Farmingdale, New York 11735

The primary goal of our active experiments at Arecibo, Puerto Rico with the ACTIVE satellite was to investigate the nonlinear interactions of VLF waves with ionospheric plasmas. We will discuss some results obtained in the experiments though the ACTIVE satellite did not work as originally planned. In addition, we will examine the observations of sideband modes displayed symmetrically above and below the transmitted frequency reported recently by Solnikov et al. (1991) in the VLF wave injection experiments conducted at Komsomolsk-on-Amur Alpha Station. The displacement of 500 Hz from the injected VLF frequencies of 11.9 and 12.65 kHz was measured. Sotnikov et al. suggested that a nonlinear coupling mechanism between the injected VLF wave and the naturally occurring ELF emission in the ionosphere was responsible for the generation of symmetric sideband modes. We, however, examine the possibility that the injected VLF waves excite symmetric sideband modes directly. Our proposed sideband modes are electrostatic in nature having large wave numbers, while those suggested by Sotnikov et al. are electromagnetic modes with rather small wave numbers.

GH3-8 STUDIES OF HIGH POWER RADIOWAVE HEATING OF THE  
 1140 LAMINAR AND TURBULENT IONOSPHERE

M.J. Keskinen<sup>(1)</sup>, P.K. Chaturvedi<sup>(1)</sup> and  
 S.L. Ossakow<sup>(2)</sup>  
<sup>(1)</sup>Space Plasma Branch  
<sup>(2)</sup>Plasma Physics Division  
 Naval Research Laboratory  
 Washington, DC 20375-5000

Recently, much interest both experimental and theoretical, has been directed towards a more complete understanding of the physics of the interaction of high power radio frequency (RF) waves and the ionosphere. Several diverse phenomena have been investigated. For the general topic of plasma dynamics and structure development during ionospheric heating observational and theoretical studies can generally be classified as emphasizing either large or small scale phenomena. The majority of studies on the large scale aspects of ionospheric heating have not considered, in a self-consistent manner, the role of ambient ionospheric electric fields, thermospheric winds, gravitational drifts, etc. on the evolution of heated regions. We have constructed models of large scale RF heating processes for both the unstructured and turbulent ionospheric space plasma.

For the unstructured case we have considered the long-time scale evolution of high power RF heating of the coupled ionosphere-thermosphere system. We show that the RF-heated ionosphere will convect and steepen due to ionosphere-thermosphere coupling effects. We treat high power RF propagation including nonlinear self-induced thermal effects. We find that the beam is distorted, shifts in direction, and changes its peak intensity. For weak beams, we find a decrease in beam intensity while for strong beams we observe and increase in beam intensity.

For the turbulent ionosphere, we discuss parametric coupling processes of a large amplitude RF pump wave with both F-region, e.g., interchange and ion-cyclotron and E-region, e.g., two stream and gradient-drift ionospheric instabilities. We show that these instabilities may be stabilized or destabilized using high power RF heaters.

J6-1  
0840

**NEW GENERATION OF COLOGNE ACOUSTO-OPTICAL  
SPECTROMETERS**

V. Tolls, M. Klumb, and R. Schieder  
I Physikalisches Institut  
Universität zu Köln  
Zùlpicher Str. 77  
D-5000 Köln 41

Acousto Optical Spectrometers (AOS) are in operation at the KOSMA 3m-radiotelescope on Gornergrat/Switzerland since more than 7 years. At present a new generation of AOS is prepared in Cologne with several new features, which will be discussed in detail.

The performance of the major AOS parts, i. e. the laser diode, the deflector, and the CCD sensor has been studied and their impact on the performance of the AOS has been characterized and found to be rather critical. The precise knowledge of the performance of laser diodes and CCD sensors under various conditions is found to be important for the 1.4 GHz bandwidth AOS of the Submillimeter Wave Astronomy Satellite (SWAS). The environmental conditions on this small satellite require a careful analysis, e. g. the temperature of the AOS will change by about  $\pm 0.3$  K during one orbit and about several degrees during its lifetime of three years. For a stable AOS (Allan plot minimum time more than 100 sec) the temperature of the laserdiode should be stable within a tenth of a degree. Therefore the mode characteristics of the laser diode is a very critical parameter for the design of the AOS. To achieve best performance, criteria have been defined. For the test and selection of proper laser diodes, a special test facility was installed at Cologne. First results will be presented together with the design of the SWAS-AOS.

Not only the laser diode, but the whole optical setup defines the performance of the spectrometer. The collimating optics and the imaging optics must match to the resolution and the aperture of the deflector. For best use of an acousto optical deflector a theoretical analysis of its resolution has been made. In consequence it is found that the number of resolvable spots of a Bragg cell can be increased significantly by modifying the illumination of the deflector aperture. The result is that the resolution of the deflector is not limited by the acoustic attenuation but by the effective (or desired) efficiency, and the size of the interacting crystal. Based on these results the setup of an AOS with variable resolution and first test measurements are presented.

J6-2  
0900**ABOUT OPTIMIZED USAGE OF ACOUSTO OPTICAL SPECTROMETERS**

**R.Schieder, M.Klumb, and V.Tolls**  
I. Physics Institute, University of Cologne  
Zùlpicher Str. 77  
D5000 Köln 41  
Germany

The amplitude stability of acousto optical spectrometers (AOS) determines the ultimate sensitivity of the instrument of radiotelescopes. It has been recognized that the performance of AOS has become competitive with and in certain applications superior to other spectroscopic instrumentation like filterbanks etc. This has been clearly established by measurements of the Allan variance, which has been developed as a standard tool at the KOSMA observatory in order to characterize the performance of spectrometers. The method is used intensively for routine performance test analyses of several components of the AOS being built in Cologne for the Submillimeter Wave Astronomy Satellite (SWAS). In particular, the impact of CCD noise on the final signal to noise ratio is determined. Based on a simple theoretical model for the structure of the Allan plot a mathematical procedure can be found, which establishes reliable rules for an efficient observing strategy usable for any existing radioastronomical instrumentation. This investigation is particularly valuable for spaceborne activities like SWAS or similar.

As derived from the statistical analysis it is also found, that acousto optical techniques can be applied for sensitive rf-power detection, especially also required for continuum measurements with heterodyne receivers. The advantage is, that the linear dynamic range obtainable with a Bragg cell can be close to 60 dB, which is much more than the linear range of an ordinary rf-detector. A detailed analysis of the signal to noise of acousto-optic detection will be given, and first results of holographic measurements of the KOSMA telescope using a modified AOS as rf-power detector will be shown. Possibilities for high dynamic range continuum detectors will be discussed.

J6-3  
0920

A MULTICHANNEL ACOUSTO-OPTIC SPECTROMETER \*  
James A. Carter, III and Dennis R. Pape  
Photonic Systems Incorporated  
1800 Penn Street, Suite 4B  
Melbourne, FL 32901

Radiometer spectrometers are used in millimeter-wave radio astronomy for the spectral measurement of molecular rotational transitions. The spectrum of interest spans 10's of GHz and the measurement time is large in order to obtain useful signal-to-noise ratio. The low power per channel and simplicity of acousto-optic technology has led to the current development of acousto-optic spectrometers (AOS) with 1 GHz bandwidth and 1000 channels. Additional AOS bandwidth and channelization is needed to increase spectral coverage and reduce overall data acquisition time. We describe here the design and analysis of the performance of a small, rugged, multichannel acousto-optic spectrometer (MCAOS) for radio astronomy spectroscopy applications. This instrument has 4 channels and can process signals from 4 separate sources simultaneously. The bandwidth of each channel is 1 GHz and the frequency resolution is 1 MHz, providing simultaneous processing over 4,000 1 MHz channels. The instrument's optical train is integrated into one common path using a 4-channel acousto-optic Bragg cell with properties (including low optical scatter using a shear acoustic mode) required for stable AOS systems. The MCAOS will be packaged in a laboratory instrument that includes the optical processor as well as digitization, acquisition and accumulation electronics. Key features of this new multichannel spectrometer instrument include small size ( $< 6000 \text{ cm}^3$ ), low power consumption ( $< 100 \text{ W}$ ), and capability of long integration time ( $> 30 \text{ s}$ ) without dynamic range loss. Analog data is read out at 1 million 1 MHz channels per second, digitized to 12 bits and accumulated in 32 bit memory registers. External TTL control logic can switch digital data to two separate memory banks for "ON" and "OFF" state data gathering and reduction on a 50 millisecond frame basis. Further, the design accommodates expandability to as many as 16 separate source channels without significant modification. These performance features are the result of innovative design features including:

- Thermally stabilized single-mode semiconductor laser diode light source
- Common optical path supporting all four channels simultaneously
- Innovative multichannel Bragg cell with polarization switching allowing greater laser speckle suppression and longer integration periods
- Custom high performance transform optics
- Integrated photodetector array with custom high speed readout and digitizing electronics
- Embedded microprocessor controller and IEEE 488 interface

\* This work is supported by NASA Goddard Space Flight Center under Contract No. NAS5-31454

J6-4  
0940**ACOUSTO OPTIC SPECTROMETERS  
FOR SPACEBORNE RADIOMETERS****Mark Koontz  
Harris Corporation  
Electronic Systems Sector  
Melbourne, Florida 32902****William J. Wilson and Kumar Chandra  
Jet Propulsion Laboratory  
California Institute of Technology  
Pasadena, California 91109**

Wideband spectrometers are required for future radiometer space systems such as the EOS Microwave Limb Sounder and the Sub-Millimeter Intermediate Mission. The spectrometers will measure the radiometer signal's power over wide IF bandwidths to analyze the spectra of molecular emission lines. The best near term solution for this application appears to be the Acousto Optic Spectrometer (AOS). Harris Corporation is developing an AOS for JPL with a bandwidth of 1000 MHz and a frequency resolution of 1 MHz. This AOS will have a dynamic range >25 dB and a stability time >60 seconds. The input signal power will be ~0 dBm and the total DC power will be <5 Watts. The AOS will use the Spectra Dynamics Laboratory SDL 5412-H1 solid state laser which has a wavelength of 825 nm and an output power of 100 mW. The Bragg cell will be a Marconi anisotropic Lithium Niobate cell which rotates the input polarization 90° in the diffracted beam. Corning polarizers are used to minimize the scatter into the transform lens and the photo diode array. The photo diode array is a Thomson-CSF array with 1024 elements, low noise and a 35 dB dynamic range. A 12" x 6" x 3" titanium chassis will be used for stability. Test results from the unit will be presented.

J6-5  
1000**ACOUSTO-OPTIC SPECTROMETERS FOR  
RADIOASTRONOMY**P. Dierich, C. Rosolen, A. Lecacheux, D. Michet  
Observatoire de Meudon  
92195 MEUDON FRANCE

Acousto-optic spectrometers (AOS) have been used on radiotelescopes for almost twenty years. But they have been considered as reliable only very recently. We have developed four generations of AOS for almost ten years. We have started with a 10 mW He-Ne Laser, a 30 MHz TeO<sub>2</sub> Bragg cell and a home built movie camera, mounted on an optical bench of 1\*1,5 meter and weighting 100 kg. We last built a 10\*5\*40 cm AOS, weighting 4 kg, covering a 900 MHz bandwidth.

A 30 MHz second generation device has been working at Nançay on the decametric network, for very fast and high dynamic range observations, for the last seven years without any problem and very little maintenance. A 500 MHz AOS has been used at the 30 m IRAM telescope for more than two years. Its stability can compete with the traditional bank of filters. At the other end, broadband spectrometer (900 MHz) has been successfully tested on a 10 microns heterodyne receiver in June 1991. On this occasion, it was demonstrated that they are easily transportable and reliable. Long term behaviour and last results will be given.

Last developments on the fourth generation of AOS : New concepts, solid state optical source, Bragg cells, array of detectors, data processing, will be described.

J6-6 THE NRAO HYBRID SPECTROMETER  
1040 Andrew V. Dowd  
National Radio Astronomy Observatory  
949 N. Cherry Ave.  
Tucson, AZ 85721

This report will present results from building the NRAO hybrid spectrometer. The talk will be a mix of theoretical work, practical experiences, and results. The emphasis will be on the hybrid nature of the instrument; particularly the difficulty in aligning spectral components processed by parallel hardware channels.

The NRAO hybrid spectrometer is a wide-bandwidth, multi-channel spectrometer. It was built for use at the NRAO 12-m millimeter-wave telescope at Kitt Peak, Arizona. It has a total IF processing capability of 2.4 GHz and incorporates a digital correlation design with a filter bank to produce a wide-bandwidth hybrid.

One difficulty in producing hybrid designs is maintaining continuity between spectral sections processed by different digital correlators. Any errors in the processing will cause baseline problems. This error is termed "platforming" and has many sources. This talk will review some causes and cures for platforming.

J6-7  
1100

THE CALTECH 1-GHz CORRELATING SPECTROMETER  
Brian Von Herzen, Scientist  
Caltech Submillimeter Observatory  
1059 Kilauea Ave.  
Hilo, HI 96720

A digital autocorrelating spectrometer has been developed at the Caltech Submillimeter Observatory (CSO) with an IF bandwidth of 1 GHz divided into 320 channels. The CSO spectrometer consists of a 2 giga-sample per second (Gs/s) 2-bit digitizer coupled to a 2 Gs/s digital correlator. The correlator is extremely compact, measuring 5 by 13 inches on a single board for a personal computer. The correlator is housed in a personal computer chassis with fan cooling and augmented power supplies.

The CSO correlator is based upon a new custom CMOS chip developed at CSO containing 320 correlator lags running at a data rate of 250 Ms/s. The CSO correlator chip achieves ten times the density of existing ECL designs without sacrificing speed. The correlator chip consumes 25 mW per lag using 5-volt power supplies, and 10 mW per lag at 3.5 volts and 250 Ms/s. These chips consume less power than alternative correlators at 250 Ms/s.

The data from the digitizer enters the correlator at a rate of 2 Gs/s and is divided into eight parallel data streams of 250 Ms/s with a 1:8 time-division GaAs demultiplexer circuit. Each data stream is cross-correlated with the other data streams using eight correlator chips. The correlator chip can integrate the correlation functions for up to 100 seconds. The personal computer reconstructs the autocorrelation function from the cross-correlations, calculates the Fourier Transform and displays the resulting power spectrum interactively.

The CSO chip uses a micropipelining technique (I. E. Sutherland, Communications of the ACM, 32, 720-738, 1989) to maximize throughput. Each pipeline stage contains at most two logic gates, which permits operation at 250 MHz using a standard CMOS process. In addition, the correlator chip uses transition signaling to latch a new datum with each transition of the control signal. This scheme reduces the frequency requirements of the control signal from 250 MHz to 125 MHz and simplifies the system design.

Recent test results of the correlator will be presented, along with measurements of the spectrometer performance.

J6-8            DEVELOPMENT OF A 1 GHZ, 256-CHANNEL, CMOS,  
1120            DIGITAL CORRELATOR CHIP  
                 C. Timoc, T. Tran, and J. Wongso  
                 Spaceborne, Inc.  
                 742 Foothill Blvd., Suite 2B  
                 La Canada, CA 91011  
                 (818) 952-0126

This paper describes the development of a digital correlator chip with the following features: (a) 1 Giga-sample/second, (b) 256 channels, (c) a 32-bit counter providing up to 4 seconds integration time at 1 GHz, and (d) 40 milliwatts of DC power dissipation per channel.

The improvements in the performance-to-cost ratio of the digital correlator chip will be achieved with a combination of: (a) systolic architecture, (b) novel pipelined differential logic circuits, and (c) standard 0.8 um CMOS process.

The development of CMOS digital logic circuits which are suitable for implementing high performance pipelined systems has been the goal of our prior research and development efforts. A total of 17 different designs employing a novel circuit, called PDL (Pipelined Differential Logic), were fabricated for the past 3 years through the MOSIS service. The most successful PDL integrated circuit was a 1K bit shift register which was fabricated with a 0.8 um CMOS process and operated at a maximum clock frequency of 1 GHz. The voltage swings inside the chip was reduced from a 5V swing, which is commonly used in conventional CMOS circuits, to only 1V. A PDL off-chip receiver amplifies an input ECL signal, with voltage swings as low as 350 mV, to PDL signals of 1V. An off-chip driver has the capability to deliver ECL levels (up to 800 mv) on 50 ohm transmission lines at a clock frequency of 1 GHz. The clock distribution network of the shift register employs microwave power dividers and on-chip transmission lines to reduce the clock skew to less than 50 psec.

Presently, most high-performance digital correlators are implemented with ECL circuits. They operate typically at frequencies ranging from 100 to 500 MHz. A broad range of functions which are currently implemented with ECL circuits could also be implemented with PDL circuits. The most significant advantage of the PDL products over the ECL products is cost. The former are fabricated with standard CMOS processes capable of integrating several millions of transistors per chip whereas the latter are fabricated with more expensive bipolar processes with a level of integration of only a few hundred thousand transistors.

J6-9  
1140**A DIGITAL CROSS-CORRELATOR FOR THE OWENS VALLEY  
MILLIMETER ARRAY****S. Padin and S.L. Scott**  
California Institute of Technology  
Owens Valley Radio Observatory  
Big Pine, CA 93513

Design and performance details for the new Owens Valley Digital Correlator are presented. The correlator serves the Owens Valley Millimeter Array which consists of three 10.4 m telescopes operating in the 80-115 GHz and 210-270 GHz bands. The array is currently being expanded to five telescopes.

The correlator computes the real cross-correlation function for signals in up to four frequency bands each up to 128 MHz wide giving a maximum total bandwidth of 512 MHz. The four bands can be independently positioned anywhere in the 1-2 GHz receiver IF band allowing simultaneous observations of up to four transitions.

A simple serial correlator architecture is used with the multipliers always operating at the maximum clock frequency of 256 MHz. The frequency resolution is controlled by the digitizer input bandwidth and the frequency of the shift register clock (S. Padin *et al.*, *Publications of the Astronomical Society of the Pacific*, **103**, 461-467, 1991). Each baseline in the array has 512 correlator lags divided into four modules. The modules can be associated with independent bands or can be cascaded to give different resolution options.

The high-speed sections of the correlator are realized in an ECL gate array. Each gate array contains the multiplier and shift register circuits for eight lags along with switches which select different signal sources. The accumulators are realized in a CMOS gate array containing 32 18-bit counters.

A correlator module (128 lags) comprises two 9U VME circuit boards. Each circuit board holds eight ECL and two CMOS gate arrays along with the circuits which interface the correlator to a VME bus. A high-speed pattern generator is also provided on each board for testing. The four correlator modules associated with a baseline fit into a standard VME chassis along with a 68030 processor. The processor controls the operating mode of each module, data integration and phase-switch demodulation.

The correlator uses 3-threshold digitization with 2-bit encoding and a multiplication scheme in which the low level products are deleted (B.F.C. Cooper, *Aust. J. Phys.*, **23**, 521-527, 1970). This results in a sensitivity of 0.88 relative to a perfect analog correlator. Digitization is performed by three high-speed ECL sampling comparators (S. Padin and M.S. Ewing, *IEEE Trans. on Instrumentation and Measurement*, **IM-38**, 1109-1115, 1989). The output states of the three comparators are monitored by counters and this information is used to compute the comparator thresholds so that digitizer-induced offsets and scale-factor errors can be corrected at the correlator output.

Friday Afternoon, 10 January, 1335-1520

Session J-7 1335-Fri. CR2-26

SPECTROMETERS FOR RADIO ASTRONOMY-II

Chairman: William J. Wilson, Jet Propulsion Laboratory,  
California Institute of Technology, Pasadena, CA 91109

J7-1  
1340

### THE HAYSTACK WIDEBAND SPECTROMETER

J. I. Levine, Staff Member  
Haystack Observatory  
Westford, Mass. 01886

A digital autocorrelation spectrometer has been constructed for use at the Haystack Observatory. Signal rates to 640 Msamples/second can be processed in real time.

The system uses 320 semi-custom gate array chips, contained on 5 multilayer printed circuit modules. Both the gate arrays and the correlator modules were designed at the Netherlands Foundation for Radio Astronomy, Dwingeloo, The Netherlands.

Each of the 5 system modules processes signals at up to 40 Msamples/second and yields a 1024 point autocorrelation function. At higher rates, samples are processed 2,4,8, or 16 at a time (with a corresponding reduction in the number of output points).

Five video and A/D converters supply input to the correlator system. The 5 signal channels are completely independent and can be tuned to different frequency bands, limited only by the digital processing hardware. Numerous signal configurations are possible under software control.

A 386-class computer services the new correlator and connects to the HP pointing computer, to our Ethernet TCP/IP network, and, through gateways, to Internet and the world. This new computer has a Unix operating system, which allows multiple users over Ethernet and allows a disk with spectra and an archive tape to be local to this machine.

J7-2  
1400

THE VERY LONG BASELINE ARRAY CORRELATOR  
R. P. Escoffier, J. D. Romney and C. M. Broadwell  
National Radio Astronomy Observatory  
Edgemont Rd.  
Charlottesville, VA 22903-2475

The Very Long Baseline Array (VLBA) interferometer for radio astronomy is currently under construction by the NRAO. The correlator for the VLBA, now being tested in Charlottesville, VA, will process the information recorded at the ten new, dedicated VLBA antennas along with data from up to ten existing VLBI antennas.

The VLBA correlator uses the 'FX' architecture in which fast digital Fourier transforms are performed directly on the samples of a baseband radio telescope output. Complex cross visibility spectra are measured by performing cross multiplication and integration on the resulting station spectra. Spectral resolution ranges from 8 channels of continuum (low resolution) data, to a single channel resolved into 1024 spectral points.

An Application Specific Integrated Circuit (ASIC) was developed to perform either a FFT butterfly operation or a complex cross multiply and accumulate function (MAC) with sample rates of 32-Msamples per second. This ASIC and its use in performing FFT and MAC operations is described as is the unique complex floating point number system used in the FFT computation.

Auto- and cross-spectra obtained during initial system testing are presented.

The full 20-station correlator is to be installed in the VLBA Array Operations Center in Socorro, NM, in mid 1992.

J7-3 FAAS: AUTOCORRELATION SPECTROMETER FOR A 3 MM ARRAY  
 1420 C.R. Predmore, P.F. Goldsmith and F.P. Schloerb  
 Five College Radio Astronomy Observatory  
 Department of Physics and Astronomy  
 GRC Towers - 619  
 University of Massachusetts  
 Amherst, MA 01003

The FCRAO 3mm array (QUARRY for Quabbin ARRAy) consists of 15 elements in a 3 by 5 pattern. Each row of 5 pixels is spaced one beamwidth apart on the sky with each of the 3 rows being spaced by two beamwidths. QUARRY operates over the 86 to 115 GHz range.

For each pixel three different filter banks are available and the Focal plane Array Autocorrelation Spectrometer (FAAS) is under development. The bandwidth and resolution per pixel of these spectrometers is summarized in the following table. The velocity resolution is calculated for the CO (1-0) line at 115.3 GHz.

Spectrometer	Channels	Total Bandwidth		Resolution	
		MHz	(Km/s)	KHz	(Km/s)
Filter Bank	32	8	( 21)	250	( .65 )
Filter Bank	32	32	( 83)	1000	( 2.60 )
Filter Bank	64	320	(832)	5000	(13.0 )
FAAS	1024	2.5	( 7)	3.0	( .007)
FAAS	1024	5	( 13)	6.0	( .015)
FAAS	1024	10	( 26)	11.9	( .031)
FAAS	1024	20	( 52)	23.8	( .062)
FAAS	512	40	(104)	95.3	( .25 )
FAAS	256	80	(208)	381	( .99 )

The higher resolution and versatile capability of FAAS will be used for mapping of molecular clouds, comets, circumstellar envelopes, bipolar outflows and for determining the galactic distribution of molecular clouds.

In addition to the array mode of the FAAS, it will also have a hybrid mode for use with the FCRAO single pixel receivers at 7, 3, 2 and 1.3mm. These receivers have single or dual polarization. The 16 boards of FAAS can be arranged into one contiguous spectrometer with 15,000 channels at or can be split in to spectrometers of various bandwidths at different parts of the spectral band.

J7-4  
1440

THE BIMA WIDEBAND CORRELATION SPECTROMETER  
MR. D. Thornton  
Radio Astronomy Laboratoru  
University of California  
Berkeley CA. 94720

With the increase of the BIMA array to nine antennas, and in order to observe external galaxies in a single observation, it was decided to increase the working bandwidth of the I.F. and the correlator system to 800 Mhz. Expanding the current correlator was deemed to be unworkable since its design was based on small scale integration.

A new design based on the Boss chip has been developed. It operates at a clock rate of 50 Mhz, is multiplexed by a factor of four, and hence can analyze an analog bandwidth of 100 Mhz. per module. Each interferometer pair utilizes eight of these modules giving a total bandwidth of 800 Mhz. The eight modules process the video output from four single sideband mixers (upper and lower outputs) that can operate over the total I.F. frequency of 100 to 900 Mhz. Four third local oscillators are provided that also cover the range so that each receiver may be located at any frequency in the I.F. band.

Some of the telescope system design will also be covered to explain the method of processing the fringe data and first L.O. sideband separation.

J7-5  
1500DIGITAL AUTOCORRELATOR SPECTROMETERS FOR  
SPACEBORNE APPLICATIONSKumar Chandra and William J. Wilson  
Jet Propulsion Laboratory  
California Institute of Technology  
Pasadena, California 91109John Canaris and Gary Maki  
NASA Space Engineering Reserach Center  
University of Idaho  
Moscow, Idaho 83843

The National Aeronautics and Space Administration (NASA) supports programs in the remote sensing of the Earth's atmosphere and in astrophysics using mm-wave and submm wave radiometers. The Jet Propulsion Laboratory is currently working on low power digital autocorrelator spectrometers for these radiometers. We have designed a 26-channel, 2-bit correlator chip and the chip was fabricated by Raytheon Corporation in Emitter-Coupled-Logic (ECL) using gate array technology. The 26-channel correlator chip is mounted in a 229-pin package, consumes 3 Watts of DC power and can work up to 300 MHz clock speed. We have used data pipelining technique in the digital delay line and in the correlator multiplier paths to achieve high clock speed. Each channel has a 3-bit prescaler to reduce the channel output rate. This allows use of low power CMOS counter chips for further integration outside the correlator chip. JPL in collaboration with the University of California at Santa Barbara (UCSB), will fly a 52-channel autocorrelator spectrometer using this ECL correlator chip in a balloon-borne observations of interstellar Oxygen. A second ECL spectrometer covering 400 MHz bandwidth with 2.5 MHz spectrum resolution will also be built for the Balloon Microwave Limb Sounder instrument. In addition to the ECL correlator chip, JPL in collaboration with the Microelectronic Research Center at the University of Idaho, has custom-designed a 2-bit CMOS correlator chip for low power, narrowband spectrometers. Hewlett-Packard (HP) fabricated the CMOS correlator chip in 1.0 micron technology and the chip is mounted in a 48-pin flat pack. The CMOS chip contains 32 channels, consumes  $\leq 300$  mWatts DC power and can be clocked up to 25 MHz. The chip also contains 24-bit counters on each channel output and the counters can be interfaced to the computer with minimal interface circuitry. Under user control, the channel counters can be read either in word serial or byte serial. A low power spectrometer with 10 MHz input bandwidth and 100 kHz resolution will be built using the CMOS correlator chips. The narrowband spectrometer may be used in the future Earth Observing System Microwave Limb Sounder instrument.

**INDEX****A**

Aarons, J., 25  
Adve, R.S., 177  
Al-Mahdawi, T.I., 219  
Albertson, V.D., 67  
Ali, J.D., 8  
Allen, J.W., 5  
Allen, K.C., 115  
Allen, O.E., 176  
Allen, R.J., 217  
Alvarez, L., 163  
Amey, D., 278  
Anderson, K.D., 71, 136  
Anderson, R.R., 151  
Andrawis, M., 278, 280  
Angell, T.S., 63  
Argo, P.E., 28, 173  
Armstrong, J.W., 33  
Arora, R.K., 11  
Asvestas, J.S., 228  
Aydin, K., 139

**B**

Babichenko, A., 265  
Bahar, E., 253  
Baker, G., 130  
Baker-Jarvis, J., 282  
Balakrishnan, N., 139  
Bansal, R., 114  
Barber, P.W., 287  
Barker, R.J., 261  
Barnes, F.S., 46, 194  
Barrios, A.E., 72  
Barts, R.M., 62  
Basu, S., 31  
Basu, Su., 31  
Batelaan, P., 187  
Bauer, R., 22  
Baum, C.E., 9, 134, 222, 290  
Baumback, M.M., 152, 298  
Baysar, A., 283, 284  
Bellamine, F.H., 111  
Benalla, A., 65, 236  
Benson, R.F., 94  
Berkey, F.T., 149  
Bernhardt, P.A., 153, 154, 298, 300  
Berry, L.A., 18

Berthaud, P., 55  
Bhapkar, U., 186  
Bhasin, K.B., 192, 193  
Biederman, W., 21  
Biggs, A.W., 133  
Blemker, A.R., 192  
Bleszynski, E., 121  
Bleszynski, M., 121, 181  
Boisvert, P., 219  
Bolomey, J.Ch., 55  
Bolourchi, N., 127  
Bonetti, R.R., 193  
Booton, R.C., Jr., 182, 240

Bowen, M.M., 247, 249  
Brandt, R.G., 258  
Breakall, J.K., 64  
Brennan, T., 186  
Brent, R., 86  
Bringi, V.N., 139  
Broadwell, C.M., 314  
Brown, G.S., 119  
Bryans, L.G., 49  
Buchau, J., 81, 144, 145  
Bundy, S.C., 189  
Bunting, C., 278  
Buonsanto, M.J., 83  
Burch, J.L., 93  
Butler, C.M., 226

**C**

Canales, N., 51  
Canaris, J., 317  
Cannon, P.S., 144  
Carlson, H.C., 147  
Carter, J.A., III, 306  
Castillo, J.P., 130  
Cavanagh, J.F., 77  
Cavcey, K.H., 113  
Chandra, K., 307, 317  
Chang, D.C., 182, 231, 240  
Chaturvedi, P.K., 30, 303  
Chen, C.F., 83  
Chen, K.M., 184, 221  
Chew, W.C., 292  
Chorey, C.M., 193  
Choudhury, D., 187  
Chowdhury, D.Q., 287  
Clark, M.H., 212

Clegg, A.W., 39  
Clodius, W.B., 156  
Cohen, D.J., 19  
Cohen, L., 110  
Conkright, R.O., 29  
Constable, S., 68  
Cordes, J.M., 37, 39  
Cottard, G., 55  
Cown, B.J., 55  
Crane, P.C., 102  
Croes, G., 209  
Crowley, G., 144  
Curilla, J., 278

**D**

Dalkir, Y., 302  
Davis, W.A., 62, 278, 280  
Dawe, B.R., 116  
Daywitt, W.C., 3  
DeLyser, R.R., 233  
DeMinco, N., 115  
Desai, K.M., 95  
DeSanto, J.A., 118  
DiCarlo, E., 114  
Dierich, P., 308  
Djuth, F.T., 146, 147, 200  
Dowd, A.V., 309  
Drosopoulos, A., 14  
Duan, D.W., 59, 135  
DuBois, D.F., 204, 205  
Dudley, D.G., 174  
Duncan, L.M., 259  
Dusenbery, P.B., 91  
Dvorak, S.L., 178

**E**

Egbert, G., 70  
El-Ghazaly, S.M., 220, 283  
Elder, J.H., 147, 200  
Eldred, D., 164  
Elshabini-Riad, A., 224, 278, 280  
Emerson, D.T., 159, 168  
Engel, A.G., Jr., 242  
Engheta, N., 243  
Escoffier, R.P., 314  
Estrada, J.P., 55

- F**
- Falco, F., 122  
 Fedder, J.A., 30  
 Fejer, J.A., 200, 201, 202  
 Ferraro, A.J., 296  
 Ferraro, R.D., 183  
 Ferriere, K., 97  
 Fidanboyllu, K.M., 224, 278  
 Field, E.C., Jr., 248  
 Fisher, J.R., 212  
 Fishman, L., 86, 295  
 Fitzgerald, T.J., 173  
 Flanagan, C., 95  
 Flemming, M., 161  
 Foldes, P., 58  
 Folkers, T.W., 159  
 Forster, J.R., 161  
 Foster, R.S., 38  
 Fougere, P.F., 170  
 Franke, P.M., 85  
 Franke, S.J., 27  
 Frasch, L., 279  
 Fraser-Smith, A.C., 247, 249  
 Freeman, M.J., 260  
 Frerking, M.A., 187  
 Frolov, V.L., 263, 265, 266  
 Fung, S.F., 158
- G**
- Gallawa, R.L., 105  
 Gamache, R.R., 83  
 Ganguli, G., 91  
 Ganguli, G.I., 154  
 Gans, W.L., 218  
 Gardner, R.L., 131  
 Gasiewski, A.J., 100, 140  
 Gerace, G.C., 78  
 Gergely, T.E., 99  
 Geyer, R.G., 282  
 Glisson, A.W., 122  
 Goddard, R., 164  
 Goldsmith, P.F., 267, 315  
 Goodman, A.A., 273  
 Goodman, S., 206, 264, 265, 266  
 Gossard, E.E., 138
- Goyal, I.C., 105  
 Grace, M., 41  
 Grach, S.M., 263, 265, 266  
 Green, J.L., 158  
 Grimm, J.M., 6, 279  
 Grondin, R.O., 220  
 Groves, K.M., 203, 302  
 Guanghua, H., 12, 190  
 Guerrieri, J.R., 51  
 Guo, Y., 106  
 Gupta, K.C., 7, 10, 65, 236  
 Gwinn, C.R., 95
- H**
- Haas, D.G., 298  
 Habashy, T.M., 293  
 Hagfors, T., 142  
 Hagn, G.H., 244, 246  
 Haines, D.M., 262  
 Hale, L.C., 157  
 Hall, W., 121  
 Hand, G.R., 87  
 Hanisch, R.J., 216, 246  
 Hansen, T.B., 229  
 Hanson, G., 279  
 Hanssen, A., 204, 205  
 Harnish, L.O., 246  
 Harrison, M.G., 107  
 Hashemi-Yeganeh, S., 230  
 Hatfield, D.N., 17  
 Haupt, R.L., 227  
 Haykin, S., 14  
 Heckscher, J.L., 262  
 Hicks, M., 116  
 Hill, D.A., 112, 176  
 Hill, S.C., 287  
 Hitney, H.V., 73, 137  
 Hjellming, R.M., 209  
 Hjelme, D.R., 235, 238, 239, 241  
 Hoffman, W., 161  
 Holdaway, M.A., 210  
 Hooper, W.P., 196, 197  
 Hoppe, D.J., 125  
 Hoshmand, B., 135  
 Howard, A.Q., Jr., 291  
 Hower, G.L., 289  
 Huang, J., 208, 299  
 Huang, X., 79, 83, 84  
 Huang, Y., 262
- Huba, J.D., 155  
 Huffman, J., 64  
 Hughes, H.G., 195, 198, 199
- I**
- Imbriale, W.A., 60  
 Inan, U.S., 172, 301  
 Itoh, T., 188
- J**
- Jahn, D., 231  
 Jaroszewicz, T., 181  
 Jauncey, D., 95  
 Jensen, D.R., 197, 198  
 Jewell, P.R., 159  
 Johnk, R.T., 113, 185  
 Johnson, R.L., 252  
 Jones, D.L., 95  
 Jordan, A.K., 294  
 Jordan, D., 114  
 Jurgens, R.F., 270
- K**
- Kahrizi, M., 232  
 Kakaes, A.K., 129  
 Kanda, M., 185  
 Kappenman, J.G., 67  
 Karashtin, A.N., 263, 265, 266  
 Kasevich, R.S., 109  
 Katehi, P.B., 242  
 Kawalko, S.F., 123  
 Kawasaki, S., 188  
 Keskinen, M.J., 30, 303  
 Kiiss, A., 44  
 King, E.A., 95  
 Kirsch, A., 63  
 Kleinman, R.E., 63, 228  
 Klumb, M., 304, 305  
 Kohl, H., 200  
 Komrakov, G.P., 263, 265, 266  
 Kong, J.A., 293  
 Koons, H.C., 152  
 Koontz, M., 307  
 Koppel, D., 122  
 Kossey, P.A., 258, 261, 262  
 Kotik, D.S., 263, 265, 266

Kremer, D.P., 51  
 Kudeki, E., 27  
 Kuester, E.F., 111, 231, 233  
 Kuester, J.L., 283, 284  
 Kuklinski, W.S., 81  
 Kulkarni, S.R., 275  
 Kullback, M., 21  
 Kunkee, D.B., 140  
 Kuo, S.P., 203, 208, 261, 297, 299, 302  
 Kwok, S.C., 46  
 Kzadri, B., 279

**L**

Lafflin, M.G., 251  
 Landecker, T.L., 272  
 Lau, K., 164  
 Lauber, W.R., 116  
 Laxpati, S.R., 123  
 Lecacheux, A., 308  
 Lee, H.M., 74  
 Lee, M.C., 203, 208, 261, 297, 302  
 Lee, S.H., 236  
 Lev-Tov, S., 301  
 Levine, J.I., 313  
 Lewis, R.L., 54  
 Leyser, T.B., 92, 263, 265, 266  
 Li, D., 126  
 Liewer, P.C., 183  
 Lillie, P.A., 48  
 Lin, C.S., 89, 90  
 Lin, K.H., 29  
 Lindell, I.V., 120  
 Lis, D.C., 274  
 Lucas, M.S.P., 43  
 Lyles, J., 278  
 Lyon, E., III, 23

**M**

MacKenzie, E., 31  
 Mader, T.B., 189  
 Maki, G., 317  
 Mannikko, P.D., 226  
 Maradudin, A.A., 256, 257  
 Maricevic, Z.A., 232  
 Martinez-Miranda, L.J., 243  
 Masson, C.R., 162

Matheson, R.J., 20, 47  
 Mattauach, R.J., 186  
 Matthaeus, W.H., 36  
 McGurn, A.R., 256, 257  
 McKinnon, M.M., 271  
 McNamara, L.F., 80  
 McPherson, J.E., 289  
 Menietti, J.D., 89, 90, 93  
 Merewether, D.E., 132  
 Michet, D., 308  
 Mickelson, A.R., 104, 235, 237, 238, 239, 241  
 Milikh, G.M., 260  
 Miller, E.K., 169, 225  
 Milman, A.S., 141  
 Milstein, L.B., 21, 128  
 Mjohhus, E., 205  
 Moghaddam, M., 292  
 Moran, K.P., 175  
 Mudaliar, S., 254, 255  
 Murphy, A., 278  
 Murphy, W.D., 180  
 Mutel, R.L., 40

**N**

Nathan, J., 221  
 Nerheim, N., 164  
 Nicholson, D.R., 207  
 Nicholson, G., 95  
 Nickisch, L.J., 85  
 Norgard, J.D., 107  
 Novak, G., 267  
 Nyquist, D.P., 6, 184, 221, 279

**O**

O'Brien, K.B., 243  
 O'Brien, T.C., 270  
 Ohnuki, S., 184  
 Olsen, R.G., 250, 289  
 Omid, N., 88  
 Ondrejka, A.R., 176  
 Orman, M., 122  
 Ossakow, S.L., 303

**P**

Padin, S., 312  
 Pal, B.P., 105  
 Papa, R.J., 117

Papazian, P.B., 115  
 Pape, D.R., 306  
 Parker, J.W., 183  
 Parlow, R.D., 16  
 Parrikar, R.P., 7  
 Paul, A.K., 82, 150  
 Paulson, M.R., 195, 198, 199  
 Pavlasek, T.J.F., 219  
 Payne, G.L., 207  
 Payne, J.M., 165  
 Percival, D.B., 13  
 Perera, S., 1, 2  
 Perini, J., 110  
 Petrakos, S., 231  
 Petre, P., 52, 179, 234  
 Phillips, J.A., 268, 275  
 Pickholtz, R., 128  
 Pickholtz, R.L., 21  
 Pizzo, V.J., 35  
 Platt, I.G., 262  
 Pongratz, M.B., 156  
 Popovic, Z.B., 189, 238  
 Pospieszalski, M.W., 42, 191  
 Poulin, T., 278  
 Predmore, C.R., 267, 315  
 Preston, R.A., 95  
 Price, R.M., 101  
 Price, S.L., 109  
 Primas, L.E., 237

**R**

Radisic, V., 238  
 Raggio, J., 45  
 Rahmat-Samii, Y., 56, 59, 125, 135, 167  
 Rao, S.M., 286  
 Reid, M.J., 171  
 Reinisch, B.W., 79, 81, 83, 84, 144, 145  
 Repjar, A.G., 51  
 Reynolds, J., 95  
 Riad, S.M., 223, 224, 278, 280  
 Richter, J.H., 195, 199  
 Rietveld, M.T., 200  
 Roberts, D.H., 277  
 Rochblatt, D.J., 167  
 Rodriguez, J.V., 301  
 Rodriguez, P., 152,

- 154, 298  
Rokhlin, V., 180  
Romero, H., 91  
Romney, J.D., 314  
Rose, H., 204, 205  
Rosolen, C., 308  
Ross, J., 221  
Rothwell, E., 184, 221  
Roussel-Dupre, R.A.,  
156  
Routledge, D., 272  
Rowland, H.L., 300
- S**
- Sailors, D.B., 245  
Sakurai, T., 34  
Salerno, D.C., 21  
Sales, G.S., 81, 262  
Sarkar, T.K., 52, 169,  
177, 179, 225, 232,  
234  
Sarrafzadeh, H.R., 129  
Satyanarayana, P., 30  
Scales, W.A., 153, 154  
Scali, J.L., 83, 145  
Scheid, R., 164  
Schieder, R., 304, 305  
Schilling, D.L., 21,  
126, 127, 128  
Schinckel, A., 166  
Schloerb, F.P., 315  
Scott, S.L., 160, 312  
Sega, R.M., 107  
Sevaston, G., 164  
Shin, R.T., 293  
Shukla, A.K., 148  
Sibbald, C., 281  
Siefring, C.L., 152,  
298  
Sihvola, A.H., 120  
Sime, D.G., 35  
Simonetti, J.H., 96  
Simons, D.J., 156  
Slade, M.A., 270  
Smegal, R.J., 272  
Smith, E.K., 78  
Song, J., 184  
Spangler, S.R., 34  
Spaulding, A.D., 244  
Srikanth, S., 269  
Stapleton, J.K., 76  
Stiles, G.S., 149  
Stone, A.P., 9
- Strauch, R.G., 175  
Stubbe, P., 200  
Stubenrauch, C.F., 50  
Stuchly, S.S., 281  
Stutzman, W.L., 58, 62  
Su, W., 223, 278  
Sulzer, M.P., 146, 147,  
200, 201, 202  
Surette, M.R., 241  
Syed, H.H., 124
- T**
- Takamizawa, K., 58  
Taylor, D.J., 288  
Thide, B., 263, 265,  
266  
Thieman, J.R., 158  
Thng, C., 240  
Thompson, T.W., 214  
Thomson, D.J., 15, 69  
Thorland, M., 279  
Thornton, D.D., 161,  
316  
Thorsett, S.E., 275,  
276  
Timoc, C., 311  
Tolls, V., 304, 305  
Toncich, S.S., 193  
Tran, T., 311  
Trzaska, H., 108  
Tsai, C.M., 10  
Tsai, L.C., 149  
Tsunoda, R.T., 26
- U**
- Uberall, H., 106, 288  
Uslenghi, P.L.E., 8,  
123
- V**
- Valco, G.J., 192  
Valladares, C.E., 143  
Vaneldik, J.F., 272  
Vanzura, E.J., 285  
Vasisht, G., 275  
Vassiliou, M.S., 180  
Vechinski, D.A., 286  
Velice, K., 203  
Vendelin, G., 41  
Veszelei, E., 263, 265  
Veszely, G., 234
- Viitanen, A.J., 120  
Volakis, J.L., 124  
Von Herzen, B., 310
- W**
- Wait, D.F., 4  
Walden, A.T., 13  
Waldenvik, M., 263,  
265, 266  
Walker, D.N., 152  
Wang, J., 207  
Warber, C.R., 248  
Ward, B.D., 83  
Webster, A.R., 75  
Welch, W.J., 161  
Wells, D., 116  
Wepman, J.A., 24  
Werner, D.H., 64, 66,  
296  
Werner, P.L., 66, 296  
Werntz, P., 58  
White, R.L., 215, 216  
Williams, A.E., 193  
Williams, K.L., 200  
Wilson, W.J., 307, 317  
Winglee, R.M., 90, 93  
Winske, D., 88  
Wittmann, R.C., 53  
Wolcott, J.H., 156  
Wolszczan, A., 213  
Wong, H.K., 89  
Wongso, J., 311  
Woodworth, M.B., 117  
Woody, D.P., 160, 166  
Wright, J.W., 28, 32  
Wright, M., 211  
Wright, M.C.H., 161
- X**
- Xia, J., 293, 294  
Xu, F.X., 43
- Y**
- Yadlowsky, M.J., 235,  
239  
Yaghjian, A.D., 57, 229  
Yang, G., 126  
Yang, S., 104  
Yeh, K.C., 29

**Z**

Zank, G.P., 36  
Zengingonul, H.P., 27  
Zhang, X., 61  
Zhang, Y.S., 261  
Zhang, Z., 194  
Ziegler, C.L., 139  
Zombory, L., 234  
Zrnic, D.S., 139

**Wednesday, 8 January (cont.)**

1355-1700

A-4	MICROWAVE AND OPTICAL METROLOGY	CR1-9
A-5	EMI/EMC MEASUREMENTS	CR0-30
E-2	HIGH POWER ELECTROMAGNETICS	CR1-46
F-2	REMOTE SENSING OF ATMOSPHERE AND OCEAN	CR1-40
H-2	PLASMA WAVES AND STRUCTURE INITIATED BY CHEMICAL RELEASES	CR1-42

1535-1700

B-4	IMPEDANCE BOUNDARY CONDITIONS	CR2-28
-----	-------------------------------	--------

1700-1800

Commission B	Business Meeting	CR2-28
Commission H	Business Meeting	CR1-42
Commission J	Business Meeting	CR2-26

**Thursday, 9 January**

0835-1200

A-6	TIME DOMAIN SIGNAL PROCESSING	CR1-42
B-5	NUMERICAL METHODS	CR2-06
D-1	HIGH FREQUENCY DEVICES	CR1-9
F-3	LIDAR REMOTE SENSING	CR1-40
GH-1	DWIGHT R. NICHOLSON MEMORIAL SESSION	CR0-30
J-4	IMAGE PROCESSING AND COMPUTERS	CR2-26

1335-1700

A-7	TIME DOMAIN METROLOGY	CR2-06
B-6	SLOTS, STRIPS, AND STRIP GRATINGS	CR2-28
D-2	THEORETICAL ASPECTS OF WAVEGUIDES AND STRUCTURES	CR1-9
E-3	NOISE MEASUREMENTS AND MODEL VALIDATION	CR1-46
F-4	SCATTERING OF RADIO AND OPTICAL WAVES	CR1-40
GH-2	IONOSPHERIC MODIFICATION-I	CR0-30
J-5	POLARIZATION: TECHNIQUES AND OBSERVATIONS	CR2-26

1700-1800

Commission D	Business Meeting	CR1-9
Commission E	Business Meeting	CR1-46
Commission G	Business Meeting	CR0-30

**Friday, 10 January**

0835-1200

A-8	METROLOGY FOR MATERIAL CHARACTERIZATION	CR1-42
J-6	SPECTROMETERS FOR RADIO ASTRONOMY-I	CR2-26

0835-1020

B-7	TRANSIENT AND RESONANT SCATTERING	CR2-28
-----	-----------------------------------	--------

0855-1200

GH-3	IONOSPHERIC MODIFICATION-II	CR0-30
------	-----------------------------	--------

1015-1200

B-8	INVERSE SCATTERING	CR2-28
-----	--------------------	--------

1335-1520

J-7	SPECTROMETERS FOR RADIO ASTRONOMY-II	CR2-26
-----	--------------------------------------	--------

